

CHEMICAL MODIFICATION OF FUEL CELL  
CATALYSTS AND ELECTROCHEMISTRY OF PROTON  
EXCHANGE MEMBRANE FUEL CELL ELECTRODES

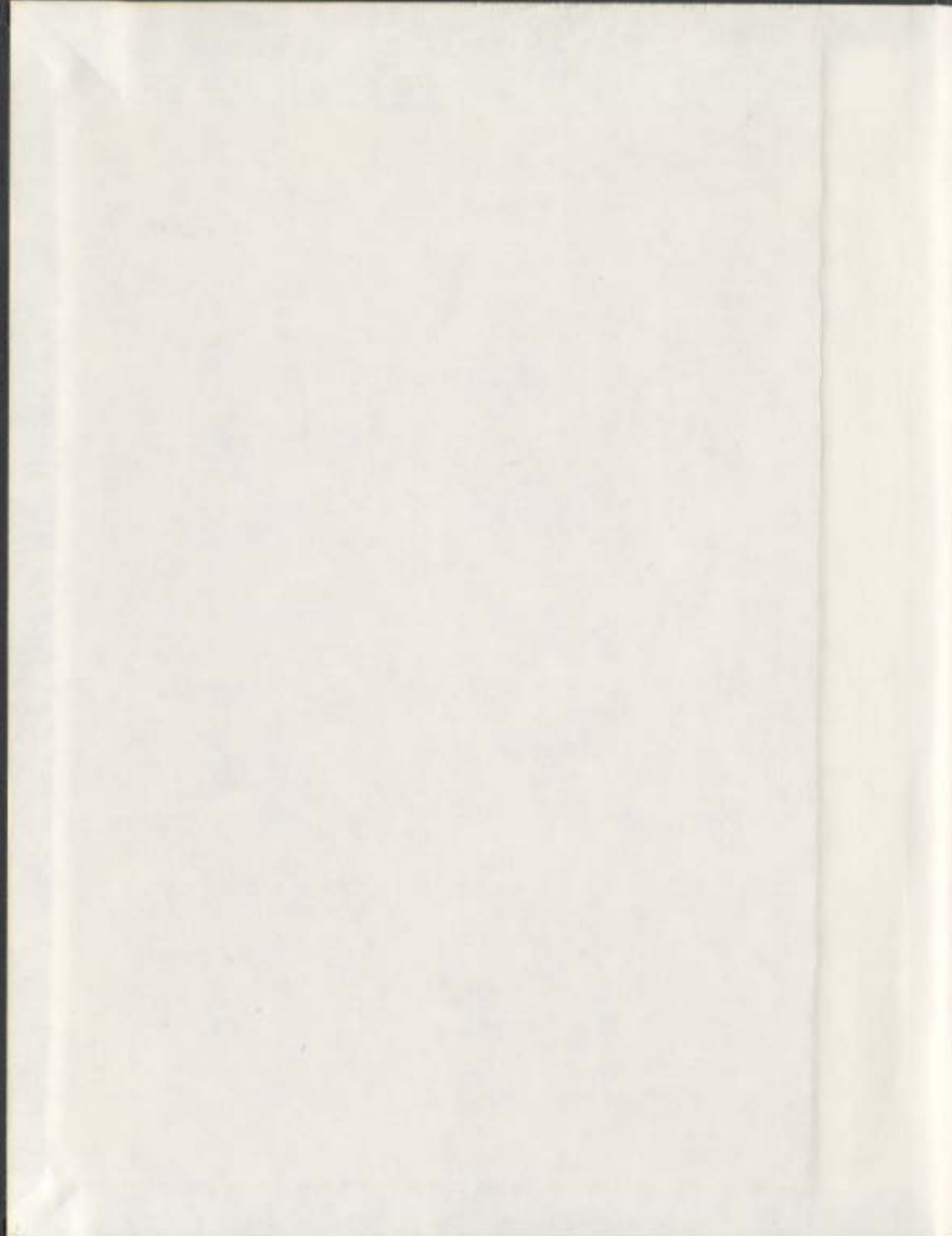
CENTRE FOR NEWFOUNDLAND STUDIES

---

TOTAL OF 10 PAGES ONLY  
MAY BE XEROXED

(Without Author's Permission)

E. BRADLEY EASTON









National Library  
of Canada

Bibliothèque nationale  
du Canada

Acquisitions and  
Bibliographic Services

Acquisitions et  
services bibliographiques

395 Wellington Street  
Ottawa ON K1A 0N4  
Canada

395, rue Wellington  
Ottawa ON K1A 0N4  
Canada

*Your file* *Votre référence*

*ISBN: 0-612-89692-7*

*Our file* *Notre référence*

*ISBN: 0-612-89692-7*

The author has granted a non-exclusive licence allowing the National Library of Canada to reproduce, loan, distribute or sell copies of this thesis in microform, paper or electronic formats.

L'auteur a accordé une licence non exclusive permettant à la Bibliothèque nationale du Canada de reproduire, prêter, distribuer ou vendre des copies de cette thèse sous la forme de microfiche/film, de reproduction sur papier ou sur format électronique.

The author retains ownership of the copyright in this thesis. Neither the thesis nor substantial extracts from it may be printed or otherwise reproduced without the author's permission.

L'auteur conserve la propriété du droit d'auteur qui protège cette thèse. Ni la thèse ni des extraits substantiels de celle-ci ne doivent être imprimés ou autrement reproduits sans son autorisation.

---

In compliance with the Canadian Privacy Act some supporting forms may have been removed from this dissertation.

Conformément à la loi canadienne sur la protection de la vie privée, quelques formulaires secondaires ont été enlevés de ce manuscrit.

While these forms may be included in the document page count, their removal does not represent any loss of content from the dissertation.

Bien que ces formulaires aient inclus dans la pagination, il n'y aura aucun contenu manquant.

**Canada**



Chemical Modification of Fuel Cell  
Catalysts and Electrochemistry of Proton  
Exchange Membrane Fuel Cell Electrodes

by

**E. Bradley Easton**

B.Sc. (Hons), Memorial University of Newfoundland  
St. John's, Newfoundland 1998

A thesis submitted to the School of Graduate Studies in partial fulfillment of the  
requirements for the degree of Doctor of Philosophy

Department of Chemistry  
Memorial University of Newfoundland  
St. John's, Newfoundland, Canada  
January 2003

## Abstract

One of the major goals of this research was to investigate ion transport within the catalyst layer of fuel cell electrodes and attempt to improve it.

One method used to study ion transport within fuel cell electrodes was to incorporate electroactive metal complexes into the catalyst layer to act as a probe. It was found that a lower fraction of the complexes were electrochemically active in the cathode of an operating fuel cell, compared to similar electrodes in contact with an aqueous sulfuric acid solution. It is anticipated that in many cases, the method of electroactive probes will be more advantageous than (or complimentary to) standard methods.

Electrochemical impedance spectroscopy was also used to study ion transport in fuel cell catalyst layers. It was found that limiting capacitance correlates with active area. Also, results indicate that the non-ideal impedance behavior of fuel cell electrodes is due to variation of their ionic conductivity with distance from the membrane.

In order to increase proton conductivity in the catalyst layer, we have explored the attachment of a sulfonated silane directly to the catalyst surface. It was found that the modified catalysts outperformed the unmodified catalyst at low Nafion loadings (<15%). The optimum performance achieved with the modified catalyst was similar to that of the untreated catalyst, despite the fact it contained 66% less Nafion. This result is explained by the fact that both optimized catalyst layers contained approximately the same concentration of sulfonate groups.

Another major goal of this work was to study the materials from which direct methanol fuel cells (DMFC) are constructed. Here we report the systematic optimization of all membrane-electrode assembly components, using standard fuel cell materials. This has led to significant improvement in performance.

To combat the issue of methanol crossover in DMFCs, we have prepared polypyrrole/Nafion composite membranes, which have previously been shown to be significantly less permeable to methanol. DMFC performance achieved with composite membranes was superior to that achieved with Nafion membranes. The improved performance results from increased cathode activity, which is due to less methanol crossover and a lower water flux across the membrane.

## **Acknowledgements**

I would like to express my deepest appreciation to Dr. Peter Pickup for his guidance and supervision throughout the duration of this project. I would also like to thank my supervisory committee, Dr. W. Machin, Dr. R. Poirier and Dr. P. Tremaine for all their helpful comments and advice throughout the course of my studies.

A special thanks the members of the Pickup research group for all their help over the last few years. In particular, I would like to thank Jeremy Hughes and Brandi Langsdorf for the synthesis of composite membranes. Also, I would like to thank Brian MacLean and Chris Kean for their helpful (and often comical) discussions.

I would also like to express my sincerest gratitude to Dr. Zhigang Qi for all his guidance during my time at H Power. Thanks to Arthur Kaufman, Chunzhi He, Mark Hollett, Victor Conti and the entire H Power R&D staff for all their assistance.

Financial support from the School of Graduate Studies, the Chemistry Department, NSERC and H Power Corp. (in the form of industrial postgraduate scholarships) are gratefully acknowledged.

Finally, I would like to thank my parents, my soon to be wife Maria, and my family and friends for all their support and encouragement throughout my studies.

## Table of Contents

Title	i
Abstract	ii
Acknowledgments	iv
Table of Contents	v
List of Abbreviations	xi
List of Tables	xiv
List of Figures	xiv
List of Schemes	xxiii
<b>Chapter 1 – General Review of Fuel Cells</b>	<b>1</b>
1.1 Introduction to Fuel Cells	1
1.2 Proton Exchange Membrane Fuel Cells (PEMFC)	3
1.2.1 The Proton Exchange Membrane	4
1.2.2 PEMFC Electrodes	7
1.2.2.1 PEMFC Anodes	10
1.2.2.2 PEMFC Cathodes	12
1.3 Other Types of Hydrogen-Air Fuel Cells	17
1.3.1 Alkaline Fuel Cells	17
1.3.2 Phosphoric Acid Fuel Cells	18
1.3.3 Molten Carbonate Fuel Cells	19

1.3.4 Solid Oxide Cells	20
1.4 Direct Methanol Fuel Cells (DMFC)	21
1.4.1 Introduction to Direct Methanol Fuel Cells	21
1.4.2 Direct Methanol Fuel Cell Anodes	22
1.4.3 Direct Methanol Fuel Cell Cathodes	25
1.4.4 Direct Methanol Fuel Cell Proton Exchange Membranes	25
1.5 Other Fuels	27
1.6 Evaluating Fuel Cell Performance	27
1.7 Thesis Objectives	28
<b>Chapter 2 – Chemicals and Instrumentation</b>	<b>39</b>
2.1 Electrochemical Instruments	40
2.2 Fuel Cell Testing	40
2.2.1 Fuel Cell Electrode Preparation	40
2.2.2 MEA Preparation	41
2.2.3 Fuel Cell MEA Testing	42
2.2.3 Reproducibility of Fuel Cell Results	46
2.3 Nuclear Magnetic Resonance Spectra	46
2.4 Electron Microprobe Energy Dispersive X-ray Analysis	46
2.5 Fourier Transform Infrared Spectroscopy	47
2.6 Electronic Absorption Spectroscopy	47
2.7 X-ray Diffraction Spectra	47

<b>Chapter 3 – Probing Electrochemical Activity in Proton Exchange</b>	
<b>Membrane Fuel Cell Electrodes using Electroactive Probes</b>	<b>48</b>
3.1 Introduction to Electroactive Probes	49
3.2 Experimental	51
3.2.1 Preparation of Modified Electrodes Containing Os(bpy) <sub>3</sub> <sup>2+</sup>	51
3.2.2 Preparation of Modified Electrodes Containing Silane Tethered Ru(terpy)(dabpy) <sup>+</sup>	51
3.2.3 Electrochemical Notes	53
3.3 Results and Discussion	54
3.3.1 Os(bpy) <sub>3</sub> <sup>2+</sup> Modified Electrodes	54
3.3.2 Silane-tethered Ru(2,2',6',2''-terpyridine)(4,4'-dicarboxylic acid- 2,2'-bipyridine)Cl <sup>+</sup>	58
3.4 Conclusion	68
<b>Chapter 4 – Chemical Modification of Proton Exchange Membrane Fuel</b>	
<b>Cell Catalysts with a Sulfonated Silane</b>	<b>72</b>
4.1 Introduction to Sulfonated Silanes	73
4.2 Experimental	74
4.2.1 Silane Treatment Procedure	74
4.2.2 Electrode and MEA Fabrication and Testing	75
4.3 Catalyst Characterization	76

4.3.1 Catalyst Loading	76
4.3.2 Average Pt Particle Size	76
4.3.3 Fourier Transform Infrared Spectroscopy	80
4.3.4 Relative Elemental Composition	83
4.4 Fuel Cell Performance	88
4.4.1 Performance vs. Nafion Loading	88
4.4.2 Discussion	90
4.5 Application of the Sulfonated Silane onto Preformed Electrodes	97
4.6 Conclusions	101
<b>Chapter 5 – Development of Direct Methanol Fuel Cell Membrane and Electrode Assemblies</b>	<b>105</b>
5.1 Introduction Direct Methanol Fuel Cells	106
5.2 Anode Optimization	106
5.2.1 Introduction	106
5.2.2 Electrode and MEA Preparation	107
5.2.3 Anode Electrode Backing	107
5.2.4 Anode Catalyst Loading	110
5.2.5 Nafion Content in the Anode Catalyst Layer	110
5.2.6 Optimized Anode Components	114
5.3 Cathode Optimization	114
5.3.1 Introduction	114

5.3.2 Electrode and MEA Preparation	115
5.3.3 Nafion Content in the Cathode Catalyst Layer	116
5.3.4 PTFE Content in the Cathode Catalyst Layer	116
5.3.5 Optimized Anode Components	116
5.4 Nafion Membrane	119
5.4.1 Introduction	119
5.4.2 Anode Performance Using Different Nafion Membranes	120
5.4.3 DMFC Performance Using Different Nafion Membranes	123
5.4.4 Methanol Crossover of Different Nafion Membranes	123
5.5 Conclusions	127
<b>Chapter 6 – Characterization of Polypyrrole/Nafion Composite</b>	
<b>Membranes in a Direct Methanol Fuel Cell</b>	133
6.1 Introduction to Conducting Polymer/Nafion Composite Membranes	134
6.2 Experimental	134
6.2.1 Preparation of Polypyrrole/Nafion Composite Membranes	134
6.2.2 MEA Preparation and Testing Procedure	135
6.3 Composite Membranes Prepared via Fe <sup>3+</sup> Oxidative Polymerization	136
6.3.1 Performance of Composite Membranes Prepared via Fe <sup>3+</sup>	136
6.3.2 Membrane Treatment to Enhance Electrode/Membrane Interface	139
6.4 Performance of Composite Membranes Prepared via H <sub>2</sub> O <sub>2</sub> Oxidative Polymerization	142

6.5 Discussion	144
6.6 Conclusion	155
<b>Chapter 7 – Electrochemical Impedance Spectroscopy Studies of Fuel Cell</b>	
<b>Electrodes</b>	158
7.1 Introduction to Electrochemical Impedance Spectroscopy	159
7.2 Modeling a Fuel Cell Electrode	162
7.3 Catalyst Layers Immobilized onto Glassy Carbon Electrodes	167
7.3.1 Experimental	167
7.3.2 Results and Discussion	167
7.3.2.1 Cyclic Voltammetry Experiments	167
7.3.2.2 EIS Experiments	170
7.4 Electrodes Containing Os(bpy) <sub>3</sub> <sup>2+</sup> Electroactive Probes	183
7.5 Conclusion	190
<b>Chapter 8 – Summary and Future Work</b>	193

## List of Abbreviations and Symbols

AC – Alternating Current

AFC – Alkaline Fuel Cell

BET - Brunauer-Emmett-Teller

bpy - 2,2'-bipyridine

$C_m$  – methanol concentration

CFP - carbon fiber paper

CV - cyclic voltammetry or cyclic voltammogram

d – membrane thickness

$D_m$  – methanol diffusion coefficient

$D_m C_m$  – methanol permeability

dabpy - 2,2'-bipyridine-4,4' dicarboxylic acid

DC – Direct current

DHE – Dynamic hydrogen electrode

DMFC – Direct Methanol Fuel Cell

E - potential

EIS - Electrochemical impedance spectroscopy

EDX - energy dispersive X-ray emission analysis

FTIR - Fourier Transform Infrared spectra

GDC - Gas Diffusion Cell

GDL - gas diffusion layer

I – current

$i_o$  – exchange current

$j - (-1)^{1/2}$

$j_{lim}$  – limiting methanol crossover current density

$j_o$  – exchange current density

$k_{dl}$  – drag coefficient

MEA - Membrane-Electrode Assembly

MCFC - Molten carbonate fuel cell

NHE – Normal hydrogen electrode

NMR - Nuclear magnetic resonance

ORR – Oxygen Reduction Reaction

PAFC - Phosphoric acid fuel cell

PBI – polybenzimidazole

PEM - Proton exchange membrane

PEMFC - Proton exchange membrane Fuel cell

Ppy - polypyrrole

PTFE - polytetrafluoroethylene

R - resistance

RHE – Reference hydrogen electrode

SAXS - Small angle X-ray scattering

SD – sputter deposition

SEM - scanning electron microscope

SOFC - Solid oxide fuel cell

SSCE - saturated sodium chloride calomel electrode

TEAP - Tetraethylammonium perchlorate

terpy – 2,2':6',2''-terpyridine

TMS -  $(\text{CH}_3)_4\text{Si}$

XAFS - X-ray absorption fine structure

XRD – X-ray diffraction

YSZ - yttria-stabilized zirconia

Z – impedance

$\omega$  - frequency

$\lambda$  – water uptake

$\epsilon$  – porosity

$\rho$  - density

$x_{\text{H}_2\text{O}}$  – mole fraction of water

## List of Tables

Table 4.1	Summary and assignment of peaks observed in the FT-IR spectrum of Vulcan XC72 carbon black.	83
Table 4.2	Summary of catalyst properties	88
Table 5.1:	Methanol Transport Properties in Nafion Membranes	127
Table 6.1	Methanol Crossover and Resistance Properties of Polypyrrole/Nafion Composite Membranes	138
Table 6.2	Water and Methanol Uptake Properties of Polypyrrole/Nafion Composite Membranes	152

## List of Figures

### Chapter 1

Figure 1.1	The structure of Nafion.	4
Figure 1.2	Yeager's three phase model of Nafion; a fluorocarbon region (A), an interfacial zone (B) and an ionic cluster region (C).	6
Figure 1.3	The membrane and electrode assembly.	9
Figure 1.4	Figure 1.4 Exploded view of a 3-cell PEMFC stack.	10
Figure 1.5	The bridge model of oxygen reduction on Pt.	12

Figure 1.6	Current-potential curve for a platinum electrode in 0.5M H <sub>2</sub> SO <sub>4</sub> . Regions of oxide formation (Q <sub>A</sub> ) and reduction (Q <sub>C</sub> ) as well as formation of Hydrogen (H <sub>A</sub> ) and its reduction (H <sub>C</sub> ) are indicated.	14
Figure 1.7	Contributions to fuel cell performance by the anode and the cathode, displaying the kinetic, ohmic and mass transport regions.	28
<b>Chapter 2</b>		
Figure 2.1	Schematic diagram of a fuel cell with serpentine flow fields.	42
Figure 2.2	Schematic diagram of a direct methanol fuel cell testing system.	43
Figure 2.3	Schematic representation of the measurement of methanol crossover in a fuel cell	44
Figure 2.4	Half-cell configuration for testing gas diffusion electrodes.	45
<b>Chapter 3</b>		
Figure 3.1	CVs (20 mV/s) of 1 cm <sup>2</sup> gas diffusion electrodes containing 0.80 mg/cm <sup>2</sup> 20%Pt/C, 0.98 mg/cm <sup>2</sup> Nafion, and 0.15 mg/cm <sup>2</sup> Os(bpy) <sub>3</sub> Cl <sub>2</sub> ·6H <sub>2</sub> O, in 0.5 M H <sub>2</sub> SO <sub>4</sub> (aq). The dashed line is for a similar electrode without the Os complex.	55

Figure 3.2	Figure 3.2 CVs (20 mV/s) of 1 cm <sup>2</sup> gas diffusion electrodes containing 0.80 mg/cm <sup>2</sup> 20%Pt/C, 0.98 mg/cm <sup>2</sup> Nafion, and 0.15 mg/cm <sup>2</sup> Os(bpy) <sub>3</sub> Cl <sub>2</sub> ·6H <sub>2</sub> O, in a fuel cell . The dashed line is for a similar electrode without the Os complex.	56
Figure 3.3	The EDX spectrum of Ru(terpy)(dabpy)Cl <sup>+</sup> modified XC-72 carbon black.	60
Figure 3.4	FTIR Spectrum of Ru(terpy)(dabpy)Cl <sup>+</sup> .	61
Figure 3.5	FTIR Spectrum of Ru(terpy)(dabpy)Cl <sup>+</sup> modified carbon black.	62
Figure 3.6	CVs (5 mV/s) of Ru(terpy)(dabpy)Cl <sup>+</sup> modified XC-72 carbon black (2.4 mg/cm <sup>2</sup> ) in 0.5 M LiClO <sub>4</sub> (aq). The dashed line is for a similar electrode without the Ru complex.	64
Figure 3.7	CVs (5 mV/s) of Ru(terpy)(dabpy)Cl <sup>+</sup> modified XC-72 carbon black (2.4 mg/cm <sup>2</sup> ) in a fuel cell. The dashed line is for a similar electrode without the Ru complex.	65
Figure 3.8	CVs (5 mV/s) of electrodes containing various amounts of Ru(terpy)(dabpy)Cl <sup>+</sup> modified XC-72 carbon black in 0.5 M LiClO <sub>4</sub> (aq).	66
Figure 3.9	Variation of peak cathodic current with mass of Ru modified carbon.	67
Figure 3.10	CVs (5 mV/s) of Ru(terpy)(dabpy)Cl <sup>+</sup> modified XC-72 carbon black in 0.1 M H <sub>3</sub> PO <sub>4</sub> (aq). Current decreases with scan number.	69

## Chapter 4

Figure 4.1	The XRD powder spectrum of the untreated catalyst (Etek 20% Pt/Vulcan XC72).	77
Figure 4.2	The XRD powder spectrum of the treated catalyst.	78
Figure 4.3	The XRD powder spectrum of the pretreated catalyst.	79
Figure 4.4	FT-IR Spectrum of (untreated) Vulcan XC-72 carbon black.	81
Figure 4.5	FT-IR Spectra of sulfonated silane treated Vulcan XC72 carbon black.	82
Figure 4.6	EDX spectrum of the untreated catalyst (Etek 20% Pt/Vulcan XC72).	84
Figure 4.7	EDX spectrum of the treated catalyst.	85
Figure 4.8	EDX spectrum of the pretreated catalyst.	86
Figure 4.9	Fuel cell polarization curves at 35°C for the untreated catalysts at various Nafion loadings.	89
Figure 4.10	Fuel cell performances at 35°C of the treated catalyst with various Nafion loadings.	91
Figure 4.11	Fuel cell performances at 35°C of the pretreated catalyst with various Nafion loadings.	92
Figure 4.12	Fuel cell polarization curves at 35°C for all catalysts at 10% Nafion loading, and the untreated catalyst at 30% Nafion loading.	93
Figure 4.13	Variation of fuel cell performance at 35°C with Nafion loading.	95
Figure 4.14	Variation of fuel cell performance at 35°C with sulfonate loading.	96

Figure 4.15	Fuel cell polarization curves at 75°C for all catalysts at 10% Nafion loading, and the untreated catalyst at 30% Nafion loading.	98
Figure 4.16	Comparison of fuel cell polarization curves at 35°C obtained with various amounts of sulfonated silane or Nafion brush applied onto preformed electrodes (Pt = 1.7 mg/cm <sup>2</sup> ).	100
 <b>Chapter 5</b>		
Figure 5.1	Anode performances at 60°C achieved using various electrode backings (2 mg/cm <sup>2</sup> Pt/Ru black, 20% Nafion).	109
Figure 5.2	Anode performance at 60°C vs. Nafion content in the CFP backing.	111
Figure 5.3	Anode performance at 60°C of electrodes composed of various Pt/Ru loadings (20% Nafion, 6 mil CFP impregnated with 20% Nafion).	112
Figure 5.4	Anode performance at 60°C as a function of Nafion content in the catalyst layer.	113
Figure 5.5	Effect of cathode Nafion loading on DMFC Performance at 60°C (4.9x air stoichiometry).	117
Figure 5.6	The effect of cathode PTFE content on DMFC performance at 60°C (4.9x air stoichiometry).	118
Figure 5.7	Variation of anode performance at 60°C with Nafion membrane thickness.	121

Figure 5.8	Variation of anode performance at 60°C with Nafion membrane thickness.	122
Figure 5.9	DMFC performances at 60°C of various Nafion membranes, 1.7x air stoichiometry.	124
Figure 5.10	DMFC performances at 60°C of various Nafion membranes 4.9x air stoichiometry.	125
Figure 5.11	Methanol crossover as a function of Nafion membrane thickness.	128
Figure 5.12	Progress of DMFC MEA development, 60°C.	129
 <b>Chapter 6</b>		
Figure 6.1	DMFC and anode performances (60°C, 1 M MeOH) of composite membranes prepared using Fe <sup>3+</sup> oxidative polymerization.	137
Figure 6.2	The DMFC performance at 60 °C (1.7x air stoichiometry) of composite membranes prepared using Fe <sup>3+</sup> oxidative polymerization before and after being dipped in Nafion solution.	140
Figure 6.3	Comparison of the anode and cathode performances at 60°C (1.7x air stoichiometry) obtained with a Nafion dipped composite membrane and Nafion 115.	141
Figure 6.4	DMFC performance at 60 °C (1.7x air stoichiometry) of composite membranes prepared using H <sub>2</sub> O <sub>2</sub> oxidative polymerization.	143

Figure 6.5	Comparison of the anode and cathode performances at 60 °C (1.7x air stoichiometry) obtained with a BL2_91 (modified Nafion 115 membranes prepared using H <sub>2</sub> O <sub>2</sub> oxidant) and Nafion 115.	145
Figure 6.6	Comparison of the anode and cathode performances at 60 °C (1.7x air stoichiometry) obtained with a BL2_92 (modified Nafion 112 membranes prepared using H <sub>2</sub> O <sub>2</sub> oxidant) and Nafion 112.	146
Figure 6.7	Variation of the 60°C DMFC performance over time of a composite membrane prepared using H <sub>2</sub> O <sub>2</sub> as the oxidant.	147
Figure 6.8	DMFC performance at 60°C (1.7x air stoichiometry) of composite membranes with and without IR correction.	149
Figure 6.9	Electrostatic Interaction of Polypyrrole and Nafion side chains.	151
Figure 6.10	The effect of airflow rate on DMFC performance at 60 °C for Nafion 115 and a composite membrane prepared using H <sub>2</sub> O <sub>2</sub> oxidant.	154
 <b>Chapter 7</b>		
Figure 7.1	The Nyquist impedance responses of different circuit element combinations.	161
Figure 7.2	Finite transmission line equivalent circuit describing the impedance behavior of a PEMFC electrode.	162

Figure 7.3	Nyquist impedance plots for different ionic resistance profiles, simulated on the basis of the transmission-line equivalent circuit (Figure 7.2) for 1000 resistor-capacitor combinations (with $R_{\text{electronic}} = 0$ and $R_{\text{membrane}} = 0$ ) with a total capacitance of 1 F and a total resistance of $0.5\Omega$ .	164
Figure 7.4	Capacitance plots for different ionic resistance profiles, simulated on the basis of the transmission-line equivalent circuit (Figure 7.2) for 1000 resistor-capacitor combinations (with $R_{\text{electronic}} = 0$ and $R_{\text{membrane}} = 0$ ) with a total capacitance of 1 F and a total resistance of $0.5\Omega$ .	166
Figure 7.5	CVs (100 mV/s) obtained in 0.5 M $\text{H}_2\text{SO}_4$ (aq) with 1- 3 $\mu\text{L}$ of catalyst ink applied.	168
Figure 7.6	CVs (100 mV/s) obtained in 0.5 M $\text{H}_2\text{SO}_4$ (aq) with 4- 6 $\mu\text{L}$ of catalyst ink applied.	169
Figure 7.7	Hydrogen adsorption charge as a function of the volume of catalyst ink applied.	171
Figure 7.8	Nyquist plots obtained for electrodes with various amounts of catalysts ink applied over a frequency range of 100 kHz to 1 Hz.	172
Figure 7.9	Enlarged view of Nyquist plots obtained for electrodes with various amounts of catalyst ink applied over a frequency range of 100 kHz to 1 Hz.	173

Figure 7.10	Capacitance plots obtained for electrodes with 1-3 $\mu\text{L}$ of catalyst ink applied.	175
Figure 7.11	Capacitance plots obtained for electrodes with 4-6 $\mu\text{L}$ of catalyst ink applied.	176
Figure 7.12	Volume normalized capacitance plots obtained for electrodes with different volumes of catalyst ink applied over a frequency range of 100 kHz to 1 Hz.	177
Figure 7.13	Limiting capacitance as a function of the volume of catalyst ink applied.	178
Figure 7.14	Comparison of capacitance plots obtained with a 0.071 $\text{cm}^2$ glassy carbon electrode prepared with 2 $\mu\text{L}$ of catalyst ink applied, to that obtained with a 1 $\text{cm}^2$ gas diffusion electrode equivalent to ca. 2.2 $\mu\text{L}$ of catalyst ink.	180
Figure 7.15	Limiting capacitance as a function of DC Potential. Data obtained using 1 $\mu\text{L}$ of catalyst ink.	181
Figure 7.16	Limiting capacitance as a function of DC Potential. Expanded view of the area outside the hydrogen adsorption/desorption region. Data obtained using 1 $\mu\text{L}$ of catalyst ink.	182
Figure 7.17	Comparison of Nyquist plots obtained on the Os redox wave both in a fuel cell and in a half-cell.	184

Figure 7.18	Comparison of capacitance plots obtained on the Os redox wave both in a fuel cell and in a half-cell.	185
Figure 7.19	Comparison of simulated and experimental Nyquist plots obtained on and off the Os redox wave.	187
Figure 7.20	Comparison of simulated and experimental capacitance plots obtained on and off the Os redox wave.	188
Figure 7.21	Conductivity profiles simulated from EIS obtained on and off the Os redox wave.	189

### **List of Schemes**

Scheme 3.1	Synthetic route to tethering Ru(terpy)(dabpy)Cl <sup>+</sup> to the carbon surface.	52
Scheme 4.1	Treatment of the catalyst surface with a sulfonated silane.	74

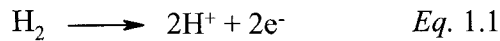
# **Chapter 1**

## **General Review of Fuel Cells**

## 1.1. Introduction to Fuel Cells

In today's society there is an enormous demand for energy. Environmental concerns necessitate that new energy sources must be highly efficient and have zero (or very low) emissions. The fuel cell is an emerging technology that can meet these demands.

A fuel cell is defined as an electrochemical device that can continuously convert chemical energy into electrical energy.<sup>1</sup> Much like a battery, a fuel cell produces electrical energy. However, unlike a battery, the reactants are continuously supplied and products are continuously removed. Hence, a fuel cell does not store energy. Typically, hydrogen is the fuel consumed at the anode; oxygen (usually from air) is consumed at the cathode. In an acid electrolyte, the cell reaction occurs as follows:



The main advantage a fuel cell has over heat engines is that they are theoretically more efficient<sup>2</sup> and produce no noxious emissions. Also, fuel cells operate very quietly, reducing noise pollution.<sup>3</sup> Because of these advantages, fuel cells are being developed for numerous commercial and military applications, such as automobiles, portable electronic devices, and mobile and stationary power generation.

Sir William Grove first demonstrated a hydrogen-air fuel cell in 1839.<sup>4</sup> Almost a century later, in 1932, Francis Bacon produced a successful device in the first major fuel

cell project. Subsequently, fuel cells were used in the Gemini and Apollo Space programs in the 1960s.<sup>5</sup>

There are, however, several hurdles that must be overcome before fuel cells can become a commercially viable technology on a large scale. Cost is one such factor. The required catalyst, membrane and cell hardware (e.g. bipolar plates) are expensive, resulting in a very high initial cost. Also, hydrogen storage requires a large (weight and volume) storage system. This reduces the operational range of portable fuel cell devices. There is much research for better ways to store hydrogen. In particular, storing hydrogen in carbon nanotubes<sup>6,7,8</sup> and metal hydrides<sup>9,10,11</sup> has received a great deal of attention recently.

There are also issues when it comes to delivering hydrogen. Currently there is no infrastructure to distribute hydrogen on a large scale. Adapting the current fossil fuel distribution infrastructure would be very costly.<sup>12</sup>

There are various types of hydrogen/air fuel cells. They differ mainly by their electrolyte. Proton exchange membrane fuel cells (PEMFC) are the focus of this thesis and will therefore be reviewed in detail. All others will only be briefly discussed.

## **1.2 Proton Exchange Membrane Fuel Cells (PEMFC)**

The following sections discuss the main components of a proton exchange membrane fuel cell (PEMFC), namely the membrane and the electrodes.

### 1.2.1 The Proton Exchange Membrane (PEM)

As the name implies, a PEMFC employs a proton exchange membrane (PEM). The PEM serves as a physical barrier between the anode and cathode gases and also as the electrolyte (hence it is also known as a solid polymer electrolyte). Today, the most common PEM is Nafion<sup>\*</sup>, a perfluorosulfonic acid membrane developed by E.I. DuPont de Nemours & Co. The structure of Nafion is shown in Figure 1.1. The values of x and y can be varied to create materials with different equivalent weights (EW). 1100 EW is the most common, though EWs of 900-1400 are available. Since Nafion is similar in structure to polytetrafluoroethylene (PTFE or Teflon), it has excellent mechanical strength, water insolubility, and chemical and thermal stability. The sulfonated side chains endow Nafion with high proton conductivity and cation exchange capacity. Nafion has found numerous applications, such as liquid and gas separations, fuel cells, and the chloro-alkali industry.

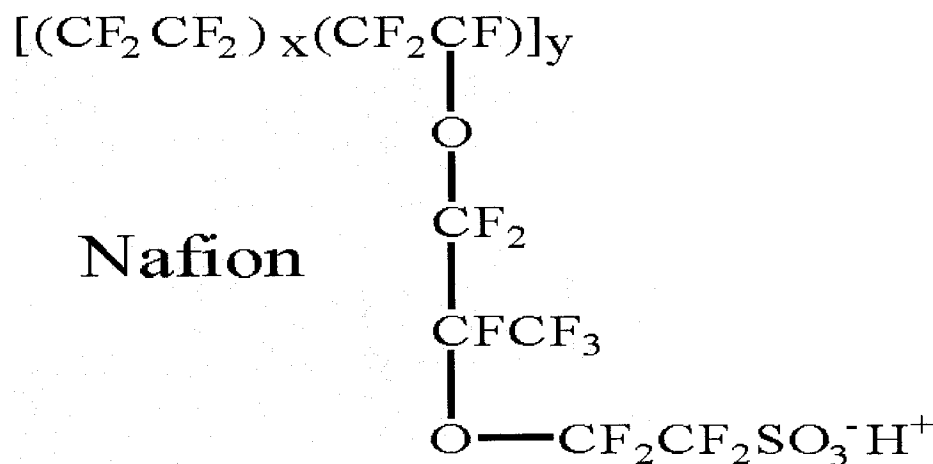


**Figure 1.1:** The structure of Nafion.

<sup>\*</sup> Nafion is a registered trademark of E.I. DuPont de Nemours & Co.

Structurally, Nafion is a fascinating polymeric material. The exact structure of Nafion is not known but there have been several models proposed to describe the way in which ionic groups aggregate within Nafion membranes. These models include the Mauritz-Hopfinger Model,<sup>13</sup> the Yeager Three-Phase Model,<sup>14</sup> the Eisenberg-Hird-More Model of Hydrocarbon Ionomers,<sup>15</sup> and the Gierke Cluster Network Model.<sup>16</sup> Each of these models attempts to predict the fundamental features of equilibrium ionic selectivities and ionic transport. Electrostatic interactions cause the ionic groups to aggregate and form tightly packed regions referred to as clusters.<sup>17</sup> These electrostatic interactions (between the ions and the ion-pairs) enhance the intermolecular forces and considerably influence the properties of the parent polymer. Small angle X-ray scattering (SAXS)<sup>18</sup> and neutron scattering experiments clearly indicate that ionic clustering is present in Nafion. However, details on the arrangement of matter within these clusters are not fully understood. Although no one model has been found to provide a complete explanation of the properties and selectivities found, several models base these properties and selectivities on an extensive micro-phase separated morphology.<sup>19,20</sup>

Yeager's model describes Nafion as consisting of three regions: a fluorocarbon region (A), an interfacial zone (B) and an ionic cluster region (C). These regions are depicted in Figure 1.2. Region A consists of the fluorocarbon backbone and is quite hydrophobic. Region C consists of clusters of pendant sulfonate groups. This region is quite hydrophilic, most absorbed water and counterions exist in this region. Gierke has proposed that these ionic clusters are spherical and exist as a network interconnected by smaller channels.<sup>21</sup> Region B is an interfacial region containing the pendant side chain

material and sulfonate groups that are not clustered. Hence, only part of the absorbed water and counterions exist in this region (typically larger, more hydrophobic cations such as  $\text{Ru}(2,2' - \text{bipyridine})_3^{2+}$ ).

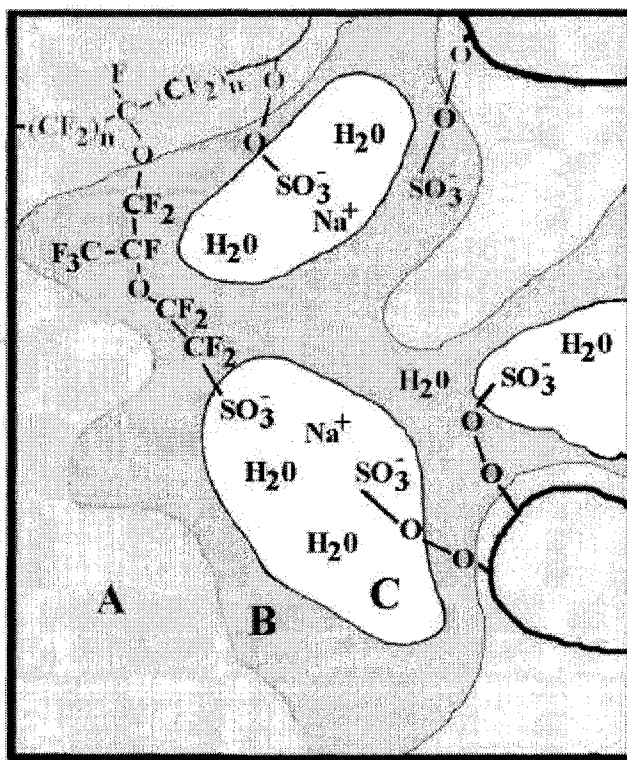


**Figure 1.2:** Yeager's three-phase model of Nafion; a fluorocarbon region (A), an interfacial zone (B) and an ionic cluster region (C).

Reprinted from Yeager, H. L.; Steck, A. J. *Electrochem. Soc.* **1981**, 128, 1880., Copyright 1981. Reproduced with permission of the Electrochemical Society.

The proton conductivity of Nafion is dependant on its hydration state. In the dry state, Nafion is a poor ion conductor, but ionic conductivity increases sharply with water content.<sup>22</sup> Because of this, reactant gases are often humidified before they enter a PEMFC. This can however induce water management issues at the cathode. This also

limits the operational temperature of Nafion based PEMFCs to under ca. 100°C since sufficient liquid water must be present for good conductivity. However, if too much water is present, electrode pores and flow fields are filled by water, leading to mass transport issues (i.e. by preventing reactant gas from reaching active catalyst sites). This is often referred to as “flooding”. Therefore, water management is often a delicate balance that is critical to good performance.

Companies such as Dow, Aciplex, Gore, and Ballard have developed other membranes. The scientific community has studied these membranes in less detail since they are proprietary to the companies that developed them. Generally, they have similar sulfonated perfluorocarbon structures.

### **1.2.2 PEMFC Electrodes**

PEMFC electrodes are complex three-dimensional structures consisting of a number of different materials in a heterogeneous mix. Much skill and art have been developed to produce structures with improved performances. Usually a 10-50 μm thick layer, consisting of carbon-supported Pt catalyst (or Pt black) bonded with recast Nafion and/or PTFE is applied onto a gas diffusion backing. The backing is typically carbon fiber paper (CFP) or carbon cloth (carbon fibers woven into a cloth-like material) that serves as a current collector and gas conduit. The backing is often treated to aid water management within the cell. The recast Nafion in the catalyst layer originates from a Nafion solution that can be mixed with the catalyst before electrode preparation or added once the catalyst layer has been formed. Its primary purpose is to provide a medium for

proton conduction within the catalyst layer, because only those Pt sites that are in ionic contact with the membrane can be active for oxidation or reduction of the fuel (typically hydrogen) or oxidant (typically oxygen). The purpose of PTFE is to bind together the electrode particles and to aid in water management.

The catalyst, Nafion and PTFE are typically mixed together with water and alcohol(s) to form an ink. This ink is then either spray-applied, brush-applied or even screen printed<sup>23</sup> onto the backing. Recently, several proprietary methods have been reported where the catalyst mixture is applied directly onto the membrane.<sup>24,25,26</sup>

Typically, electrodes are hot-bonded to each side of the membrane to form the membrane and electrode assembly (MEA). An MEA is shown in Figure 1.3. The thin size (ca. 75-300  $\mu\text{m}$ ) and low mass of the MEA is the main advantage of a PEMFC. This allows for the formation of compact lightweight “stacks”. A fuel cell stack consists of several MEAs (2 or more) electrically connected in series by bipolar plates. The bipolar plate serves as an electrical connection between the MEAs and also physically separates the reactant gases. A schematic diagram of a 3-cell PEMFC stack is shown in Figure 1.4. Bipolar plates have flow fields machined onto each side to distribute the reactant gases throughout the entire area of the electrode. The most common flow field shapes are serpentine and interdigitated. There is much engineering research devoted to optimizing fuel cell flow field design,<sup>27,28,29,30,31,32</sup> but this will not be discussed here.

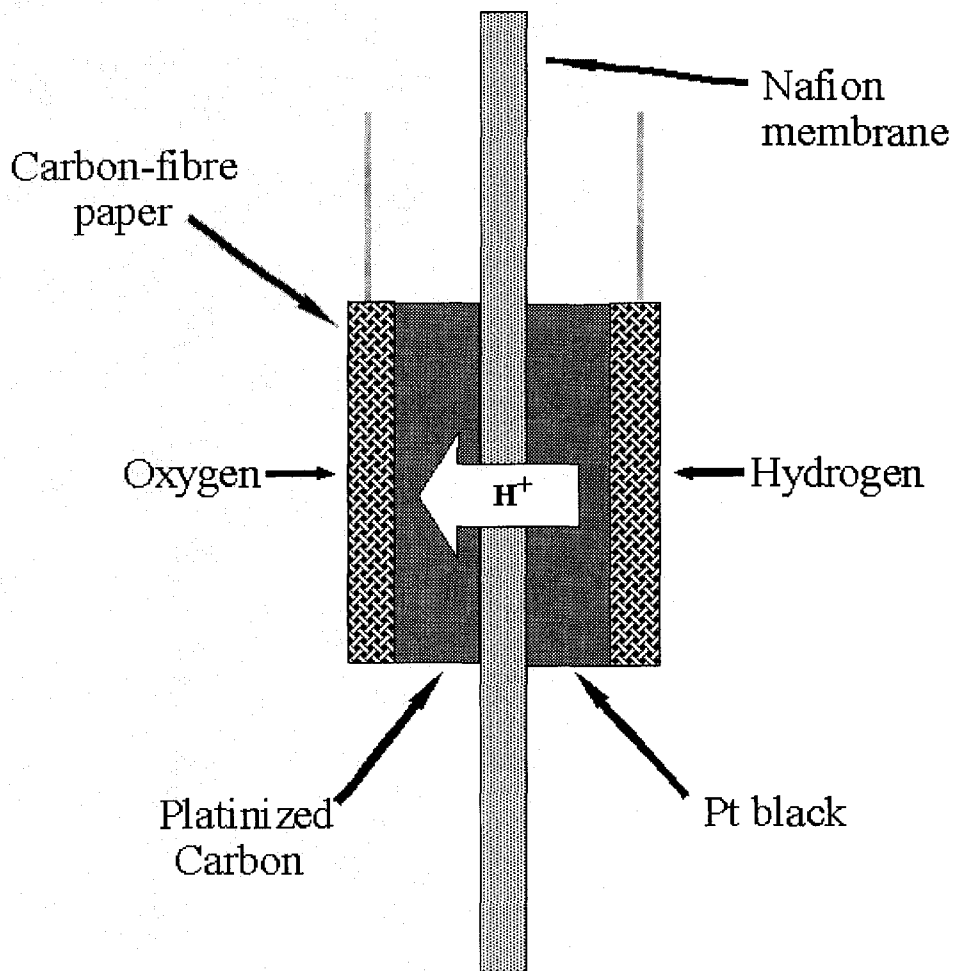


**Figure 1.3:** The membrane and electrode assembly (MEA).

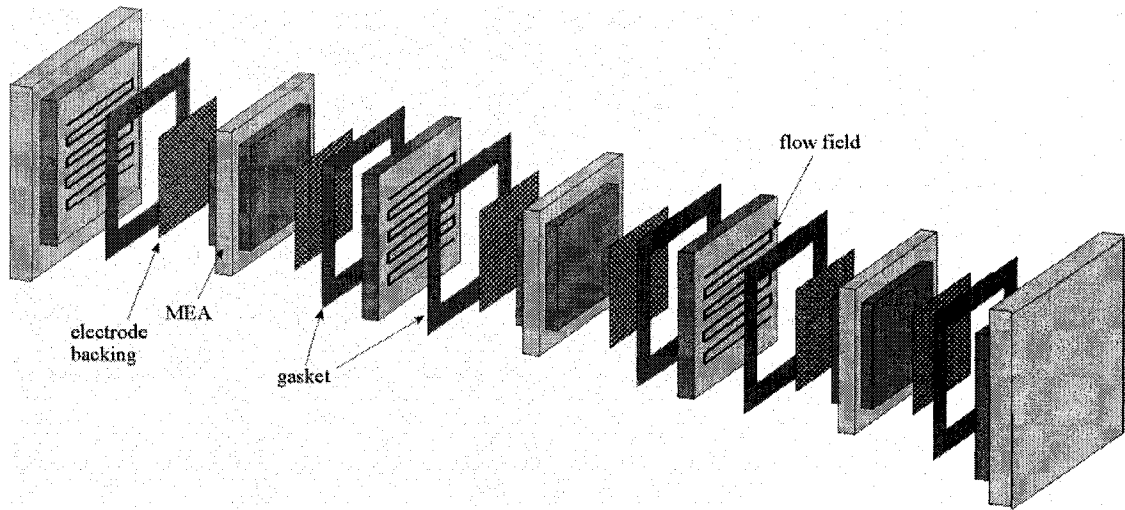


**Figure 1.4:** Exploded view of a 3-cell PEMFC stack.

### 1.2.2.1 PEMFC Anodes

PEMFC anodes typically consist of a Pt catalyst, either Pt black or Pt on a carbon support. These anodes perform very well when pure hydrogen is used, but storage and infrastructure issues make hydrogen an inconvenient fuel to supply. To circumvent these issues, hydrogen can be generated *in situ* by reforming other fuels (methanol, propane, natural gas, etc.).<sup>33</sup> For example, methane can be steam reformed to produce hydrogen:



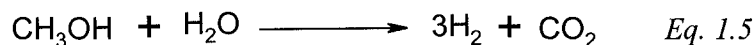
However, reformat gas also has a major drawback: carbon monoxide. CO poisons a Pt catalyst by adsorbing strongly onto its surface, blocking active sites for hydrogen electro-oxidation, resulting in losses of electrical current. There is an unacceptable performance loss when as little as 10 ppm of CO is present in the fuel

mixture. To reduce CO levels in the reformat, the “water-gas shift reaction” can be employed:



Even after using a “state of the art” water-gas shift reactor, CO levels are still greater than 2500 ppm.<sup>34</sup> Further gas processing (e.g. selective oxidation, methanation) is required to reduce CO levels, but these reactors are bulky and expensive.<sup>35</sup>

Methanol can also be steam reformed:



Although steam reforming of methanol does not produce CO directly, CO is still present in small quantities because the water-gas shift reaction is reversible (see Eq. 1.4).<sup>36</sup>

In order to use reformat gas in a PEMFC, even after being processed, CO must be tolerated in concentrations up to 100 ppm. One method that has been proven effective is the use an “air bleed”. When air is mixed with the reformat feed (ca. 2% O<sub>2</sub>), it will react with CO adsorbed on Pt (producing CO<sub>2</sub>), freeing active sites for H<sub>2</sub> oxidation.<sup>37,38</sup> However, any O<sub>2</sub> that does not react with CO will react with H<sub>2</sub>, thereby wasting fuel.

Obviously, a CO tolerant catalyst is desired. Pt is easily poisoned but bi-metallic Pt/X co-catalysts (X = Ru, Mo, Sn) have been shown to be more tolerant to CO. The second (promoter) metal is deposited with Pt and will either reduce poisoning or decrease the potential at which CO is removed. Ru has been shown to be the most effective.<sup>39</sup>

However, adding Ru further increases the cost of the anode. Operating at higher temperatures can also decrease the effect of CO poisoning.

### 1.2.2.2 PEMFC Cathodes

The oxygen reduction reaction (ORR) is a multi-electron process consisting of numerous elementary steps, involving both series and parallel pathways. It is generally accepted that oxygen reduction on Pt (in acid) occurs via dissociative adsorption of  $O_2$  followed by protonation of the adsorbed species, with the former being the rate-determining step. There have been several models that attempt to describe these pathways.<sup>40,41,42,43,44</sup> Several models successfully interpret the same data due to their similarity (often the only differences are the inclusion/exclusion of adsorbed species that cannot be proven to exist). One such model is the bridge model<sup>45</sup> of the ORR on Pt in acid, illustrated in Figure 1.5.

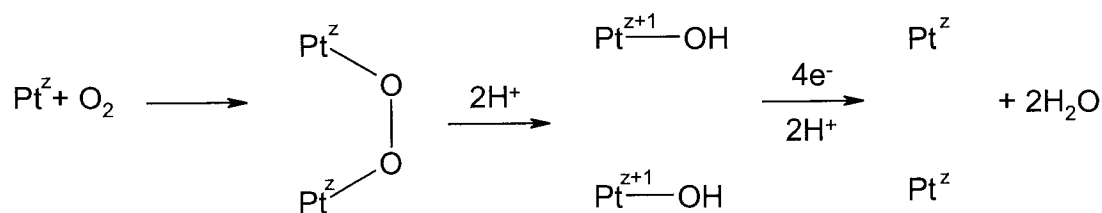


**Figure 1.5:** The bridge model of oxygen reduction on Pt, where z represents the oxidation state.

Because of the bridging oxygen system, it is obvious that optimal Pt particle spacing (and size) is of critical importance.<sup>46</sup>

The complicated pathway(s) of the ORR results in slow electrochemical kinetics. One measure of the rate of an electrochemical reaction is its exchange current density,  $j_0$ .  $j_0$  for the ORR on Pt is  $10^5$  less than  $j_0$  for hydrogen oxidation at Pt.<sup>47</sup> It is because of this huge difference that the activity at the cathode most influences hydrogen/air cell fuel cell performance. Therefore, enhancing the cathode activity has been a major focus for PEMFC electrode development.

In order to increase cathode activity, one must increase catalyst utilization. This will not only increase performance but can also lead to a lowering of the required Pt loading. In order for a catalyst site to be electrochemically active, a pathway for electron, proton and gas transport must all be present.<sup>48</sup> The active area of Pt is typically measured using cyclic voltammetry (CV) in acid electrolyte. Specifically, the area under the hydrogen adsorption/desorption peaks is determined,<sup>49</sup> as shown in Figure 1.6.<sup>50</sup> A larger area (per mass of Pt) indicates a larger active area.

One very successful method to increase catalyst utilization is to employ a carbon supported Pt catalyst. Typically, Pt particles (3-10 nm) are dispersed onto the electronically conducting carbon particles, ca. 30-50 nm.<sup>51</sup> The ideal carbon support should possess high chemical/electrochemical stability, good electronic conductivity, and a suitably high surface area and pore size distribution.<sup>52</sup> The type of carbon that appears to be best suited to be a fuel cell catalyst support is carbon black. There are several types of commercial carbon blacks that have been studied for use with fuel cells, Vulcan XC72 (Cabot Corp.) is the most common.

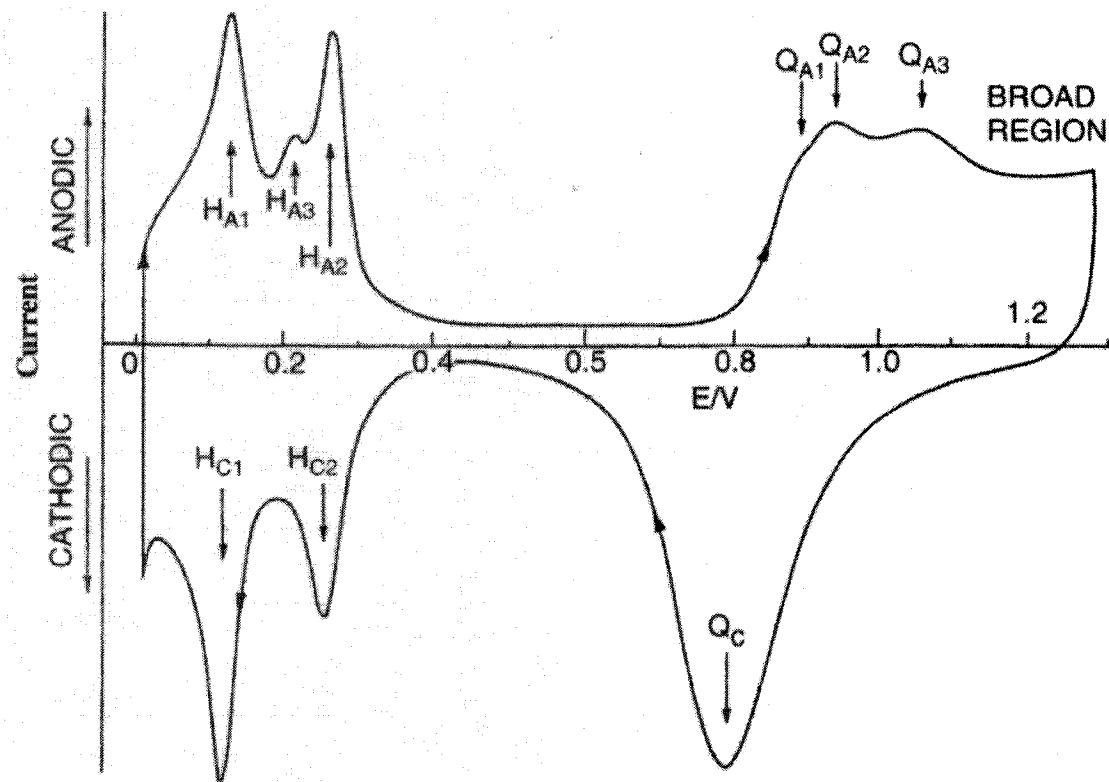


**Figure 1.6:** Current-potential curve for a platinum electrode in 0.5M  $\text{H}_2\text{SO}_4(\text{aq})$ . Regions of oxide formation ( $Q_A$ ) and reduction ( $Q_C$ ) as well as formation of Hydrogen ( $H_A$ ) and its reduction ( $H_C$ ) are indicated.

Reprinted from Kozławska, H; Conway, B.; Sharp, W. *J. Electroanal. Chem.* **1973**, 43, 9., Copyright 1993, with permission from Elsevier Science.

Although carbon is an excellent electronic conductor, it is a very poor proton conductor. This is mainly because carbon is hydrophobic. However, the carbon surface does consist of some hydrophilic moieties. Carbon-oxygen complexes, such as phenol, carbonyl, carboxyl, quinone and lactone groups can all be found on the carbon surface. Typically, exposing the carbon to an oxidizing agent forms these complexes.

In order to study the effect that carbon surface functional groups have on fuel cell performance, Pickup *et al.* explored the effect of increasing the hydrophilicity of the

carbon support. Supported catalysts treated with nitric acid were shown to outperform untreated catalysts.<sup>53</sup> This was attributed to increased proton conductivity of the catalyst layer, most likely due to the formation of surface carboxylic acid groups.

One serious issue with Pt/carbon fuel cell catalysts is the “sintering” of the Pt particles. Sintering occurs when Pt particles become larger over their lifetime.<sup>54</sup> This decreases the Pt surface area, and ultimately leads to a decline in performance throughout the lifetime of operation.

Ideally, a catalyst support material that is both electronically and ionically conductive is desired. Pickup *et al.*, have studied such a material, a conducting polymer composite.<sup>55</sup> The composite consists of one polymer that is electronically conductive (*e.g.* polyprrole, poly(3,4-ethylenedioxythiophene)), and one that is a proton conductor (*e.g.* polystyrenesulfonate). This material was tested as a replacement for carbon and reasonable performance was achieved. However, low Pt utilization and polymer stability are still issues.<sup>56</sup>

Another method to increase catalyst utilization is to add a proton-conducting polymer (such as Nafion) into the catalyst layer. Pt catalyst near or directly in contact with the Nafion membrane is utilized most efficiently. However, utilization drops off deeper into the catalyst layer, largely due to the limited proton conductivity of the catalyst layer. Nafion solution can be applied onto preformed electrodes or directly mixed with the catalyst during ink preparation.<sup>57,58,59,60</sup> This increases the proton conductivity of the catalyst layer. In 1986, Raistrick was able to demonstrate that carbon-supported Pt catalyst mixed with Nafion could outperform conventional Pt black electrodes that had

ten times the Pt loading.<sup>61</sup> This was a major breakthrough in fuel cell development in that it made the cost of Pt required much more feasible.

When designing an electrode using carbon-supported catalyst and Nafion, they must be mixed in proper proportions to form a stable “three-phase” boundary where the gas, ion conductor and catalytically active electronically conducting phase are all present. This requirement limits the amount of Nafion that can be added since the morphology, low gas permeability, and poor electronic conductivity of Nafion disrupts this boundary and adversely affects cell performance.<sup>62,63</sup> Because of this, and the high cost of Nafion, alternative methods for providing proton conductivity in the catalyst layer are of interest.

Another approach to increase Pt utilization is to simply deposit Pt only in the areas of the electrode where it would be electroactive. This can be done by sputter deposition (SD) where layers as thin as 2 nm can be deposited. There have been many studies that use SD to localize Pt catalyst at the front surface of the electrode or even directly onto the membrane surface. Srinivsan *et al.* applied a 50 nm thick layer of Pt onto an uncatalyzed gas diffusion layer (GDL) by SD and achieved a 10-fold reduction in Pt loading (from 4 mg/cm<sup>2</sup> to 0.4 mg/cm<sup>2</sup>) without a loss in performance.<sup>64</sup> Hirano *et al.* later showed that electrodes prepared by sputter deposition with a Pt loading of 0.1 mg/cm<sup>2</sup> could perform the same as those prepared using standard materials (Pt/C) at a 0.4 mg/cm<sup>2</sup> Pt loading.<sup>65</sup> Cha and Lee have further reduced the Pt loading to 0.04 mg/cm<sup>2</sup> by alternating sputter deposited Pt layers and painted Nafion/Carbon ink layers, with successively lower amounts of Pt in each layer.<sup>66</sup> This leads to very efficient utilization of Pt.

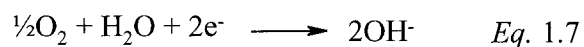
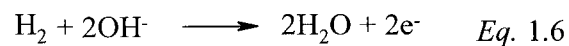
SD is promising for fuel cells since a larger percentage of Pt is electrochemically active (or utilized). Also, it allows for the fabrication of very thin active layers, which decrease ohmic and mass transport overpotentials in the catalysts layer. Also, SD is a well established industrial technique in areas such as thin films and integrated circuits<sup>67</sup> and it is anticipated that this technique could be readily applied to micro-fuel cell applications.

### 1.3 Other Types of Hydrogen-Air Fuel Cell

Most other types of hydrogen/air fuel cell are classed by the electrolyte used. The following section will briefly describe them.

#### 1.3.1 Alkaline Fuel Cells

Alkaline fuel cells (AFC) have found use in the Apollo space missions as well as the space shuttle program. AFCs operate at temperatures between 60-90 °C and employ KOH as the electrolyte, typically in a stabilized matrix. Electrodes (both anode and cathode) are generally fabricated from Pt catalysts supported on carbon. The half cell reactions in an AFC are slightly different than those in a PEM because of the electrolytes and are as follows:



The main advantage of an AFC is that the kinetics of the ORR are significantly faster in base. This results in a higher efficiency. However, AFC do have significant drawbacks. For example, very pure gases are required. Even small amounts of CO<sub>2</sub> can lead to “carbonation” of the electrolyte. Circulation of the electrolyte has been found to reduce this effect.<sup>68</sup> Also, hydrogen oxidation kinetics are slower in base (than in acid).

### 1.3.2 Phosphoric Acid Fuel Cells

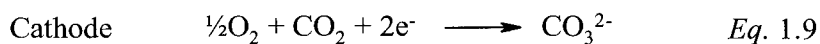
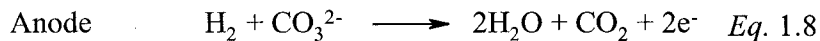
Phosphoric acid fuel cells (PAFC) are the most advanced type of fuel cell with respect to commercial development. As the name implies, phosphoric acid is the electrolyte, it is usually stabilized in a SiC-based matrix. Recently, polybenzimidazole (PBI) membranes that are doped with phosphoric acid have been developed.<sup>69</sup> Since the electrolyte is an acid, the half-cell reactions are the same as those for a PEMFC (see Eq. 1.1 and 1.2).

Electrodes are usually fabricated from Pt/C. Water management can be a problem since a liquid electrolyte is used. The use of a hydrophobic backing layer and the proper amount of PTFE within the catalyst layer is critical for good performance. Also, leakage of the liquid electrolyte over time can be a problem.

PAFCs typically operate at temperatures near 200°C. Because of this, they have a better CO tolerance (up to 2% CO) than PEMFCs, thus allowing the use of reformat.<sup>70</sup> Likewise, the higher temperature of the PAFC results in better cathode performance.

### 1.3.3 Molten Carbonate Fuel Cells

Molten carbonate fuel cells (MCFC) employ a eutectic melt of either potassium or sodium carbonate and lithium carbonate, usually stabilized by either an alumina or ceria based matrix. The use of a molten carbonate as the electrolyte solves the problem of electrolyte carbonation quite elegantly. Since carbonate is the electrolyte, the half-cell reactions are slightly different than those of a PEMFC. The reactions are as follows:



MCFCs operate at ca. 650°C; hence there are significantly less polarization losses at the cathode. Also, the increased ORR kinetics allow for the use of a less expensive NiO catalyst (as opposed to Pt) at the cathode. Ni/Al and Ni/Cr alloys are common anode catalysts. The higher temperature also allows for the internal reforming of methane.

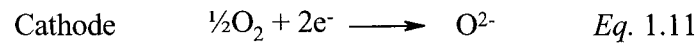
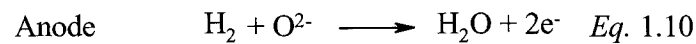
The largest problem associated with developing MCFC (or any high temperature fuel cell) is the selection of materials from which to construct the cells. Degradation, sealing and thermal expansion are major problems for many materials constantly in a high temperature environment. Cell materials will not be discussed here. An overview of MCFC cell materials has been published.<sup>71</sup>

### 1.3.4 Solid Oxide Fuel Cells

Solid oxide fuel cells (SOFC) operate at temperatures above 900°C. Also, the higher temperature increases the ORR kinetics at the cathode, leading to increased performance as well as the ability to use less expensive catalysts.

SOFC's employ a thin ceramic electrolyte of yttria-stabilized zirconia (YSZ) electrolyte, which conducts oxygen ions. The advantage of the solid electrolyte is that, unlike liquid electrolytes, it cannot leak. Also, carbonation from CO/CO<sub>2</sub> content in the fuel stream does not occur.

The half-cell reactions are slightly different than those of a PEMFC because of the electrolyte. The reactions are as follows:



SOFC cathodes often consist of LaSrMnO<sub>3</sub>/YSZ composite electrodes that perform quite well.<sup>72,73</sup> Anodes are typically made from Ni cermet (ceramic-metallic) materials. Internal reforming of fuels is possible, as is the direct oxidation of different fuels.<sup>74,75,76</sup>

Similar to MCFC, cell materials that can withstand high temperatures is a major issue for SOFCs.

## 1.4 Direct Methanol Fuel Cells (DMFC)

### 1.4.1 Introduction to Direct Methanol Fuel Cells

In a direct methanol fuel cell (DMFC), methanol is oxidized at the anode and oxygen (usually in air) is reduced at the cathode. The electrochemical oxidation of methanol (in acid electrolyte) occurs as follows:



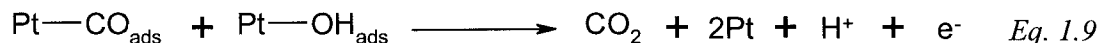
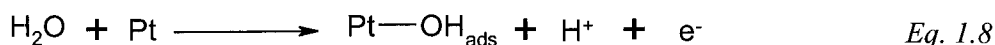
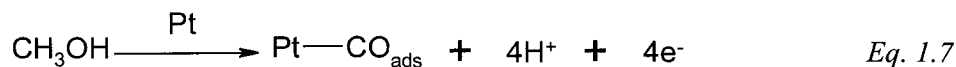
There are many advantages to employing methanol as the fuel (as opposed to hydrogen). Methanol is a liquid, hence its storage and transportation is less complicated. Also, methanol could be supplied through the existing gasoline infrastructure. Although hydrogen can be generated *in situ* from methanol using a reforming process (see section 1.2.2.1), the reformer unit further complicates the fuel cell system. Also, reformed hydrogen contains significant levels of CO that poison the Pt catalyst.

DMFCs were first studied over 40 years ago. At that time, an alkaline electrolyte was used. However, carbonation of the electrolyte (caused by the evolved CO<sub>2</sub>) decreased efficiency by reducing the electrolyte conductivity and de-polarizing the cathode.<sup>77</sup> In the late 1970s/early 1980s, several researchers explored the use of H<sub>2</sub>SO<sub>4</sub> as an electrolyte.<sup>78</sup> Currently, researchers mainly focus on the use of a polymer electrolyte membrane (PEM), largely due its proliferation in hydrogen/air cells. A PEM has the same advantages in a DMFC as it does in an H<sub>2</sub>/air PEMFC (*e.g.* lightweight, good proton conductivity, etc., see Section 1.2.1).

The next sections describe the development of the individual components of a DMFC MEA.

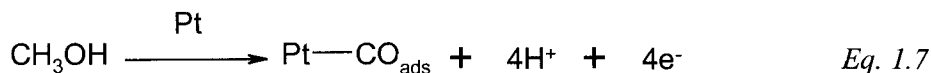
### 1.4.2 Direct Methanol Fuel Cell Anodes

MeOH oxidation is a complicated process; it has many steps and many intermediates. The best catalyst to facilitate this oxidation process is Pt, however, CO intermediates strongly adsorb and therefore poison the Pt catalyst. These CO intermediates are only removed when there are oxygenated species present on the Pt surface. There is still much debate as to the exact nature of the CO intermediates formed. Still, the mechanism can be generally represented as follows:



When water is present, oxygenated species only form on the Pt surface (via Eq. 1.8) when the potential is greater than 0.5 - 0.6 V.<sup>79,80</sup> This large overpotential results in severe performance losses. Higher temperatures increase the rate of methanol oxidation and removal of CO intermediates; hence temperatures of 60-100 °C are employed. To decrease the poisoning effect, a bi-metallic catalyst can be used (see Section 1.2.2.1). Historically, only a few metals have been shown to give positive results.<sup>81</sup> Ru has been shown to be the most effective, although Sn and Mo show promise.

Currently, Pt-Ru is the most effective bimetallic catalyst used for MeOH oxidation. The simplified mechanism for methanol oxidation using Pt-Ru is as follows:



The main advantage of Pt-Ru is that it lowers the MeOH oxidation potential (compared to just using Pt).<sup>82,83,84</sup> This is because oxygenated species form on Ru (via Eq. 1.8') at lower potentials and Ru also decreases the amount of CO intermediates formed on Pt.<sup>85</sup> Additionally, Ru is a fairly noble metal and therefore much more stable than other promoters under the conditions of DMFC operation.

There is still much debate regarding the ideal Pt-Ru catalyst composition. Much of this debate arises from the methods by which the catalysts are made. Pt-Ru catalysts can be prepared by numerous methods, such as chemical deposition,<sup>86</sup> electrodeposition,<sup>87</sup> sputter deposition,<sup>88</sup> ball milling,<sup>89</sup> arc melting,<sup>90</sup> and organometallic routes.<sup>91</sup> Each method results in a catalyst with inherently different properties. These properties, such as morphology, particle size, structure, composition, uniformity, dispersion state and alloying state, all influence catalytic activity.<sup>92,93</sup> Also, catalyst “activation” techniques can greatly influence performance.<sup>94,95</sup>

The oxidation state of Ru is one such issue (that arises from the preparation method) that is disputed. Rolison *et al.*<sup>96</sup> have claimed that Pt<sup>0</sup>Ru<sup>0</sup> (pure metallic alloy) catalysts are much less active for methanol oxidation than mixed phase PtRuO<sub>x</sub>H<sub>y</sub>

catalysts. They based their conclusions on the fact that the presence of hydrous oxides would be expected to increase the rate of methanol oxidation by promoting the formation of Ru-OH<sub>ads</sub> species.<sup>97</sup> Also, RuO<sub>x</sub>H<sub>y</sub> are proton conductors. In fact, DMFC anodes containing RuO<sub>x</sub>H<sub>y</sub> have been shown to require less Nafion ionomer in the catalyst layer because of the proton conductivity of RuO<sub>x</sub>H<sub>y</sub>.<sup>98</sup>

However, the role of RuO<sub>x</sub>H<sub>y</sub> as a methanol oxidation catalyst is debated. X-ray absorption experiments by Grady *et al.*<sup>99</sup> indicated that at the potentials at which methanol oxidation occurs, the metal oxides were reduced to their metallic form. Furthermore, using *in situ* X-ray absorption fine structure (XAFS) experiments on well-mixed Pt-Ru/carbon catalysts, Russell *et al.*<sup>100</sup> have concluded that both metal oxides were reduced to their metallic form existing as a bi-metallic alloy.

This structural debate also feeds into the debate over the optimal atomic ratios of Pt to Ru. For example, Gasteiger *et al.*<sup>101</sup> reported that 30% Ru is optimal for Pt-Ru alloys prepared by arc melting. However, catalyst manufacturer Johnson Matthey claims that their 50% Pt-50% Ru is the most active. This was explained by Garau *et al.*,<sup>102</sup> who studied the lattice parameters of both arc melted Pt-Ru alloys and high surface area mixed phase Pt-Ru catalysts prepared by borohydride reduction. They found that for the mixed phase catalysts, smaller Ru atoms phased out of the alloy, leaving a more Pt-rich alloy whose surface composition was very similar to arc-melted Pt/Ru alloys with higher Pt contents.

### **1.4.3 Direct Methanol Fuel Cell Cathodes**

Cathode activity is a very important, but often ignored, part of a DMFC. The use of an aqueous methanol feed at the anode, and its subsequent crossover into the cathode compartment, can cause a drastic reduction in cathode activity. Methanol (or other organics) will be oxidized at the cathode. This creates a “mixed” electrode potential that will be lower than the standard potential for oxygen reduction. For example, if methanol is present in a concentration of 0.01 M at the cathode, it will cause a 300 mV reduction in electrode potential.<sup>103</sup> Poisoning of the Pt cathode catalyst by CO intermediates can also occur, reducing the cathode activity over time.

Additionally, the crossover of water from the anode feed to the cathode can cause flooding. This is often overcome by increasing the airflow rate. However, from a system design standpoint, higher airflows are not desirable as they would require a more powerful pump/compressor and decrease the system’s overall efficiency.

In order to circumvent some of these issues, one can optimize the electrode composition. High Pt loadings are employed to reduce the mixed potential loss. Generally, a large degree of hydrophobicity is incorporated into the cathode catalyst layer and backing to aid water removal. Research to develop methanol tolerant catalysts is ongoing.<sup>104</sup>

### **1.4.4 Direct Methanol Fuel Cell Proton Exchange Membranes**

Although significant performance gains have been achieved using PEMs, many problems still exist that must be overcome before the DMFC becomes marketable. The

best available PEM to date is Nafion. However, Nafion is permeable to methanol (and of course water). This permeability enables methanol to “crossover” from the anode to the cathode and has drastic effect on cathode performance. Because of this, several alternatives to Nafion are being proposed and developed. One common approach is to create membranes that exhibit less methanol crossover. Sulfonated poly(ether ketone),<sup>105</sup> sulfonated polysulfones and poly(ether sulfones)<sup>106</sup> based membranes have been developed and tested. While these membranes exhibit less methanol permeability than Nafion, their proton conductivities are substantially lower and hence they do not perform as well. Pickup *et al.*<sup>107, 108</sup> have developed composite poly(1-methylpyrrole)/Nafion membranes. These membranes exhibit ca. 50% less methanol crossover without a significant increase in the resistance (or decrease in conductivity) of the composite membrane.

Another approach is to develop membranes that can be used at higher temperatures. Increasing cell temperature can increase the rate of methanol oxidation and reduce the rate of CO poisoning. However, Nafion is essentially limited to temperatures below ca. 100 °C, since at higher temperature its proton conductivity drastically decreases and it begins to degrade. Polybenzimidazole membranes doped with phosphoric acid have been shown to have good proton conductivity up to ca. 200 °C and are currently being studied for DMFC applications.<sup>109</sup> Also, Nafion /zirconium phosphate composite membranes<sup>110</sup> and Nafion/silica composite membranes<sup>111</sup> are promising candidates for DMFC applications at elevated temperatures.

## 1.5 Other Fuels

While methanol is the most common hydrocarbon that is being explored for direct oxidation in fuel cells, many other hydrocarbons have been either proposed or studied. Savadogo's group has studied running fuel cells directly on both propane<sup>112</sup> and acetals.<sup>113</sup> H Power has recently reported good low-current density performance for cells running on 2-propanol.<sup>114</sup> Ethanol is also being explored as a possible fuel.<sup>115</sup>

## 1.6 Evaluating Fuel Cell Performance

The performance of a PEMFC is usually determined by obtaining a polarization curve (or V-I curve), where cell voltage is plotted as a function of current density. Naturally, a higher cell voltage at a specific current indicates better performance. However, we can also gain information from the polarization curve about factors that are affecting cell performance. Performance losses caused by slow kinetics, ohmic resistance and mass transport can all be diagnosed from a polarization curve. Figure 1.7 shows a typical polarization curve for a fuel cell. Also shown are the regions where kinetic, ohmic and mass transport losses occur. Kinetic losses are typically seen as a sharp drop in potential at low current densities. Ohmic losses (*i.e.* from the membranes/electrode resistances) are usually observed in the linear region at intermediate current densities. Mass transport losses can be diagnosed from sudden drops in potential at high current densities.

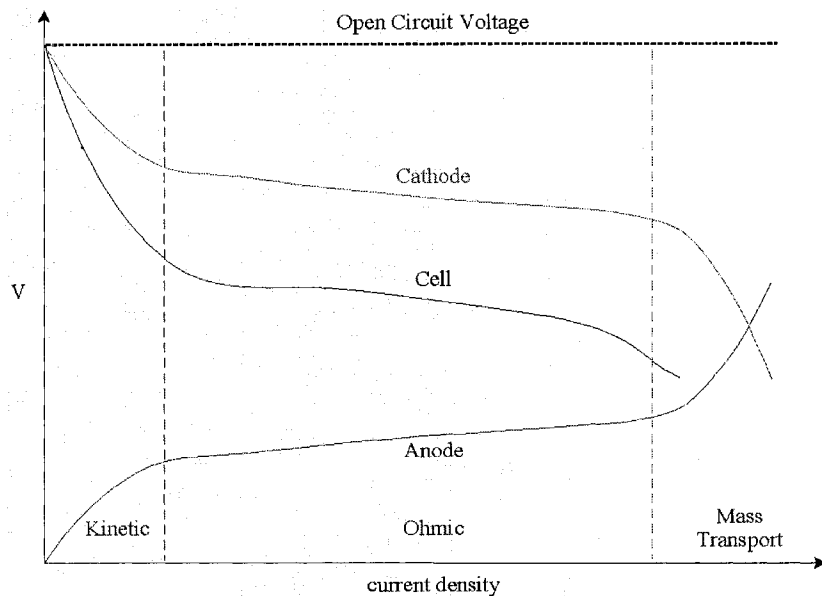


**Figure 1.7:** Contributions to fuel cell performance by the anode and the cathode, displaying the kinetic, ohmic and mass transport regions.

## 1.7. Thesis Objectives

The general goals of this thesis are to improve PEMFC and DMFC performance and understand the underlying factors that influence it. Chapter 3 explores the use of electroactive probes as a diagnostic technique to determine the degree of electrochemical activity within a PEMFC electrode. We demonstrate two strategies for incorporating electroactive probes into PEM fuel cell electrodes and show how they can provide insight into the transport properties of the electrodes.

Chapter 4 describes PEMFC cathode catalysts that have been treated with a sulfonated silane. The treatment procedure endows the surface with a chemically bonded silane monolayer that contains a proton conducting sulfonate group. The effect of the treatment on fuel cell performance and catalyst layer proton conductivity is described.

While there have been numerous studies of the various phenomena associated with DMFCs, there is virtually no literature that describes the optimization of all MEA components. With that in mind, Chapter 5 deals with the systematic optimization of all (standard) MEA components and the characterization of Nafion membranes of different thickness.

Conducting polymer/Nafion composite membranes are promising candidates for DMFC applications because of their reduced methanol crossover. Chapter 6 describes the characteristics that these membranes display in a DMFC.

Electrochemical impedance spectroscopy (EIS) is a powerful technique to characterize electrochemical systems. In Chapter 7, EIS is used to characterize the fundamental behavior of different cathode catalyst mixtures.

## References

- 
- <sup>1</sup> Radel, S.; Navidi, M.; *Chemistry* West Publishing Company: New York, 1990.
- <sup>2</sup> Plzak, V.; Rohland, B. Advanced Electrochemical Hydrogen Technologies, in *Modern Aspects of Electrochemistry* No. 26, Conway, B. E., Bockris, J. O'M.; White, R. E., Eds.; Plenum Press: New York, 1994; pp 105-163.
- <sup>3</sup> Kordesch, K. V.; Simander, G. R. *Chem. Rev.* **1995**, 95, 191-201.
- <sup>4</sup> Grove, W. R. *Philos. Mag.* **1839**, 14, 127.
- <sup>5</sup> Grubb, W. T.; Niedrach, L. W. *J. Electrochem. Soc.* **1960**, 107, 131.
- <sup>6</sup> Huczko, A. *Przm. Chem*, **2002**, 81, 19-24.
- <sup>7</sup> Ding, R. G.; Lu, G. Q.; Yan, Z. F.; Wilson, M. A. *J. Nano. Nanotechno.* **2001**, 1, 7-29.
- <sup>8</sup> Darkrim, F. L.; Malbrunot, P.; Tartaglia, G. P. *Int. J. Hydrogen Energy* **2002**, 27, 193-202.
- <sup>9</sup> Lee, S. M.; Kim, J. H.; Lee, H. H.; Lee, P. S.; Lee, J. Y. *J. Electrochem. Soc.* **149**, A603-A606.
- <sup>10</sup> Guther, V.; Otto, A. *J. Alloys Compounds* **1999**, 295, 889-892.
- <sup>11</sup> Kong, V. C. Y.; Foulkes, F. R.; Kirk, D. W.; Hinatsu, J. T. *Int. J. Hydrogen Energ.*, **1999**, 24, 665-675.
- <sup>12</sup> Ogden, J. M.; Steinbugler, M. M.; Kruetz, T. G. *J. Power Sources* **1999**, 79, 143-168.
- <sup>13</sup> Mauritz, K. A.; Hora, C. J.; Hopfinger, A. J. in: *Ions in Polymers*; ed. A. Eisenberg, ACS Advances in Chemistry Ser. No. 187, American Chemical Society: Washington, DC, 1980, pp. 124-154.
- <sup>14</sup> Yeager, H. L.; Steck, A. *J. Electrochem. Soc.* **1981**, 128, 1880.

- 
- <sup>15</sup> Eisenberg, A.; Hird, B.; Moore, R. B. *Macromolecules* **1990**, *23*, 4098.
- <sup>16</sup> Gierke, T. D.; Munn, G. E.; Wilson, F. C. *J. Polym. Sci. Polym. Phys. Ed.* **1981**, *19*, 1687.
- <sup>17</sup> Butler, G. B.; O'Driscoll, K. F.; Wilkes, G. L. *JMS Macromol. Chem. Phys.* **1994**, C34, 325-373.
- <sup>18</sup> Yeager, H. J.; Eisenberg, A. in: *Perfluorinated Ionomer Membranes*; eds. A. Eisenberg and H. L. Yeager, ACS Symp. Ser. No.180, American Chemical Society: Washington, DC, 1982, pp. 1-6, 41-63.
- <sup>19</sup> Mauritz, K. A.; Storey, R. F.; Jones, C. K. in: *Multiphase Polymer Materials: Blends, Ionomers, and Interpenetrating Networks*; eds. L.A. Utracki and R.A. Weiss, ACS Symp. Ser. No. 395; American Chemical Society: Washington, DC, 1989, p. 401-417.
- <sup>20</sup> A. Eisenberg and M. King, *Ion-Containing Polymers: Physical Properties and Structure*, Vol. 2., Academic Press: New York, 1977, pp. 163-169.
- <sup>21</sup> Hsu, W. Y.; Gierke, T. D. *Macromolecules* **1982**, *15*, 101.
- <sup>22</sup> Anantaraman, A. V.; Gardner, C. L. *J. Electroanal. Chem.* **1996**, *414*, 115-120.
- <sup>23</sup> Kim, C. S.; Chun, Y. G.; Peck, D. H.; Shin, D. R. *Int. J. Hydrogen Energy* **1998**, *23*, 1045-1048.
- <sup>24</sup> Bevers, D.; Wagner, N.; VonBradke, M. *Int. J. Hydrogen Energy* **1998**, *24*, 57-63.
- <sup>25</sup> Giorgi, L.; Antolini, E.; Pozio, A.; Passalacqua, E. *Electrochim. Acta* **1998**, *43*, 3675-3680.

- 
- <sup>26</sup> Ralph, T.; Hards, G.; Keating, J.; Campbell, S.; Wilkinson, D.; Davis, H.; St. Pierre, J.; Johnson, M. *Electrochim. Acta* **1997**, 144, 3845-3857.
- <sup>27</sup> Scott, K.; Taama, W. M.; Argyropoulos, P. *J. Power Sources*, **1999**, 79, 43-59.
- <sup>28</sup> Qi, Z.; Kaufman, A. *J. Power Source*, **2002**, 109, 469-476.
- <sup>29</sup> Hwang, J. J.; Hwang, H. S. *J. Power Sources* **2002**, 104, 24-32.
- <sup>30</sup> Costamagna, P.; Srinivasan, S. *J. Power Sources*, **2001**, 102, 253-269.
- <sup>31</sup> Hentall, P. L.; Lakeman, J. B.; Mepsted, G. O.; Adcock, P. L.; Moore, J. M. *J. Power Sources* **1999**, 80, 235-239.
- <sup>32</sup> Arico, A. S.; Creti, P.; Baglio, V.; Modica, E.; Antonucci, V. *J. Power Sources* **2000**, 91, 202-209.
- <sup>33</sup> Ogden, J. M.; Steinbugler, M. M.; Kruetz, T. G. *J. Power Sources* **1999**, 79, 143-168.
- <sup>34</sup> Cross, J. C. Hydrocarbon Reforming for Fuel Cell Application, in *Proceedings of the European Fuel Cell Forum Portable Fuel Cell Conference*, Lucerne, 1999, pp205-213.
- <sup>35</sup> Larminie, J.; Dicks, A. *Fuel Cell Systems Explained*; Wiley Publishing: New York, 2000, p200.
- <sup>36</sup> Rostrup-Neilson, J. R. *Catalysis Today* **1993**, 18, 305-324.
- <sup>37</sup> Stumper, J.; Campbell, S.; Wilkinson, D.; Johnson, M.; Davis, M. *Electrochim. Acta*, **1998**, 43, 3773-3783.
- <sup>38</sup> Gottesfeld, S.; Pafford, J. *J. Electrochem. Soc.* **1998**, 135, 2651.
- <sup>39</sup> Janssen, M. M. P.; Moolhuysen, J. *Electrochim. Acta* **1976**, 21, 869.
- <sup>40</sup> Damjanovic, A.; Grenshaw, M. A.; Bockris, J. O'M. *J. Chem. Phys.* **1966**, 45, 4057.

- 
- <sup>41</sup> Wroblowa, H. S.; Pan, Y. C.; Razumnet, G. *J. Electroanal. Chem.* **1976**, 69, 195.
- <sup>42</sup> Appleby, A. J.; Savy, M. *J. Electroanal. Chem.* **1978**, 92, 15.
- <sup>43</sup> Zurilla, R. W.; Sen, R. K.; Yeager, E. *J. Electrochem. Soc.* **1978**, 125, 1103.
- <sup>44</sup> Bagotskii, V. S.; Tarasevich, M. R.; Filinovskii, V. Y. *Elektrokhimiya* **1978**, 5, 1218.
- <sup>45</sup> Yeager, E. *Electrochim. Acta* **1984**, 29, 1527
- <sup>46</sup> Kinoshita, K. *Electrochemical Oxygen Technology*; Wiley: New York, 1992.
- <sup>47</sup> Appleby, A. J.; Foulkes, F. R. *A Fuel Cell Handbook*, 2<sup>nd</sup> Ed.; Kreiger Publishing :  
New York, 1993, p22
- <sup>48</sup> Ticianelli, E.A.; Derouin, C. R.; Srinivasan, S. *J. Electroanal. Chem.* **1988**, 251, 275-  
295.
- <sup>49</sup> Biegler, T.; Rand, A. J.; Woods, R.; *J. Electroanal. Chem.* **1971**, 29, 269-277.
- <sup>50</sup> Kozlowska, H; Conway, B.; Sharp, W. *J. Electroanal. Chem.* **1973**, 43, 9.
- <sup>51</sup> Jordan, L.R.; Shukla, A. K.; Behrsing, T.; Avery, N. R.; Muddle, B. C.; Forsyth, M. *J. Appl. Electrochem.* **2000**, 30, 641
- <sup>52</sup> Kinoshita, K. *Carbon: Electrochemical and Physicochemical Properties*; Wiley: New  
York, 1988.
- <sup>53</sup> Jia, N.Y.; Martin, R.B.; Qi, Z.; Lefebvre, M.C.; Pickup, P.G. *Electrochim. Acta* **2001**,  
46, 2863-2869.
- <sup>54</sup> Gruver, G. A.; Pascoe, R. F.; Kunz, H. R. *J. Electrochem. Soc.* **1980**, 127, 1219.
- <sup>55</sup> Lefebvre, M. C.; Qi, Z.; Pickup, P. G. *J. Electrochem. Soc.* **1999**, 146, 2054.
- <sup>56</sup> Shan, J.; Pickup, P. G. *Electrochim. Acta* **2000**, 46, 119-125.
- <sup>57</sup> Wilson, M. S.; Gottesfeld, S. *J. Appl. Electrochem.* **1992**, 22, 1-7.

- 
- <sup>58</sup> Wilson, M. S.; Gottesfeld, S. *J. Electrochem. Soc.* **1992**, 139, L28.
- <sup>59</sup> Murphy, O. J.; Hitchens, G. D.; Manko, D. J. *J. Power Sources* **1994**, 47, 353-368.
- <sup>60</sup> Poltarzewski, Z.; Staiti, P.; Alderucci, V.; Weiczorek, W.; Giordano, N. *J. Electrochem. Soc.* **1992**, 139, 761.
- <sup>61</sup> Raistri, I. D. in *Proceedings of the Symposium on Diaphragms, Separators, and Ion-Exchange Membranes*, J. W. Van Zee, R. E. White, K. Kinoshita, and H. S. Burney, Eds.; The Electrochemical Society Inc.: Pennington, NJ, 1986, p. 172.
- <sup>62</sup> Lee, S. J.; Mukerjee, S.; McBreen, J.; Rho, Y. W.; Kho, Y. T.; Lee, T. H. *Electrochim. Acta* **1998**, 43, 3693.
- <sup>63</sup> Cheng, X. L.; Yi, B. L.; Han, M.; Zhang, J. X.; Qiao, Y. G.; Yu, J. R. *J. Power Sources* **1999**, 79, 75.
- <sup>64</sup> Srinivasan, S.; Manko, D. J.; Koch, H.; Enayetullah, M. A.; Appleby, A.J. *J. Power Sources* **1990**, 29, 367.
- <sup>65</sup> Hirano, S.; Kim, J.; Srinivasan, S. *Electrochim. Acta* **1997**, 42, 1587.
- <sup>66</sup> Cha, S. Y.; Lee, W. M. *J. Electrochem. Soc.* **1999**, 146, 4055.
- <sup>67</sup> O'Hayre, R.; Lee, S.J.; Cha, S. W.; Prinz, F. B. *J. Power Sources* **2002**, 109, 483-493.
- <sup>68</sup> Kordesch, K.; Hacker, V.; Bachhiesl, U. *J. Power Sources* **2001**, 96, 200-203.
- <sup>69</sup> Li, Q. F.; Hjuler, H. A.; Bjerrum, N. J. *J. Appl. Electrochem.* **2001**, 31, 773-779.
- <sup>70</sup> Kordesch, K. V.; Simander, G. R. *Chem. Rev.* **1995**, 95, 191-201.
- <sup>71</sup> Yuh, C.; Johnsen, R. Farooque, M.; Maru, H. *J. Power Sources* **1995**, 56, 1.

- 
- <sup>72</sup> Shibuya, Y.; Nagamoto, H. in *Proc. Fifth Int. Symp. Solid Oxide Fuel Cells*, U. Stimming, S.C. Singhal, H. Tagawa, W. Lehnert, Eds.; Aachen, Germany, 1997, p. 510.
- <sup>73</sup> Doshi, R.; Richards, V. L., Krumpelt, M. in *Proc. Fifth Int. Symp. Solid Oxide Fuel Cells*, U. Stimming, S.C. Singhal, H. Tagawa, W. Lehnert, Eds.; Aachen, Germany, 1997, p. 379.
- <sup>74</sup> Hamakawa, S.; Shiozaki, R.; Hayakawa, T.; Suzuki, K.; Murata, K.; Takehira, K.; Koizumi, KM, Nakamura, J.; Uchijima, T.; *J. Electrochem. Soc.* **2000**, 147, 839.
- <sup>75</sup> Ihara, M.; Yokohama, C.; Abdula, A.; Kato, R.; Komiyama, H.; Yamada, K.; *J. Electrochem. Soc.* **1999**, 146, 3481.
- <sup>76</sup> Park, S.; Vohs, J. M.; Gorte, R. J.; *Nature* **2000**, 404, 265.
- <sup>77</sup> Murray, J. N.; Grimes, P. G. in *Fuel Cells*; American Institute of Chemical Engineers: New York, 1963, p. 57.
- <sup>78</sup> Glazebrook, R. W. *J. Power Sources* **1982**, 7, 15.
- <sup>79</sup> Tilak, B. V.; Conway, B. E.; Angerstein-Kozlowska, H. W. *J. Electroanal. Chem.* **1973**, 48, 1.
- <sup>80</sup> Li, N. H.; Sun, S. G.; Chen, S. P. *J. Electroanal. Chem.* **1997**, 430, 57.
- <sup>81</sup> Janssen, M. M. P.; Moolhuysen, J. *Electrochim. Acta* **1976**, 21, 869.
- <sup>82</sup> Parsons, R.; & Vandernoot, T. *J. Electroanal. Chem.* **1989**, 257, 9.
- <sup>83</sup> Lamy, C.; Léger, J-M.; Hahn, F.; Bedan, B.; Durand, R.; Kabbabi, A. in *Electrode Process IV*, Weickowski, A., Itaya, K., Eds.; The Electrochem. Society: Pennington, NJ, PV96-8, 1996; pp 356-370.

- 
- <sup>84</sup> Ianniello, R.; Schmidt, V. M.; Stimming, U.; Stumper, J.; Wallau, A. *Electrochim. Acta* **1994**, 39,1863.
- <sup>85</sup> Lamy, C.; Léger, J-M.; Srinivasan, S.; Direct Methanol Fuel Cells: From a Twentieth Century Electrochemist's Dream to a Twenty-first Century Technology, in *Modern Aspects of Electrochemistry*, No. 34, Bockris, J. O'M.; Conway, B. E., Eds.; KluwerAcademic/Plenum Publishers: New York, 2001; pp 53-118.
- <sup>86</sup> Swathirajan, S; Mikhail, M. *J. Electrochem. Soc.* **1991**, 138, 5.
- <sup>87</sup> Watanabe, M.; Genjima, Y, Turimi, K. *J. Electrochem. Soc.* **1997**, 144, 423.
- <sup>88</sup> Witham, C. K.; Chun, W.; Valdez, T. I.; Narayanan, S. R. *Electrochem. Solid-State Lett.* **2000**, 3, 497.
- <sup>89</sup> Denis, M. C.; Lalande, G.; Guay, D.; Dodelet, J. P.; Schulz, R. *J. Appl. Electrochem.* **1999**, 29, 951-960.
- <sup>90</sup> Gasteiger, H. A.; Markovic, M.; Ross, P. N.; Cairns, E. J. *J. Electrochem Soc.* **1994**, 141, 1795.
- <sup>91</sup> Lee, C. L.; Bergens, S. H. *J. Phys. Chem. B* **1998**, 102, 193-199.
- <sup>92</sup> Takasu, Y.; Fujiwara, T.; Murakami, Y.; Sasaki, K.; Oguri, M.; Asaki, T.; Sugimoto, W. *J. Electrochem. Soc.* **2000**, 147, 4421-4427.
- <sup>93</sup> Nordland, J.; Roessler, A.; Lindbergh, G. *J. Appl. Electrochem.* **2002**, 35, 259-265.
- <sup>94</sup> McNicol, B. D.; Short, R. T. *J. Electroanal. Chem.* 1977, 81, 249.
- <sup>95</sup> He, C.; Qi, Z.; Hollett, M.; Kaufman, A. *Electrochem. Solid-State Lett.* **2002**, 5, A181-A183.

- 
- <sup>96</sup> Long, J. W.; Stroud, R. M.; Swider-Lyons, K. E.; Rolison, D. R. *J. Phys. Chem. B* **2000**, 104, 9772.
- <sup>97</sup> Rolison, D. R.; Hagans, P. L.; Swider, P. L.; Long, K. E.; *Langmuir* **1999**, 15, 774.
- <sup>98</sup> Thomsa, S. C.; Ren, X.; Gottesfeld, S. *J. Electrochem. Soc.* **1999**, 146, 4354.
- <sup>99</sup> O'Grady, W. E.; Hagans, P. L.; Pandya, K. I.; Maricle, D. L. *Langmuir* **2001**, 14, 3047.
- <sup>100</sup> Lampitt, R. A.; Carrette, L. P. L.; Hogarth, M. P.; Russell, A. E. *J. Electroanal. Chem.* **1999**, 460, 80.
- <sup>101</sup> Gasteiger, H. A.; Markovic, M.; Ross, P. N.; Cairns, E. J. *J. Electrochem Soc.* **1994**, 141, 1795.
- <sup>102</sup> Gurau, B.; Viswanathan, R.; Liu, R. X.; Lafrenz, T. J.; Ley, K. L.; Smotkin, E. S.; Reddington, E.; Sapienza, A.; Chan, B. C.; Mallouk, T. E.; Sarangapani, S. *J. Phys. Chem. B* **1998**, 102, 9997.
- <sup>103</sup> Lamy, C.; Léger, J.-M. In *Proceedings of the 1<sup>st</sup> International Symposium on New Materials for Fuel Cell Systems*, Savadogo, O., Roberge, P. R., Veziroglu, T. N., Eds.; Ecole Polytechnique: Montreal, 1995, pp. 296-309.
- <sup>104</sup> Tributsch, H.; Bron, M.; Hilgendorff, M.; Schulenburg, H.; Dorbandt, I.; Eyert, V.; Bogdanoff, P.; Fiechter, S. *J. Appl. Electrochem.* **2001**, 31, 739-748.
- <sup>105</sup> Kerres, J.; Urlich, A.; Haring, Th.; Preidel, W.; Baldauf, M.; Gebhardt, U. *J. New Mater. Electrochem. Syst.* **2000**, 3, 229.
- <sup>106</sup> Nolte, R.; Ledjeff, K.; Bauer, M.; Mulhaupt, R. *J. Membr. Sci.* **1993**, 82, 221.
- <sup>107</sup> Jia, N.; Lefebvre, M. C.; Halfyard, J.; Qi, Z.; Pickup, P. G.; *Electrochem. Solid-State Lett.* **2000**, 3, 529-531.

- 
- <sup>108</sup> Pickup, P. G.; Qi, Z. *Canadian Patent Application No. 2,310,310*, PCT/CA 01/00767  
**2000.**
- <sup>109</sup> Wainright, J. S.; Wang, J.-T.; Wend, D.; Savinell, R. F.; Litt, M. H. *J. Electrochem. Soc.* **1995**, 142, L121.
- <sup>110</sup> Yang, C.; Srinivasan, S.; Arico, A.S.; Creti, P.; Baglio, V.; Antonucci, V.  
*Electrochem. Solid-State Lett.* **2001**, 4, A31-A34.
- <sup>111</sup> Antonucci, P. L.; Arico, A. S.; Creti, P.; Ramunni, E.; Antonucci, V. *Solid State Ionics* **1999**, 125, 431-437.
- <sup>112</sup> Savadogo, O.; Varela, F. J. R. *J. New Mat. Electr. Sys.* **2001**, 4, 93-97.
- <sup>113</sup> Savadogo, O.; Yang, X. *J. Appl. Electrochem.* **2001**, 31, 787-792.
- <sup>114</sup> Qi, Z.; Hollett, M.; Attia, A.; Kaufman, A. *Electrochem. Solid-State Lett.* **2002**, 5,  
A129-A130.
- <sup>115</sup> Neto, A. O.; Giz, M. J.; Perez, J.; Ticianelli, A.; Gonzalez; E. R. *J. Electrochem. Soc.*  
**149**, 3, A272-A279.

## **Chapter 2 :**

# **Chemicals and Instrumentation**

Unless stated otherwise, all commercial chemicals and solvents were used as received without further purification. Reported yields are not optimized. Experimental details relevant to a particular topic are written in each chapter.

## **2.1. Electrochemical Instruments**

Electrochemical experiments were performed using the two following instruments:

### **Solartron 1286/1250**

A Solartron (Schlumberger) 1286 electrochemical interface and 1250-frequency response analyzer controlled using custom software. Electrochemical Impedance Spectra (EIS) were collected using Z-plot software (Scribner Associates, Inc).

### **EG&G PAR 273A Potentiostat/Galvanostat/ 5210 Lock-in Amplifier**

An EG&G PAR 273A Potentiostat/Galvanostat, equipped with a 5210 lock-in amplifier, controlled using EG&G/PAR M270 electrochemical software. EIS data was acquired with PAR Powersine software.

## **2.2 Fuel Cell Testing**

### **2.2.1 Fuel Cell Electrode Preparation**

Fuel cell electrodes were prepared by thoroughly mixing and sonicating the dry catalyst with the desired proportions of Nafion and/or PTFE (Teflon), water and/or

2-propanol to create an “ink”. The ink was then applied to the electrode backing (*e.g.* carbon fiber paper) by using either a brush or a spray gun.

If the electrode contained Nafion (no PTFE), the electrode was dried at 135 °C for *ca.* 30 minutes. However, if the electrode contained PTFE, it was “sintered” at a temperature step of 110 °C, 280 °C, and 360 °C, each for 30 minutes. Sintering allows the PTFE to form an evenly distributed gas diffusion network. After cooling to room temperature, Nafion solution (5% in alcohols/water, Dupont) was either spray or brush applied to the electrode (Note: Nafion partially decomposes at temperatures greater than 200 °C and therefore electrodes containing Nafion cannot be sintered).

Catalyst, Nafion and PTFE loadings were determined gravimetrically using either a top-loading balance (for larger/heavier samples) or an analytical balance (for smaller/lighter samples).

### **2.2.2 MEA Preparation**

Full cell MEAs were prepared by hot-pressing two electrodes across a Nafion membrane at 130 °C with a pressure of 140-180 kg/cm<sup>2</sup> for 90-180s using a Carver laboratory press equipped with temperature controlled heating block to maintain temperature while pressure was applied. Reinforced Teflon templates were used to achieve proper alignment of electrodes. Half-cell MEAs were prepared in a similar manner as full-cell MEAs except that only one electrode was used.

### 2.2.3 Fuel Cell MEA Testing

MEA's were tested in 1, 5, 10 or 25 cm<sup>2</sup> cells. The 5, 10 and 25 cm<sup>2</sup> fuel cells were commercial models sold by Fuel Cell Technologies, constructed from graphite blocks with serpentine flow-fields. A schematic of these cells are shown in Figure 2.1. The 1 cm<sup>2</sup> cell was constructed from Plexiglas with an open current collector ring on each side which allowed gas to flow to each electrode. All cells were sealed using silicone rubber gaskets.

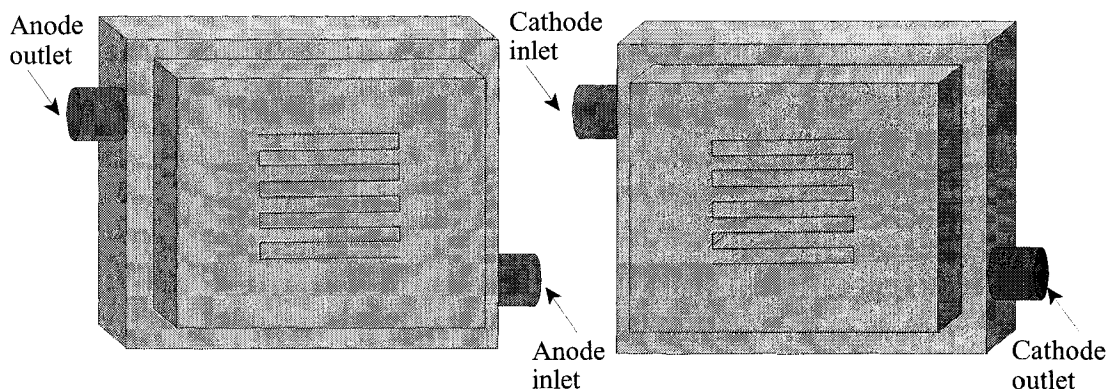


**Figure 2.1:** Schematic diagram of a fuel cell with serpentine flow fields.

Gas flow was controlled by flow meters (Cole-Parmer). Humidification of gases was achieved by passing the gas flow through a bubbler prior to entering the cell. The temperature of the bubbler was the same as that of the cell unless otherwise specified and was controlled using a temperature controller. Flow rates are reported as the reactant stoichiometry at 200 mA/cm<sup>2</sup> where relevant. Flow rates are reported as the reactant stoichiometry at 200 mA/cm<sup>2</sup> where relevant.

When using a direct methanol fuel cell (DMFC), air was not humidified.

Methanol solution was supplied from a heated 4 L tank using a Micropump 180 series magnetically driven suction shoe pump head equipped with a variable flow DC pump drive. The methanol solution was first passed through a pre-heating tube (to ensure it was at the cell temperature) before entering the cell. Since only a fraction of the methanol supplied to the cell is actually oxidized, the anode effluent was returned to the original tank and reused. The tank was large enough so that the methanol concentration changed very little over the course of a typical eight-hour experiment. A schematic diagram of the DMFC test system is shown in Figure 2.2. The methanol solution was supplied at a flow rate of 25 mL/min unless otherwise specified.

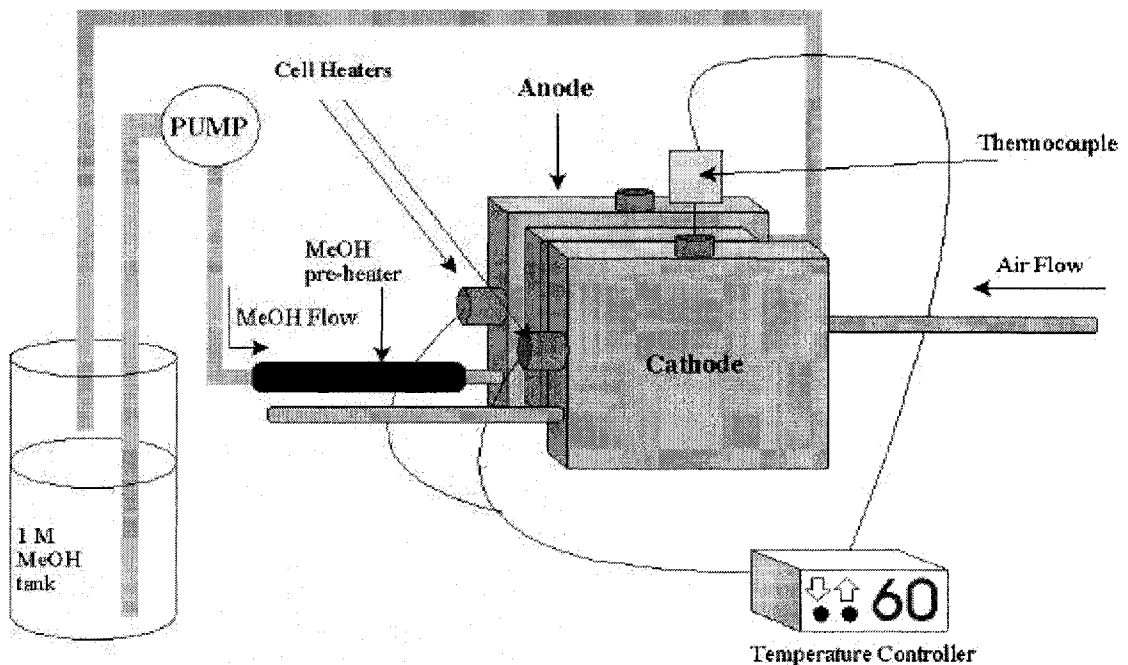


**Figure 2.2:** Schematic diagram of a direct methanol fuel cell testing system.

Fuel cells were tested by applying either a constant current or voltage from a potentiostat or power supply, or by applying a constant resistance from a rheostat. The method used in specific experiments is stated in the experimental section of the each chapter. Voltage and current measurements were made using either a potentiostat or a digital multi-meter. Measurements were recorded after allowing sufficient time for the reading to stabilize, typically 30-60 seconds.

Methanol crossover measurements were made in a fuel cell by passing humidified nitrogen through the cathode compartment and increasing the cell voltage to +0.85 V. Under these conditions, methanol can only be oxidized at the cathode and must first diffuse through the membrane ( $H_2$  is evolved at the anode).<sup>1</sup> This is depicted in Figure 2.3. Crossover current was measured after ca. 5 minutes, although readings typically stabilized in less than 2 minutes.

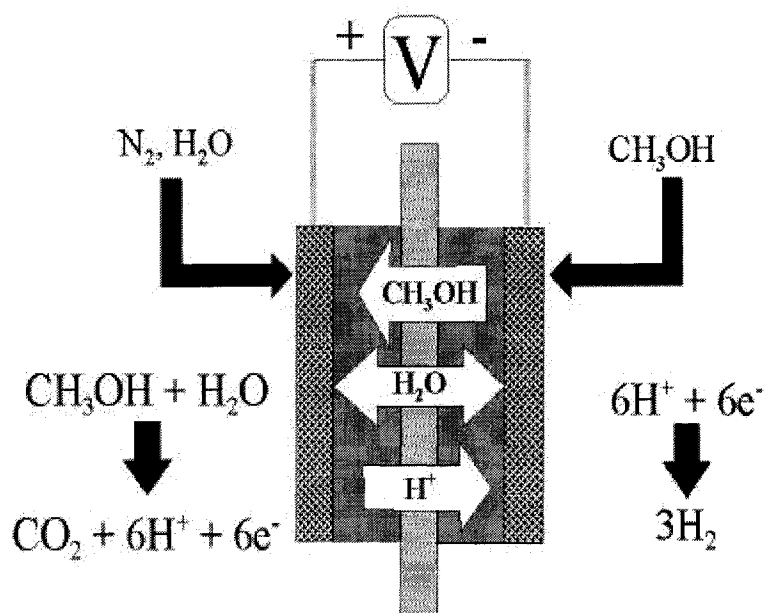


**Figure 2.3:** Schematic representation of the measurement of methanol crossover in a fuel cell.

Half-cell measurements were performed in a three-electrode configuration by exposing the test electrode to aqueous sulfuric acid solution. A schematic diagram of the half-cell is shown in Figure 2.4.

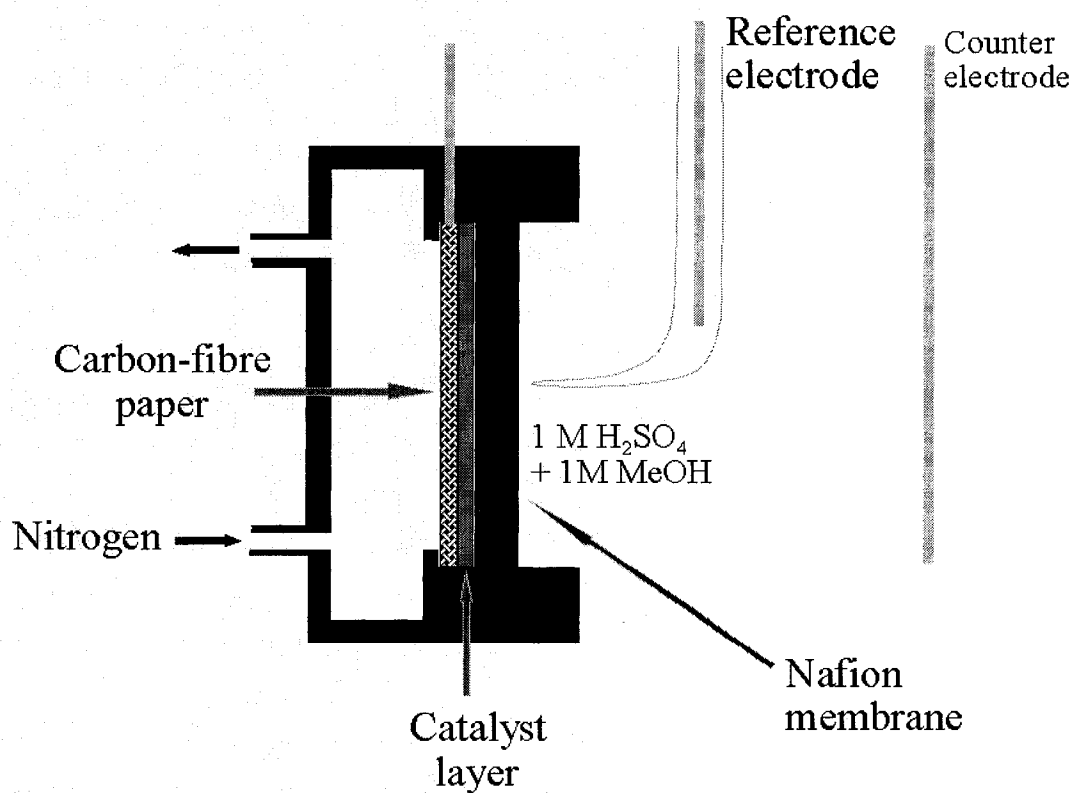


**Figure 2.4:** Half-cell configuration for testing gas diffusion electrodes.

#### **2.2.4 Reproducibility of Fuel Cell Results**

The fabrication methods used to prepare electrode surfaces make it extremely difficult to precisely reproduce results. Nonetheless, reasonably results were reasonably reproducible. Approximately 5% variation in electrode performance was typical for all experiments.

#### **2.3 Nuclear Magnetic Resonance Spectra**

Nuclear magnetic resonance (NMR) spectra were acquired on a GE-300NB instrument at 300 MHz. Chemical shifts are reported against TMS ( $(\text{CH}_3)_4\text{Si}$ ) as an internal standard. For all spectra, peaks are reported as chemical shift,  $\sigma$  (ppm), multiplicity (s = singlet, d = doublet, dd = double doublet, t = triplet, m = multiplet), and relative integration ratio. Data processing was accomplished with the NUTS software package (Acorn).

#### **2.4 Electron Microprobe Energy Dispersive X-ray Analysis**

Elemental compositions of electrodes and MEAs were investigated using electron microprobe energy dispersive X-ray (EDX) emission analysis with a Tracor Northern 5500 energy dispersive X-ray analyser in conjunction with a Hitachi S-570 scanning electron microscope. Relative element concentrations were estimated using Tracor Northern's software package "SQ" (Standardless Quantitative Analysis). This program provides a rapid, easy and standardless analysis of X-ray spectra acquired from bulk

specimens. It removes background, extracts peaks areas, calculates normalized intensity ratios, and corrects for matrix effects.

## **2.5 Fourier Transform Infrared Spectroscopy**

Fourier Transform Infrared (FTIR) spectra were obtained from KBr/analyte pellets using a Matheson Polaris FT-IR spectrometer. Data processing, including KBr background subtraction, was performed using the Matheson Polaris software package.

## **2.6 Electronic Absorption Spectroscopy**

All electronic absorption measurements were carried out on a CARY-5E UV-Vis-NIR spectrophotometer. Absorption spectra were collected from solutions contained in quartz cuvettes (path length = 1 cm).

## **2.7 X-ray Diffraction Spectra**

Powder X-ray diffraction was used to determine the Pt particle size of various catalysts. Spectra were acquired using a Rigaku Ru 200 diffractometer using  $\text{CuK}\alpha$  radiation (0.15405 nm). Average particle sizes were estimated from the spectral line broadening using commercial software (Jade 1994, Materials Inc.) that uses the Scherrer equation and includes an instrument calibration parameter.

## **References**

---

<sup>1</sup> Ren, X.; Springer, T. Gottesfeld, S.; *J. Electrochem. Soc.* **2000**, 147, 92-98.

## **Chapter 3**

# **Probing Electrochemical Activity in Proton Exchange Membrane Fuel Cell Electrodes using Electroactive Probes**

### 3.1 Introduction to Electroactive Probes

The chemical modification of electrodes is now a mature subject area, and there are many methods for functionalizing electrodes and to thereby endow them with desirable properties.<sup>1</sup> One of the major scientific benefits of modified electrodes is the insight that they have provided into the chemistry and structure of diverse classes of materials, from ion-exchange polymers to carbon nanostructures and inorganic materials such as clays and zeolites.<sup>2, 3, 4</sup> In this chapter, we demonstrate how some of the concepts and techniques developed over more than 20 years of research on modified electrodes can be applied to the investigation of the electrochemistry of gas diffusion electrodes used in proton exchange membrane fuel cells (PEMFC).

One of the key parameters for a PEMFC electrode is its electrochemically active catalyst area. This is generally determined by cyclic voltammetry in which the areas of the peaks for electrochemical hydrogen adsorption/desorption provide a measure of the active Pt area (discussed in detail in Chapter 1). However, the use of this parameter has a number of limitations, including the fact that it cannot be measured while the fuel cell is actually operating. Furthermore, the full Pt area that is active for hydrogen adsorption is unlikely to be active for the fuel cell reaction because of insufficient reactant gas access (to the Pt particle) and resistance losses at high current densities.

The chemical modification of fuel cell electrodes with electroactive probes has the potential to improve the diagnostic value of data obtained by techniques such as cyclic voltammetry (CV) and electrochemical impedance spectroscopy (EIS). The quantity of the probe present can be accurately controlled so that the percentage that is

active can be determined. Furthermore, probes can be deliberately placed in certain regions (macroscopic or microscopic) of the catalyst layer to monitor local properties. Electroactive probes can provide better accuracy and precision in active-area determinations and simplify the analysis of impedance data. In addition, chemical modification methods can be used to improve the characteristics of the electrode, such as proton conductivity and hydrophilicity/hydrophobicity. They can also be used to immobilize transition metal complex catalysts within the electrode.

In this chapter, we demonstrate two strategies for incorporating electroactive probes into PEM fuel cell electrodes, and show how they can provide insight into the transport properties of the electrodes. In the first strategy  $\text{Os}(\text{bpy})_3^{2+}$  (bpy = 2,2'-bipyridine) was incorporated into the Nafion binder as counterions.  $\text{M}(\text{bpy})_3^{2+}$  (M = Ru, Os, Fe) complexes have been commonly used to explore ion and charge transport with thin polymer films (including Nafion) on electrodes.<sup>5,6</sup> Here, we apply that methodology to three-dimensional gas-diffusion electrodes to gain similar insights.

The second strategy was to covalently bind  $\text{Ru}(\text{terpy})(\text{dabpy})\text{Cl}^+$  (terpy = 2,2',6',2''-terpyridine, dabpy = 4,4'-dicarboxylic acid-2,2'-bipyridine) to the surface of the carbon particles via a silane linkage. Silanes have been widely used to anchor desired functional groups, including metal complexes, to electrode surfaces. For example, Murray and coworkers studied the electrochemistry of several ferrocene complexes that were covalently attached to Pt electrodes via silane linkages.<sup>7</sup> This methodology has also been used for carbon electrodes. Here, we again applied that methodology to three-dimensional gas-diffusion electrodes to gain insight into their electroactivity.

The work described in this chapter has been published as:

Easton, E. B.; Pickup, P. G. *Electrochem. Solid-State Lett.* **2000**, 3(8) 259-261.

## 3.2 Experimental

### 3.2.1 Preparation of Modified Electrodes Containing Os(bpy)<sub>3</sub><sup>2+</sup>

Os(bpy)<sub>3</sub>Cl<sub>2</sub>·6H<sub>2</sub>O was prepared by a method similar to that of Anson et al.<sup>8</sup> A solution of K<sub>2</sub>OsCl<sub>6</sub> (Aldrich) (0.48 g) and 2,2'-bipyridine (0.68 g) in glycerol (10 mL) was refluxed for 5 hours. The dark green product was collected and purified by mixed solvent crystallization using a mixture of glycerol (5 mL), methanol (25 mL), and ether (1.5 L). After cooling in an ice bath, dark green crystals were collected via suction filtration (0.76 g, 89% yield). The purity of Os(bpy)<sub>3</sub>Cl<sub>2</sub>·6H<sub>2</sub>O was confirmed by NMR spectroscopy, cyclic voltammametry and electronic absorption spectroscopy.

Os(bpy)<sub>3</sub><sup>2+</sup> modified electrodes were prepared by spreading a suspension of 20% Pt/C (Electrosynthesis) in a mixture of Os(bpy)<sub>3</sub>Cl<sub>2</sub> in 0.1 M H<sub>2</sub>SO<sub>4</sub> (aq) and Nafion solution (5% in alcohols, Solution Technology), each in determined amounts, onto wetproofed carbon fiber paper (Toray TGPH090).

### 3.2.2 Preparation of Modified Electrodes Containing Silane Tethered

#### Ru(terpy)(dabpy)<sup>+</sup>

The route by which the silane tether Ru(terpy)(dabpy)Cl<sup>+</sup> was prepared is illustrated in Scheme 3.1.



dicarboxylic acid-2,2'-bipyridine) by refluxing the mixture in dry acetonitrile (15 mL) with N,N'- dicyclohexylcarbodiimide (DCC, 20 mg) for 24 h (DCC is a commonly used coupling agent). The product was collected by suction filtration, washed with acetonitrile (2x) and acetone (1x), and dried at 120°C for 2 h.

Ru(terpy)(dabpy)Cl<sup>+</sup> modified electrodes were prepared by mixing the modified carbon (11.3 mg) with a 15% polytetrafluoroethylene (PTFE) suspension (21.3mg, DuPont) and spreading the resulting slurry on wetproofed carbon fiber paper.

### 3.2.3 Electrochemical Notes

Electrochemical measurements on electrodes exposed to electrolyte solutions were performed in a three-electrode cell configuration with a Pt wire counter electrode and a saturated sodium chloride calomel reference electrode (SSCE), as shown in Figure 2.4.

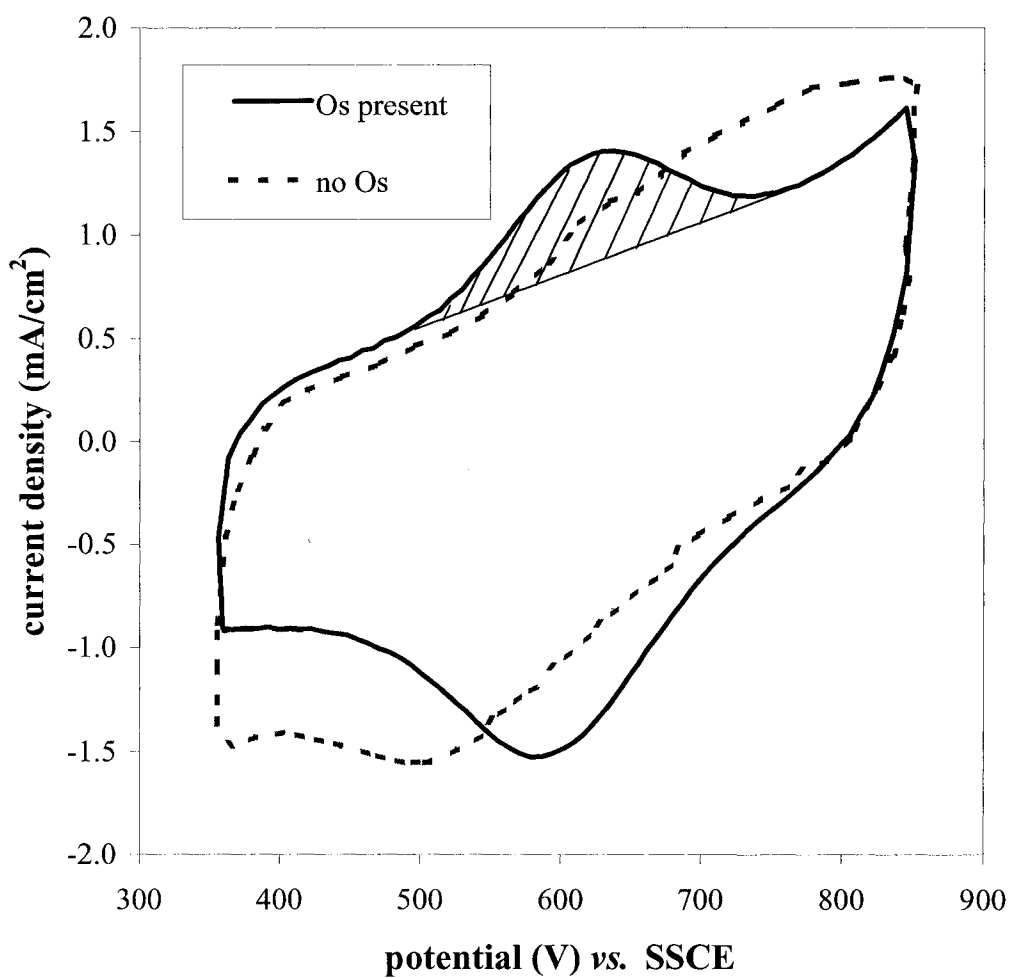
For measurements in fuel cells, membrane and electrode assemblies (MEAs) were prepared by hot-pressing the modified electrode and a similar Pt black catalyzed electrode onto each side of a Nafion membrane. The electrochemistry of the MEAs were investigated with cyclic voltammetry in a two-electrode configuration while humidified hydrogen was passed over the Pt black electrode, which acted as both counter and reference electrode; nitrogen was passed over the test electrode. The MEA was run as a H<sub>2</sub>/O<sub>2</sub> fuel cell (O<sub>2</sub> passed over the test electrode) for 30 min at 0.5 V immediately before the voltammetric experiments were performed.

### 3.3 Results and Discussion

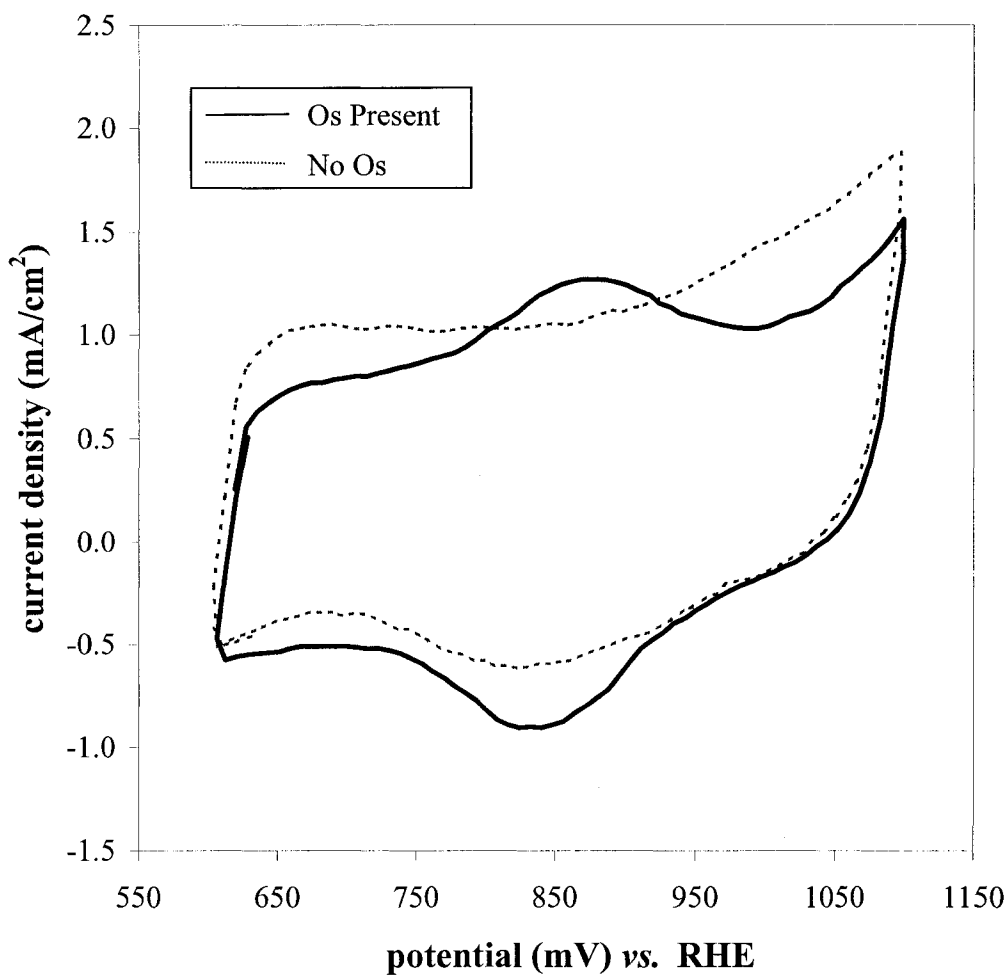
#### 3.3.1 Os(bpy)<sub>3</sub><sup>2+</sup> Modified Electrodes

Figure 3.1 shows a cyclic voltammogram of an electrode that was immersed in 0.5 H<sub>2</sub>SO<sub>4</sub> (aq) (i.e., the catalyst layer was in direct contact with the electrolyte solution) for which Os(bpy)<sub>3</sub><sup>2+</sup> was added to the Nafion binder. Figure 3.2 shows a cyclic voltammogram of an identical electrode that was bonded to a Nafion membrane and operated as the cathode of a H<sub>2</sub>/O<sub>2</sub> fuel cell prior to the voltammetric measurements. The background voltammograms (dashed lines) in both figures are for electrodes without the added osmium complex, which show background currents due to Pt oxide formation and stripping in the potential region of interest. These Pt waves were clearly suppressed when the osmium complex was present. The reversible redox waves at E°' = 0.60 V vs. SSCE in Figure 3.1 and +0.85 V vs. H<sup>+</sup>/H<sub>2</sub> in Figure 3.2 were therefore attributed to the Os(III/II) electrochemistry of the added complex. The cathodic waves for this couple appeared to be slightly enhanced by Pt oxide stripping, and so the quantitative measurements reported below were based on the charge under the anodic Os(III/II) wave only.

Determination of the area under the Os(bpy)<sub>3</sub><sup>3+/2+</sup> wave when the electrode was exposed to solution (Figure 3.1) corresponded to 51% of the total amount added to the layer. Two factors may be responsible for the lack of electroactivity of some of the Os(bpy)<sub>3</sub><sup>2+</sup>. First, it is known that the method of incorporation used allows some Os(bpy)<sub>3</sub><sup>2+</sup> to enter regions of the Nafion structure where it would become



**Figure 3.1:** CVs (20 mV/s) of 1 cm<sup>2</sup> gas diffusion electrodes containing 0.80 mg/cm<sup>2</sup> 20%Pt/C, 0.98 mg/cm<sup>2</sup> Nafion, and 0.15 mg/cm<sup>2</sup> Os(bpy)<sub>3</sub>Cl<sub>2</sub>·6H<sub>2</sub>O, in 0.5 M H<sub>2</sub>SO<sub>4</sub>(aq). The dashed line is for a similar electrode without the Os complex.



**Figure 3.2:** CVs (20 mV/s) of 1 cm<sup>2</sup> gas diffusion electrodes containing 0.80 mg/cm<sup>2</sup> 20%Pt/C, 0.98 mg/cm<sup>2</sup> Nafion, and 0.15 mg/cm<sup>2</sup> Os(bpy)<sub>3</sub>Cl<sub>2</sub>·6H<sub>2</sub>O, in a fuel cell. The dashed lines is for a similar electrode without the Os complex.

electrochemically inactive (*i.e.* the interfacial and hydrophobic regions).<sup>11</sup> A 30-60% loss of activity would be expected based on literature results for  $\text{Ru}(\text{bpy})_3^{2+}$  in Nafion. In addition, regions of the gas diffusion electrode may be electrochemically inactive because of poor electronic or ionic conductivity with the current collector or electrolyte.

When operated as a fuel cell cathode (Figure 3.2), the area under the Os(III/II) wave corresponded to only 28% of the total  $\text{Os}(\text{bpy})_3^{2+}$  in the layer. If it can be assumed that the same percentage of the catalyst layer was in electrical and ionic contact with both the current collector and electrolyte (membrane) as in the half-cell experiments, and that the same percentage of Os(III/II) in the Nafion was electroactive, then it can be reasoned that the lower Os(III/II) wave in the fuel cell is indicative that the fuel cell electrode has a lower ionic conductivity than the half-cell electrode (a lower electronic conductivity would not be expected). This is a reasonable result since the catalyst layer should not be as well hydrated in the fuel cell, as it would be when it was in contact with  $\text{H}_2\text{SO}_4$  (aq).

One concern in these experiments was that  $\text{Os}(\text{bpy})_3^{2+}$  could leach out of the catalyst layer into the Nafion membrane. However, the area under the Os oxidation wave decreased only slightly over 12 h in the fuel cell, indicating that leaching was not a significant problem. Thus the Os complex could easily diffuse over the short distances to the nearest catalyst particle during cyclic voltammetry experiments, but moved too slowly to diffuse far from the catalyst layer.

The hydrogen adsorption/desorption waves of the Os containing electrodes were similar in magnitude to those obtained with Os-free electrodes, although surprisingly the Os complex suppressed these waves slightly when the electrode was in contact with

H<sub>2</sub>SO<sub>4</sub> (aq), but not when in a fuel cell. It was not possible to make meaningful comparisons between H adsorption charges for electrodes in the fuel cell with those obtained in H<sub>2</sub>SO<sub>4</sub> (aq) because the poor definition of the H adsorption waves in the fuel cell made it impossible to determine the appropriate lower potential limit for integration. This highlights one of the advantages of using the Os complex as an electroactive probe, which allowed for accurate integration of the charge in both cases.

The fuel cell with the Os complex in its cathode catalyst layer gave a significantly lower current at 0.5 V (ca. 60 mA) than one without the Os complex (ca. 130 mA). This difference can presumably be attributed to the partial displacement of H<sup>+</sup> from the Nafion in the catalyst layer by the Os complex. The consequent decrease in [H<sup>+</sup>] in the catalyst layer would decrease both the rate of the oxygen reduction reaction, and the rate of proton transport to catalytic sites.

### **3.3.2 Silane-tethered Ru(2,2',6',2''-terpyridine)(4,4'-dicarboxylic acid-2,2'-bipyridine)Cl<sup>+</sup>**

Immobilization of an electroactive probe on the surface of the catalyst has a number of advantages over adding an unbound probe to the Nafion binder. Its electrochemistry should be more rapid because it does not need to diffuse to the catalyst surface (nor do electrons need to be transported through the Nafion), and it can be used to investigate ion transport and electrochemical utilization in the absence of Nafion in the catalyst layer. To demonstrate the feasibility of preparing such modified catalysts we report here on the electrochemistry of carbon black modified as outlined in Scheme 3.1.

This immobilization scheme is based on work reported by Murray and co-workers.<sup>12</sup> The Ru(terpy)(dabpy)Cl<sup>+</sup> moiety was chosen to give a redox wave at a suitable potential for studies in fuel cells.

### 3.3.2.1 Chemical Characterization of Modified Carbon

Relative elemental compositions were determined by electron microprobe energy dispersive X-ray (EDX) analysis with an electron microscope. Figure 3.3 shows the EDX spectrum of the Ru(terpy)(dabpy)Cl<sup>+</sup> modified XC-72 carbon black. A distinct peak for Si is observed, as are peaks for Ru and Cl. However, quantification of Ru and Cl was not possible since their peaks overlap (Ru L<sub>α1</sub> line = 2.56 keV, Cl K<sub>α1</sub> line = 2.60 keV). The instrument used was unable to resolve the two peaks. Nonetheless, the spectrum does confirm the presence of the complex on the carbon surface.

Fourier Transform Infrared Spectroscopy (FTIR) was also used to characterize the modified carbon. Figure 3.4 shows the FTIR spectrum of [Ru(terpy)(dabpy)Cl]PF<sub>6</sub> and Figure 3.5 shows the FTIR spectrum of Ru(terpy)(dabpy)Cl<sup>+</sup> modified XC-72 carbon black. The most compelling aspects of these spectra is the shift in the carbonyl stretching frequencies, from 1700 cm<sup>-1</sup> for the complex to 1624 cm<sup>-1</sup> for the modified carbon. This indicates the formation of the amide bond that attached the complex to the silane-modified carbon. Also, the peak at 1113 cm<sup>-1</sup> in Figure 3.5 is indicative of an amide bond (C-N stretch).

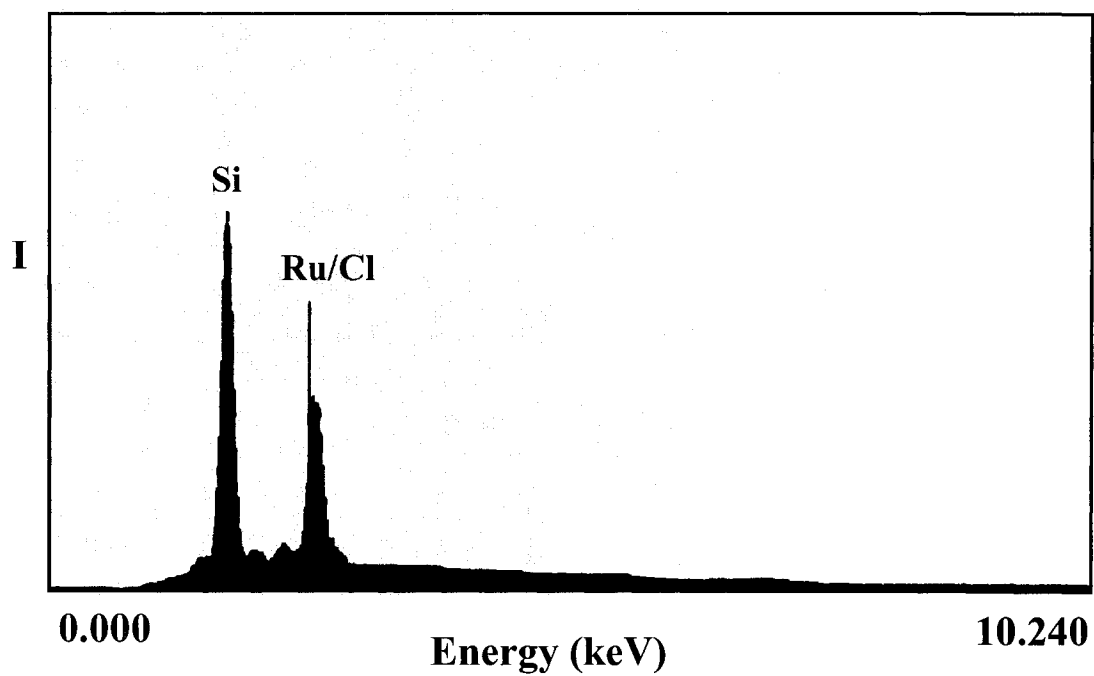


**Figure 3.3:** The EDX spectrum of Ru(terpy)(dabpy)Cl<sup>+</sup> modified XC-72 carbon black.

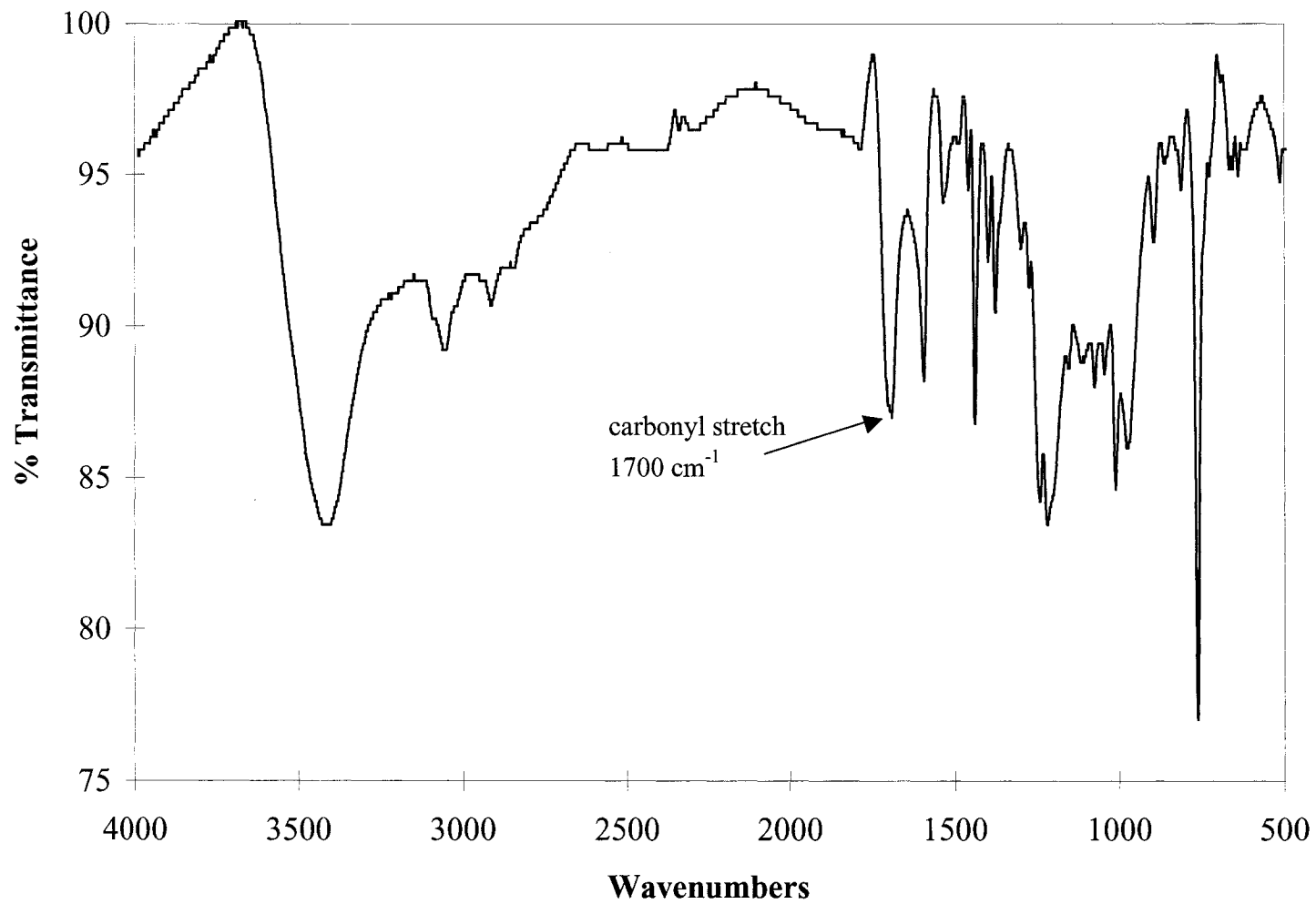


**Figure 3.4:** FTIR Spectrum of Ru(terpy)(dabpy)Cl<sup>+</sup>.

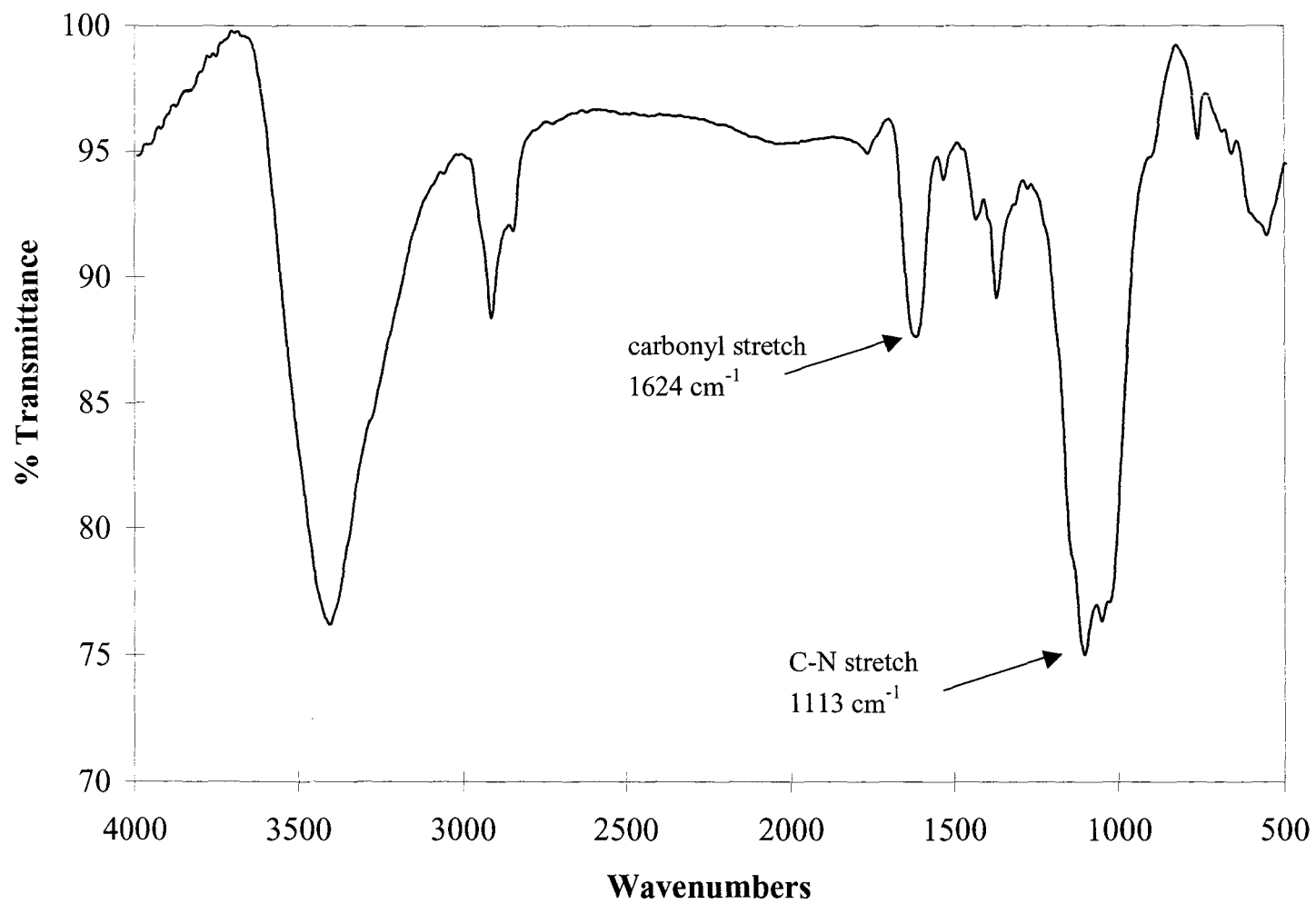


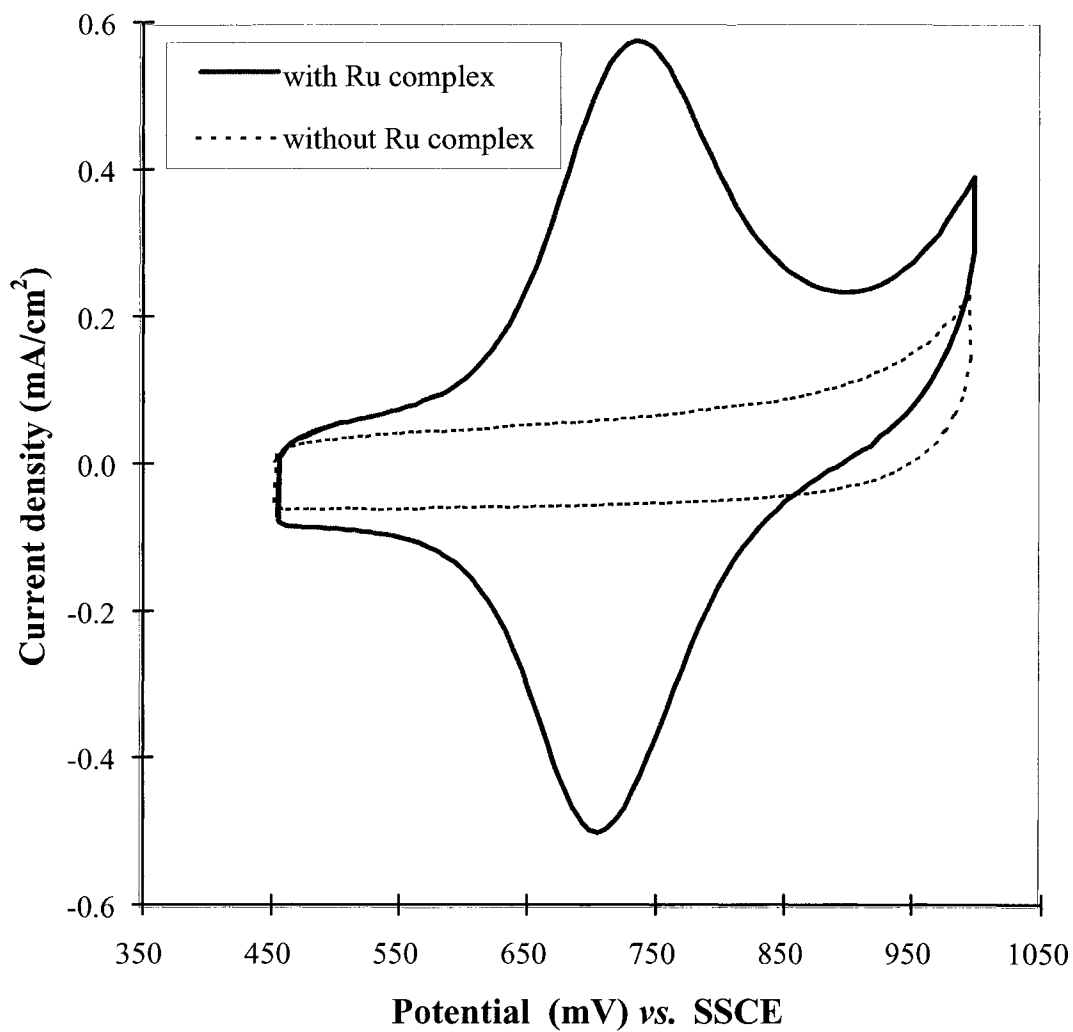
**Figure 3.5:** FT-IR Spectrum of Ru(terpy)(dabpy)Cl<sup>+</sup> modified Vulcan XC-72 carbon black

### 3.3.2.1 Electrochemistry of Modified Catalysts

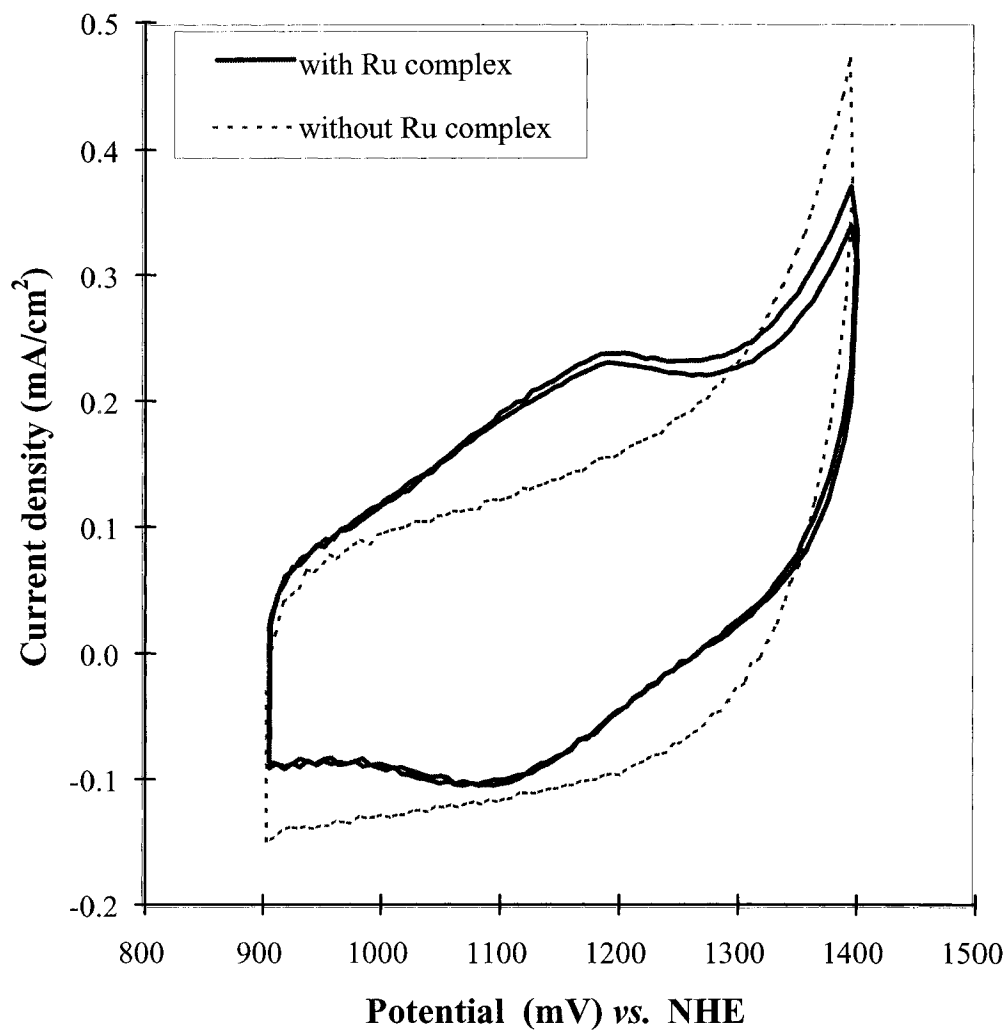
Figure 3.6 shows a cyclic voltammogram of the modified carbon, supported on carbon fiber paper, in 0.5M LiClO<sub>4</sub> (aq). The dashed line is a CV obtained with a similar electrode that did not contain the Ru complex (just PTFE bound carbon). The immobilized Ru complex exhibited a well-defined and relatively stable Ru(III/II) wave at ca. +0.70 V vs. SSCE.

Figure 3.7 shows the cyclic voltammogram of the modified carbon in a fuel cell MEA. The dashed line is a CV obtained with a similar electrode that did not contain Ru the complex (just PTFE bound carbon). Here the Ru(III/II) wave is shifted to ca. +1.15 V vs. H<sup>+</sup>/H<sub>2</sub> and became much smaller. The diminished size indicates that only a small fraction of the modified carbon layer was electroactive, presumably because of poor ionic conductivity. The fraction of the layer that was active in this case (ca. 20 %) was smaller than for the Os(bpy)<sub>3</sub><sup>2+</sup> - loaded electrodes of Figure. 3.2 (ca. 55 %) because we did not add an ionic conductor (e.g. Nafion) to the layer. The potential shift is due in part to the difference in reference electrode, but also appears to contain an environmental component because it is larger than the expected value of ca. +0.24 V that was seen for the Os(bpy)<sub>3</sub><sup>2+</sup> - loaded electrodes.

Figure 3.8 shows CVs obtained for electrodes that contained various amounts of Ru(terpy)(dabpy)Cl<sup>+</sup> modified XC-72 carbon black. A plot of peak cathodic current vs. mass is plotted in Figure 3.9. From these, we see that current scaled quite linearly with mass. This indicates that there is an even dispersion of the Ru complex on the carbon surface.



**Figure 3.6:** CVs (5 mV/s) of Ru(terpy)(dabpy)Cl<sup>+</sup> modified XC-72 carbon black (2.4 mg/cm<sup>2</sup>) in 0.5 M LiClO<sub>4</sub>(aq). The dashed line is for a similar electrode without the Ru complex.



**Figure 3.7:** CVs (5 mV/s) of Ru(terpy)(dabpy)Cl<sup>+</sup> modified XC-72 carbon black (2.4 mg/cm<sup>2</sup>) in a fuel cell MEA. The dashed line is for a similar electrode without the Ru complex.

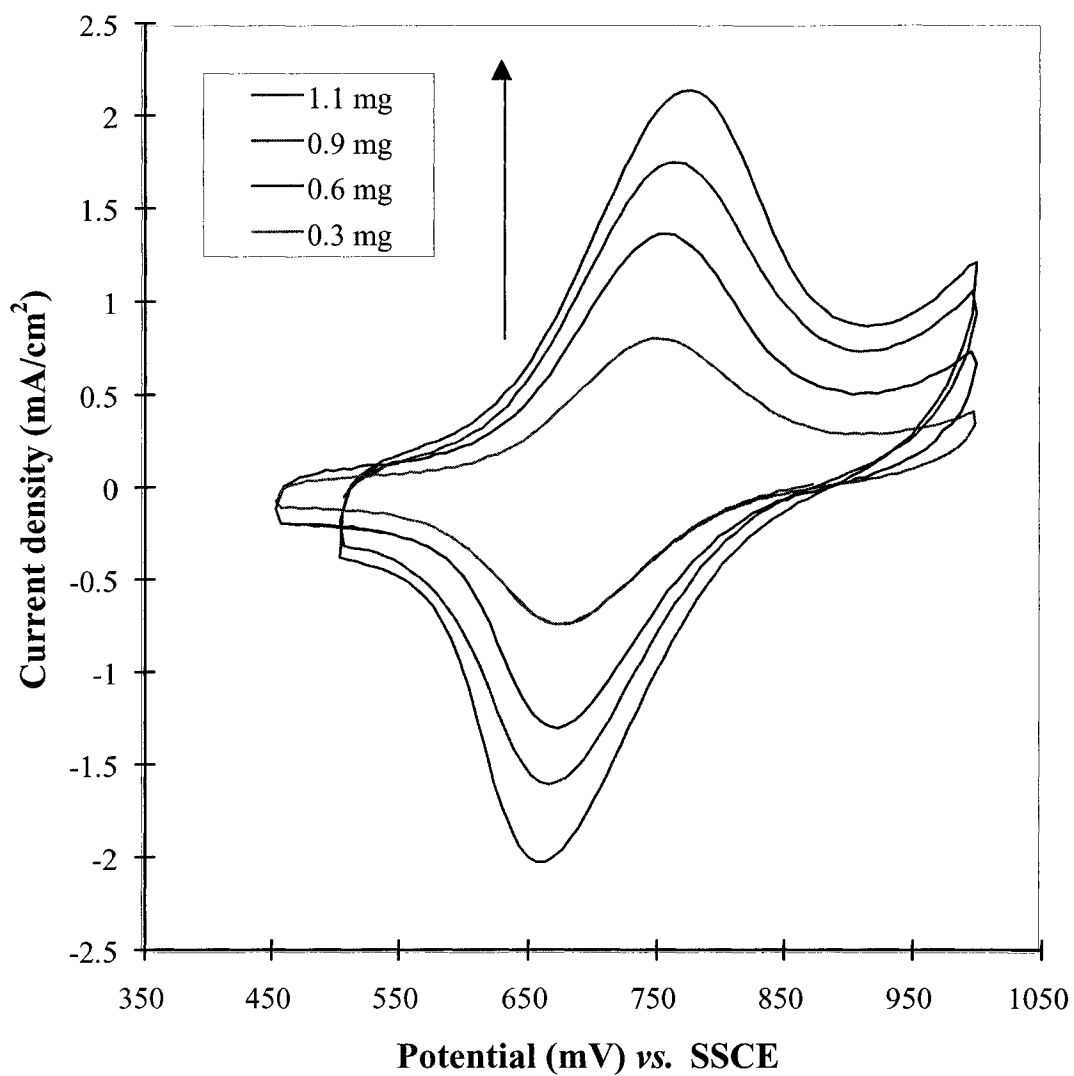


**Figure 3.8:** CVs (5 mV/s) of electrodes containing various amounts of Ru(terpy)(dabpy)Cl<sup>+</sup> modified XC-72 carbon black in 0.5 M LiClO<sub>4</sub>(aq).

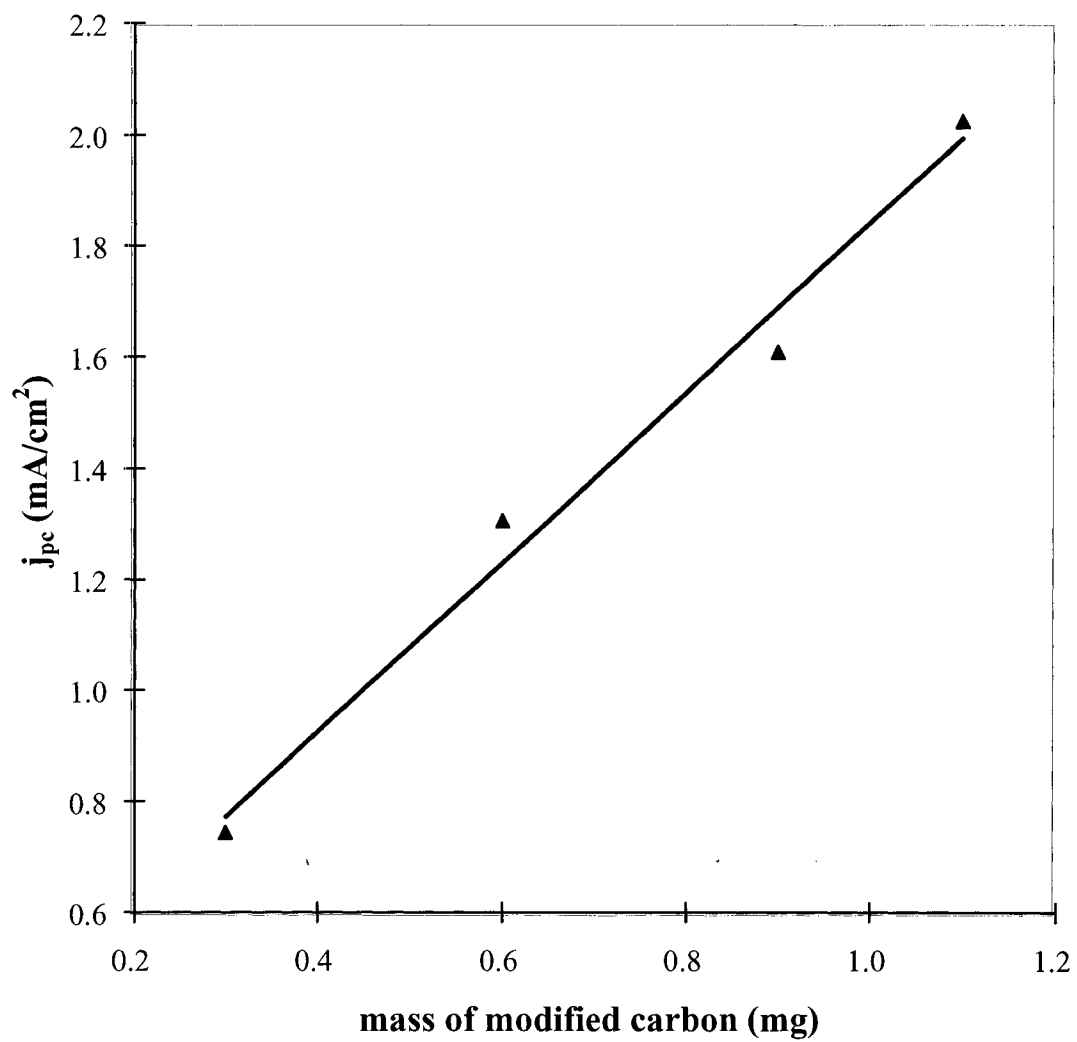


**Figure 3.9:** Variation of peak cathodic current with mass of Ru modified carbon.

The stability of the amide bond that tethers the Ru complex to the surface was a major concern. Amide bonds can easily be hydrolyzed in an acidic environment; therefore we studied the electrochemistry of the modified carbon black in acidic electrolyte. Figure 3.10 shows the electrochemistry of the Ru(terpy)(dabpy)Cl<sup>+</sup> modified XC-72 carbon black using 0.1M H<sub>3</sub>PO<sub>4</sub> (aq) electrolyte. From this we see that the Ru(II)/(III) peaks become smaller with each successive scan, indicating cleavage of the amide bond. This cleavage was not observed in non-acidic electrolytes such as LiClO<sub>4</sub>, KPF<sub>6</sub>, and CH<sub>3</sub>CN. This could be a potential problem in fuel cell electrodes that have good proton conductivity (*i.e.* containing Nafion).

### 3.4 Conclusion

The methodology of electroactive probes has been used to show that, even under ideal conditions, the entire catalyst layer of a fuel cell electrode is not electroactive. Also, only about half of the catalyst layer that was electroactive in the half-cell, was electroactive in the full cell.

Attaching the electroactive probe directly to the catalyst surface has many benefits. For example, it could complement the use of the Pt hydrogen absorption/desorption charge in determining electroactive areas and could also provide a reference point and pseudocapacitance for impedance studies. In many cases, it should be easier to quantify the charge due to the probe, particularly for catalysts with low Pt percentages, or alloys that show indistinct hydrogen waves.

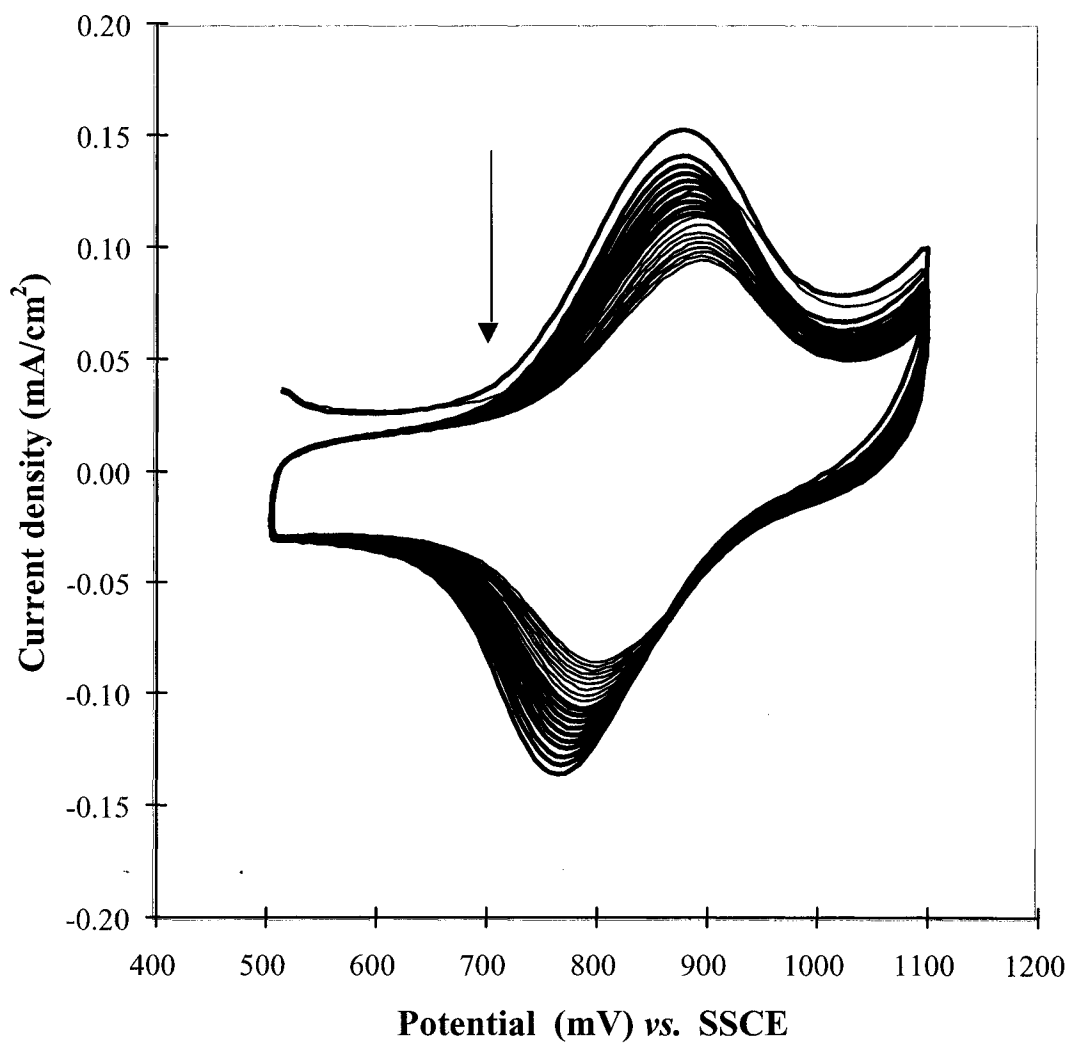


**Figure 3.10:** CVs (5 mV/s) of Ru(terpy)(dabpy)Cl<sup>+</sup> modified XC-72 carbon black in 0.1 M H<sub>3</sub>PO<sub>4</sub>(aq). Current decreases with scan number.

The stability of the amide linkage that tethered the Ru complex to the surface is an issue in the presence of acid. Because of this, Nafion could not be used as a binder. A non-hydrolyzable linkage is desired, perhaps through direct co-ordination of the complex to an immobilized bi-dentate ligand such as 2,2'-bipyridine.

## References

- 
- <sup>1</sup> Durst, R. A.; Baumner, A. J.; Murray, R. W.; Buck, R. P.; Andrieux, C. P. *Pure Appl. Chem.* **1997**, 69, 1317.
- <sup>2</sup> *Molecular Design of Electrode Surfaces*, Vol. XXII; Murray, R. W., Ed.; John Wiley & Sons: New York, 1992.
- <sup>3</sup> Abruna, H. D. in *Electroresponsive Molecular and Polymeric Systems*, Skotheim, T. A., Ed.; Marcel Dekker: New York 1991, p. 97.
- <sup>4</sup> Murray, R. W. *Electroanal. Chem.* **1984**, 13, 191.
- <sup>5</sup> White, H. S.; Leddy, J.; Bard, A. J. *J. Am. Chem. Soc.* **1982**, 104, 4811.
- <sup>6</sup> Martin, C. R.; Rubinstein, I.; Bard, A. J. *J. Am. Chem. Soc.* **1982**, 104, 4817.
- <sup>7</sup> Murray, R. W.; Lenhard, J. R. *J. Am. Chem. Soc.* **1978**, 100, 7780.
- <sup>8</sup> Anson, F. C.; Blauch, D. N.; Savéant, J.-M.; Shu, C.-F. *J. Am. Chem. Soc.* **1991**, 113, 1922-1932.
- <sup>9</sup> Abruna, H. D.; Meyer, T. J.; Murray, R. W. *Inorg. Chem.* **1979**, 18, 3233.
- <sup>10</sup> P. G. Pickup, Ph.D. Thesis, Oxford University, Oxford (1981).
- <sup>11</sup> Zhang, J.; Zhao, F.; Kaneko, M. *Electrochim. Acta* **1999**, 44, 3367.
- <sup>12</sup> Abruna, H. D.; Meyer, T. J.; Murray, R. W. *Inorg. Chem.* **1979**, 18, 3233.

## **Chapter 4**

# **Chemical Modification of Proton Exchange Membrane Fuel Cell Catalysts with a Sulfonated Silane**

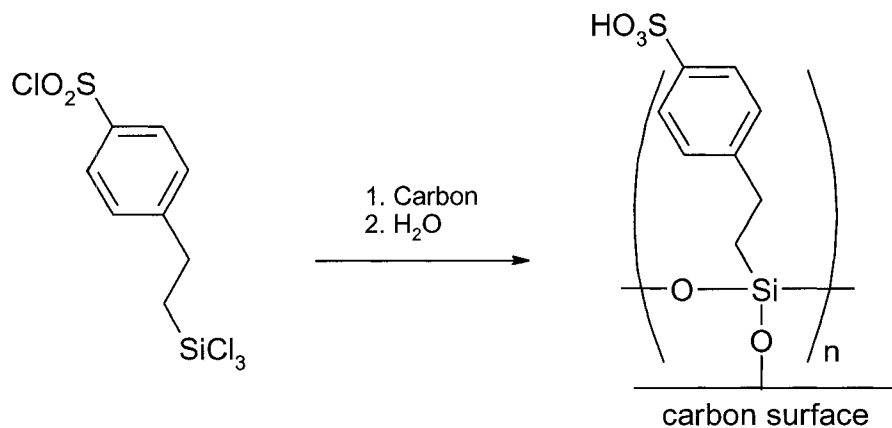
#### 4.1 Introduction to Sulfonated Silanes

The activity of a PEMFC electrode is greatly influenced by the proton conductivity within the catalyst layer. A common method employed to increase Pt utilization is to add a proton-conducting polymer, such as Nafion, into the catalyst layer. This has been shown to increase performance, but there is a limit to the quantity that can be added before adversely affecting cell performance.<sup>1,2</sup> Because of this, and the high cost of Nafion, alternative methods for increasing proton conductivity in the catalyst layer are of interest.

The objectives of the work described in this chapter were to explore the effects of treating the catalyst surface with a sulfonated silane and to characterize such modified catalysts. Silanes have been widely used to anchor desired functionalities to electrode surfaces.<sup>3,4,5</sup> Here, we tether proton conducting sulfonic acid groups to the surface of the catalyst via a silane linkage. This was accomplished by treating carbon black (with or without Pt) with 2(4-chlorosulfonylphenyl)ethyl trichlorosilane to produce a monolayer of silane on the surface as shown in Scheme 4.1. Sol-gel membranes based on this type of silane exhibit proton conductivities comparable to those of Nafion membranes.<sup>6</sup> Because the silane chemically binds directly to the surface of the catalyst layer, we anticipated that it should enhance proton conductivity without significantly blocking the pores and channels that allow gas diffusion.

Part of the work described in this chapter has been published as:

Easton, E.B.; Qi, Z.; Kaufman, A.; Pickup, P. G. *Electrochem. Solid-State Lett.* **2001**, 4(5) A59-A61.



**Scheme 4.1:** Treatment of the catalyst surface with a sulfonated silane.

## 4.2 Experimental

### 4.2.1 Silane Treatment Procedure

Dry 20% Pt on Vulcan XC-72 carbon black (E-TEK, 400 mg) was placed in a septum capped round bottom flask under a nitrogen atmosphere. To this, anhydrous dichloromethane (90 mL) and 50% 2-(4-chlorosulfonylphenyl)ethyl trichlorosilane (United Chemical Technologies) in dichloromethane (10 mL) were added via a syringe to give a final silane concentration of ca. 5%. After stirring at room temperature for ca. 2 h, the modified catalyst was collected by suction filtration, washed several times with dichloromethane, and dried at  $60^\circ\text{C}$  under vacuum for 6 h. This product is referred to hereafter as the “treated” catalyst.

Uncatalyzed Vulcan XC-72 carbon black (Electrosynthesis Corp.) was also treated with the sulfonated silane by the above procedure. It was then platinized with ca. 23% Pt by the formaldehyde reduction of  $\text{H}_2\text{PtCl}_6$ .<sup>7</sup> The treated carbon powder (200 mg) was ground gently with a mortar and pestle, then suspended in  $\text{H}_2\text{O}$  (30 mL).  $\text{H}_2\text{PtCl}_6$  was then added in an amount slightly greater than the desired loading. The suspension was stirred at 80 °C for 30 min to allow dispersion and equilibration. Next, a 25 molar excess of formaldehyde (37%) was added, followed by heating at reflux for 1 h. The catalyzed modified carbon was collected by filtration, washed thoroughly with water, and dried under vacuum (25-50 °C). This product is referred to hereafter as the “pretreated” catalyst.

#### **4.2.2 Electrode and MEA Fabrication and Testing**

Electrodes were prepared by mixing the silane treated catalysts with a Nafion solution (ca. 5% in alcohols, Solution Technology) and spreading the resulting slurry on a carbon cloth substrate (ELAT, E-TEK). Electrodes were then dried for 30 minutes at both room temperature and 135°C. Catalyst loadings ranged from 0.07 to 0.18 mg Pt/cm<sup>2</sup>. Performance was not strongly correlated with Pt loading in this range, and so this level of variation does not introduce significant uncertainty. Electrodes were also prepared using untreated E-TEK 20% Pt on Vulcan XC-72 carbon black to serve as a control (referred to hereafter as the “untreated” catalyst).

Fuel cell performance was tested in a single cell test station using membrane and electrode assemblies constructed by hot-pressing a 10 cm<sup>2</sup> test cathode and a similar Pt

catalyzed anode onto each side of a Nafion 112 membrane. After activating the cell (by running it for ca. 6 h under various loads and conditions), performance was tested at a cell temperature of 35°C, using a 45°C humidified air feed and a 45°C humidified hydrogen feed. Polarization curves were taken by applying a constant load from a rheostat. The voltage and current readings were allowed to stabilize for ca. 45 seconds before a measurement was recorded.

### **4.3 Catalyst Characterization**

#### **4.3.1 Catalyst Loading**

The total amount of Pt deposited onto the carbon surface for all samples was determined by a gravimetric analysis in which the catalyzed carbon was burned at 900 °C in a muffle furnace, and elemental Pt was assumed to be the only product since only a negligible amount of SiO<sub>2</sub> would be expected to form (discussed in more detail in Section 4.3.4). Loadings (as mass percentages) are listed in Table 4.2.

#### **4.3.2 Average Pt Particle Size**

Powder X-ray diffraction (XRD) experiments were performed on the untreated, treated and pretreated catalysts; their spectra are shown in Figures 4.1, 4.2 and 4.3 respectively. The broad peak centered at ca. 25° is due to the carbon support, while the peaks at ca. 40°, 47°, and 68° are due to Pt(111), Pt(200) and Pt(220) face-centered cubic faces respectively.<sup>8</sup> The average Pt particle diameter was estimated from the broadening

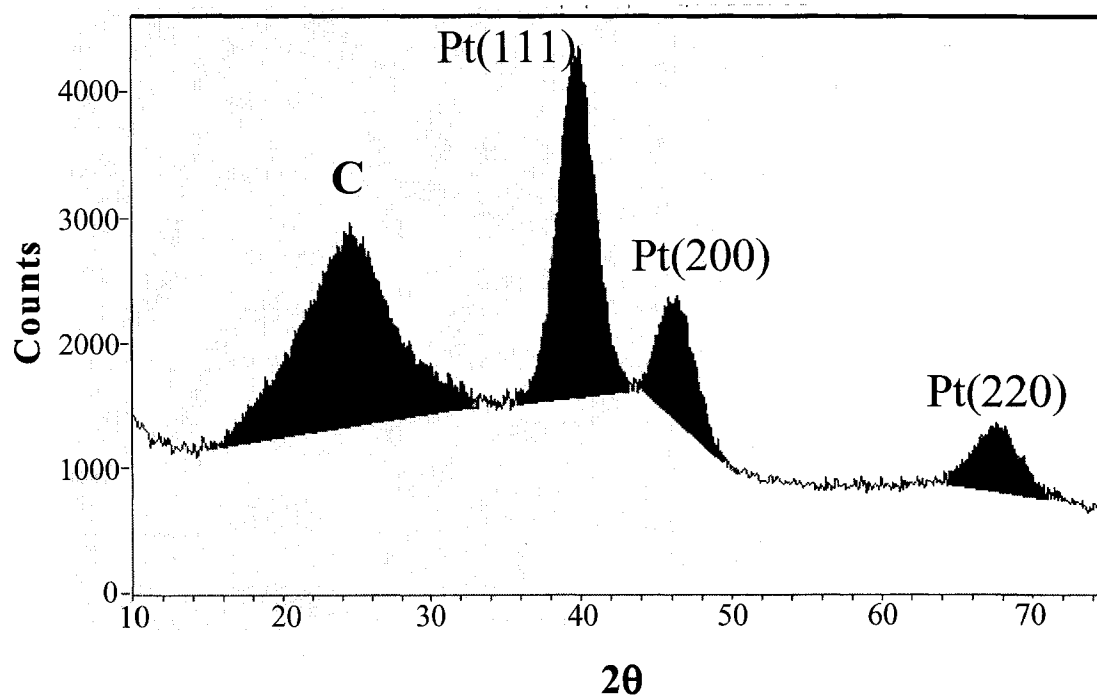


**Figure 4.1:** The XRD powder spectrum of the untreated catalyst (Etek 20% Pt/Vulcan XC72).

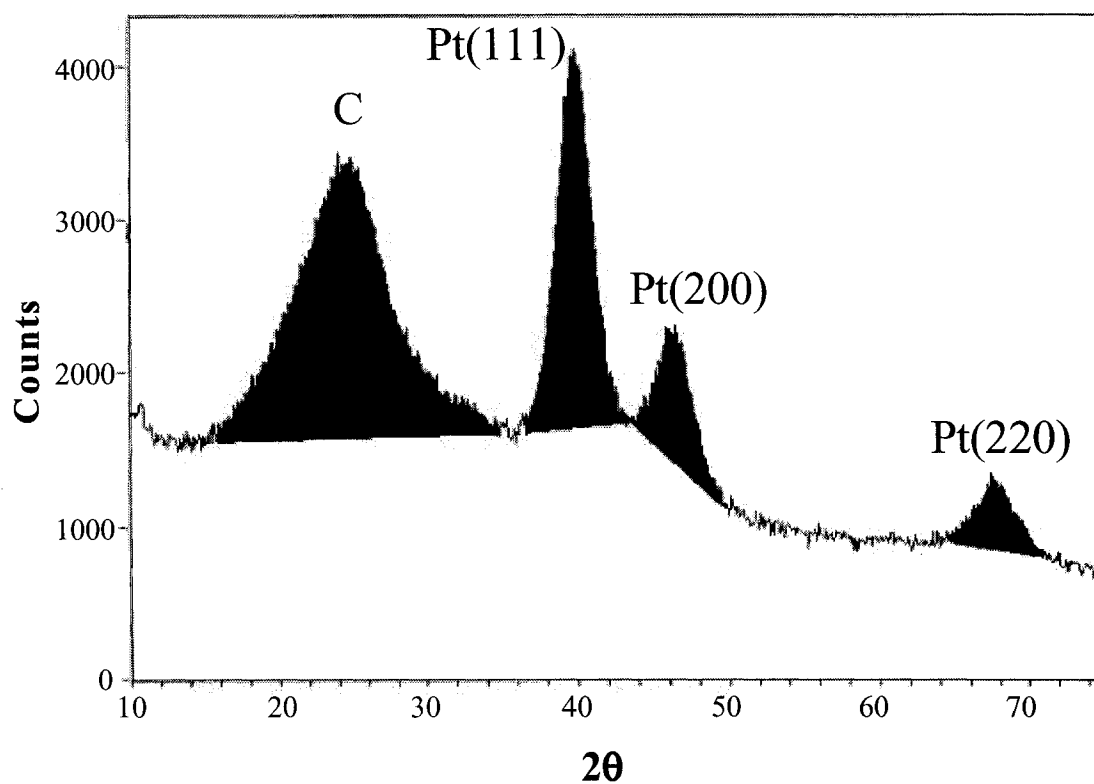


**Figure 4.2:** The XRD powder spectrum of the treated catalyst.

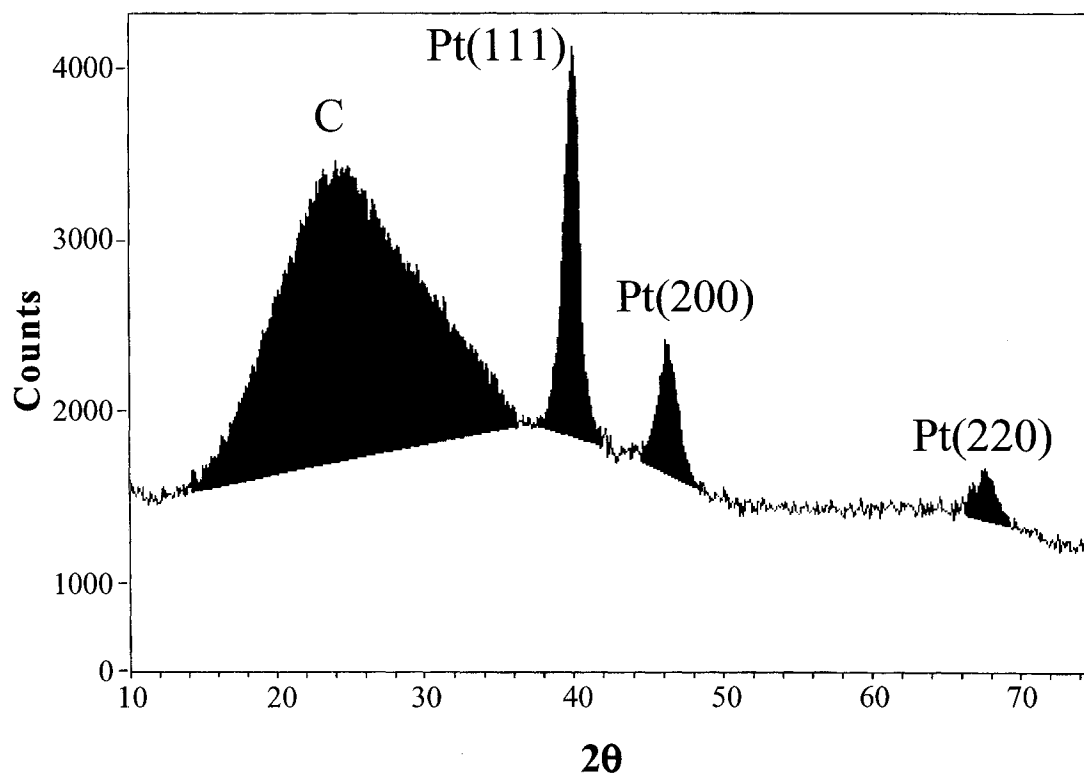


**Figure 4.3:** The XRD powder spectrum of the pretreated catalyst.

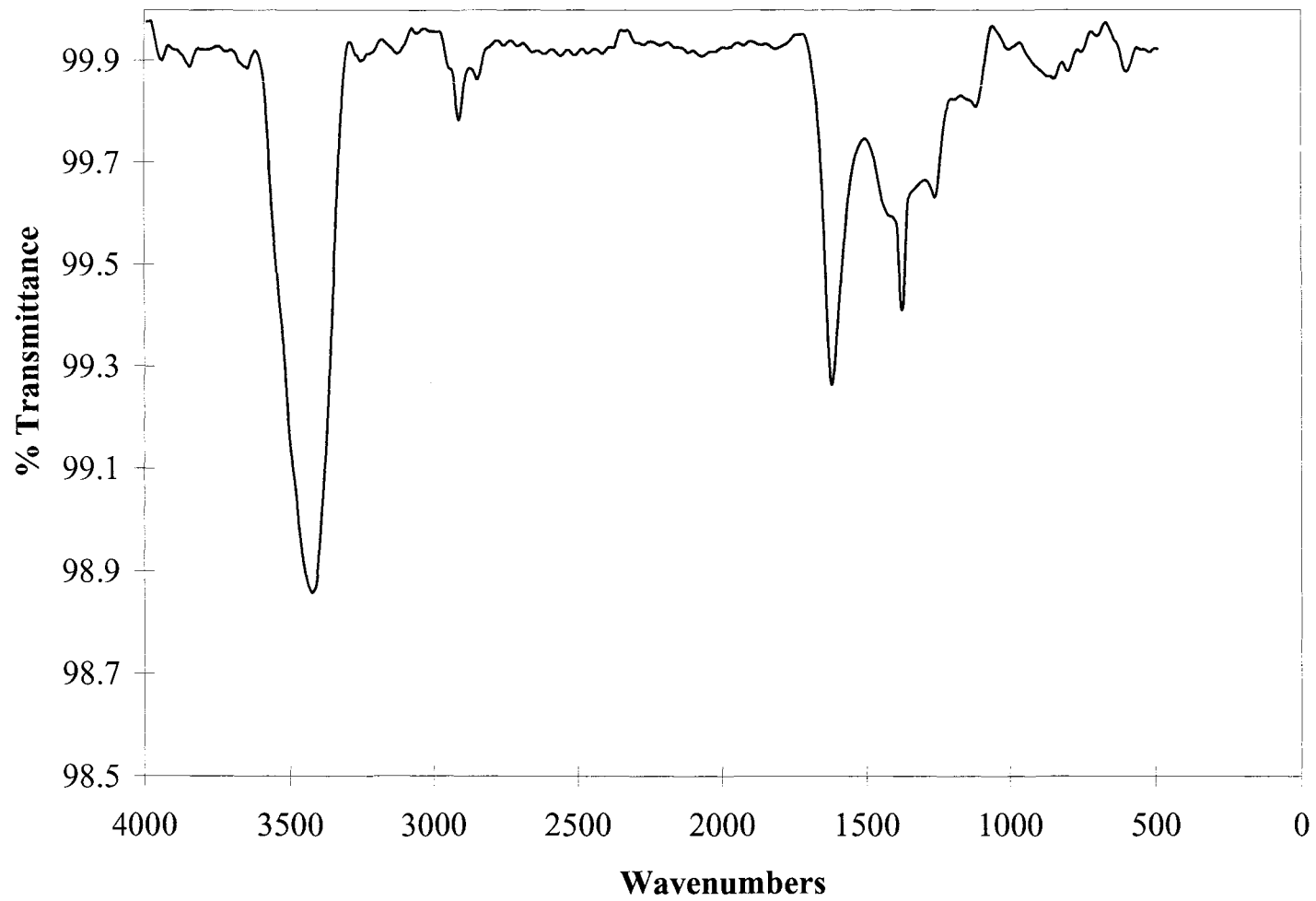
of the Pt(111) peak and was estimated to be 7.2 nm for the pretreated catalyst, 3.2 nm for the untreated catalyst and 3.4 nm for the treated catalysts. The extremely small difference in particle size between the untreated and treated catalyst indicates that the treatment procedure has little or no effect on the Pt particle size. The larger particle size for the pretreated catalyst is characteristic of the method by which the Pt was deposited. The deposition method used by E-TEK to produce the (untreated) commercial catalyst has not been revealed to us.

#### 4.3.3 Fourier Transform Infrared Spectroscopy

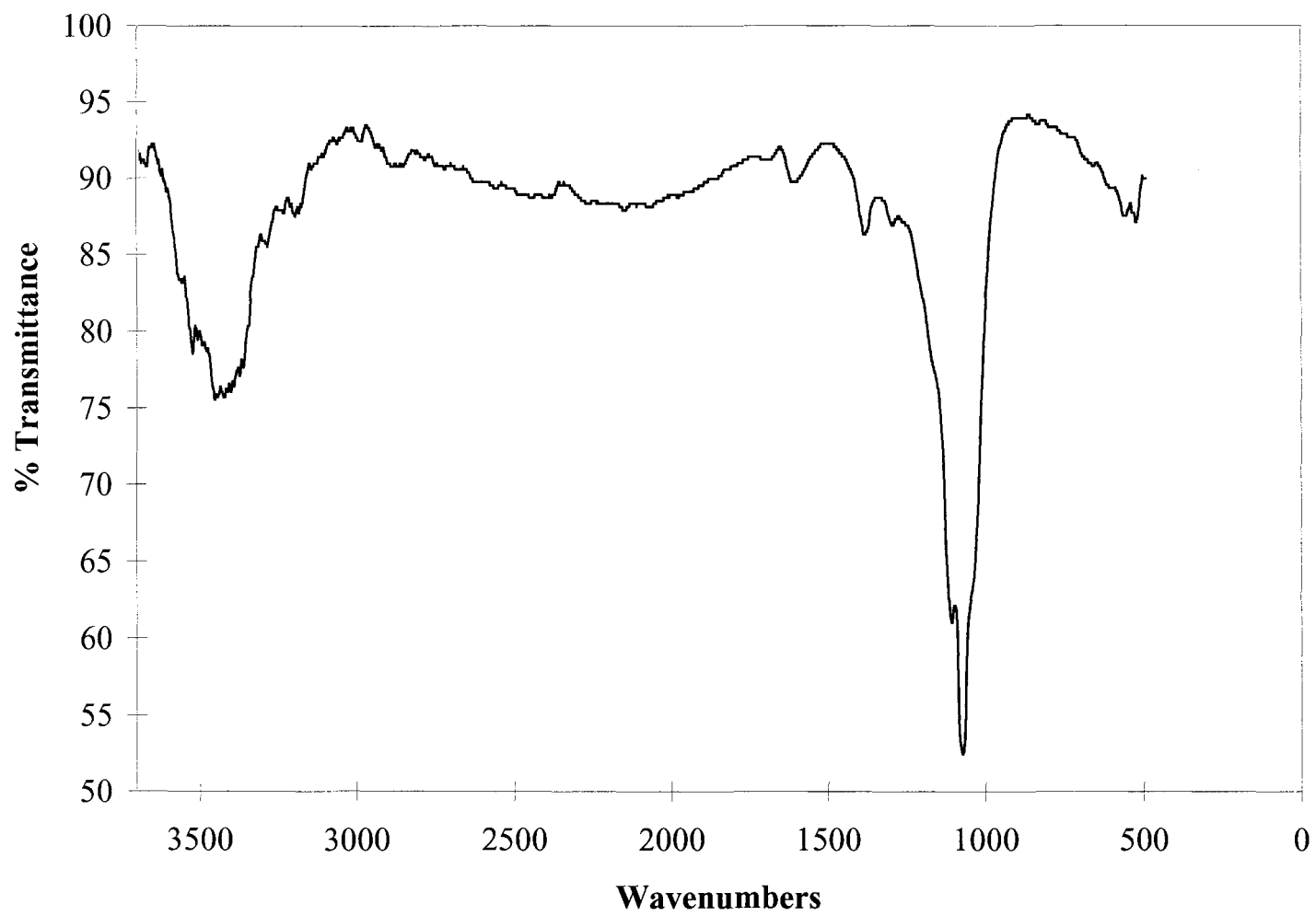
Fourier Transform Infrared Spectroscopy (FT-IR) was also used to characterize the changes in surface functionality caused by the sulfonated silane treatment and confirm the presence of the sulfonated silane on the surface after treatment.

Figure 4.4 shows an FT-IR spectrum of Vulcan XC72 carbon black (no Pt). Several peaks are observed between 1000 and 1700  $\text{cm}^{-1}$ , which originate from oxygen-containing species on the carbon surface. Table 4.1 lists the observed peaks and their assigned source based upon the literature.

Figure 4.5 shows an FT-IR spectrum of Vulcan XC72 carbon black after it has been treated with 2(4-chlorosulfonylphenyl)ethyl trichlorosilane (it is the pretreated catalyst prior to Pt deposition). The most compelling aspect of this spectrum is the appearance of intense peaks at 1120 and 1085  $\text{cm}^{-1}$ , originating from the attached sulfonate moiety. Also, the peak for absorbed water has increased which is expected since sulfonate groups are very hydrophilic.



**Figure 4.4:** FT-IR Spectrum of (untreated) Vulcan XC-72 carbon black.



**Figure 4.5:** FT-IR spectrum of sulfonated silane treated Vulcan XC72 carbon black.

Quantitative information about the carbon surface is extremely difficult to obtain through (absorption/transmission) IR spectroscopy due to the opaque nature of carbon (thus requiring very low concentrations of carbon in the KBr disc) and the low concentration of surface functionality. Nonetheless, qualitative information can be easily acquired. The differences between these two spectra clearly show the presence of new sulfonate groups on the carbon surface after treatment.

**Table 4.1:** Summary and assignment of peaks observed in the FT-IR spectrum of Vulcan XC72 carbon black (Figure 4.4).

Frequency (cm <sup>-1</sup> )	Signal Source
1126	C-O stretch <sup>9</sup>
1270	Ether <sup>10</sup>
1384	Phenol/hydroxyl <sup>11</sup>
1627	Quinone <sup>10</sup>
2920	CH <sub>2</sub> /CH <sub>3</sub> stretch <sup>12,13</sup>
3434	Absorbed water <sup>14</sup>

#### 4.3.4 Relative Elemental Compositions

Relative elemental compositions were determined by electron microprobe energy dispersive X-ray (EDX) analysis with an electron microscope. The EDX spectra for the untreated, treated and pretreated catalysts are shown in Figures 4.6, 4.7 and 4.8 respectively. The EDX spectrum of the untreated catalyst shows peaks for only Pt. However, both the pretreated and treated catalysts have peaks due to the presence of Si,

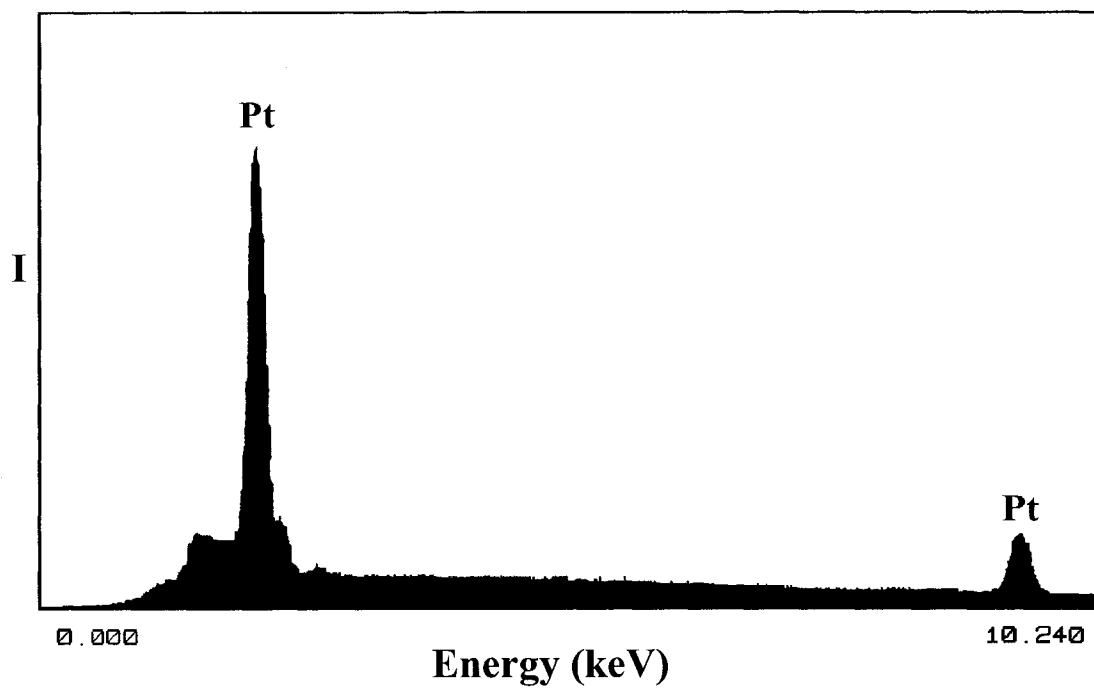


**Figure 4.6:** EDX spectrum of the untreated catalyst (Etek 20% Pt/Vulcan XC72)

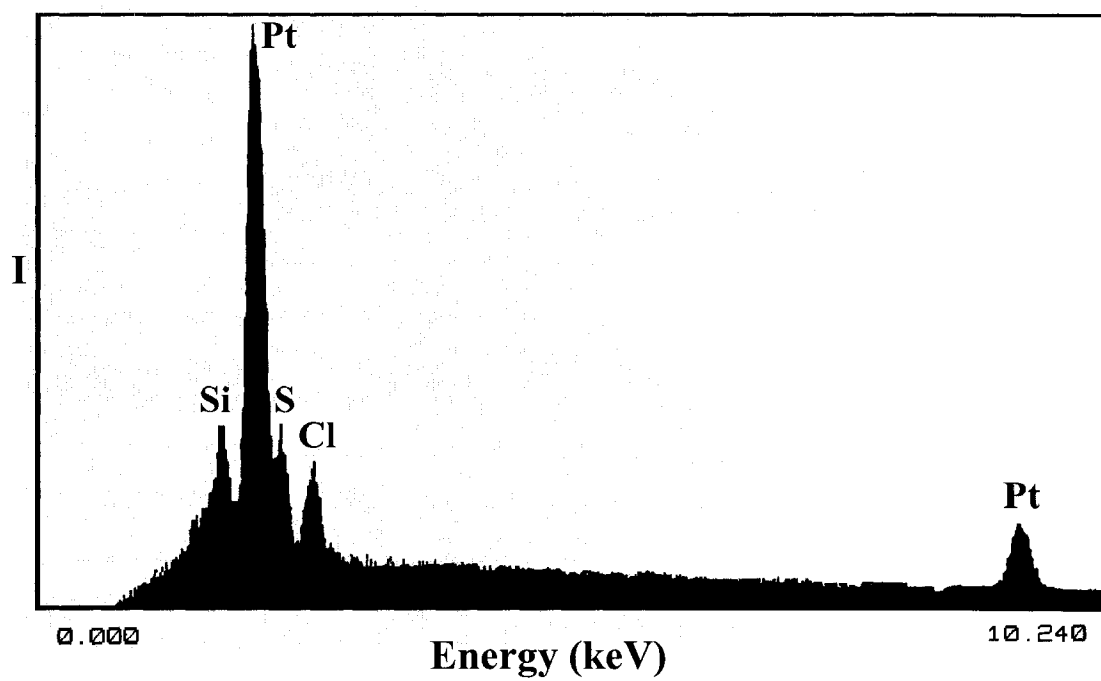


**Figure 4.7:** EDX spectrum of the treated catalyst

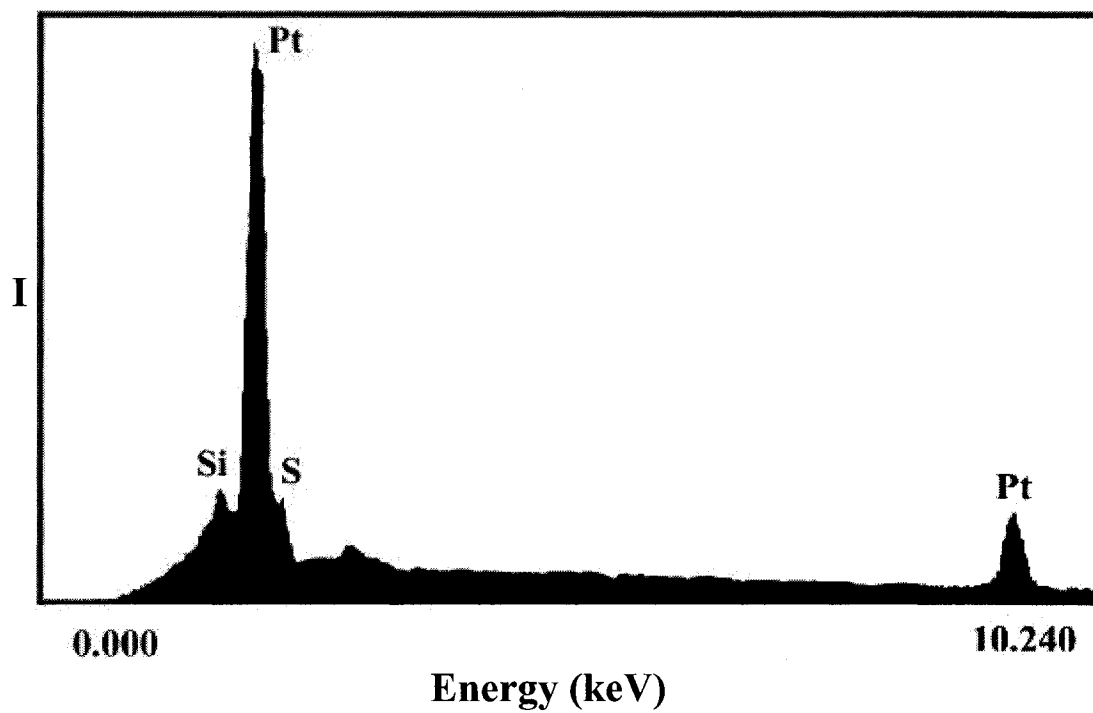


**Figure 4.8:** EDX spectrum of the pretreated catalyst.

confirming the presence of the silane on the catalyst surfaces. Also, the treated catalyst had a small signal due to Cl that originated from the trichlorosilane starting material. The Cl peak was not present for the pretreated catalyst, which was most likely removed during the Pt deposition step.

EDX analysis of the treated catalyst gave a Pt to Si mole ratio of 3.9, which was used to calculate loadings of the silane and hence total sulfonate in the electrodes. Based on the Brunauer-Emmett-Teller (BET) area of the carbon support ( $195 \text{ m}^2/\text{g}$ )<sup>15</sup> we estimate that the silane coverage on the carbon is ca.  $2.3 \times 10^{-10} \text{ mol}/\text{cm}^2$ , which is consistent with approximately monolayer coverage. The Pt to Si mole ratio of the pretreated catalyst was determined to be 5.44, which is larger than that of the treated catalyst. This disparity arises from the difference in Pt loadings of the two catalysts (17% vs. 23%). Nevertheless, the calculated silane surface coverage of the pretreated catalyst was found to be the same as for the treated catalyst, indicating reproducibility in the treatment procedure.

During combustion analysis (to determine Pt loading), it was assumed that only elemental Pt would remain and that there would be neither Si nor  $\text{SiO}_2$  present. The fact that the Pt loading of the treated catalyst was not higher than that of the untreated catalyst, suggests that this assumption is valid. Based upon this assumption, the Pt loading of the treated catalyst would in fact be lower than that of the untreated catalyst. This can be reasoned by the following calculation. First we will assume we have 1 g of untreated catalyst that we have treated with the sulfonated silane (to make the treated catalyst). The combustion analysis of the untreated catalyst gave a 19% Pt loading (i.e.

0.19 g of Pt, 0.81 g of C for every 1 g of untreated catalyst). Once treated, there will be a mass increase due to the presence of the sulfonated silane. Using the atomic ratio of Pt to Si of the treated catalyst determined from EDX (3.9:1), we calculated the mass ratio of Pt to sulfonated silane of 3.1:1. Therefore, the mass of sulfonated silane would be 0.061 g and the total mass of the treated catalyst would be 1.061 g. From these values, the %Pt was calculated to be 17.9%. This is in agreement with the combustion analysis result within experimental error. Based upon these calculations, the assumption is valid. Even if some Si remained after combustion, its mass would be too small to have a significant effect.

**Table 4.2:** Summary of catalyst properties.

<b>Catalyst</b>	<b>%Pt (mass)</b>	<b>Average particle size (nm)</b>	<b>Pt : Si Atomic ratio</b>	<b>%Si (mass)</b>	<b>Silane Coverage x 10<sup>10</sup> (mol/cm<sup>2</sup>)</b>
Untreated	19%	3.2	-	-	-
Treated	17%	3.4	3.9	0.6%	2.3
Pretreated	23%	7.2	5.4	0.6%	2.3

## 4.4 Fuel Cell Performance

### 4.4.1 Performance vs. Nafion Loading

Since the performances of all three catalysts vary with the Nafion loading in the catalyst layer, the optimal Nafion loading for each was first determined. Figure 4.9 illustrates the fuel cell performances achieved using the untreated catalyst at various Nafion loadings. From this, we see that performance increased steadily with Nafion loading up to peak performance at 30% Nafion. There was a small decline in

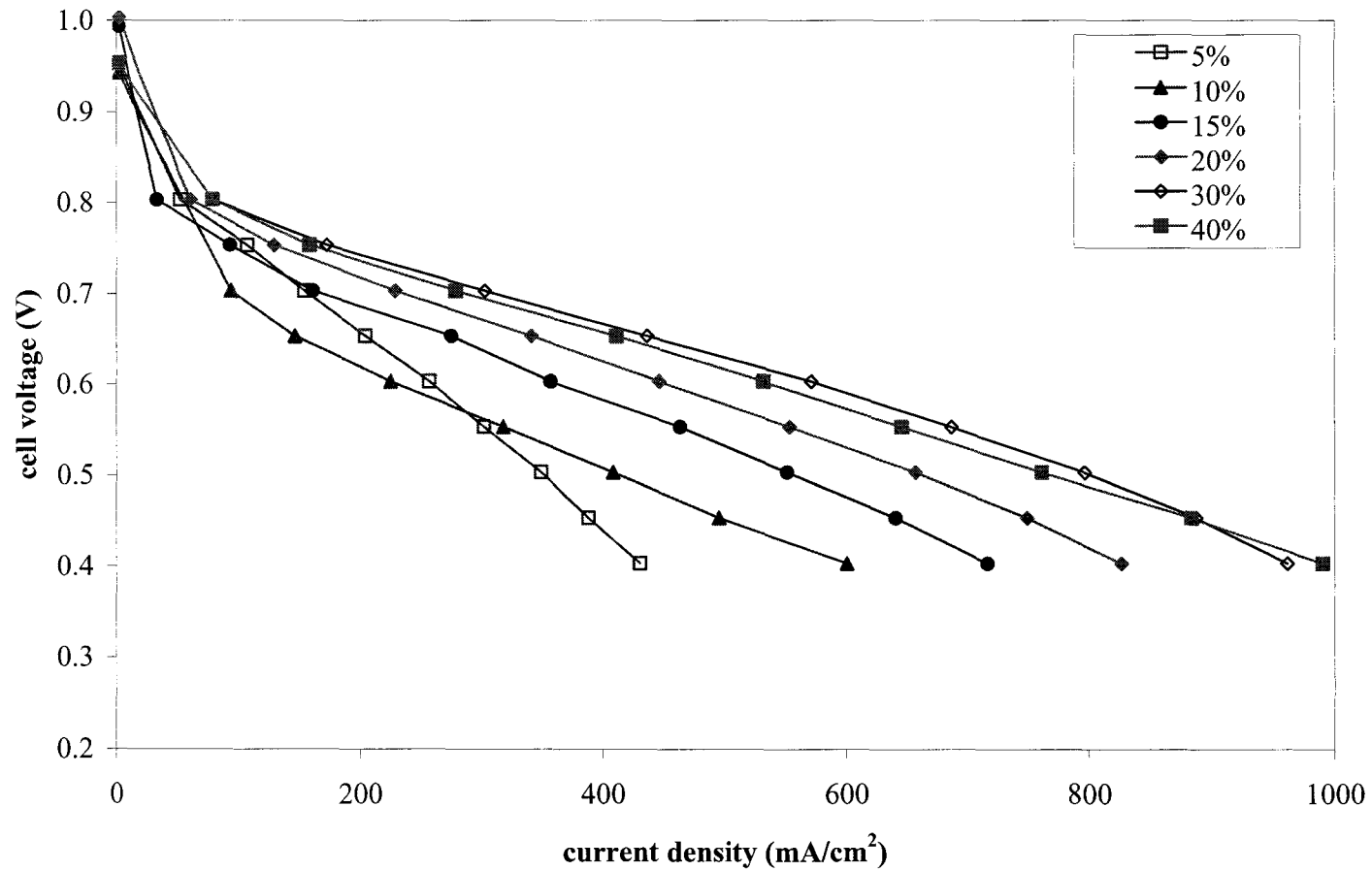


**Figure 4.9:** Fuel cell polarization curves at 35°C for the untreated catalysts at various Nafion loadings.

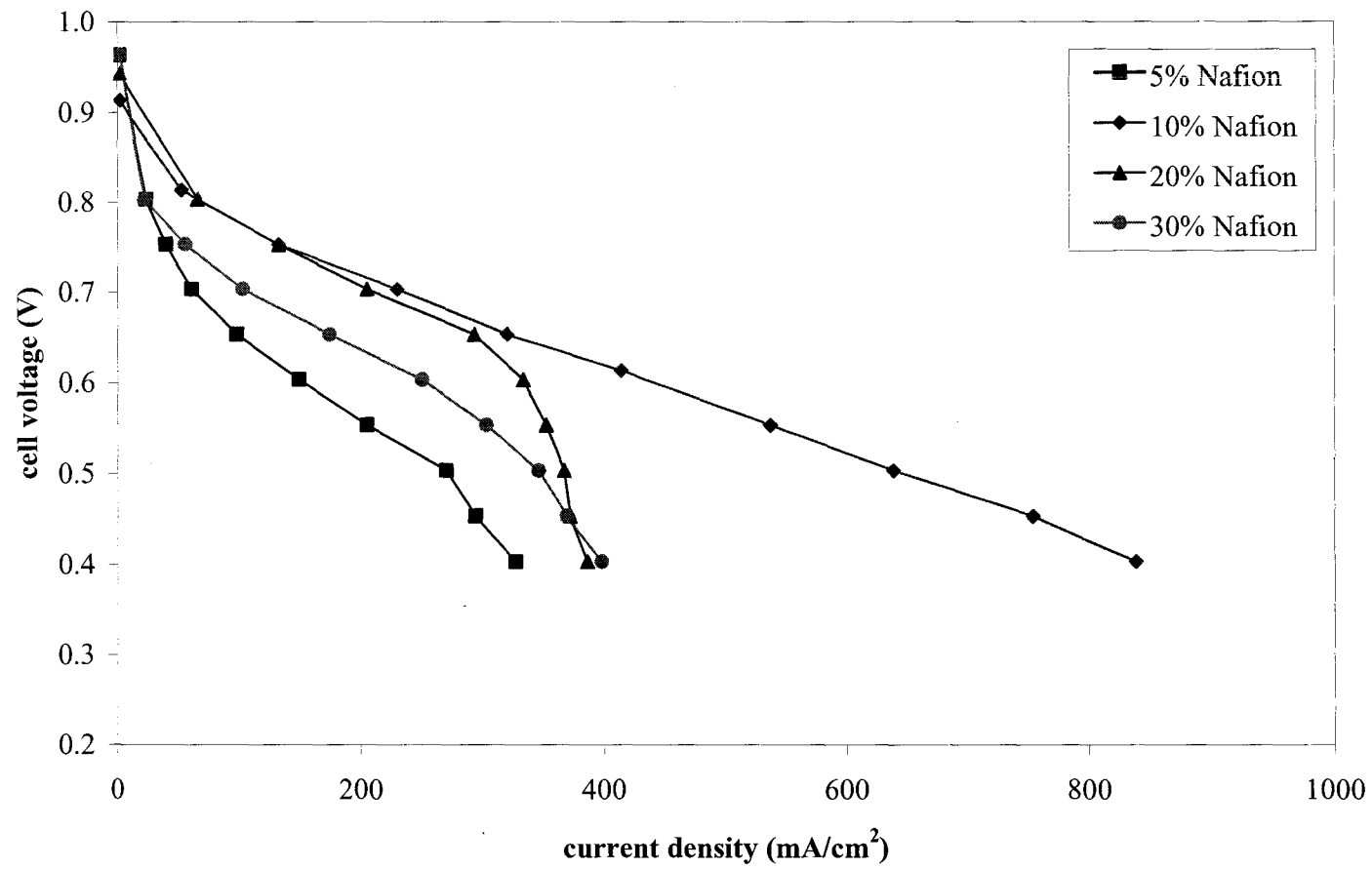
performance at Nafion loadings higher than 30%, which can be attributed to mass transport issues or increased electronic resistance in the catalyst layers.<sup>16</sup>

Figure 4.10 illustrates fuel cell performances achieved using the treated catalyst at various Nafion loadings. From this, we see that peak performance was achieved at 10% Nafion. At Nafion loadings higher than 10%, there was a steady decline in performance, most likely due to flooding. Performance was also meager when less than 10% Nafion was employed.

Figure 4.11 illustrates the fuel cell performances achieved using the pretreated catalyst at various Nafion loadings. Similar to the treated catalyst, peak performance was achieved at 10% Nafion. Also, at Nafion loadings other than 10%, there was a steady decline in performance.

#### **4.4.2 Discussion**

Knowing the optimal Nafion loading (10%) for both silane modified catalysts, they can now be compared with the untreated catalyst. Figure 4.12 shows polarization curves for all three catalysts at a 10% Nafion loading. From this it can be seen that both modified catalysts outperformed the untreated catalyst and that the pretreated catalyst exhibits better performance than the treated catalyst. For comparison, a polarization curve for the untreated catalyst at 30% Nafion (the best performing mixture for the untreated catalyst) is also plotted in Figure 4.12. It can be seen that the performance of the pretreated catalyst at 10% Nafion was comparable to that of the untreated catalyst at 30% Nafion. This similarity in performance shows significant promise for the silane treatment



**Figure 4.10:** Fuel cell performances at 35°C of the treated catalyst with various Nafion loadings.

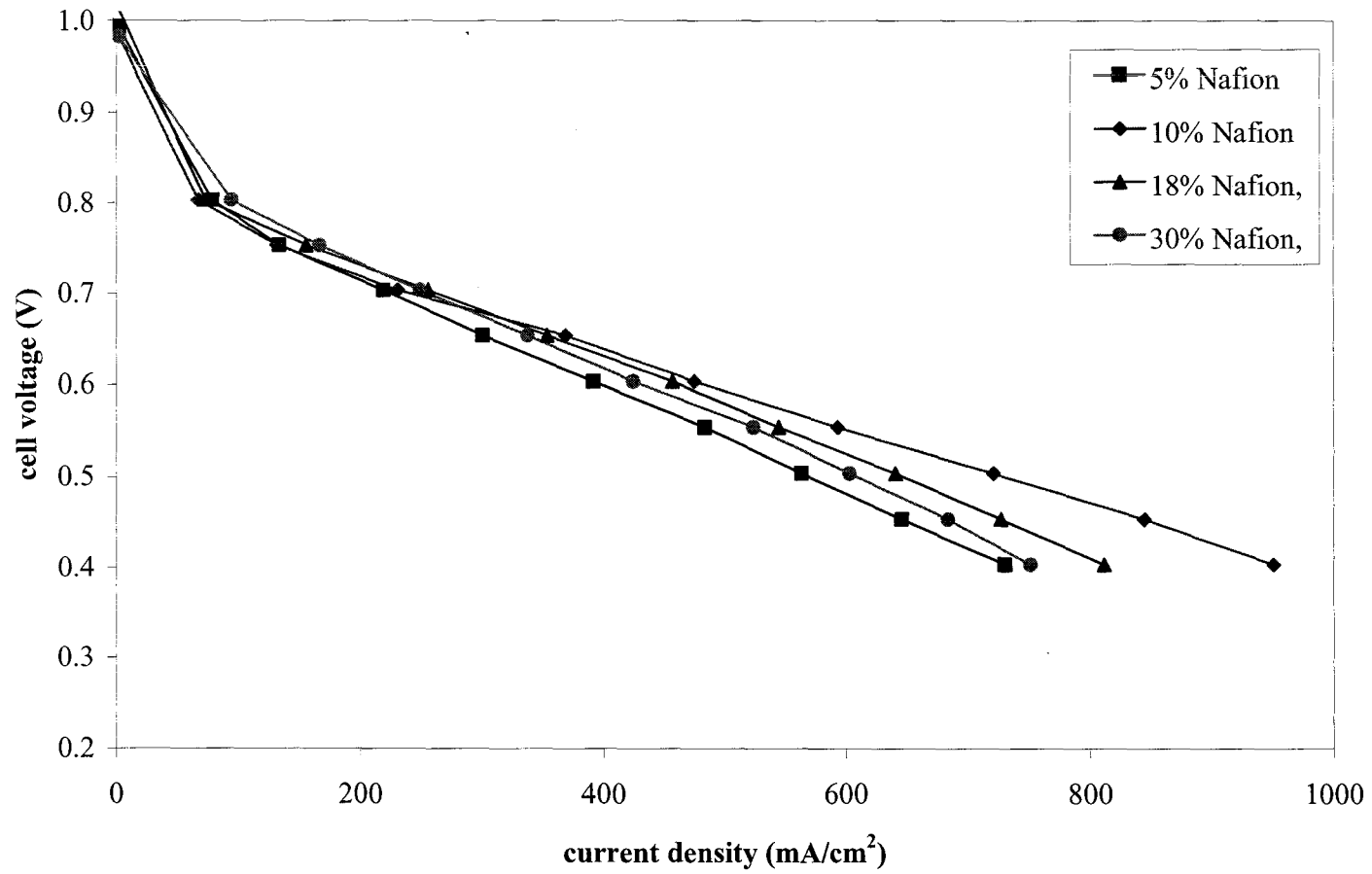
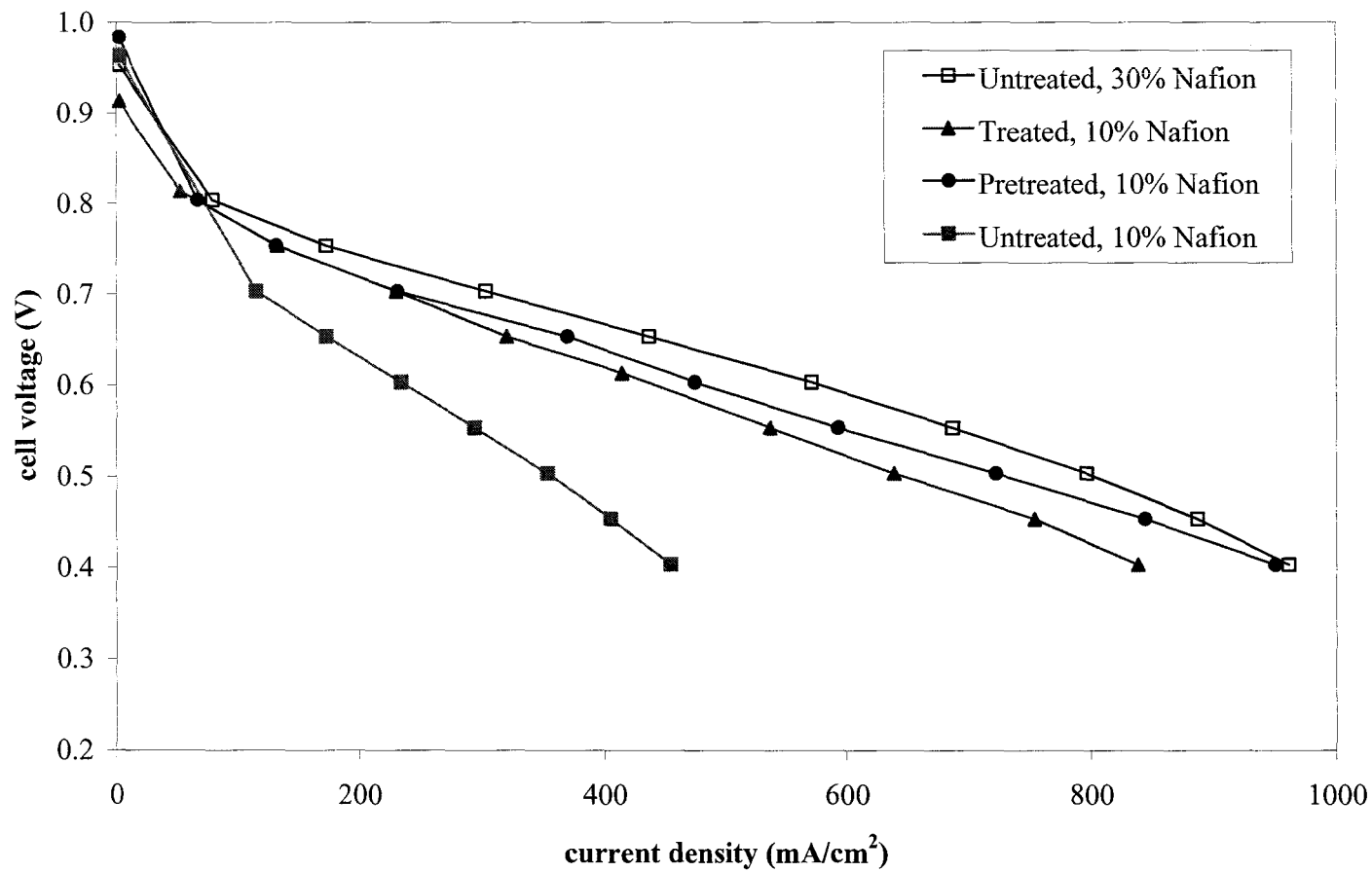


Figure 4.11: Fuel cell performances at 35°C of the pretreated catalyst with various Nafion loadings.



**Figure 4.12:** Fuel cell polarization curves at 35°C for all catalysts at 10% Nafion loading, and the untreated catalyst at 30% Nafion loading.

method because it leads to a two-thirds reduction in the amount of Nafion required in the catalyst layer.

The similarity in the performances of the two catalyst systems can be explained by comparing the total loadings (or concentrations) of sulfonate groups. For simplicity, the current density at 0.50 V vs. the Nafion loading is plotted in Figure 4.13.

EDX analysis of the Pt to Si ratio of the modified catalysts enabled estimation of the silane loading in the catalyst layers. Knowing this and the number of sulfonate groups from the Nafion in the catalyst layer, total sulfonate loadings were determined. This permitted comparison of performance as a function of sulfonate loading, shown in Figure 4.14. From this it can be seen that for all three catalysts, the performance increased with sulfonate loading up to a maximum at ca.  $1.3 \times 10^{-7}$  mol/cm<sup>2</sup> before it began to decline. Therefore, the major reason for the superior performance of the modified catalysts at low Nafion loadings would appear to be the increased proton conductivity from the silane anchored sulfonate groups.

Differences in the average Pt particle size of each catalyst has been ignored in this discussion because of the weak dependence observed for performance on Pt loading, and the fact that the lower dispersion of the Pt on the pretreated carbon is partly compensated by the higher Pt loading (23 vs. 18% measured for the untreated catalyst).

The difference in performance between the treated and pretreated catalysts can most likely be attributed to a lower active Pt area for the treated catalyst due to blocking of some of the active sites by the silane. The silane can bind onto the surface of Pt and

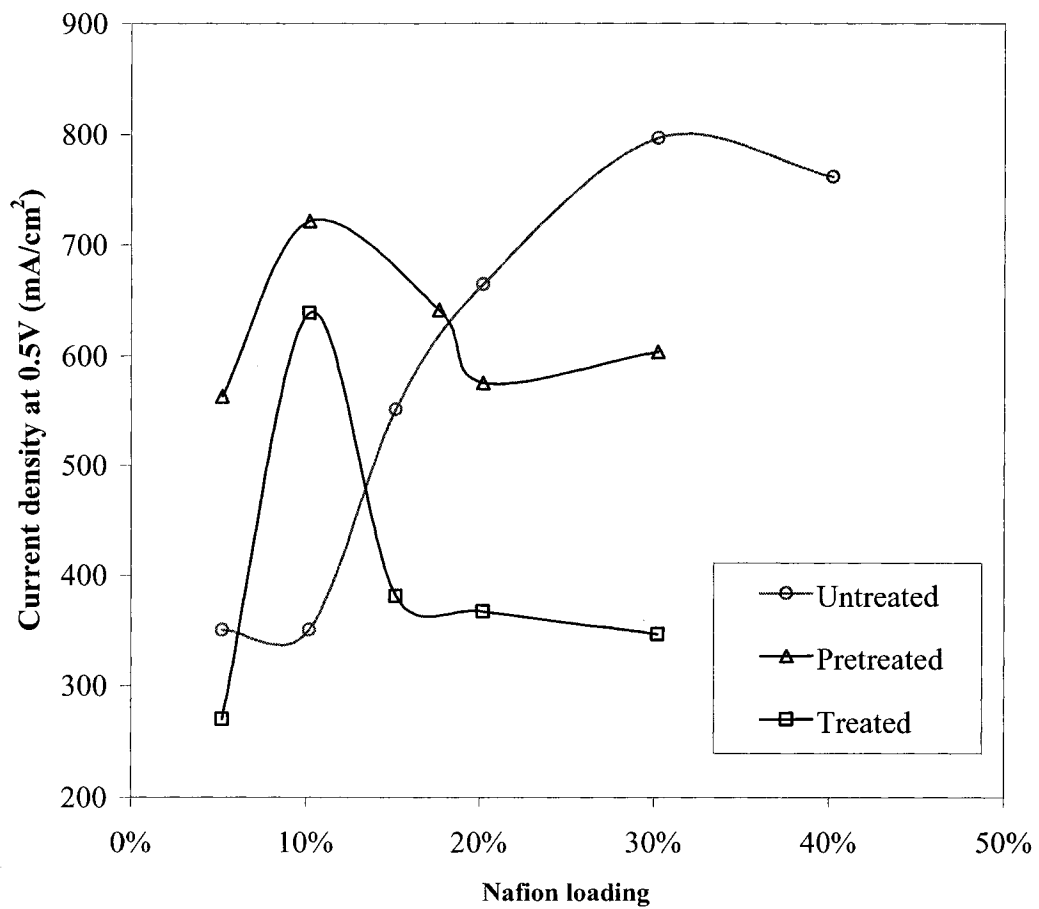


**Figure 4.13:** Variation of fuel cell performance at 35°C with Nafion loading.

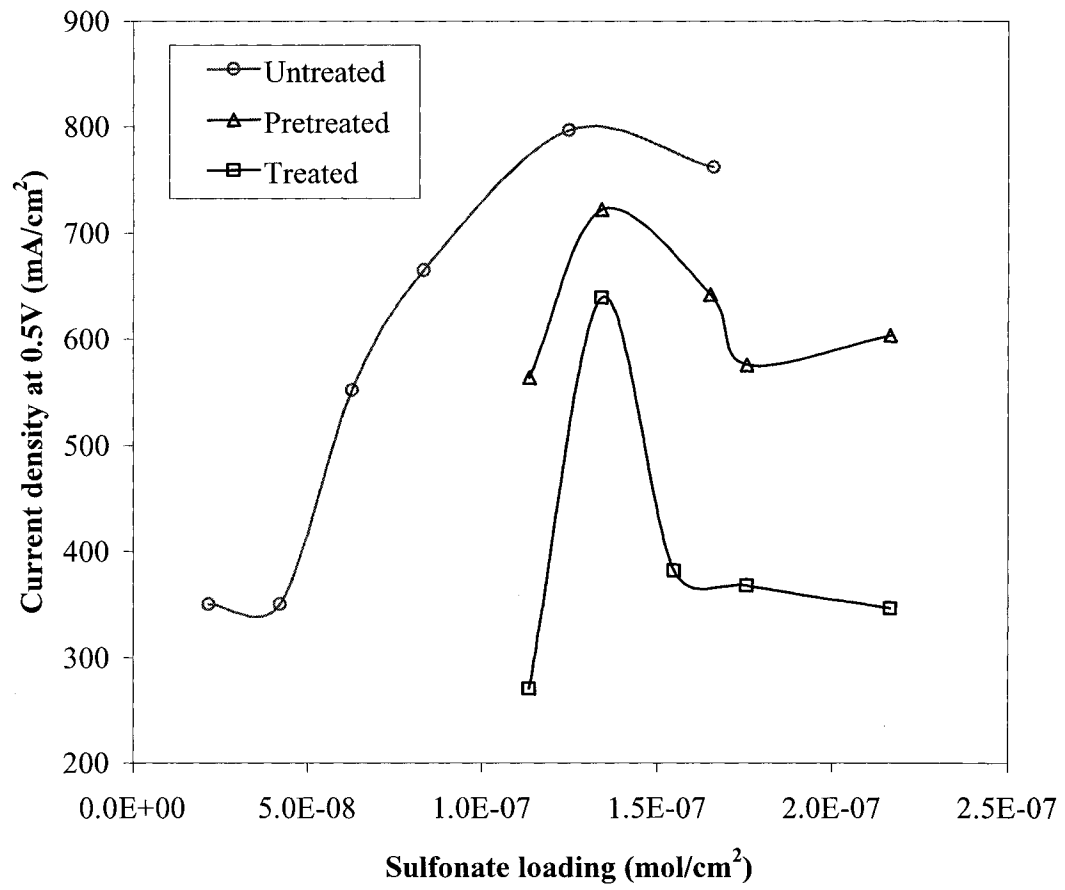


**Figure 4.14:** Variation of fuel cell performance at 35°C with sulfonate loading.

potentially block sites that would be electrochemically active. Also, the treated catalyst was much more susceptible to flooding. This may again be due to the fact that some Pt sites are covered by the silane monolayer. The sulfonate groups are extremely hydrophilic, attracting water that can cover (*i.e.* flood) the Pt particles. This type of localized flooding is much more unlikely for the pretreated catalyst since Pt was deposited after the silane monolayer.

During the course of these experiments there was no indication that the modified catalysts were unstable (*i.e.*, there were no performance losses). Experiments often extended over 2 days (minimum 12 h of fuel cell operation), and routinely involved temperature excursions to 75°C for periods of several hours. In fact, the same performance trends were observed at 75°C and 35°C. Figure 4.15 illustrates the performance of all catalysts at 10% Nafion loading at 75°C (95°C humidified hydrogen, 20 PSI backpressure/ 90°C humidified air, 20 PSI backpressure) and the untreated catalyst at 30% Nafion. As at 35°C, the pretreated and treated catalyst outperformed the untreated at 10% Nafion loadings, and the pretreated at a 10% Nafion loading performed similarly to the untreated at 30% Nafion.

#### **4.5 Application of the Sulfonated Silane onto Preformed Electrodes**

The work described above explored treating the catalyst with the sulfonated silane before electrodes were formed. However, it is quite common to apply the proton conducting ionomer after the electrodes are formed. This is most often done when PTFE is incorporated into the catalyst layer to aid water management. When PTFE is used, the

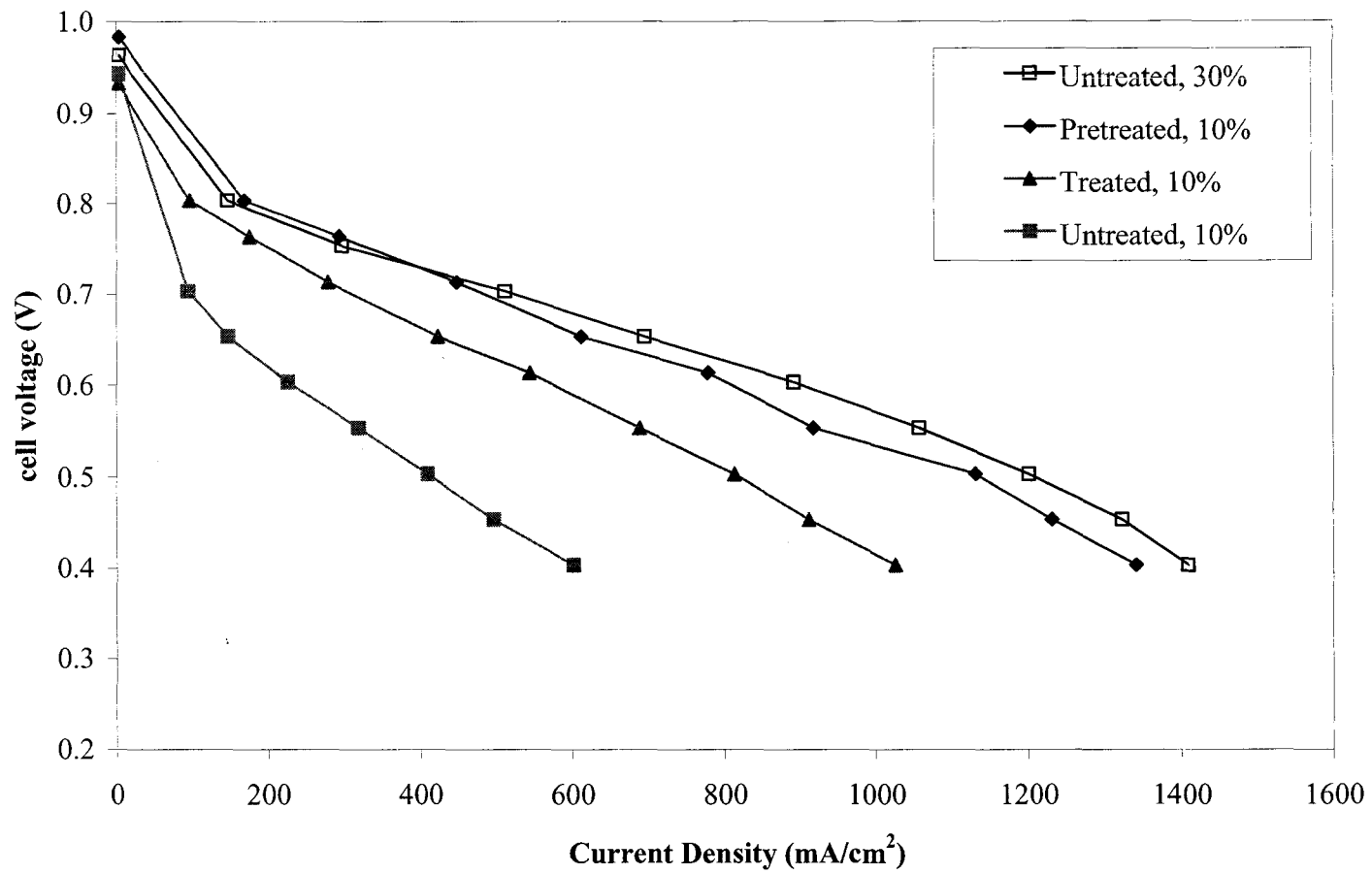


**Figure 4.15:** Fuel cell polarization curves at 75°C for all catalysts at 10% Nafion loading, and the untreated catalyst at 30% Nafion loading.

electrodes are sintered at ca. 350°C. At such a temperature, sulfonate groups (on Nafion or the silane) would be lost. Therefore these proton conductors can only be added after sintering. We have therefore tested the effect of applying the sulfonated silane to preformed electrodes.

A dilute solution (ca. 5%) of the sulfonated silane was brushed onto sintered PTFE bound Pt black electrodes (1.7 mg/cm<sup>2</sup>, no Nafion), followed by a small amount of acetone. The electrodes were then dried for 30 minutes at both room temperature and 135°C. The sulfonated silane loading was determined gravimetrically. Nafion solution (5%) was also applied by the same method for comparison.

MEAs were made for single-cell testing (10 cm<sup>2</sup>) by hot pressing the electrodes across a Nafion 112 membrane with a sintered PTFE bound Pt black (1.7 mg/cm<sup>2</sup>) electrode as the anode.

As can be seen from Figure 4.16, cell performance increased with the amount of sulfonated silane applied, and it reached values significantly higher than for an electrode without any sulfonated silane (or Nafion) applied. The largest sulfonated silane level studied was 3.3 mg/cm<sup>2</sup> and this performed almost as well as the electrode with 1.6 mg/cm<sup>2</sup> of Nafion brush applied.

Unfortunately, we were not able to study levels of sulfonated silane greater than 3.3 mg/cm<sup>2</sup> due to an excessive amount of gel formation. Since the sulfonated silane is moisture sensitive, application of large amounts is quite difficult since a gel rapidly forms on the outer surface of the electrode. Nevertheless, the formation of gel material within the electrode may be beneficial. Recent reports tout “carbon-ceramic electrodes” as

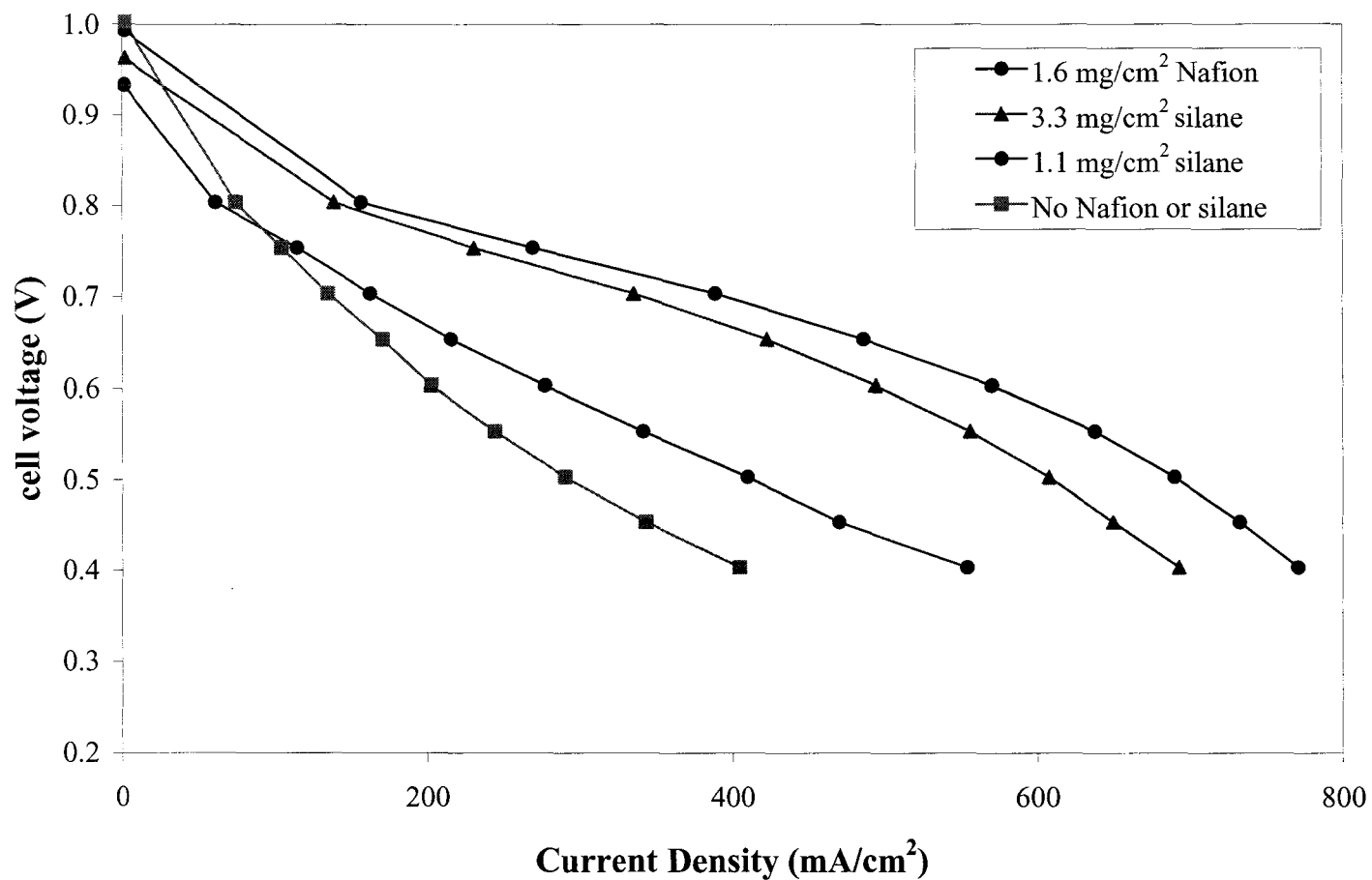


**Figure 4.16:** Comparison of fuel cell polarization curves at 35°C obtained with various amounts of sulfonated silane or Nafion brush applied onto preformed electrodes (Pt= 1.7 mg/cm<sup>2</sup>).

promising candidates for fuel cell electrodes due to their porous structure and robust characteristics.<sup>17,18</sup>

The loadings of sulfonated silane are much larger here than when attached directly to the surface (as in Section 4.2-4.4). This was partially due to the fact that attachment method described in Section 4.2 leads to only a monolayer of silane on the catalyst surface. This large quantity of sulfonated silane material did not appear to cause significant mass transport issues, most likely since the gel formed was sufficiently porous.

#### **4.6 Conclusions**

Surface modification of PEMFC catalysts with sulfonated groups allows them to outperform their untreated counterparts at low Nafion loadings (<15%). Modification of the carbon support before Pt deposition was more effective than modification of precatalyzed carbon, presumably because of blocking of active Pt sites in the latter case. At optimal Nafion loadings, the pretreated catalyst and the untreated catalyst perform similarly, yet the pretreated catalyst requires the use of only one-third the quantity of Nafion in the catalyst layer. Although there is a difference in Nafion loading, the sulfonate loading for each is similar; hence proton conductivity and performance are similar. This is promising in that proton conductivity, and not the source of proton conductivity, exerts the most influence over fuel cell performance. Therefore, less expensive proton conductors could be used in the catalyst layer without sacrificing performance.

There is also much promise for applying the sulfonated silane to preformed electrodes as it resulted in a steady increase in performance in preliminary experiments. However, the application of large amounts of silane resulted in gel formation on the outer surface of the electrode. Optimization of this strategy can be expected to result in high performance carbon-ceramic electrodes for fuel cells.

## References

- 
- <sup>1</sup> Lee, S. J.; Mukerjee, S.; McBreen, J.; Rho, Y. W.; Kho, Y. T.; Lee, T. H. *Electrochim. Acta* **1998**, 43, 3693.
- <sup>2</sup> Cheng, X. L.; Yi, B. L.; Han, M.; Zhang, J. X.; Qiao, Y. G.; Yu, J. R. *J. Power Sources* **1999**, 79, 75.
- <sup>3</sup> Murray, R. W. *Electroanal. Chem.* **1984**, 13, 191.
- <sup>4</sup> Lev, O.; Wu, Z.; Bharathi, S.; Glezer, V.; Modestov, A.; Gun, J.; Rabinovich, L.; Sampath, S. *Chem. Mater.* **1997**, 9, 2354.
- <sup>5</sup> Easton, E. B.; Pickup, P. G. *Electrochem. Solid-State Lett.* **2000**, 3 359-361.
- <sup>6</sup> Gautier-Luneau, I.; Denoyelle, A.; Sanchez, J. Y.; Poinsignon, C. *Electrochim. Acta* **1992**, 37, 1615.
- <sup>7</sup> Lefebvre, M. C.; Qi, Z.; Pickup, P. G. *J. Electrochem. Soc.* **1999**, 146, 2054.
- <sup>8</sup> Radmilovic, V.; Gasteiger, H. A.; Ross, P. N., Jr. *J. Catal.* **1995**, 154, 98-106.
- <sup>9</sup> Marti, I.; Ishizaki, C. *Carbon* **1981**, 18, 109.
- <sup>10</sup> Studebaker, M. L.; Rinehart, R. W. *Rubber Chem. Technol.* **1972**, 45, 106.
- <sup>11</sup> Smith, R. N.; Young, D. A.; Smith, R. A. *Trans. Faraday Soc.* **1966**, 62, 2280.
- <sup>12</sup> Brown, J. K. *J. Chem. Soc.* **1955**, 744.
- <sup>13</sup> Brown, J. K. *J. Chem. Soc.* **1955**, 752.
- <sup>14</sup> O'Rielly, J. M.; Mosher, R. A. *Carbon* **1983**, 21, 47.
- <sup>15</sup> Kinoshita, K. *Carbon: Electrochemical and Physicochemical Properties*; Wiley: New York, 1988.
- <sup>16</sup> Li, G.; Pickup, P. G. *In Preparation*

---

<sup>17</sup> Anderson, M. L.; Stroud, R. M.; Rolison, D. R. *Nano Letters* **2002**, 2, 235-240.

<sup>18</sup> Rabinovich, L.; Lev, O. *Electroanalysis* **2001**, 13, 265-275.

## **Chapter 5**

### **Development of Direct Methanol Fuel Cell Membrane and Electrode Assemblies**

## **5.1 Introduction to Direct Methanol Fuel Cells**

The challenges presented when designing direct methanol fuel cell (DMFC) electrodes are quite different than those of typical H<sub>2</sub>/air electrodes. For example, a Pt/Ru catalyst is usually used for methanol oxidation (as opposed to just Pt). Also, the methanol fuel is typically delivered via an aqueous solution, typically at a concentration of 1 M. This essentially floods the anode catalyst layer. In addition, both the methanol and water can diffuse through the membrane and into the cathode. While this ensures good hydration (and hence good proton conductivity) in the membrane, it also leads to poisoning of the cathode catalyst and flooding of the cathode. Because of these differences, new electrodes (with different electrode formulations) must be prepared. The objectives of the work described in this chapter were to optimize the structure and composition of DMFC electrodes and to determine the optimum Nafion membrane thickness for use in a DMFC.

## **5.2 Anode Optimization**

### **5.2.1 Introduction**

MeOH oxidation is a complicated process; it has many steps and many intermediates. The presence of poisoning CO intermediates requires the use of a bi-metallic catalyst, typically Pt/Ru. Increasing the activity of this system and reducing the precious metal loading are of paramount importance for commercialization. The optimization of a DMFC anode prepared using a commercially available Pt/Ru black catalyst was thus explored.

### 5.2.2 Electrode and MEA Preparation

Pt/Ru Black (1:1 atomic ratio, Johnson-Matthey) was thoroughly stirred with water, isopropyl alcohol (ca. 1:1 mass ratio, water was added first to avoid burning of the alcohols), and 5% Nafion solution for several hours, sonicated for 30 minutes followed by 15 minutes of mixing using a high-speed homogenizer. The mixture was then stirred again for 10 minutes before spray application to the electrode backing. After catalyst application, the electrode was dried for 30 minutes at both room temperature and 135 °C.

Membrane and electrode assemblies (MEA) were prepared by hot-pressing the anode onto a Nafion 117 membrane with a Pt black cathode (1.7 mg/cm<sup>2</sup>). MEA's were tested in a 25cm<sup>2</sup> fuel cell (Fuel Cell Technologies) at 60 °C. Anode performance was evaluated versus a dynamic hydrogen electrode (DHE, N<sub>2</sub>(g) is passed through the cathode compartment and H<sub>2</sub> evolution occurs), thereby eliminating any effects due to oxygen reduction kinetics at the cathode. MEAs were run for ca. 3 hours before data was recorded. Polarization curves were obtained at constant current using a power supply. Voltages were allowed to stabilize for ca. one minute before readings were taken.

### 5.2.3 Anode Electrode Backing

Initially, 3 different anode electrode backings were tested; plain 6 mil Toray carbon fiber paper (CFP), 6 mil plain Toray CFP with a 1 mg/cm<sup>2</sup> 20% Nafion/Carbon sub-layer, and 6 mil plain Toray CFP impregnated with 20% Nafion. The treated CFPs were prepared by spray applying either the 20% Nafion/Carbon ink or a 5% Nafion solution, onto the plain CFP. Nafion solution was sprayed onto both sides of the CFP

while the 20% Nafion/Carbon ink was applied only onto one side (to which the catalyst would be applied). After treatment, the backings were dried for 30 minutes at both room temperature and 135 °C.

As illustrated in Figure 5.1, the Nafion impregnated CFP yielded the best anode performance, CFP with a 1 mg/cm<sup>2</sup> 20% Nafion/Carbon sublayer produced the next best anode performance, and plain Toray CFP gave the worst anode performance.

Impregnating Nafion into the CFP may prevent the catalyst from penetrating deeply into the backing when applied, thereby increasing catalyst utilization. Also, Nafion imparts some hydrophilicity into the CFP, enhancing the diffusion of MeOH and water through the backing. It should also be noted that impregnation of Nafion into CFP has not been previously reported in the scientific literature. However, Zhang *et al.* have recently been granted a patent for this technique.<sup>1</sup> They claim that the treated paper allows for better transfer of methanol and also prevents the catalyst ink from penetrating into the backing, thereby increasing catalyst utilization.

The Nafion/Carbon sub-layered backing performed similarly to the Nafion impregnated backing. The Nafion impregnated backing outperformed it at low current densities, indicating it has higher catalyst utilization. This may be due to less catalyst penetrating deeply into the backing when applied. At high current densities, the sub-layered backing performs slightly better than the Nafion impregnated backing. This may be due to the increased porosity of the sub-layer.

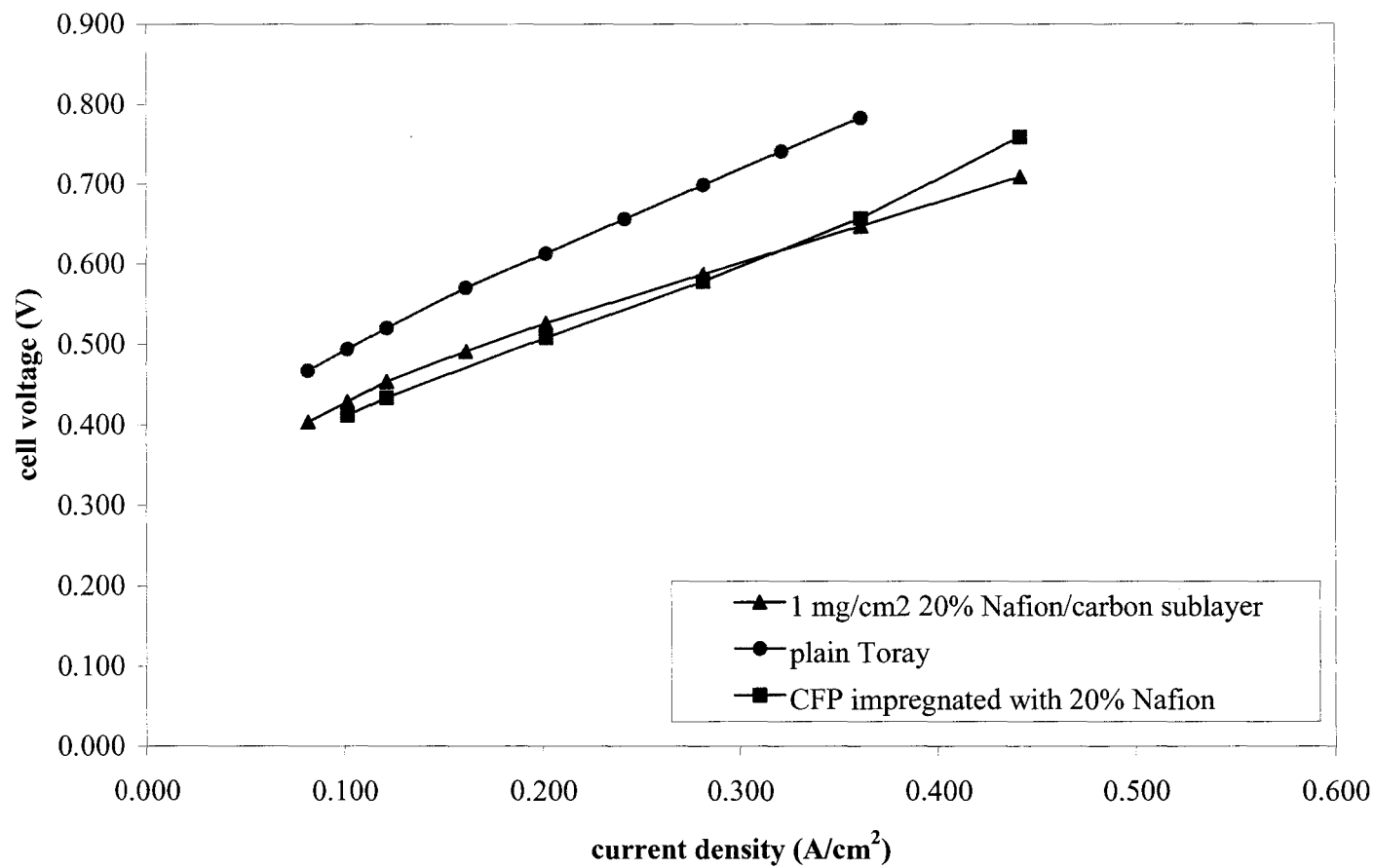


**Figure 5.1:** Anode performances at 60°C achieved using various electrode backings (2 mg/cm<sup>2</sup> Pt/Ru black, 20% Nafion)

The effect of Nafion loading within the CFP was also studied. This was accomplished by impregnating the CFP with Nafion at levels ranging between 13% and 30%. Pt/Ru black electrodes (ca. 4 mg/cm<sup>2</sup>) with ca. 15% Nafion binder were applied to the backings. Maximum performance was achieved at the lowest level tested, 13% Nafion, and decreased slightly as Nafion loading was increased as shown in Figure 5.2. Therefore, the optimum Nafion loading for CFP impregnation was therefore determined to be in the range 10-15%.

#### **5.2.4 Anode Catalyst Loading**

Pt/Ru black electrodes were prepared with Pt/Ru loadings ranging between 1.2 and 10.6 mg/cm<sup>2</sup> with 20% Nafion binder. Performance increased with catalyst loading up to a loading of ca. 4 mg/cm<sup>2</sup>, after which there was no significant gain, as shown in Figure 5.3. Addition of carbon supported Pt/Ru catalyst to the Pt/Ru black mixture was found to decrease performance. Hence, the optimal catalyst loading is ca. 4 mg/cm<sup>2</sup> Pt/Ru black.

#### **5.2.5 Nafion Content in the Anode Catalyst Layer**

Pt/Ru black (4-5 mg/cm<sup>2</sup>) electrodes were prepared with Nafion loadings ranging between 10-30%. The differences in anode performance for each loading were very small, as illustrated in Figure 5.4. A 10-20% Nafion loading was chosen for subsequent work.

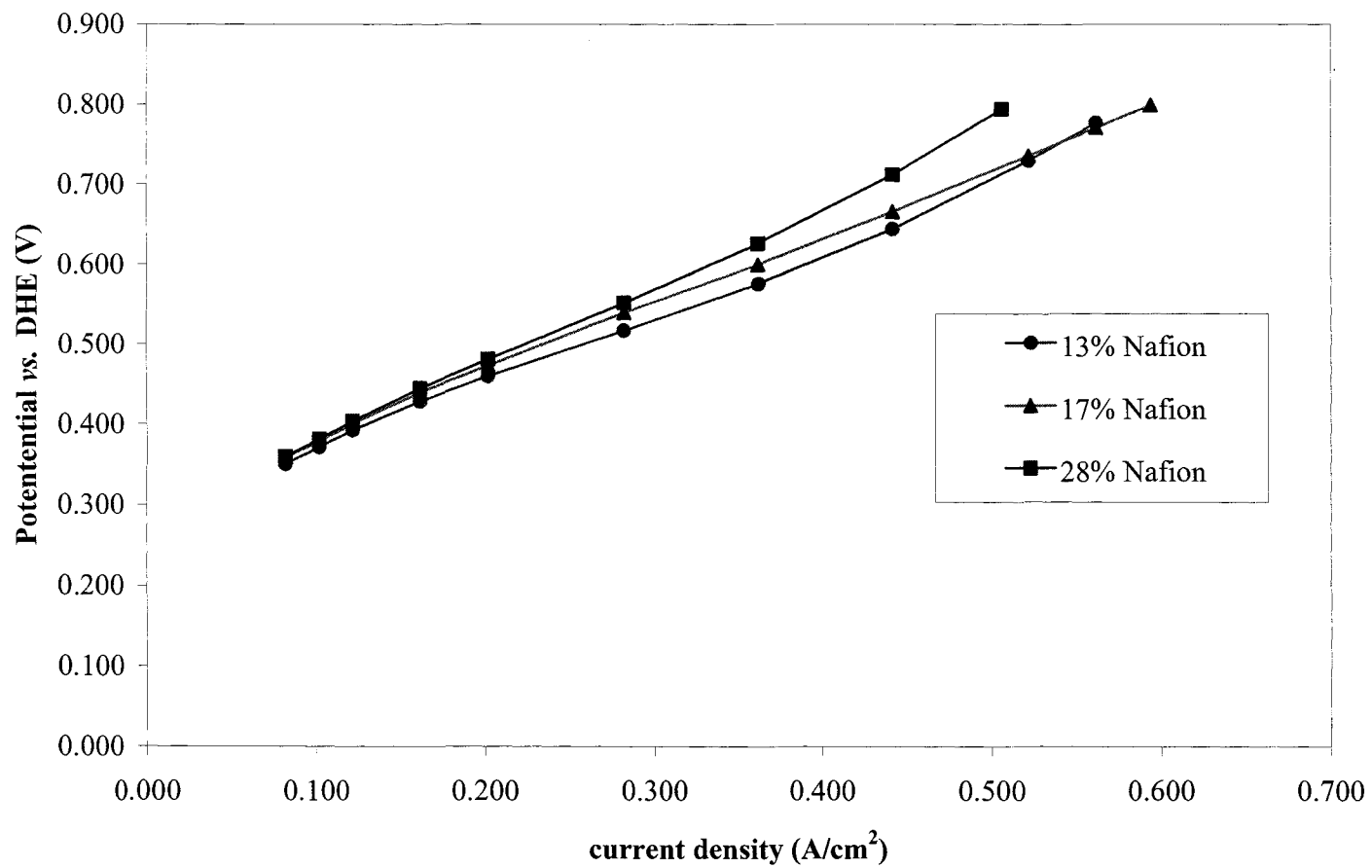
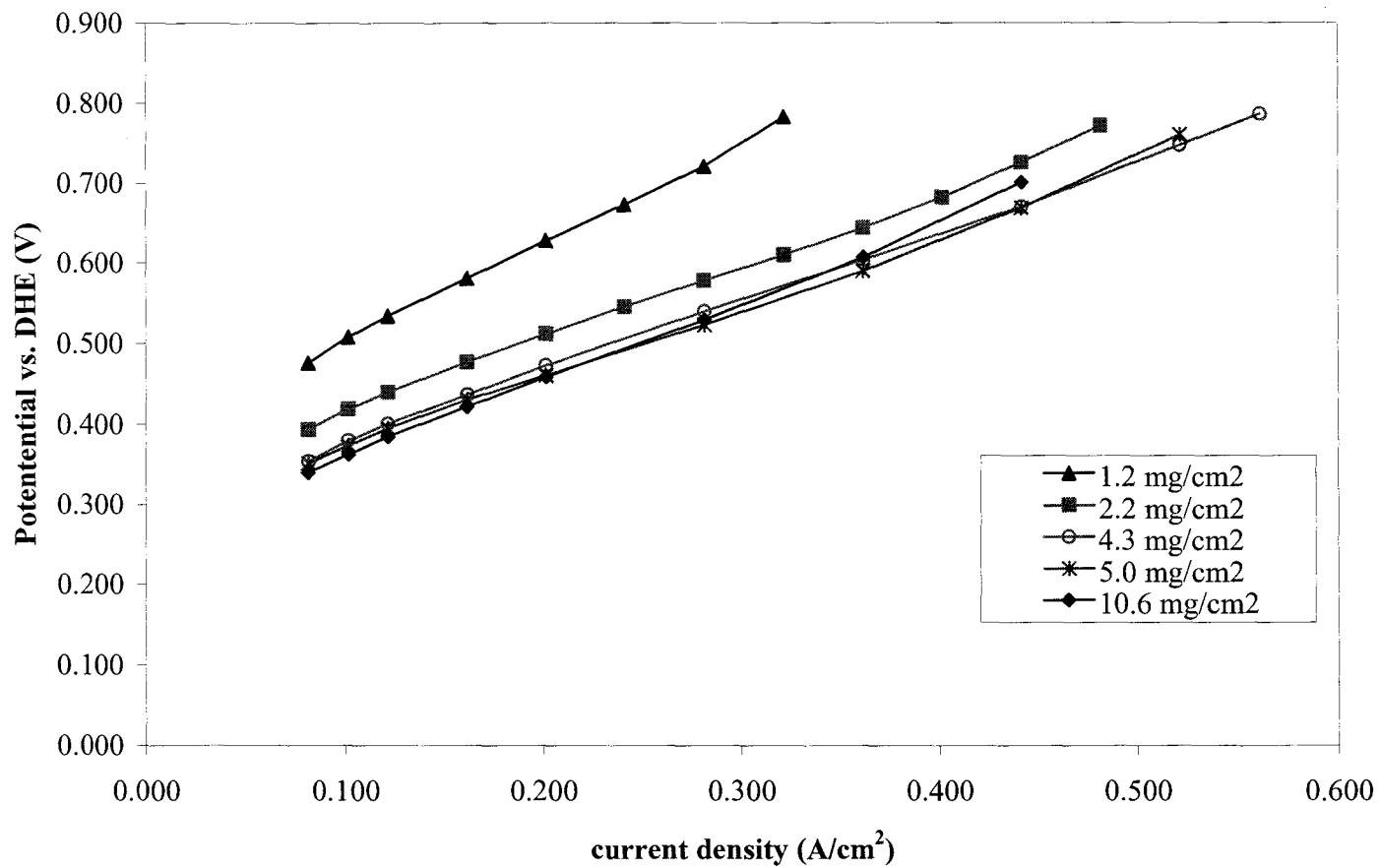
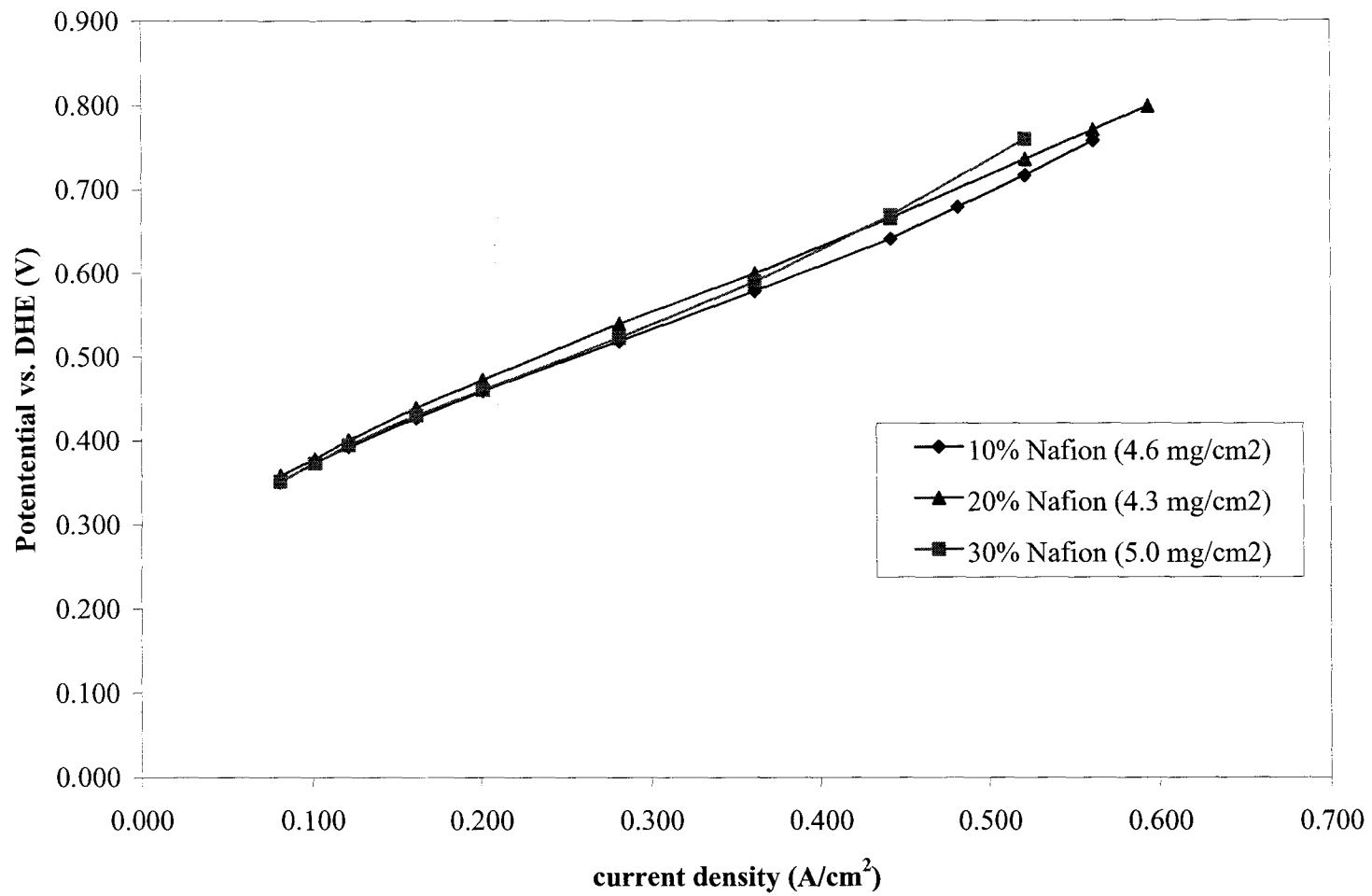


Figure 5.2: Anode performance at 60°C vs. Nafion content in the CFP backing.



**Figure 5.3:** Anode performance at 60°C of electrodes composed of various Pt/Ru loadings (20% Nafion, 6 mil CFP impregnated with 20% Nafion).



**Figure 5.4:** Anode performance at 60°C as a function of Nafion content in the catalyst layer.

### **5.2.6 Optimized Anode Components**

In summary, the optimal anode was found to be composed of ca. 4 mg/cm<sup>2</sup> Pt/Ru black mixed with 10-20% Nafion binder applied onto a 6 mil Toray CFP impregnated with 10-15% Nafion. It should be noted that the effect of CFP thickness was not explored. However, a thicker backing would not be expected to perform better as it may introduce mass transport effects.<sup>2</sup>

## **5.3 Cathode Optimization**

### **5.3.1 Introduction**

Cathode activity is an important, but often ignored, part of a DMFC. The use of an aqueous methanol feed at the anode, and its subsequent crossover into the cathode compartment, can cause a drastic reduction in cathode activity. Not only does this waste fuel but also the presence of methanol at the cathode reduces its performance and long-term activity. Additionally, the crossover of water from the anode feed to the cathode can cause flooding.

In order to circumvent some of these issues, one can optimize the electrode composition. High Pt loadings ( $\geq 4$  mg/cm<sup>2</sup>) are employed to reduce the mixed potential losses (discussed in more detail in Chapter 1). Generally, high airflow rates in conjunction with a highly hydrophobic catalyst layer and electrode backings are employed to enhance water management.

The optimization of a DMFC cathode prepared using commercially available materials was explored.

### 5.3.2 Electrode and MEA Preparation

A 9:1 mass ratio of Pt Black (Fuel Cell grade) and Etek 20% Pt on Black Pearls 2000 (added to aid ink preparation, Black Pearls was chosen due to its high surface area and hydrophilic surface<sup>3</sup>) was thoroughly stirred with water, a 60% PTFE suspension and isopropyl alcohol (water was added first to avoid burning of the alcohols) for several hours, followed by 30 minutes of sonication and 15 minutes of mixing using a high-speed homogenizer. The mixture was then stirred again for 10 minutes before spray application to the electrode backing, 10 mil Toray CFP impregnated with a proprietary “microporous” mixture (previous experiments performed at H Power have shown that the “microporous” CFP is a superior backing).<sup>4</sup> After catalyst application, the electrodes were dried at room temperature, 110 °C, 280 °C, and 360 °C (sintering) for 30 minutes at each temperature. After sintering, Nafion solution was sprayed onto the electrode, which was then dried for 30 minutes at both room temperature and 135 °C.

MEAs were prepared by hot-pressing the cathode across a Nafion 117 membrane with a Pt/Ru black anode (using the optimized formulation from section 5.2.6). MEAs were tested in a 25cm<sup>2</sup> fuel cell (Fuel Cell Technologies) at 60 °C. The cell was run as a DMFC for several hours before data was collected. Polarization curves were obtained at constant current using a power supply. Voltages were allowed to stabilize for ca. one minute before readings were taken.

### **5.3.3 Nafion Content in the Cathode Catalyst Layer**

Cathodes were prepared with a  $4.25 \text{ mg/cm}^2$  Pt loading and 10% PTFE content. After sintering, the electrode sheet was divided into four sections. Nafion solution was sprayed onto each section at various loadings ranging from 0 - 26%. Each cathode was then evaluated in a DMFC.

Figure 5.5 illustrates that performance increased with Nafion loading up to ca. 20% after which performance declined with Nafion loading. A 15-20% Nafion loading was determined to be ideal.

### **5.3.4 PTFE Content in the Cathode Catalyst Layer**

Electrodes were prepared using PTFE loadings between 10 and 30%. After sintering, Nafion solution was sprayed onto the electrode at ca. 15% loading. Figure 5.6 illustrates that the optimal PTFE content is about 10-15%. Slightly lower performance was observed at high and lower loadings.

### **5.3.5 Optimized Cathode Components**

In summary, the optimized cathode was found to be ca.  $4 \text{ mg/cm}^2$  Pt loading mixed with 10-15% PTFE binder applied onto a 10 mil “microporous” Toray CFP, with 15% Nafion (sprayed on after sintering).

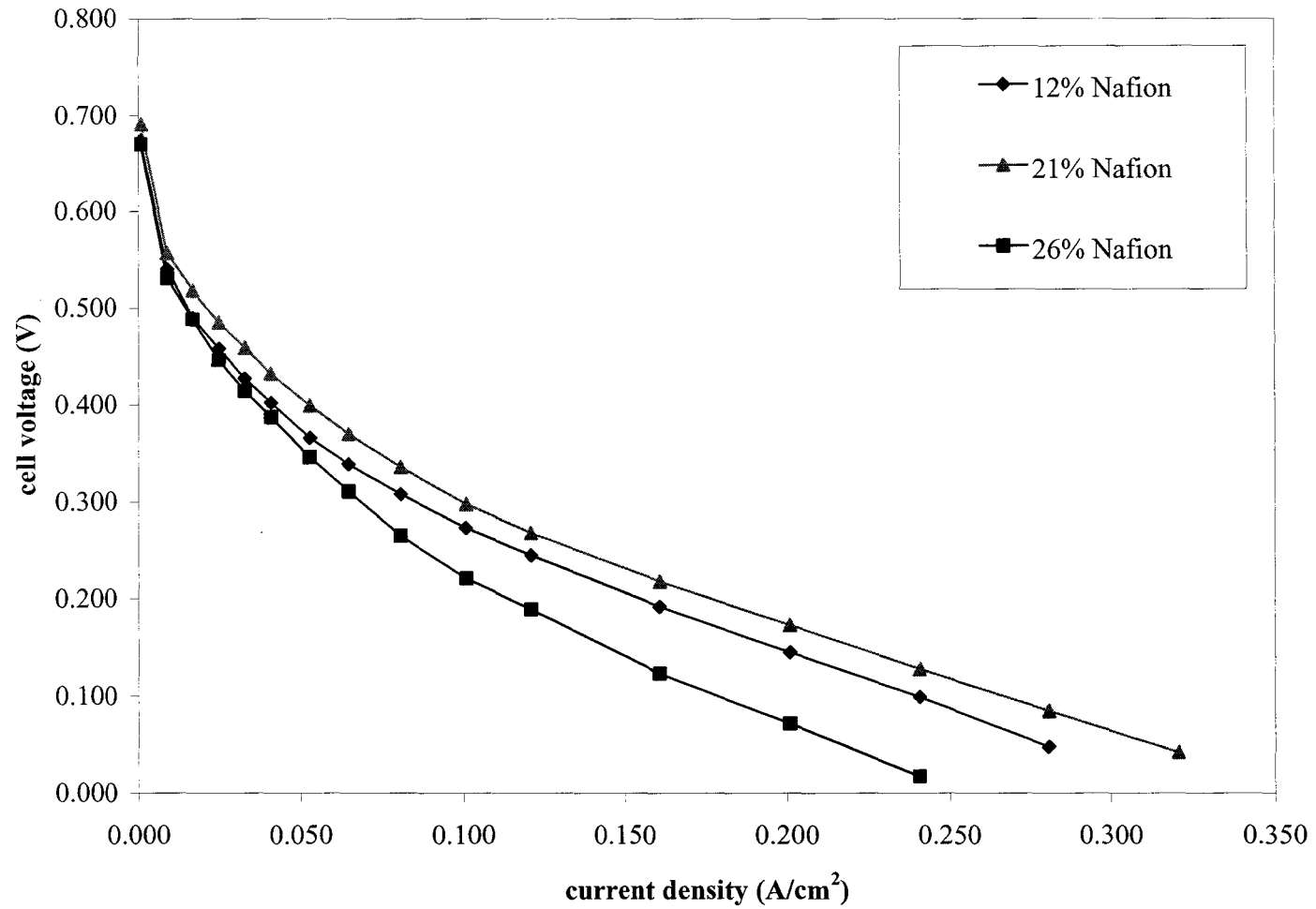


**Figure 5.5:** Effect of cathode Nafion loading on DMFC Performance at 60°C (4.9x air stoichiometry).

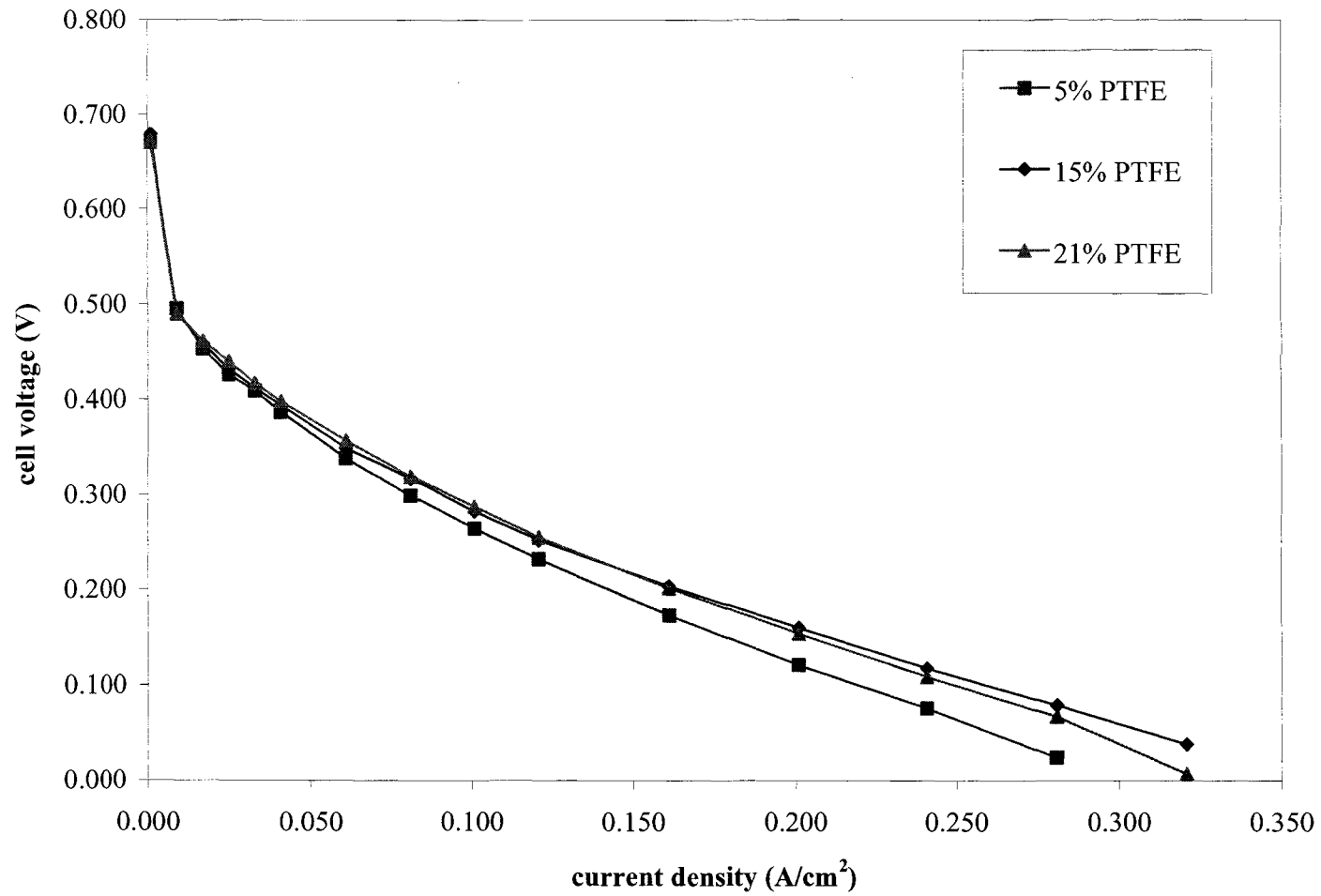


**Figure 5.6:** The effect of cathode PTFE content on DMFC Performance at 60°C (4.9x air stoichiometry).

## 5.4 Nafion Membrane

### 5.4.1 Introduction

With its success in H<sub>2</sub>/Air fuel cells, the proton exchange membrane (PEM) has received much attention for use in DMFCs. The best available PEM to date is Nafion. Nafion is a chemically and thermally durable membrane material that exhibits high proton conductivity. These properties, and the fact that the membranes are thin (ca. 100-200 μm) and lightweight, make them excellent candidates for use in a DMFC. However, Nafion is permeable to methanol (and of course water). This permeability enables methanol to diffuse from the anode to the cathode. This methanol “crossover” can have a drastic effect on cathode performance (see Chapter 1 for more details). Despite these flaws, Nafion is still the best available PEM for use in a DMFC.

The performance characteristics of 1100 equivalent weight (EW) Nafion membranes of varying thickness were evaluated in a DMFC. Experimental conditions and fabrication of electrodes and MEAs were similar to previous studies in this chapter. Briefly, MEAs were prepared by hot pressing optimized anodes and cathodes across each membrane and were then tested in a DMFC at 60 °C. Polarization curves (anode and cell) were obtained at constant current using a power supply. Voltages were allowed to stabilize for ca. one minute before readings were taken.

There is a standard nomenclature to describe Nafion is as follows. The first 2 digits indicate the molecular weight; the last digit(s) indicates the thickness of the membrane in mil (0.001 inches). For example, Nafion 115 is a membrane of 1100 EW and is 5 mil thick.

#### 5.4.2 Anode Performance Using Different Nafion Membranes

As illustrated in Figure 5.7, anode performance increases with decreasing Nafion membrane thickness. The differences in the performances of MEAs made with 115, 1135 & 112 are very small and incremental, mainly due to the differences in ionic resistance. However, the anode performance using Nafion 117 is lower than one would expect. Figure 5.8 illustrates the anode overpotential achieved at  $0.8 \text{ A/cm}^2$  for Nafion membranes of various thicknesses. The variation is highly linear for Nafion 112, 1135 and 115, but Nafion 117 does not follow this trend. In fact, the overpotential is ca. 70 mV larger than one would expect following the trend of the thinner membranes. This unusually low performance of Nafion 117 is reproducible and the best performance achieved is shown. We postulate that this difference may be due to the stress the membrane exerts upon the electrode-membrane interface when the humidification levels changes. When humidification conditions change, Nafion membranes have a tendency to swell or contract. It was often observed when using Nafion 117 that these distortions would cause the anode and/or cathode backings to partially or completely delaminate. This phenomenon was seldom observed for thinner membranes. Since Nafion 117 was the thickest of all membranes tested, it exerts the most force upon the interface when it distorts. This can lead to poor bonding, which may account for the lower anode performance. This delamination phenomenon has been reported in the literature and is believed to increase the contact resistance at the membrane/electrode interface.<sup>5</sup>

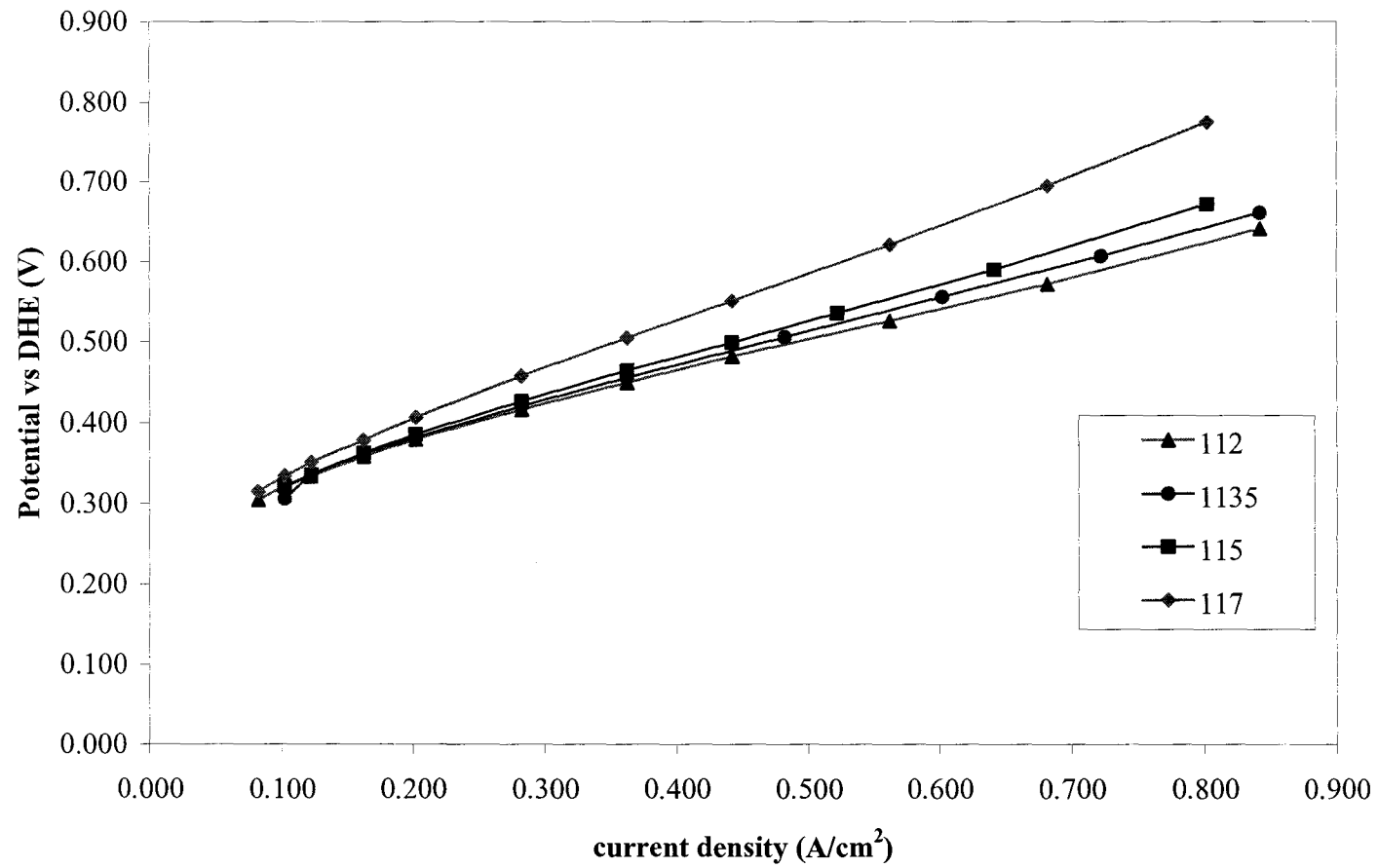
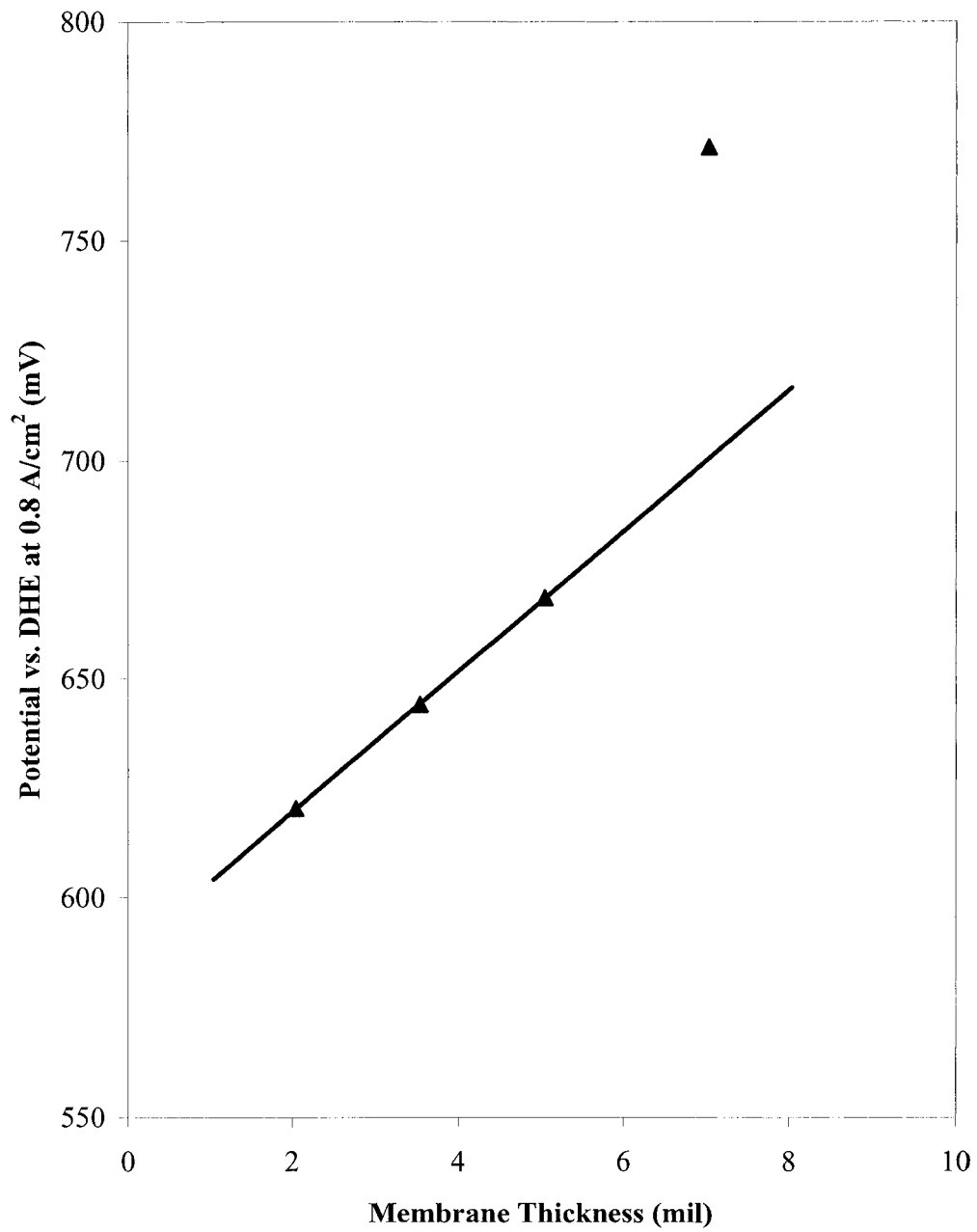


Figure 5.7: Variation of anode performance at 60°C with Nafion membrane thickness.



**Figure 5.8:** Variation of anode performance at 60°C with Nafion membrane thickness.

### 5.4.3 DMFC Performance Using Different Nafion Membranes

Figure 5.9 shows the DMFC performance of various Nafion membranes at 60 °C when low air flows (159 mL/min, ca. 1.7x air stoichiometry) are used. Nafion 115 exhibited slightly better DMFC performance compared to Nafion 1135 at high current densities, and was far superior to 112. However, when very high air flow rates (520 mL/min, ca. 4.9x air stoichiometry) are used, Nafion 1135 is slightly better than 115. This is shown in Figure 5.10. Also, Nafion 112 gave similar performance to 1135 except that it was slightly worse at high current densities. These trends can be explained by the fact that there is better water removal from the cathode at higher air flows. Hence, when using the thinner membrane at lower air flow rates, flooding (and methanol crossover) causes a decrease in cathode performance.

Surprisingly, Nafion 117 was by far the poorest performer. This may be related to the poor bonding issue discussed in the previous section.

### 5.4.4 Methanol Crossover of Different Nafion Membranes

The limiting methanol crossover current,  $j_{\text{lim}}$ , was measured by passing nitrogen through the cathode compartment and increasing the cell voltage to 0.85 V. Under these conditions, methanol can only be oxidized at the cathode and must first diffuse through the membrane (see Section 2.2.3 for more details).<sup>6</sup> Since the membrane is a diffusion barrier,  $j_{\text{lim}}$  is related to membrane thickness,  $d$ , by the following equation:

$$j_{\text{lim}} = k_{dl} \frac{nFAD_m C_m}{d} \quad \text{Eq. 5.1}$$

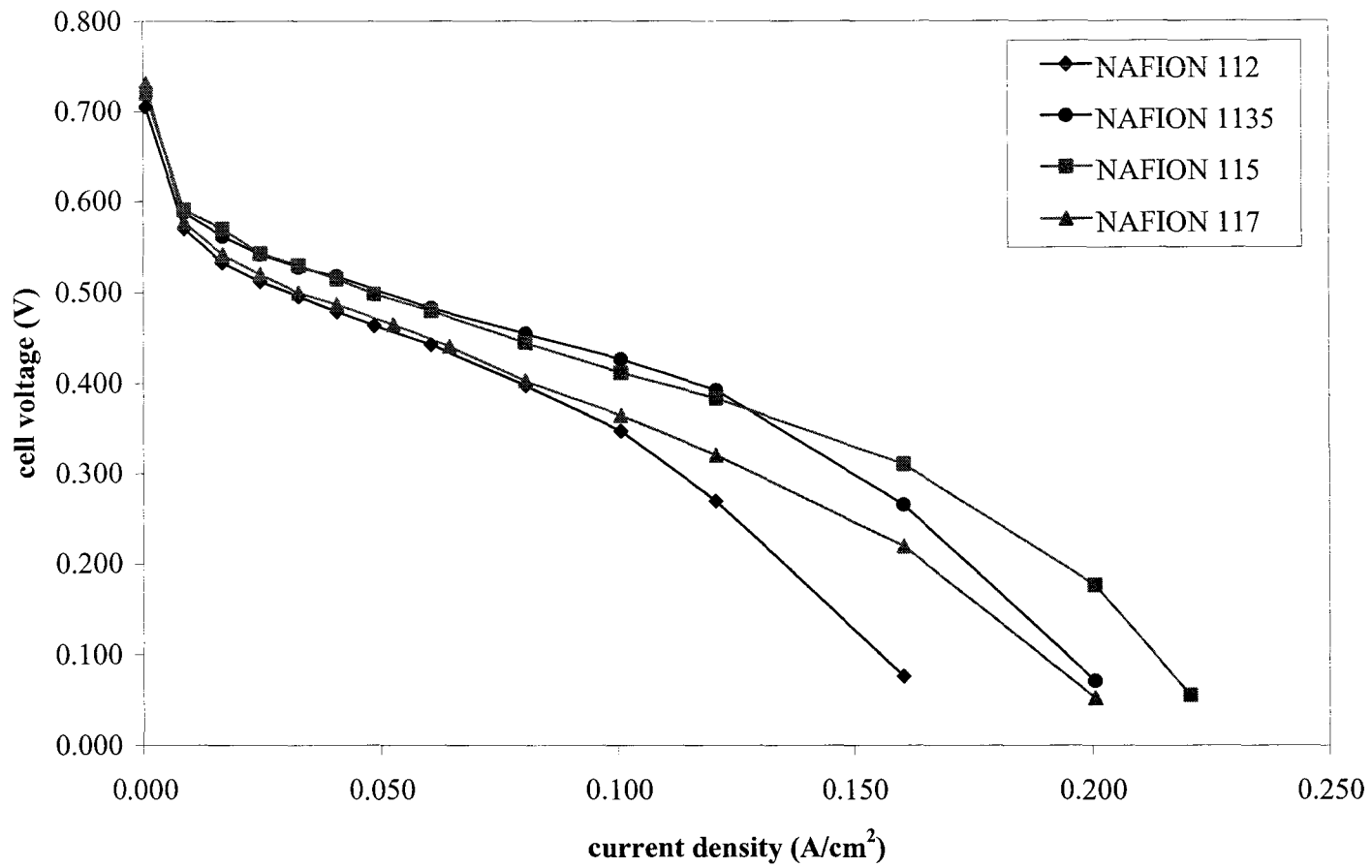
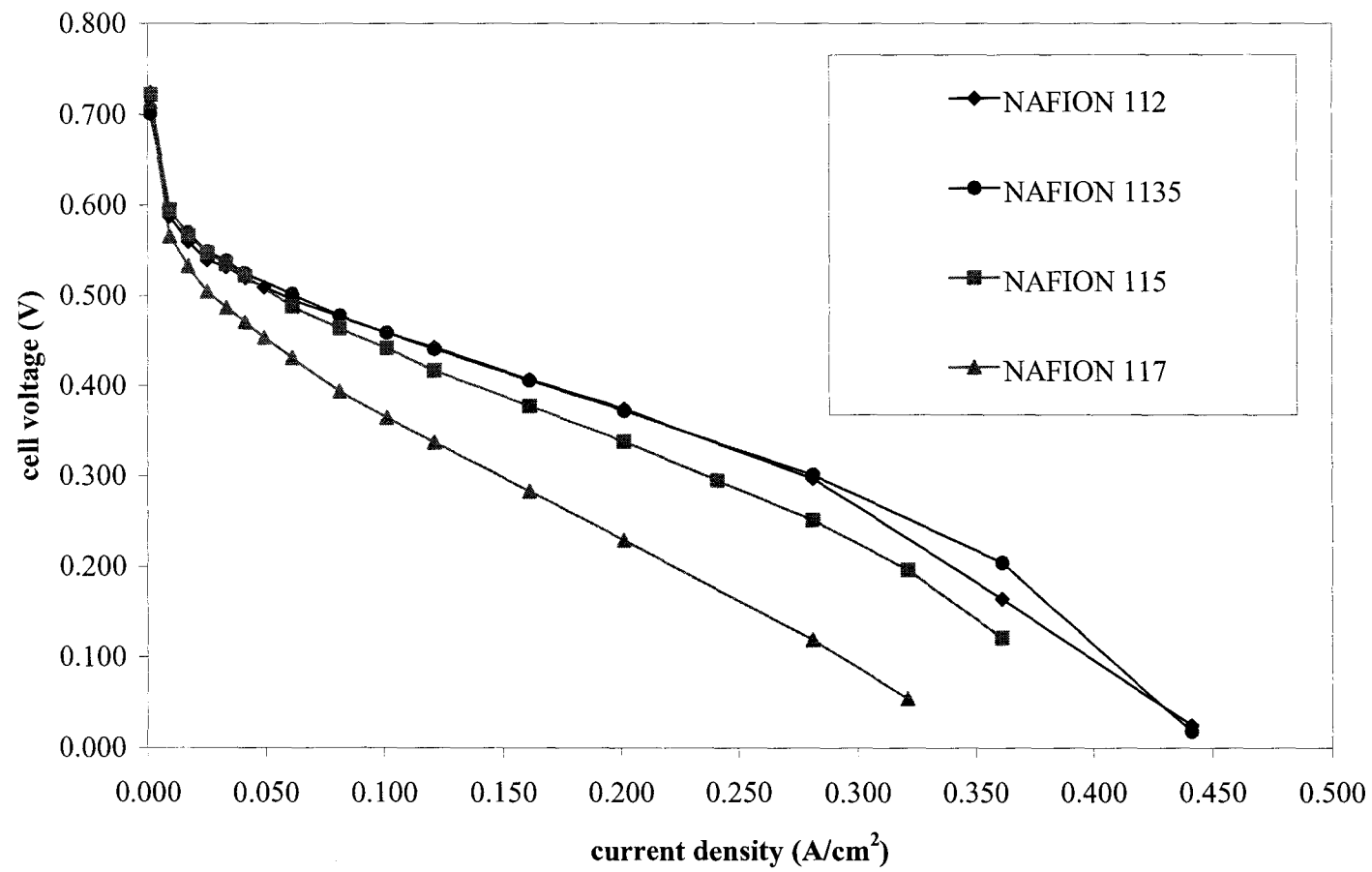


Figure 5.9: DMFC performances at 60°C of various Nafion membranes, 1.7x air stoichiometry.



**Figure 5.10:** DMFC performances at 60°C of various Nafion membranes, 4.9x air stoichiometry.

where  $D_m$  is defined as the methanol diffusion coefficient,  $C_m$  is the concentration of methanol within the membrane, and  $k_{dl}$  is the drag coefficient. Protonic current within the Nafion membrane induces electro-osmotic drag of water through the membrane.<sup>7,8,9</sup>

When methanol crossover is measured, protons migrate in the opposite direction to methanol, hence drag retards the methanol flux and the value of  $k_{dl}$  must be less than unity. Ren has determined  $k_{dl}$  to be 0.8829 for 1 M MeOH at 60 °C.<sup>10</sup>

If the anode (backing and catalyst layer) also acts as a diffusion barrier, then a constant steady state limiting current associated with the anode,  $j_{lim,anode}$ , will also exist.

Thus:

$$\frac{1}{j_{lim}} = \frac{1}{j_{lim,anode}} + \frac{1}{k_{dl}} \frac{d}{nFAD_m C_m} \quad Eq. 5.2$$

Methanol crossover was measured (using 1 M MeOH) at both 60°C and 80°C. for various membranes. Values are listed in Table 5.1.

Using this data, the diffusion coefficient of MeOH in Nafion can be calculated. Ren and co-workers have determined  $C_m$  and  $k_{dl}$  at a variety of MeOH concentrations and temperatures in Nafion. NMR experiments show that the methanol concentration within the membrane is essentially identical to that of the external solution.<sup>11</sup> However methanol is only present in the ion-cluster pores and channels (membrane porosity,  $\epsilon = 0.41$ ), hence the methanol concentration within the total volume of the membrane is actually reduced.

Ren et al. have determined that the values of  $C_m$  for 1M MeOH at 60°C and 80°C are 0.3905 M and 0.3810 M respectively.\*

A plot of  $1/j_{lim}$  vs.  $d$  is shown in Figure 5.11. Substituting the above  $C_m$  values and the slopes obtained from Figure 5.11 into Equation 5.2,  $D_m$  and values for  $J_{lim,anode}$  were calculated (listed in Table 5.1).  $D_m$  values are similar to those obtained by Ren. The differences may be due to the fact that Ren's data was acquired from both crossover measurements and potential-step measurements. Also, Ren did not study Nafion 1135 (only 112, 115 and 117).  $J_{lim,anode}$  values are significantly higher than those for even the thinnest Nafion membrane. This indicates that the anode is highly permeable to methanol and that its performance is not limited by the diffusion of methanol.

**Table 5.1:** Methanol Transport Properties in Nafion Membranes

Temperature (°C)	$J_{lim,Nafion\ 112}$ (mA/cm <sup>2</sup> )	$J_{lim,Nafion\ 1135}$ (mA/cm <sup>2</sup> )	$J_{lim,Nafion\ 115}$ (mA/cm <sup>2</sup> )	$J_{lim,Nafion\ 117}$ (mA/cm <sup>2</sup> )	$D_m \times 10^6$ (cm <sup>2</sup> /s)	$J_{lim,anode}$ (mA/cm <sup>2</sup> )
60	228	144	108	80	7.88	829
80	340	220	160	128	13.2	919
Ren, 60*	300	N/A	111	97	9.95	-
Ren 80*	353	N/A	151	134	13.8	-

## 5.5 Conclusions

Systematic optimization of MEA components has led to a dramatic improvement in DMFC performance. This is illustrated in Figure 5.12, which compares the 60°C DMFC performance achieved with our optimized MEAs to that reported in the literature. Shown is work reported in 1999 by Smotkin *et al.* (◆).<sup>12</sup> Their MEA employed 50%

\*  $C_m$  at 60°C was determined by linearly interpolating between the reported values at 50°C and 70°C.  $C_m$  at 80°C was determined by linearly interpolating between the reported values at 70°C and 90°C

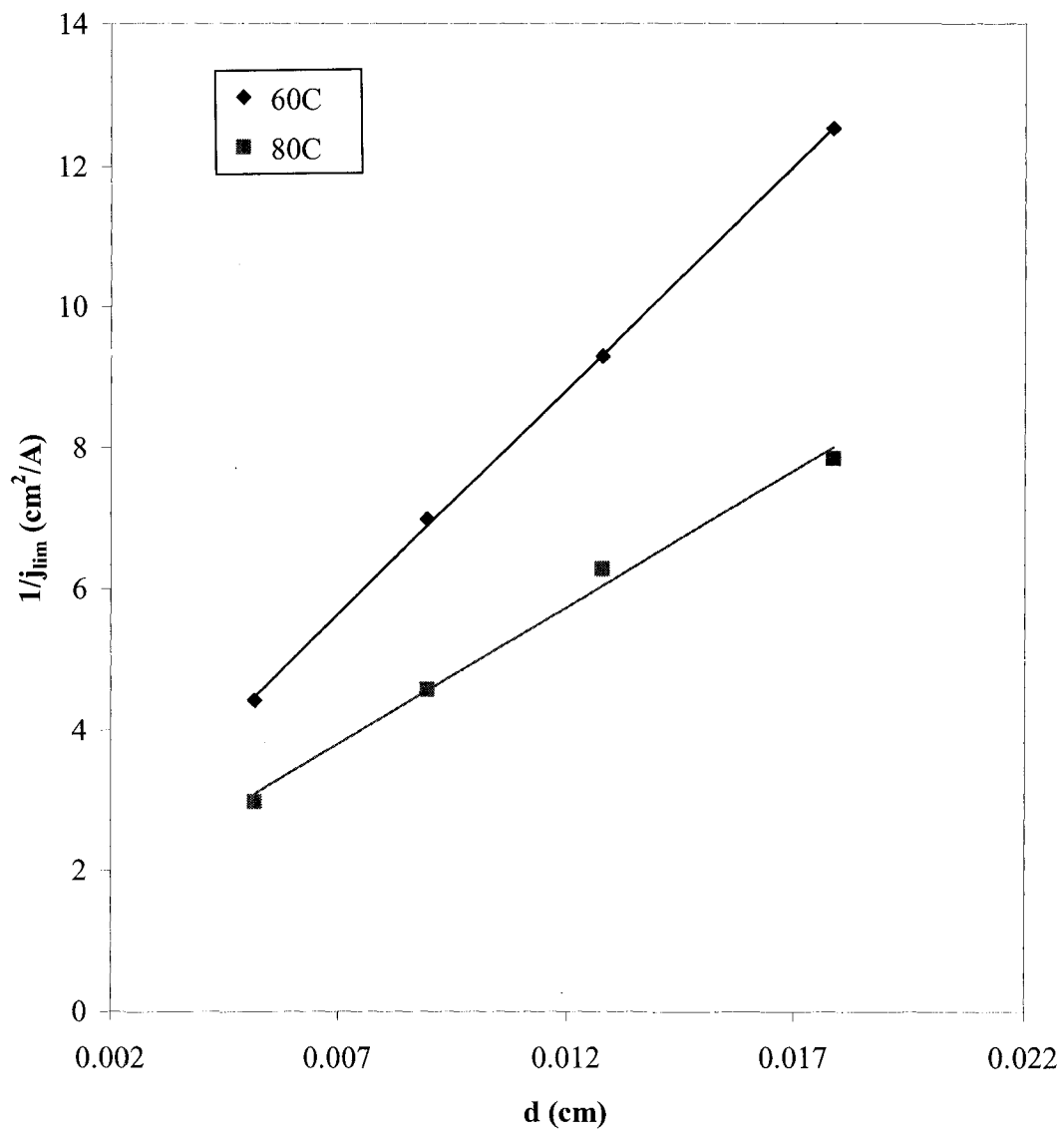


**Figure 5.11:** Methanol crossover as a function of Nafion membrane thickness

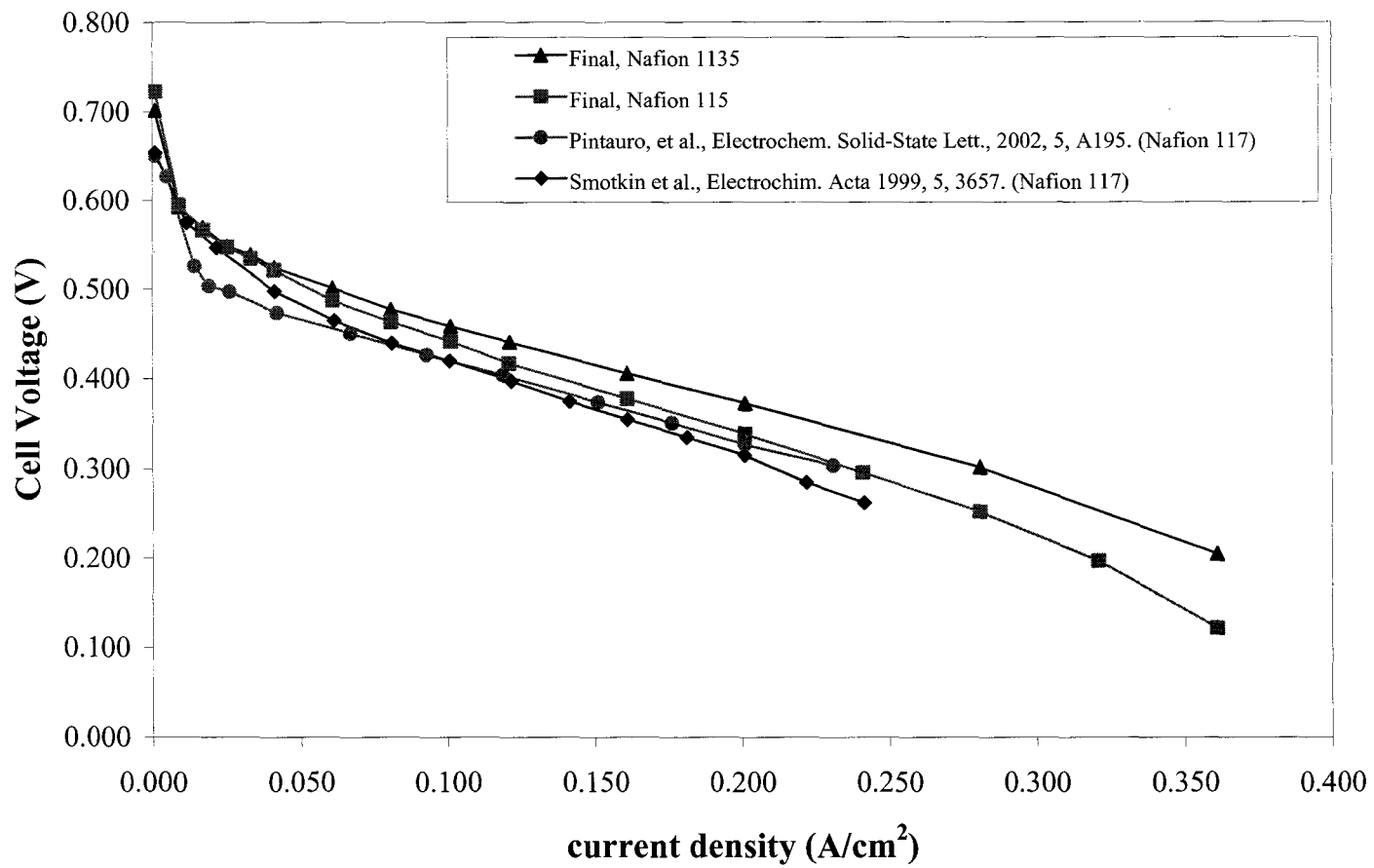


Figure 5.12: Progress of DMFC MEA development, 60°C.

higher catalyst loadings (anode = 6 mg/cm<sup>2</sup> Pt-Ru black/ Nafion 117/ cathode = 6 mg/cm<sup>2</sup> Pt black) yet our MEAs achieved superior performance.<sup>†</sup> Also shown is DMFC performance data recently reported (2002) by Pintauro *et al.*<sup>13</sup> (●). Their MEAs (anode = 4 mg/cm<sup>2</sup> Pt/Ru black, 15% Nafion on ELAT backing/ Nafion 117/ cathode = 4 mg/cm<sup>2</sup> Pt black, 10% Nafion on ELAT backing) were similar in composition to our own. However, our MEAs also outperformed them, possibly because we used a thinner Nafion membrane and a more hydrophilic anode backing.

Although excellent anode and cathode activity has been achieved, there is still room for improvement. Both the anode and cathode require high loadings of precious metals. A reduction of these loadings (without significantly decreasing performance) would greatly reduce the cost. Carbon supported Pt/Ru anode catalysts may eventually become a viable option due to their higher specific activity. However, the maximum attainable voltage is substantially lower for Pt/Ru/C<sup>14</sup> and therefore was not studied.

The superior performance of both Nafion 115 and 1135 make either one an excellent choice for DMFC applications. Despite the slightly lower performance of Nafion 115 at the higher air flow, overall it is probably a better choice due to its lower rate of methanol crossover (better fuel efficiency) and better performance at lower (and more practical) air flow rates.

---

<sup>†</sup> Smotkin's tests employed 0.5M methanol (as opposed to 1.0M MeOH employed by both Pintauro and the author). However, Smotkin also reported performance data at 90°C using both 0.5M and 1.0M methanol solutions, but no noticeable difference in cell performance was observed.

Nafion membranes still have an unacceptable level of methanol crossover. If crossover could be significantly reduced, the cathode Pt loading could in turn be greatly reduced to level more comparable to those of H<sub>2</sub>/air fuel cell cathodes.

## 5.6 References

- 
- <sup>1</sup> Zhang, J.; Colbow, K. M.; Wilkinson, D. P. US Patent 6187467, 2001
- <sup>2</sup> Nordlund, J.; Lindbergh, G. *J. Electrochem. Soc.* **2002**, 149, A1107-A1113.
- <sup>3</sup> Kinoshita, K. *Carbon: Electrochemical and Physicochemical Properties*; Wiley: New York, 1988.
- <sup>4</sup> Qi, Z. G.; Kaufman, A. *J. Power Sources* **2002**, 109, 38-46.
- <sup>5</sup> Wei, Z.; Wang, S.; Yi, B.; Liu, J.; Chen, L.; Zhou, W.; Li, W.; Xin, Q. *J. Power Sources* **2002**, 106, 364.
- <sup>6</sup> Ren, X.; Springer, T. Gottesfeld, S.; *J. Electrochem. Soc.* **2000**, 147, 92-98.
- <sup>7</sup> Fuller, T.F.; Newman, J. *J. Electrochem. Soc.* **1992**, 139, 1332.
- <sup>8</sup> Xie, G.; Okada, T. *J. Chem. Soc. Faraday Trans.* **1996**, 92, 663.
- <sup>9</sup> Zawodzinski, T.; Davey, J.; Valerio, J.; Gottesfeld, S. *Electrochim. Acta* **1995**, 40, 297.
- <sup>10</sup> Ren, X.; Springer, T.; Zawodzinski, T.; Gottesfeld, S. *J. Electrochem. Soc.* **2000**, 147, 466-474.
- <sup>11</sup> Skou, E.; Kaurenen, P.; Hentschel, J. *Solid State Ionics* **1997**, 97, 333-337.
- <sup>12</sup> Liu, L.; Pu, C.; Viswanathan, R.; Fan, Q.; Liu, R.; Smotkin, E. S. *Electrochim. Acta* **1999**, 43, 3657
- <sup>13</sup> Carter, R.; Wycisk, R.; Yoo, H.; Pintauro, P. N. *Electrochem. Solid-State Lett.* **2002**, 5, A195-A197.
- <sup>14</sup> Carrette, L.; Friedrich, K. A.; Stimming, U. *ChemPhysChem* **2000**, 1, 162-193.

## **Chapter 6**

# **Characterization of Polypyrrole/Nafion Composite Membranes in a Direct Methanol Fuel Cell**

## 6.1 Introduction to Conducting Polymer/Nafion Composite Membranes

Conducting polymer/Nafion composite membranes show excellent potential for DMFC applications. This is mainly because they are less permeable to methanol and therefore efficiency losses from methanol crossover are significantly less. Preliminary results from Pickup's group have demonstrated that composite membranes prepared using poly(1-methylpyrrole) reduce methanol crossover by as much as 50% without a significant increase in the ionic resistance of the composite membrane.<sup>1,2</sup> The mechanism by which the Nafion/poly(1-methylpyrrole) composite restricts methanol transport has not been fully determined.

The work described in this chapter is the characterization and performance of Polypyrrole/Nafion composite membranes in an operational DMFC. Pyrrole was chosen (over 1-methylpyrrole) because preliminary results indicated it performed better and also it is easier to polymerize. Methanol crossover, DMFC performance (including the separate performance of the anode and cathode) have been evaluated and results are compared with results obtained with unmodified Nafion membranes (from Chapter 5).

## 6.2 Experimental

### 6.2.1 Preparation of Polypyrrole/Nafion Composite Membranes

Polypyrrole/Nafion membranes were prepared by *in situ* polymerization of the pyrrole monomer in the Nafion membrane with the addition of an oxidizing agent, either  $\text{Fe}^{3+}$  or  $\text{H}_2\text{O}_2$ . Membranes were cleaned in 15 %  $\text{H}_2\text{O}_2(\text{aq})$ , 1 M  $\text{HNO}_3(\text{aq})$ , 1 M  $\text{H}_2\text{SO}_4(\text{aq})$  (1 h at 60-80 °C in each solution) and water. They were then immersed in a

pyrrole solution (0.08 or 0.10 M for 80 or 120 min for Fe(III) as the oxidant, 0.20 M for 5 min for H<sub>2</sub>O<sub>2</sub>) and then rinsed well with water. The pyrrole within the membrane was then polymerized by immersion in a 0.03-0.05 M Fe(NO<sub>3</sub>)<sub>3</sub>(aq) solution for 80 to 120 min or in a 30% hydrogen peroxide solution for 5 min. When Fe<sup>3+</sup> was used as the oxidant, the modified membranes were washed with 1 M or 2M HNO<sub>3</sub>(aq) until there was no further coloration of the wash solution. All membranes were washed with 1 M H<sub>2</sub>SO<sub>4</sub>, methanol, and water, and stored in water prior to use.

Membranes prepared using H<sub>2</sub>O<sub>2</sub> as the oxidizing agent were synthesized by Dr. B. Langsdorf and are therefore coded as BLXXXX (e.g. BL2\_91). Membranes prepared using Fe<sup>3+</sup> as the oxidizing agent were synthesized by Jeremy Hughes and are therefore coded as JHXXXX. Membranes were used as received unless otherwise noted.

### **6.2.2 MEA Preparation and Testing Procedure**

MEAs were prepared by hot-pressing the membrane with an optimized DMFC anode (Pt/Ru loading ca. 4 mg/cm<sup>2</sup>, described in Chapter 5) and cathode (Pt/Ru loading ca. 4 mg/cm<sup>2</sup>, described in Chapter 5). They were tested in a 25cm<sup>2</sup> DMFC at 60 °C and various other temperatures. Polarization curves (anode and cell) were obtained at constant current using a power supply. Voltages were allowed to stabilize for ca. one minute before readings were taken. Methanol crossover measurements were made in the same manner as those for Nafion membranes (see section 5.4.4).

### **6.3 Composite Membranes Prepared via Fe<sup>3+</sup> Oxidative Polymerization**

#### **6.3.1 Performance of Composite Membranes Prepared via Fe<sup>3+</sup> Oxidation**

Membranes prepared using Fe<sup>3+</sup> as the oxidizing agent exhibit excellent blockage of methanol crossover. A reduction of ca. 50-80% was achieved without a significant increase in resistance (values are tabulated in Table 6.1). However, despite this reduction in crossover these membranes generally displayed poor DMFC performance, as shown in Figure 6.1. For example, at a current density of 100 mA/cm<sup>2</sup> only 263 mV was produced when JH0727A is employed, compared to 408 mV when unmodified Nafion 115 was used.

One of the major reasons for this appears to be poor anode performance, as shown in Figure 6.1. The performance is far worse than one would expect based upon the slightly higher resistance of the composite membrane. It is indicative of a lower active area of the Pt/Ru catalyst. This is surprising since the same type of anode was used in all cases.

The poor performance of these composite membranes is believed to be due to their poor bonding to the electrodes. Delamination of electrodes occurred rather easily, similar to that observed with Nafion 117 (discussed in chapter 5). Poor bonding plagues many “alternative” fuel cell membranes.<sup>3</sup> The poor interfacial properties of these MEA's can lead to a lower catalyst utilization and increased resistance. These factors can effectively nullify any gains that would be observed from the beneficial properties that the alternative membrane might possess (in our case, decreased MeOH crossover). In

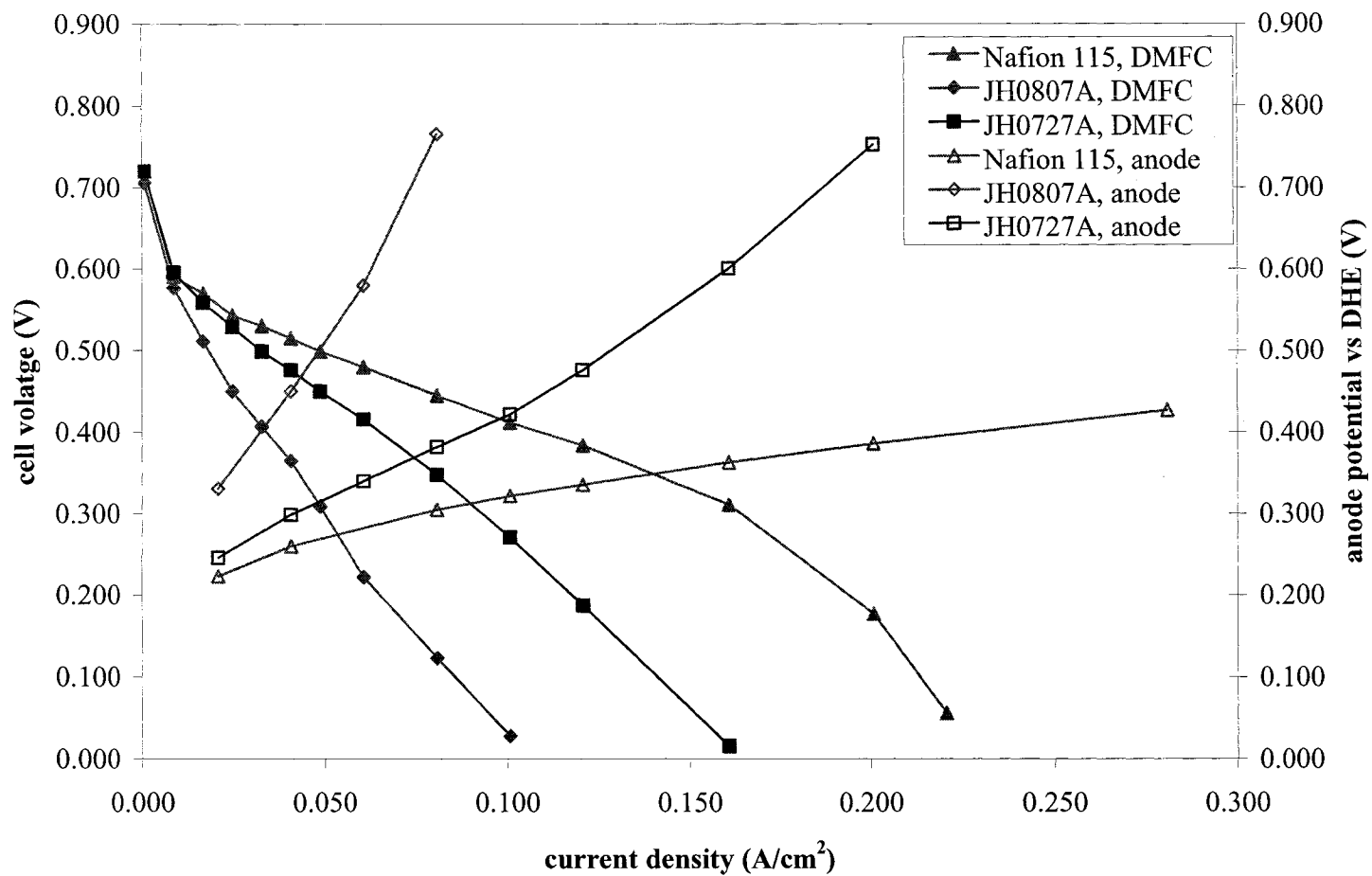


**Figure 6.1:** DMFC and anode performances (60°C, 1 M MeOH) of composite membranes prepared using Fe<sup>3+</sup> oxidative polymerization.

fact, these factors cause most alternative membranes to perform worse than (unmodified) Nafion membranes.

In this particular case,  $\text{Fe}^{3+}$  is used as the oxidizing agent. Studies performed by Sata indicate that  $\text{Fe}^{3+}$  can promote the formation of polypyrrole at the outer surface of the membrane.<sup>4</sup> High polypyrrole character (and less Nafion character) at the outer surface of the membrane is believed to retard its bonding with electrodes. This poor interface results in lower catalyst utilization at both electrodes.

**Table 6.1:** Methanol Crossover and Resistance Properties of Polypyrrole/Nafion Composite Membranes (see section 5.4.4 for definitions and details of measurements).

Membrane Code	Comment	Oxidant	$J_{\text{lim}}, 60\text{ }^{\circ}\text{C}$ (mA/cm <sup>2</sup> )	$D_m C_m \times 10^{10}$ (mol/cm/s)	$C_m, \ddagger 60\text{ }^{\circ}\text{C}$ (mol/L)	$R^*$ ( $\Omega\text{cm}^2$ )
JH0724A	Ppy/N115	$\text{Fe}^{3+}$	48			0.58
JH0724A-N	Ppy/N115, Nafion dipped	$\text{Fe}^{3+}$	60			N/A
JH0727A	Ppy/N115	$\text{Fe}^{3+}$	60			0.49
JH0807A	Ppy/N115	$\text{Fe}^{3+}$	20			0.68
JH0808A	Ppy/N115	$\text{Fe}^{3+}$	28			N/A
JH0809A	Ppy/N115 Nafion dipped	$\text{Fe}^{3+}$	48	11.9	0.171	0.75
BL2_91	Ppy/N115	$\text{H}_2\text{O}_2$	75.5	18.8	0.270	0.41
BL2_92	Ppy/N112	$\text{H}_2\text{O}_2$	128	12.7	0.183	0.25
JH0923A	Ppy/N112	$\text{Fe}^{3+}$	88			0.21
Nafion 112	Unmodified	None	228	27.2	0.391	0.11
Nafion 115	Unmodified	None	108	27.2	0.391	0.27

\* Measured by Electrochemical Impedance Spectroscopy by Dr. Brandi Langsdorf.

‡ Assuming that  $D_m$  is the same as for unmodified membranes.

### 6.3.2 Membrane Treatment to Enhance Electrode/Membrane Interface

Since (unmodified) Nafion membranes show excellent bonding to electrodes, we sought to endow the surface of the composite membranes with more “Nafion character”. Dipping the composite membrane in a 5% solution of Nafion (in water and alcohols, Solution Technologies) for ca. 20 minutes was investigated. After dipping, the membrane was allowed to “drip-dry” in air for 30 minutes and soaked in water for at least 24 h before use. The outer surface of the dipped membranes appeared to have a glossy coating. MEAs were prepared and tested at 60 °C in a DMFC.

JH0724A was one of the poorest performing membranes tested. However, after dipping in Nafion, a significant gain in performance was observed as shown in Figure 6.2. Methanol crossover increased slightly (Table 6.1) but was still substantially lower than that of an unmodified membrane. Also shown in Figure 6.2 is the performance of composite membrane JH0809A following a Nafion dip treatment. This membrane exhibits excellent DMFC performance, outperforming unmodified Nafion 115 (e.g. 427 mV vs. 408 mV at 100 mA/cm<sup>2</sup>). Methanol crossover was quite low, less than half that of Nafion 115 (Table 6.1). Figure 6.3 compares the separate anode and cathode performances achieved with JH0809A and Nafion 115. The anode performance of JH0809A is lower, most likely due to the increased resistance of the membrane (see Table 6.1). However the cathode performance achieved with JH0809A is substantially higher, hence the overall DMFC performance is better. Unfortunately a piece of JH0809A was not tested before the Nafion dip treatment due to the limited amount available. Nonetheless, based upon results for other membranes prepared via the same (or

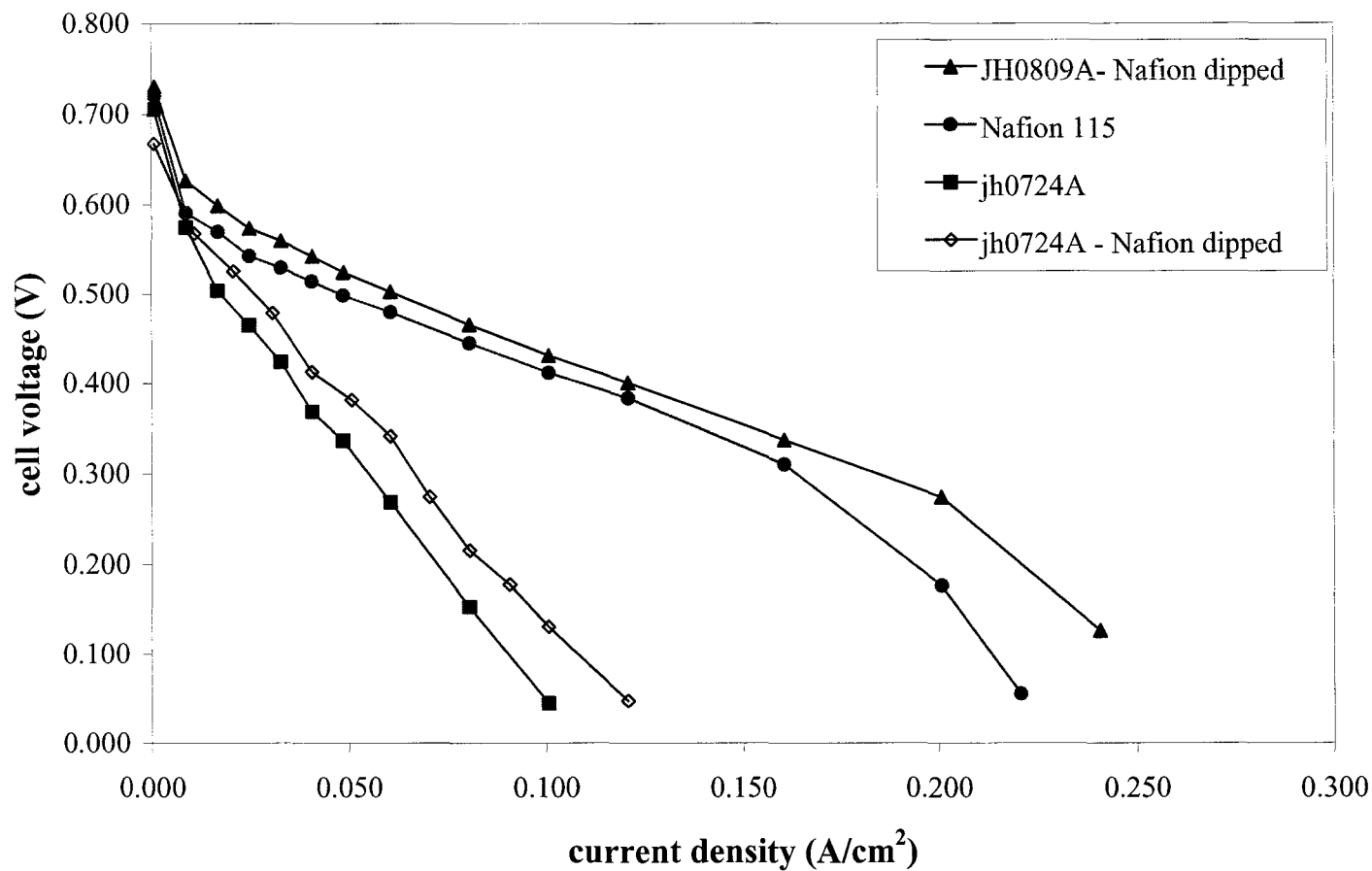


**Figure 6.2:** The DMFC performance at 60 °C (1.7x air stoich) of composite membranes prepared using Fe<sup>3+</sup> oxidative polymerization before and after being dipped in Nafion solution.

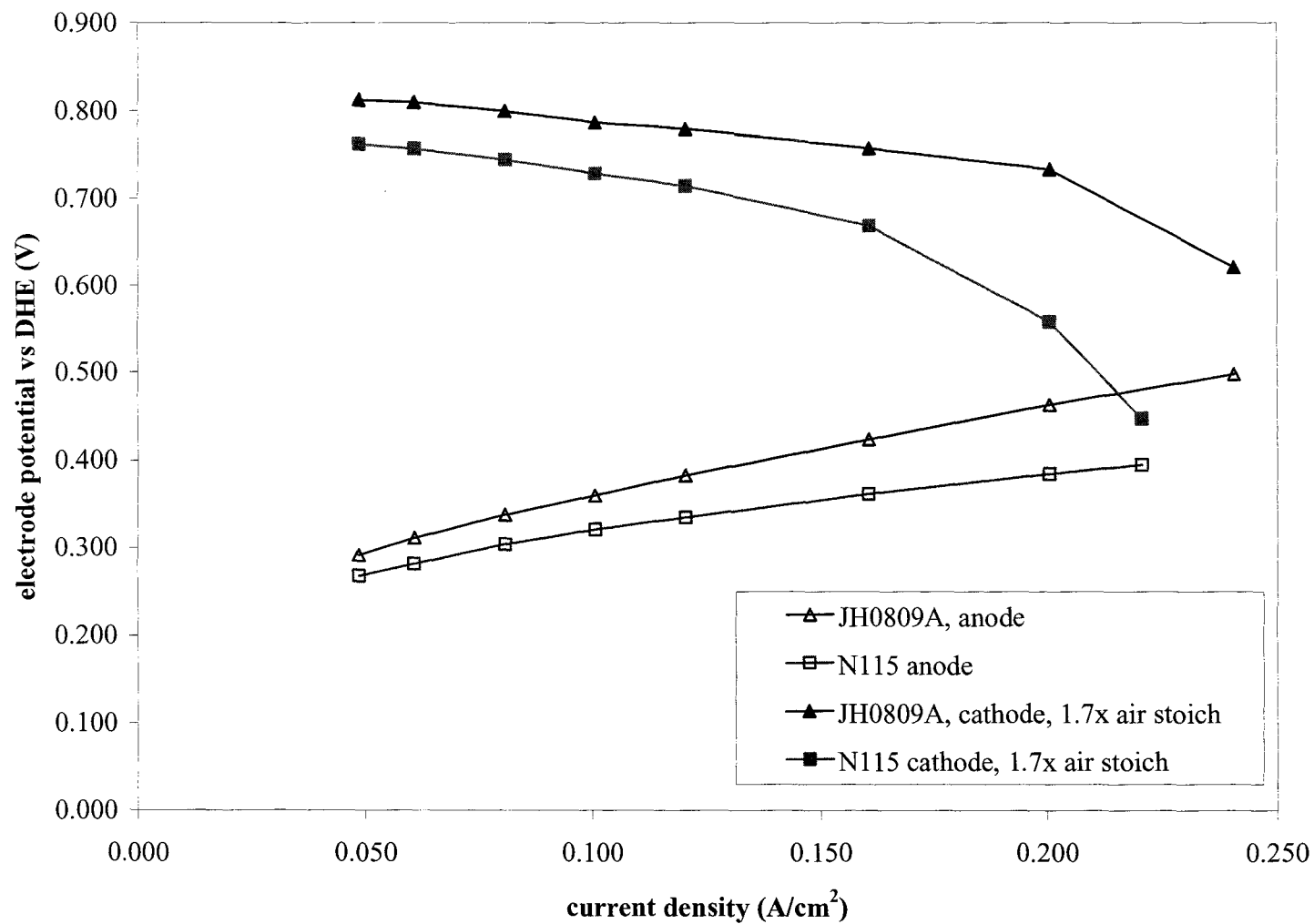


**Figure 6.3:** Comparison of the anode and cathode performances at 60°C (1.7x air stoich) obtained with a Nafion dipped composite membrane and Nafion 115.

similar) procedure and that for JH0724A, we can infer that dipping in Nafion has greatly enhanced its performance. After dipping, these membranes appear to bond much better with the electrodes (no delamination). This technique has since been applied to other “alternative” fuel cell membranes with similar results.<sup>3</sup>

## **6.4 Performance of Composite Membranes Prepared via H<sub>2</sub>O<sub>2</sub> Oxidative**

### **Polymerization**

Composite membranes prepared using H<sub>2</sub>O<sub>2</sub> as the oxidizing agent exhibit a good reduction of methanol crossover. Typically a reduction of ca. 30-50% was achieved without a large increase in resistance (values are listed in Table 6.1). These membranes also displayed good bonding properties, better than those prepared using Fe<sup>3+</sup>. Delamination rarely occurred. We presume that this is because polypyrrole formation most readily occurs within the pores and not on the outer surface of the membrane when using peroxide (since acid, which is only present within the pores, is also required for H<sub>2</sub>O<sub>2</sub> to polymerize pyrrole).<sup>5</sup>

Figure 6.4 illustrates the DMFC performance achieved using two composite membranes prepared using H<sub>2</sub>O<sub>2</sub> as the oxidant and results for unmodified Nafion 115, Nafion 112 and the best membrane from the Fe(III) series (i.e. Nafion dipped), for comparison. Excellent DMFC performances were achieved with the composite membranes. BL2\_91, a modified Nafion 115 membrane, outperforms Nafion 115 at low airflows (e.g. 432 mV vs. 408 mV at 100 mA/cm<sup>2</sup>). Also, BL2\_92, a modified Nafion

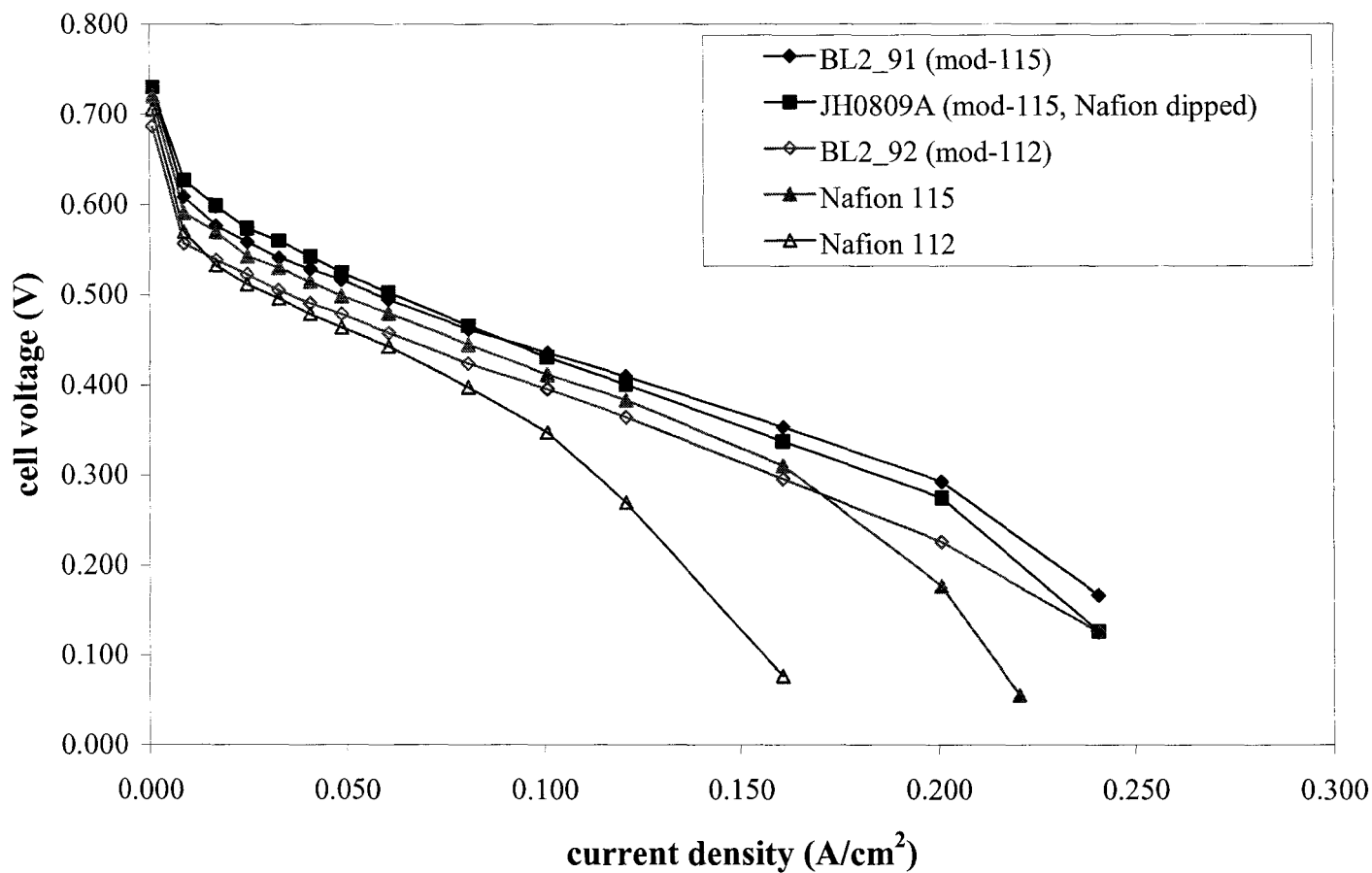


**Figure 6.4:** DMFC performance at 60 °C (1.7x air stoichiometry) of composite membranes prepared using H<sub>2</sub>O<sub>2</sub> oxidative polymerization.

112 membrane, vastly outperforms Nafion 112 (e.g. 392 mV vs. 344 mV at 100 mA/cm<sup>2</sup>) and performs similarly to Nafion 115 at low airflows.

The enhanced performances achieved with both BL2\_91 and BL2\_92 can be explained by the higher cathode activity that is a direct result of the decrease in methanol crossover. Figure 6.5 compares the anode and cathode performances obtained when BL2\_91 and Nafion 115 are used. Figure 6.6 compares the anode and cathode performances obtained when BL2\_92 and Nafion 112 are used. Despite the slightly lower anode performances of the composite membranes (most likely caused by a larger ionic resistance), the cathode performances are significantly better than those of the unmodified counterparts. This leads to the better overall DMFC performance.

The stability of the composite membranes, BL2\_91 was thoroughly tested over the course of two weeks at temperatures ranging between 35 and 80 °C. Peak performance was achieved after ca. 3 days and was then maintained throughout the course of the experiments, as shown in Figure 6.7. Methanol crossover levels also remained steady at ca. 30% lower than Nafion 115. These results indicate that the membrane is quite stable in the DMFC environment and showed no signs of polypyrrole leaching or decomposition.

## **6.5. Discussion**

It is clear that the composite membranes examined in this work effectively reduce the amount of methanol crossover. This reduction of methanol crossover leads to enhanced cathode activity and better overall DMFC performance. However, the addition

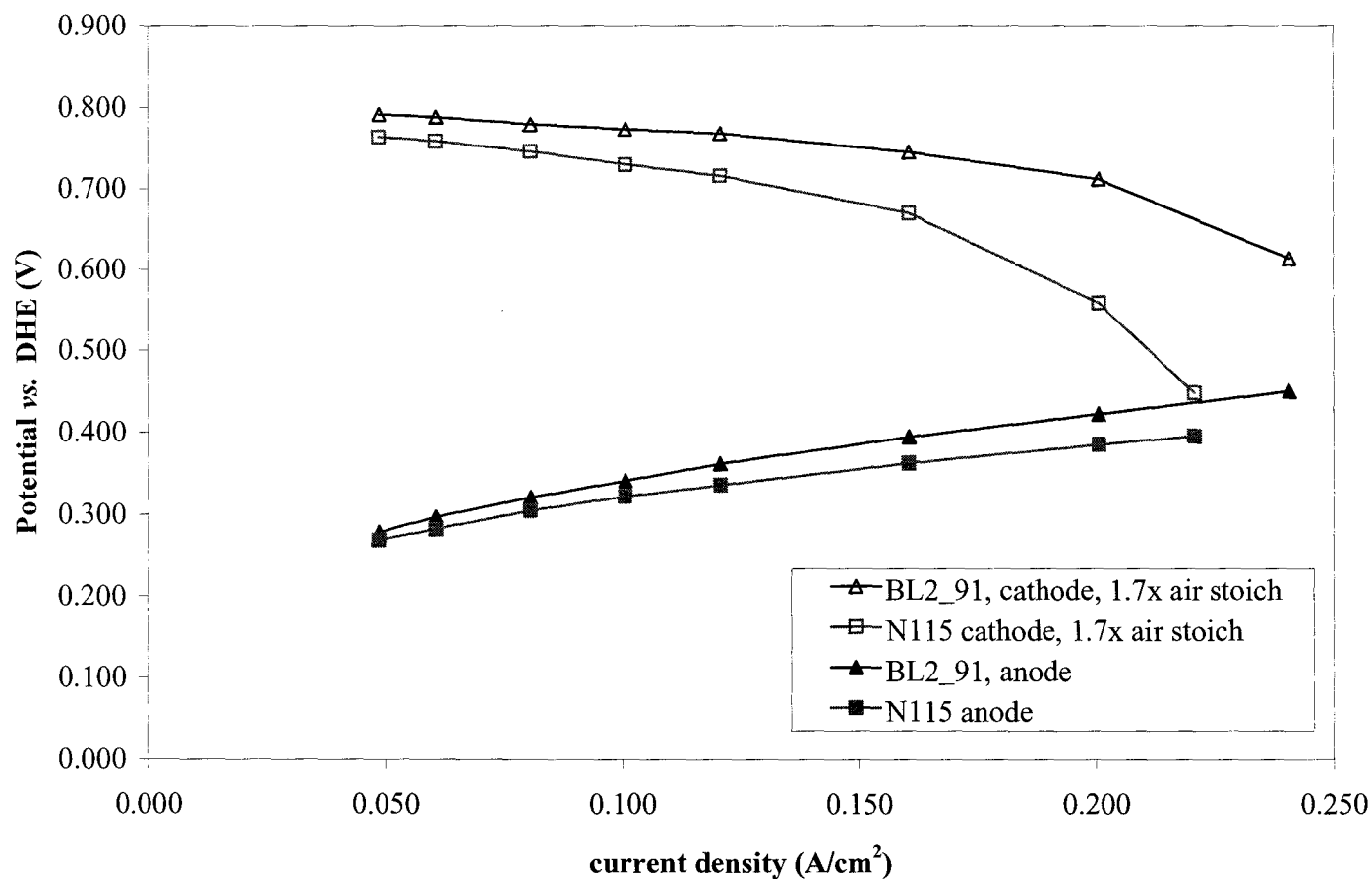


**Figure 6.5:** Comparison of the anode and cathode performances at 60 °C (1.7x air stoichiometry) obtained with a BL2\_91 (modified Nafion 115 membranes prepared using H<sub>2</sub>O<sub>2</sub> oxidative polymerization) and Nafion 115.

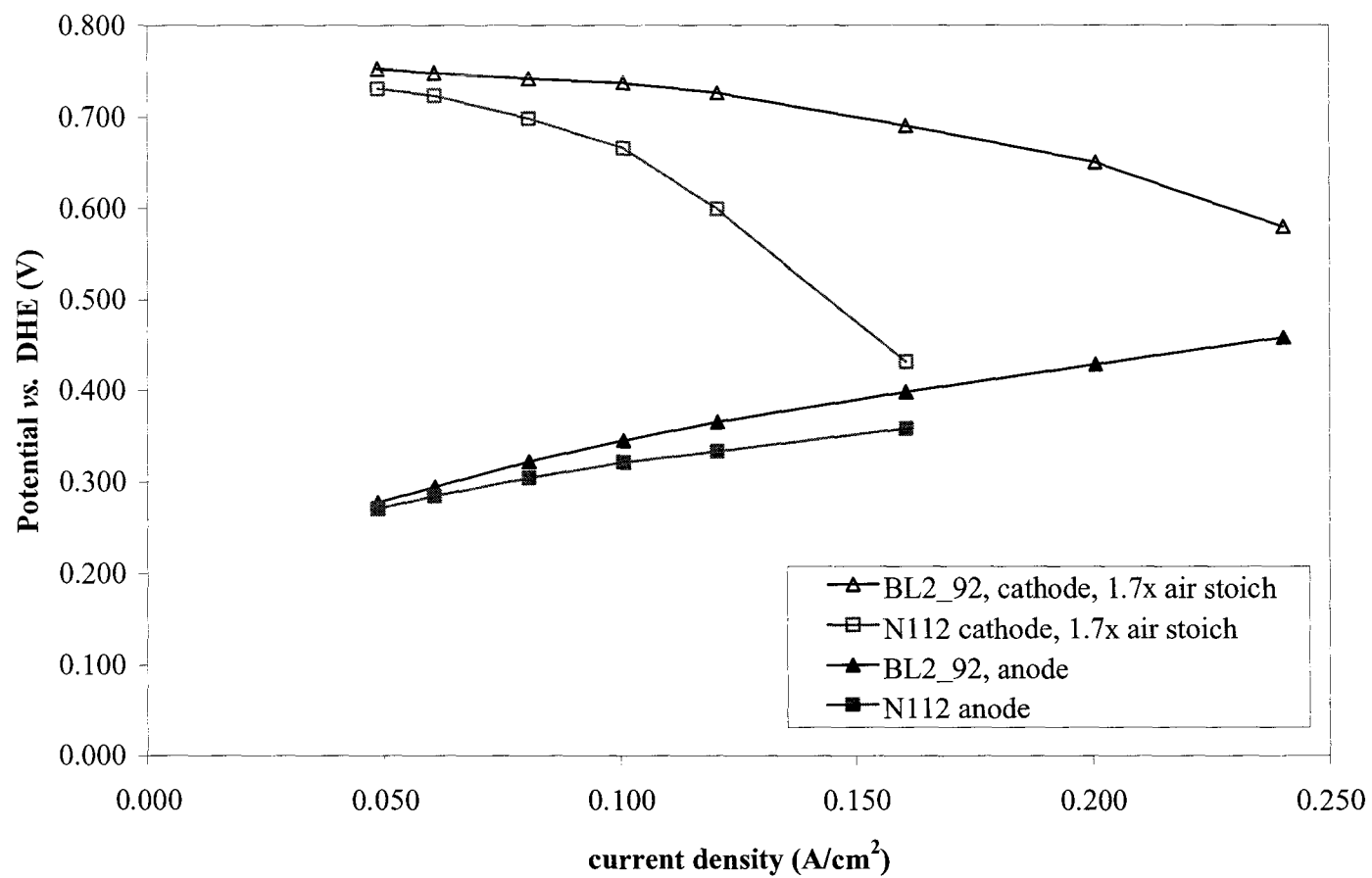


**Figure 6.6:** Comparison of the anode and cathode performances at 60 °C (1.7x air stoichiometry) obtained with a BL2\_92 (modified Nafion 112 membranes prepared using H<sub>2</sub>O<sub>2</sub> oxidative polymerization) and Nafion 112.

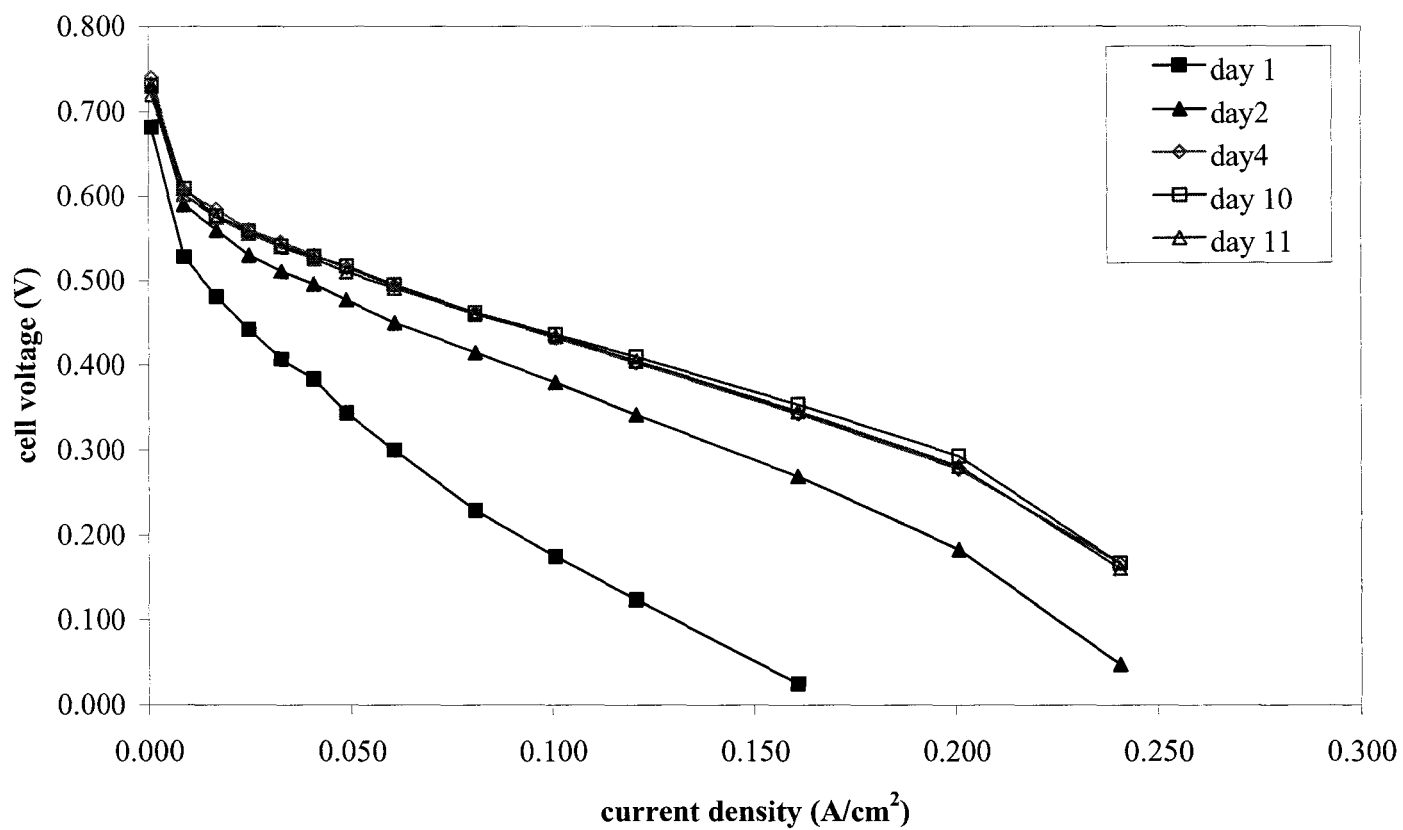


**Figure 6.7:** Variation of the 60°C DMFC performance over time of a composite membrane prepared using H<sub>2</sub>O<sub>2</sub> as the oxidant.

of polypyrrole into Nafion does increase the ionic resistance of the membrane to some extent. A small increase in resistance can be tolerated because the cathodic performance gains are larger than the Ohmic losses. Nevertheless, decreasing the ionic resistance (while maintaining the low level of methanol crossover) would lead to even further performance gains. For example, Figure 6.8 compares the DMFC performance of JH0809A (Nafion dipped) with that of Nafion 115. Even though the JH0809A membrane (Nafion soaked) has ca. three times the resistance ( $0.75 \Omega \text{ cm}^2$ , compared to  $0.27 \Omega \text{ cm}^2$  for Nafion 115) it still outperforms Nafion 115. Also shown is a polarization curve that corrects for the increased resistance of the composite membrane. Clearly, the performance difference would be enormous if the resistances of both were equal. That being said, the higher resistance is much less of an issue when low current is being drawn. For low power applications, highly resistive composite membranes with very low methanol crossover rates would be advantageous.

The lower rate of methanol crossover of composite membranes is due to their decreased methanol permeability,  $D_m C_m$ . However, it is still unclear as to exactly why there is reduced permeability. It may be due to a reduced concentration of methanol within the membrane ( $C_m$ ), a lower methanol diffusion coefficient ( $D_m$ ), or a combined reduction of both. Both Skou *et al.* and Ren *et al.*, have reported that the concentration of methanol within Nafion pores is the same as that of the bulk solution.<sup>6,7</sup> Hence  $C_m$  is a function of the membrane porosity,  $\epsilon$ , and can be expressed as:

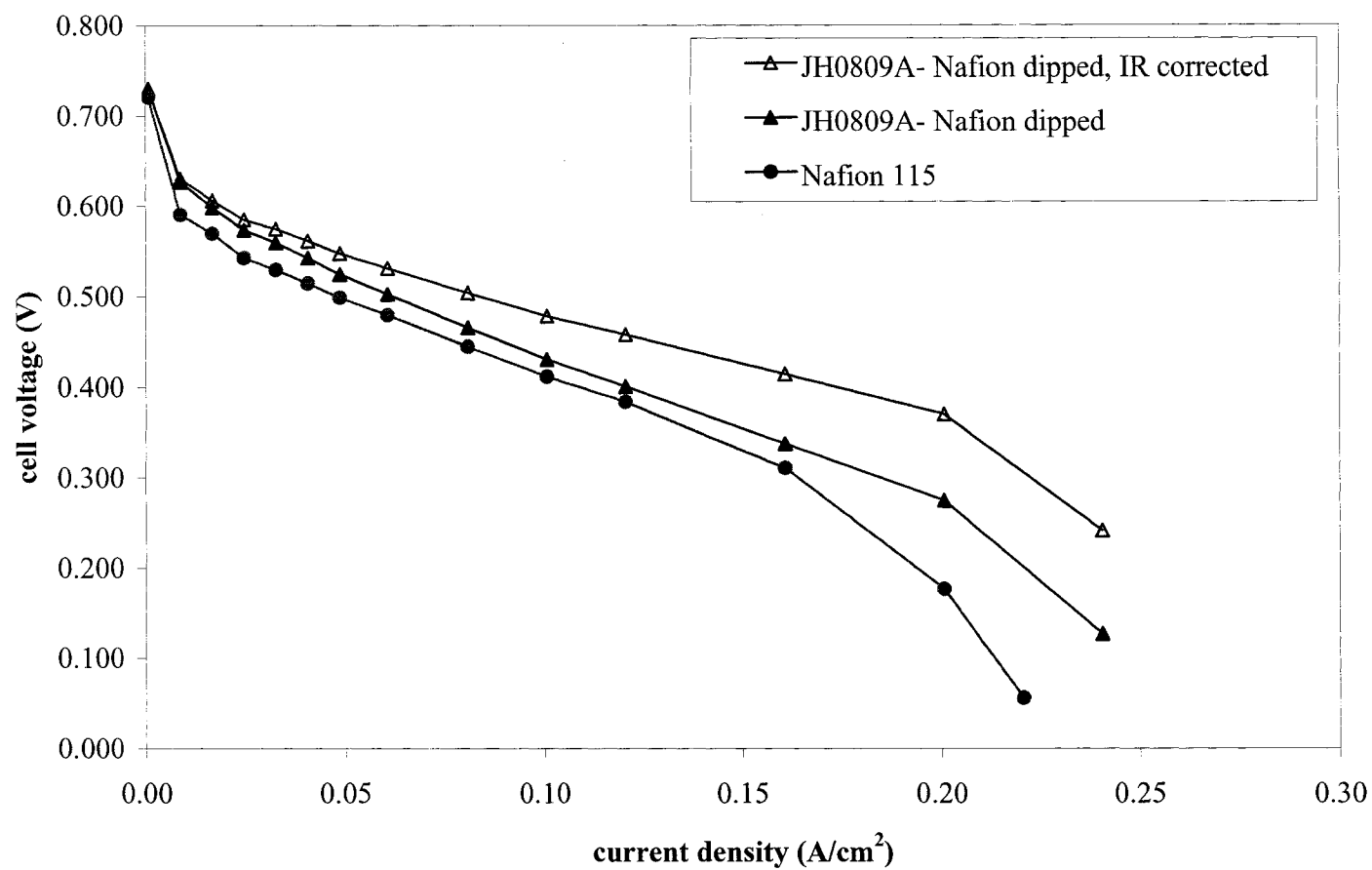


**Figure 6.8:** DMFC performance at 60°C (1.7x air stoich) of composite membranes with and without IR correction.

$$C_m = \varepsilon C_{BULK} \quad \text{Eq.6.1}$$

Assuming that  $D_m$  and the concentration of methanol within the pores of the composite membranes are the same as for Nafion membranes, the decreased permeability could be attributed to a reduction in the membrane's porosity. Using the values for  $C_m$  from Table 6.1, we can calculate  $\varepsilon$  for composite membranes when a 1 mol/L MeOH solution was employed. As can be seen from the values in Table 6.2, the composite membranes are significantly less porous. Not surprisingly, the decrease in methanol permeability is proportional to the decrease in porosity (substituting Eq. 6.1 into Eq. 5.1 can mathematically show this relationship).

Polypyrrole can decrease the pore volume of Nafion in two obvious ways. First, the volume physically occupied by polypyrrole will reduce the pore volume (assuming that the membrane does not swell to accommodate the polypyrrole). Also, electrostatic interactions between the negatively charged sulfonate groups on the Nafion side chains and the positively charged doped form of polypyrrole can further decrease the pore volume. This interaction is shown in Figure 6.9.

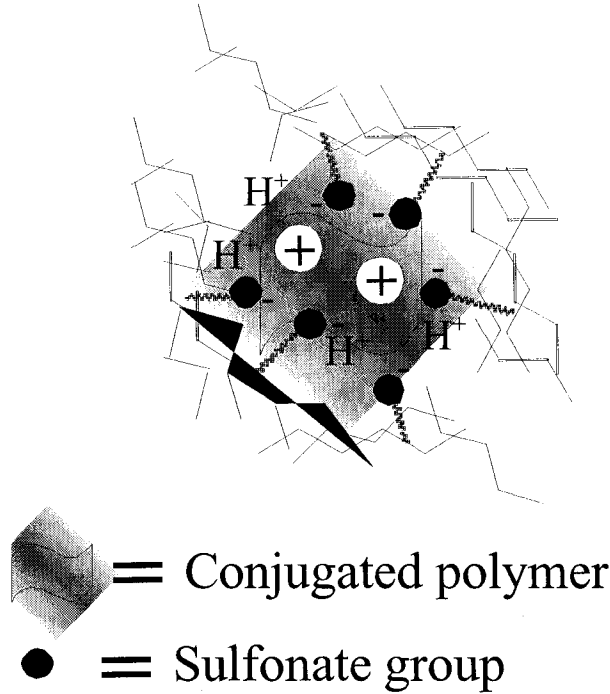


**Figure 6.9:** Electrostatic Interaction of Polypyrrole and Nafion side chains.

The decreased porosity of the composite membranes also has an effect on the hydration state of the membrane. Water (or solvent) uptake,  $\lambda$ , is defined as the molar ratio of water (or solvent) molecules in the membrane to sulfonate groups. For an aqueous methanol solution,  $\lambda_{total}$  ( $\lambda_{total} = \lambda_{H_2O} + \lambda_{MeOH}$ ) can be calculated using Equation 6.2:<sup>8,9</sup>

$$\lambda_{total} = \frac{\mathcal{E} \rho_{soln}}{(1 - \mathcal{E}) \rho_{dry}} \cdot \frac{EW_{membrane}}{18 \cdot x_{H_2O} + 32(1 - x_{H_2O})} \quad Eq. 6.2$$

where  $\rho_{soln}$  is the density of the solution,  $\rho_{dry}$  is the density of the dry membrane

( $2.075\text{g/cm}^3$  for the protonated form of Nafion<sup>10</sup>),  $\text{EW}_{\text{membrane}}$  is the equivalent weight of the membrane and  $x_{\text{H}_2\text{O}}$  is the mole fraction of water in the solution. Values of  $\lambda$  calculated for Nafion and several composite membranes are listed in Table 6.2.

**Table 6.2:** Water and Methanol Uptake Properties of Polypyrrole/Nafion Composite Membranes

Membrane	Comment	Oxidant	$C_m$ (mol/L)	$\epsilon$	$\lambda$
JH0809A	Ppy/N115, Nafion dipped	$\text{Fe}^{3+}$	0.1714	0.1714	6.12
BL2_91	Ppy/N115	$\text{H}_2\text{O}_2$	0.2697	0.2697	10.9
BL2_92	Ppy/N112	$\text{H}_2\text{O}_2$	0.1829	0.1829	6.62
Nafion	Unmodified Nafion	None	0.3905	0.3905	19.0

These calculations infer that the composite membranes do not take up as much water (and methanol) as unmodified Nafion membranes and this is supported by water uptake measurements performed by Dr. B. Langsdorf. It was found that when placed in a controlled humidity environment, composite membranes absorbed ca. 40% less water per sulfonate than unmodified membranes. These results are consistent with the slightly higher resistances of the composite membranes since conductivity is a function of water content.<sup>11,12</sup> A longer “break-in period” observed for MEAs made with composite membranes supports this theory. MEAs made with composite membranes typically reach peak DMFC performance after about 3 days (compared to less than 1 day for Nafion). The longer time may be required in order to achieve full hydration of the MEA (catalyst activation would be expected to require the same amount of time for both membranes).

The lower water uptake by composite membranes may also explain their tolerance of lower air flow rates. Figure 6.10 illustrates the DMFC performance when the air flow rate was decreased from 4.9x stoichiometry to 1.7x stoichiometry. There was only a small loss of performance when composite membranes were employed. However, a significant performance drop occurs when Nafion 115 is used. This can most likely be attributed to decreased water flux across the composite membrane<sup>13</sup> due to the decrease in  $\lambda$ . Given the fact that the anode feed is an aqueous solution, there is quite a large flux of water across the membrane. This can induce flooding problems at the cathode,<sup>14</sup> thus requiring high air flow rates. The reduced water flux across the composite membranes allows for the use of lower airflow rates, which would be quite beneficial from a system design standpoint, since a less powerful pump could be used thereby increasing the system's overall efficiency (i.e. less parasitic power).

The method by which the membrane is modified clearly has a significant effect on the properties of the resulting composite membrane. Membranes prepared using  $\text{Fe}^{3+}$  as the oxidizing agent appear to block more methanol than those made with  $\text{H}_2\text{O}_2$ . However,  $\text{Fe}^{3+}$  may promote pyrrole polymerization on or near the outer surface of the membrane, and this can lead to poor interfacial properties. Also, ionic resistances tend to be higher when  $\text{Fe}^{3+}$  is used.  $\text{H}_2\text{O}_2$  has emerged as the better method to synthesize composite membranes since they have reasonably low methanol crossover rates and better interfacial properties.

We speculate that an ideal composite membrane should consist of a high-density polypyrrole region centered within the membrane, and that the polypyrrole density should

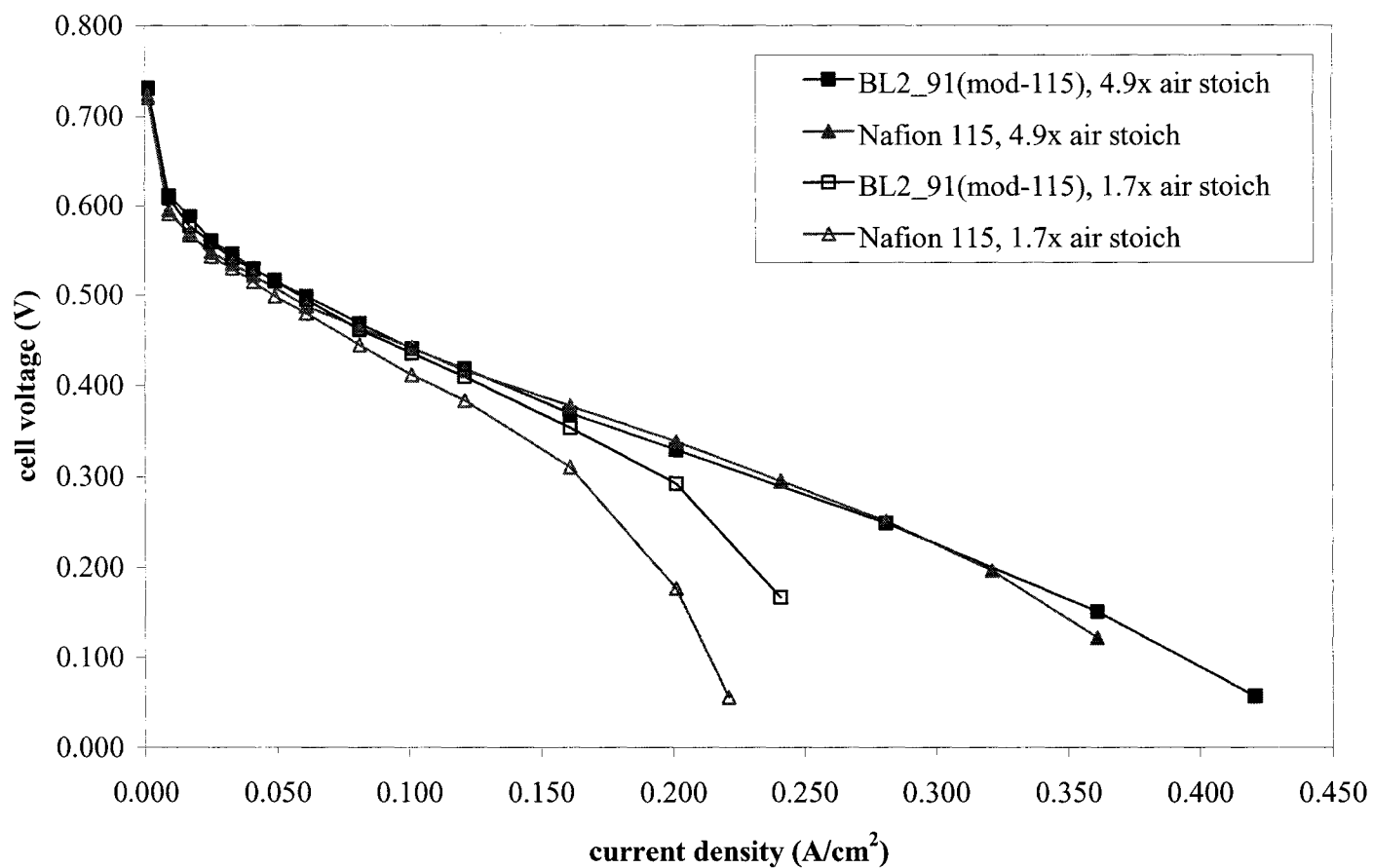


**Figure 6.10:** The effect of airflow rate on DMFC performance at 60 °C for Nafion 115 and a composite membrane prepared using H<sub>2</sub>O<sub>2</sub> oxidant.

decrease to zero near the surface. The Nafion character at the surface can promote a good interface with the electrodes and the central polypyrrole would block methanol.

There are still many other composite membrane systems that can be explored. Different monomers, such as a variety of pyrrole, thiophene and aniline derivatives could be used. Also, this methodology could be applied to other PEMFC membranes. Exploration of the numerous combinations may result in a better understanding of the system and will likely yield even better performing membranes.

## **6.6. Conclusion**

Polypyrrole/Nafion composite membranes have been shown to be superior to Nafion in a DMFC. The improved DMFC performance results from increased cathode activity, which is due to less methanol crossover and a lower water flux across the membrane. Lifetime tests have shown that the composite membranes are sufficiently stable. Because of these results, it is projected that they will be used in commercial cells in the near future.

## References

- 
- <sup>1</sup> Jia, N.; Lefebvre, M. C.; Halfyard, J.; Qi, Z.; Pickup, P. G. *Electrochem. Solid-State Lett.* 2000, 3, 529-531.
- <sup>2</sup> Pickup, P. G.; Qi, Z. Canadian Patent Application 2,310,310, 2000.
- <sup>3</sup> Qi, Z.; Easton, E. B.; Pickup, P. G.; Kaufman, A.; *US Patent Application* 10/264805, Applied October 2002.
- <sup>4</sup> Sata, T. *Chem. Mater.* 1991, 3, 838-843.
- <sup>5</sup> Langsdorf, B. L.; Pickup, P. G.; et al. *J. Phys. Chem. B.*, submitted September 2002.
- <sup>6</sup> Skou, E.; Kaurenen, P.; Hentschel, J. *Solid State Ionics* 1997, 97, 333-337.
- <sup>7</sup> Ren, X.; Springer, T.; Zawodzinski, T.; Gottesfeld, S. *J. Electrochem. Soc.* 2000, 147, 466-474.
- <sup>8</sup> Verbrugge, M. W.; Schneider, E. W.; Conell, R. S.; Hill, R. F. *J. Electrochem. Soc.* 1992, 139, 3421.
- <sup>9</sup> Verbrugge, M. W.; Schneider, E. W.; Conell, R. S.; Hill, R. F. *J. Electrochem. Soc.* 1989, 136, 417.
- <sup>10</sup> Gierke, T. D.; Hsu, W. Y.; in *Perfluorinated Ion Exchange Membranes*, Eisenberg, A., Yeager, H. L., Eds.; ACS Symposium Series 180; American Chemical Society: Washington, DC, 1982; p. 283.
- <sup>11</sup> Zawodzinski, T.; Derouin, C.; Radzinski, S.; Sherman, R.; Smith, V.; Springer, T.; Gottesfeld, S. *J. Electrochem. Soc.* 1993, 140, 1041.
- <sup>12</sup> Cappadonia, M.; Erning, J. W.; Miaki, S. M. S.; Stimming, U. *Solid State Ionics* 1995, 75, 65.

---

<sup>13</sup> Ren, X.; Springer, T.; Gottesfeld, S. *J. Electrochem. Soc.* **2000**, 147, 92-98.

<sup>14</sup> Ren, X.; Gottesfeld, S. *J. Electrochem. Soc.* **2001**, 148, A87-A93.

**Chapter 7 :**  
**Electrochemical Impedance Spectroscopy Studies**  
**of Fuel Cell Electrodes**

## 7.1. Introduction to Electrochemical Impedance Spectroscopy

Electrochemical impedance spectroscopy (EIS) is a very powerful technique, offering a vast amount of data in a period of short time, from a very simple experimental setup. Although the technique draws from basic electronics,<sup>1</sup> a full discussion of the theory involved is beyond the scope of this thesis. A rudimentary discussion of the method follows. Generally, EIS is used to characterize electrochemical systems in terms of equivalent circuits where each elementary process is described in terms of circuit elements such as resistors and capacitors. Impedance experiments involve perturbation of the cell by a potential having a small amplitude (ca. 5 mV) AC component at a fixed DC bias potential. The frequency of this component is typically scanned from high to low frequency, eliciting responses corresponding to the various processes occurring in the cell.

For resistors, Ohm's law describes the relationship between the applied potential ( $E$ ), the current ( $I$ ) and resistance ( $R$ ):

$$E = IR \qquad \text{Eq. 7.1}$$

Circuit elements like capacitors and inductors can impede electron flow under alternating current. The impedance ( $Z$ ) of these systems is described by:

$$E = IZ \qquad \text{Eq. 7.2}$$

For such systems, the current and potential sinusoidal functions are out of phase by  $\theta$  (rad), referred to as the phase angle. The AC waveform is conveniently characterized by vector analysis, and is often reported in coordinate terms of real ( $Z'$ ) and imaginary ( $Z''$ ) impedance. Thus,

$$Z' + jZ'' = \frac{(E' + jE'')}{(I' + jI'')} \quad \text{Eq. 7.3}$$

Where  $j = (-1)^{1/2}$

Nyquist (or complex plane impedance) plots are the most common representation of EIS data. Nyquist plots for various circuit elements are shown in Figure 7.1. The X-axis corresponds to real impedance ( $Z'$ ) and the Y-axis corresponds to imaginary impedance ( $Z''$ ), with a high-to-low frequency scan corresponding to left-to-right along the X-axis. Real impedance derives from the resistance component of the impedance measurements, while imaginary impedance is calculated from the capacitance ( $Z'' = -1/\omega C$ ). Figure 7.1 (a) shows the Nyquist plot obtained for a resistor ( $R_1$ ) and capacitor ( $C_1$ ) connected in series, which results in a vertical line with a high frequency intercept of  $R_1$ . The circuit elements can be connected together in different manners and will then yield different plots. For example, Figure 7.1 (b) shows the Nyquist plot obtained for a resistor ( $R_1$ ) connected in series to parallel-connected resistor ( $R_2$ ) and capacitor ( $C_1$ ). This results in a semi-circle centered on the real axis with a high frequency intercept of  $R_1$  and a low frequency intercept of  $R_1 + R_2$ .

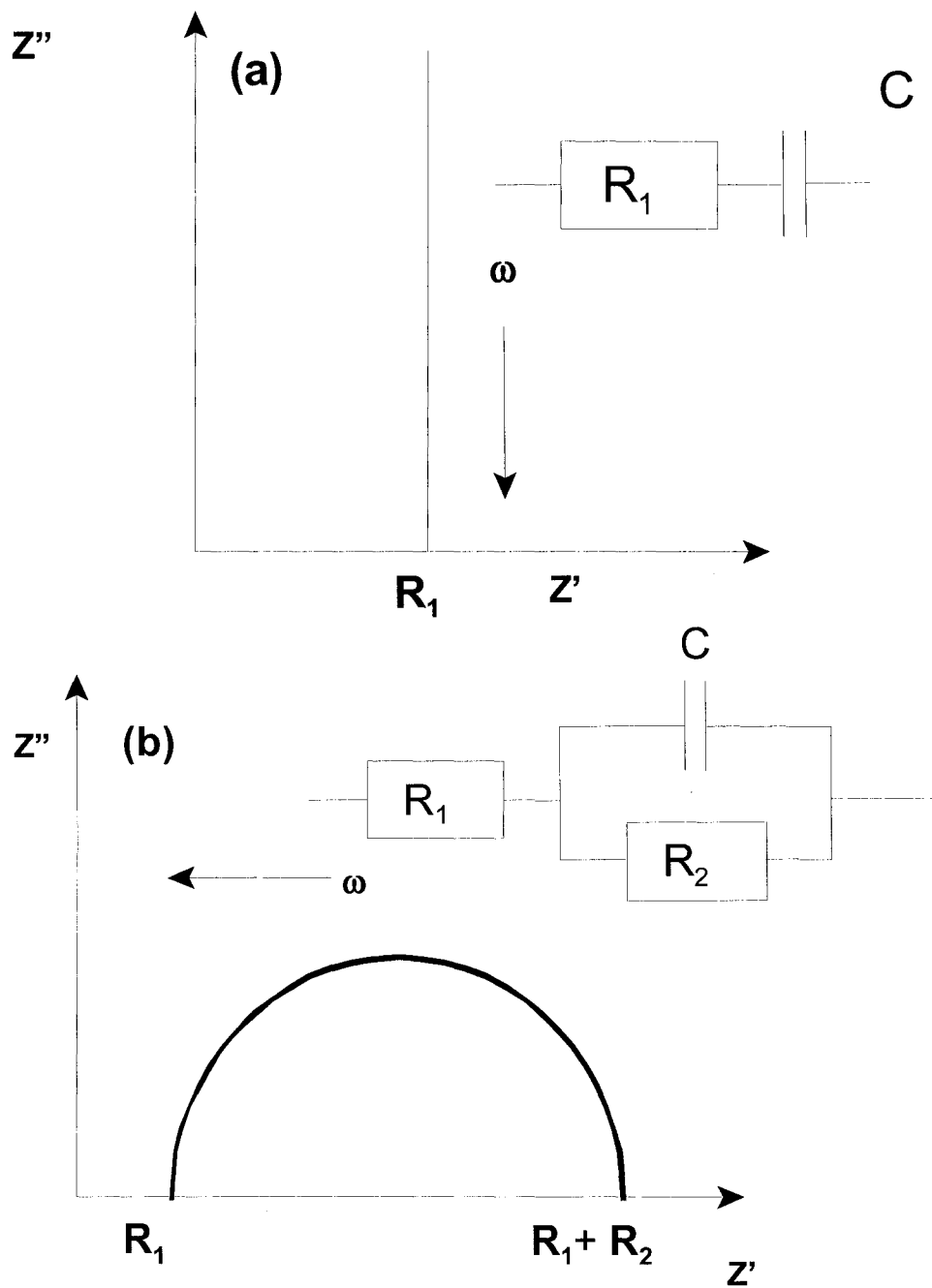


**Figure 7.1:** The Nyquist impedance responses of different circuit element combinations.

As circuits become more complex, so does their EIS spectra. Many equivalent circuits can often fit experimental data. However, a good equivalent circuit model must contain reasonable representations of real electrochemical processes in order to provide meaningful information.

## 7.2 Modeling a Fuel Cell Electrode

EIS has been applied to proton exchange membrane fuel cell (PEMFC) in a number of recent studies.<sup>2,3,4</sup> The cathode impedance typically dominates the PEMFC impedance when pure hydrogen is used at the anode. Previous work in our lab has shown that the impedance of fuel cell electrodes closely corresponds to that of porous electrodes, which can be modeled by a finite transmission-line equivalent circuit, shown in Figure 7.2.<sup>5</sup>

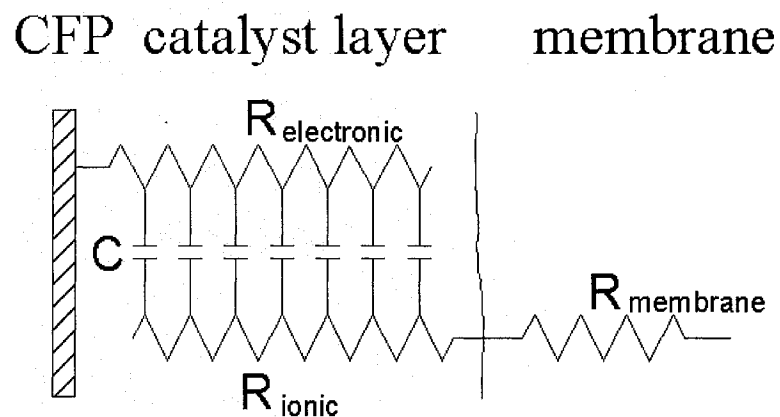


**Figure 7.2:** Finite transmission line equivalent circuit describing the impedance behavior of a PEMFC electrode.

The circuit consists of two parallel resistive rails, one for electron transport through conducting carbon particles ( $R_{\text{electronic}}$ ), the other for ion transport in the catalyst layer ( $R_{\text{ionic}}$ ). The rails are connected by capacitors representing the differential capacitance of the electrolyte-catalyst (Pt and C). We assume that this capacitance is uniformly distributed throughout the catalyst layer. Since carbon particles are excellent electronic conductors, we will also assume that  $R_{\text{electronic}}$  is negligible compared to  $R_{\text{ionic}}$ , and therefore should have a negligible effect on the impedance of the electrode. This has been confirmed by 4-point probe conductivity measurements.<sup>6</sup> We can also omit the membrane resistance ( $R_{\text{membrane}}$ ) since it would only shift the plot along the real axis.

Based upon these assumptions, we can now simulate the Nyquist impedance response of a PEMFC electrode,<sup>5</sup> as shown in Figure 7.3. Curve A simulates the response achieved when the ionic resistance is uniformly distributed across the catalyst layer. At high frequencies, a Warburg-like response ( $45^\circ$  slope) is observed. This corresponds to ion migration through the catalyst layer. At low frequencies, the plot curves upward towards a limiting capacitance response, corresponding to the electrode's total capacitance and resistance.  $R_{\text{ionic}}$  can be obtained from the real component of the length of the Warburg-like region ( $= R_{\text{ionic}}/3$ ).<sup>7</sup>

However, it is very unlikely that the ionic conductivity in a PEMFC electrode is distributed evenly across the catalyst layer. Instead, ionic conductivity should be highest near the electrode-membrane interface, and decrease deeper into the layer. This type of behavior can also be simulated. Curve B in Figure 7.3 shows the simulated response

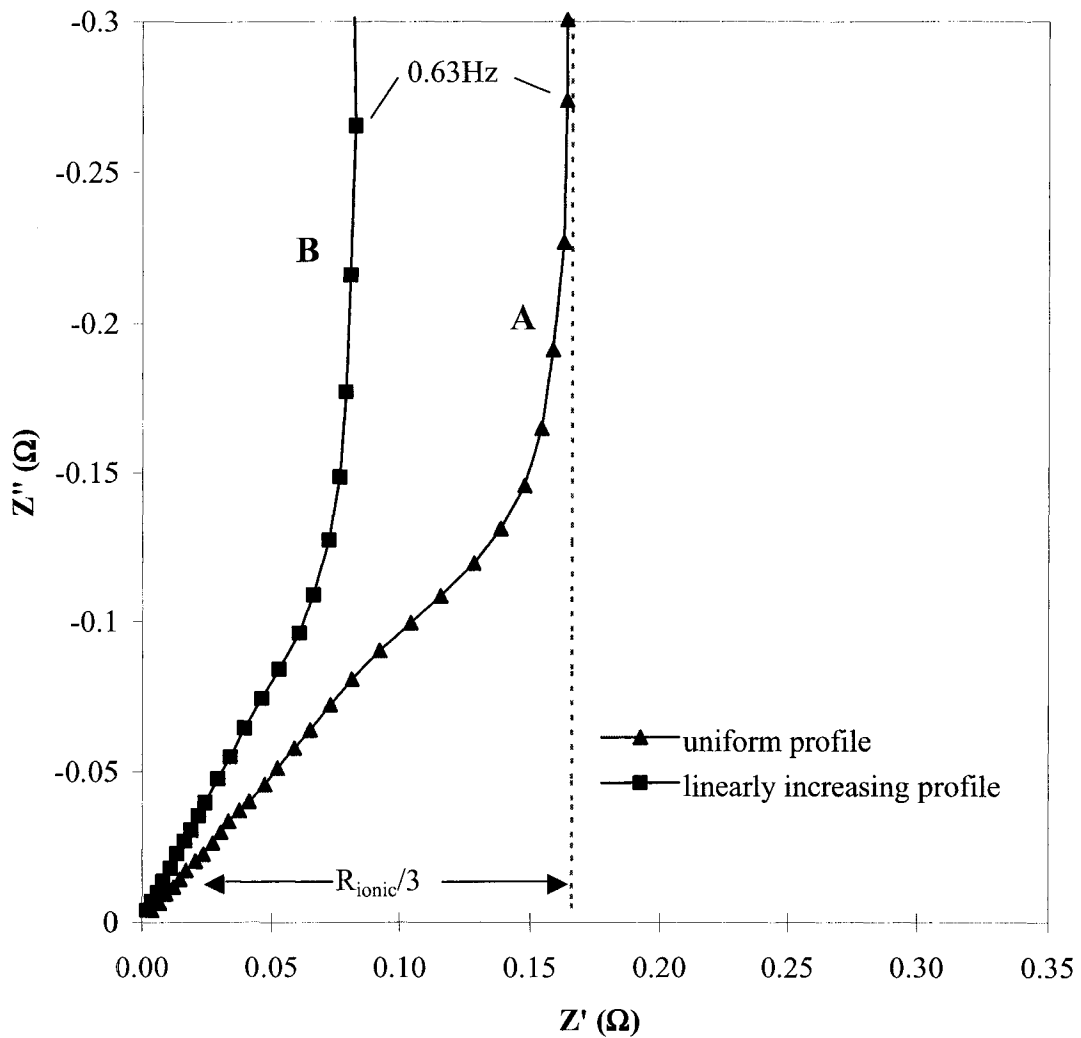


**Figure 7.3:** Nyquist impedance plots for different ionic resistance profiles, simulated on the basis of the transmission-line equivalent circuit (Figure 7.2) for 1000 resistor-capacitor combinations (with  $R_{\text{electronic}} = 0$  and  $R_{\text{membrane}} = 0$ ) with a total capacitance of 1 F and a total resistance of  $0.5\Omega$ .

when the ionic resistance linearly increases. Responses can be simulated for any ionic conductivity distribution profile.

Although Nyquist type plots are the most common, we find it more informative to convert them into “capacitance plots”, shown in Figure 7.4. This type of plot can better show how conductivity (resistivity) varies across the catalyst layer. This is because the capacitance axis can also be considered to be a distance axis since the capacitance is uniformly distributed across the layer. In practice, the capacitance measured by EIS will include both double layer capacitance and Faradaic pseudo-capacitance terms for both the Pt and carbon surfaces. However, we can assume that their relative contributions do not vary greatly between electrodes and that total capacitance is a relative measurement of electrochemically active area. This assumption is supported by cyclic voltammetry studies.<sup>8</sup>

The main objectives of the work described in this chapter are to establish a relationship between the limiting capacitance and active area, validate measurements taken on fuel cell electrodes and obtain preliminary data on their ionic conductivities.

In one case we studied the impedance behavior of catalyst layers immobilized onto glassy carbon electrodes. The impedance response was studied as a function of catalyst layer thickness and DC potential. In another case, we studied the impedance response of gas diffusion electrodes containing  $\text{Os}(\text{bpy})_3^{2+}$  electroactive probes (described in chapter 3).

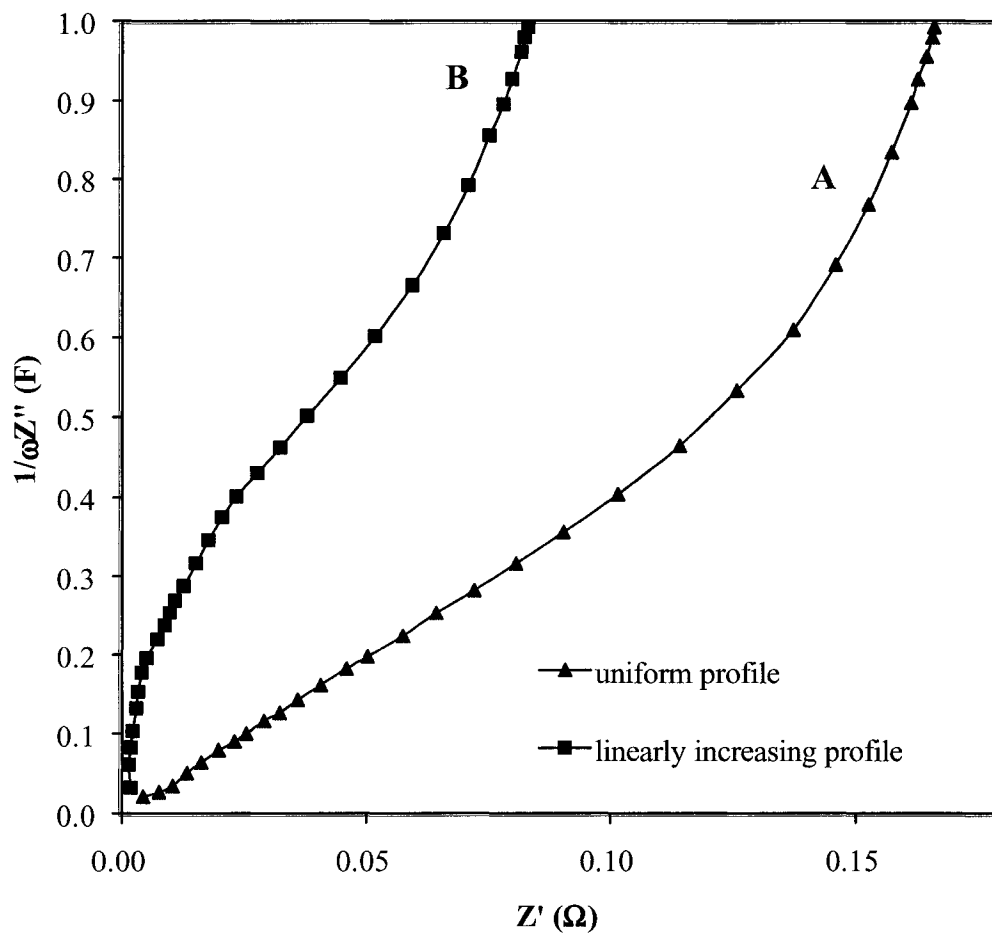


**Figure 7.4:** Capacitance plots for different ionic resistance profiles, simulated on the basis of the transmission-line equivalent circuit (Figure 7.2) for 1000 resistor-capacitor combinations (with  $R_{\text{electronic}} = 0$  and  $R_{\text{membrane}} = 0$ ) with a total capacitance of 1 F and a total resistance of  $0.5\Omega$ .

### **7.3 Catalyst Layers Immobilized onto Glassy Carbon Electrodes**

The aim of this work was to study the impedance behavior of fuel cell catalyst layers under carefully controlled conditions. Thus, the catalyst layers have been immobilized onto glassy carbon electrodes following a procedure developed by Gojkovic's group.<sup>9</sup>

#### **7.3.1 Experimental**

20% Pt/Vulcan XC72 carbon black (11.1 mg, Etek) and 5% Nafion solution (500  $\mu\text{L}$  or 420 mg, Solution Technology) were mixed thoroughly with a magnetic stirrer and sonicated to ensure a homogeneous mixture. Volumes of this catalyst ink (1-6  $\mu\text{L}$ ) were applied via a syringe onto a 0.071 $\text{cm}^2$  glass carbon electrode and allowed to dry before use. Such a large percentage of Nafion was chosen to ensure good proton conductivity and to avoid the use of other solvents in the ink preparation.

Electrochemical experiments were performed in a typical three-compartment cell using 0.5M  $\text{H}_2\text{SO}_4$  (aq) electrolyte, a Ag/AgCl reference electrode and a Pt counter electrode. EIS spectra were obtained at 0.2V vs. SSCE unless otherwise specified

#### **7.3.2 Results and Discussion**

##### **7.3.2.1 Cyclic Voltammetry Experiments**

Cyclic voltammetry (CV) is the most common technique to characterize active areas of Pt catalyst. CVs were obtained for electrodes with various amounts of catalyst ink applied. Figure 7.5 shows the CVs obtained with 1-3  $\mu\text{L}$  of ink, while Figure 7.6

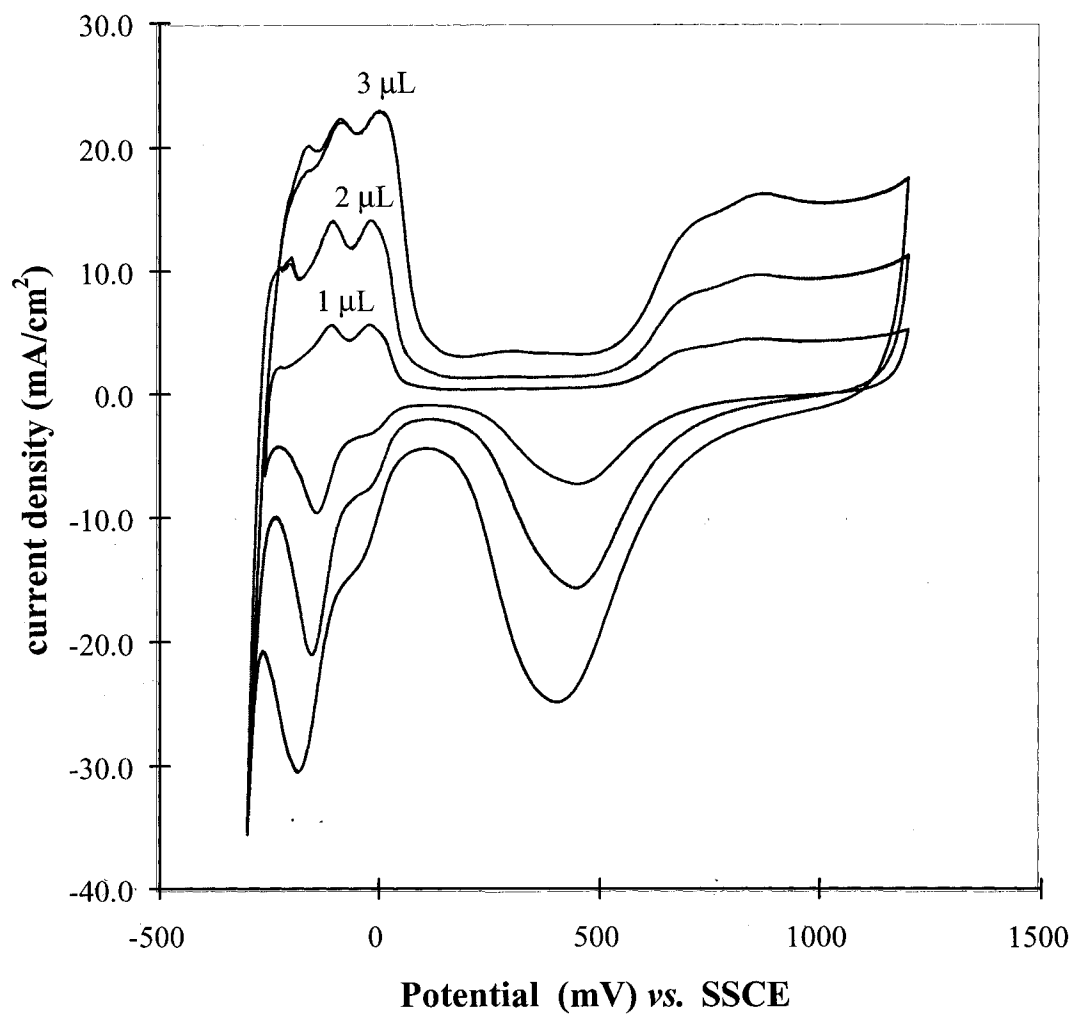


**Figure 7.5:** CVs (100 mV/s) obtained in 0.5 M H<sub>2</sub>SO<sub>4</sub> (aq) with 1- 3 μL of catalyst ink applied.

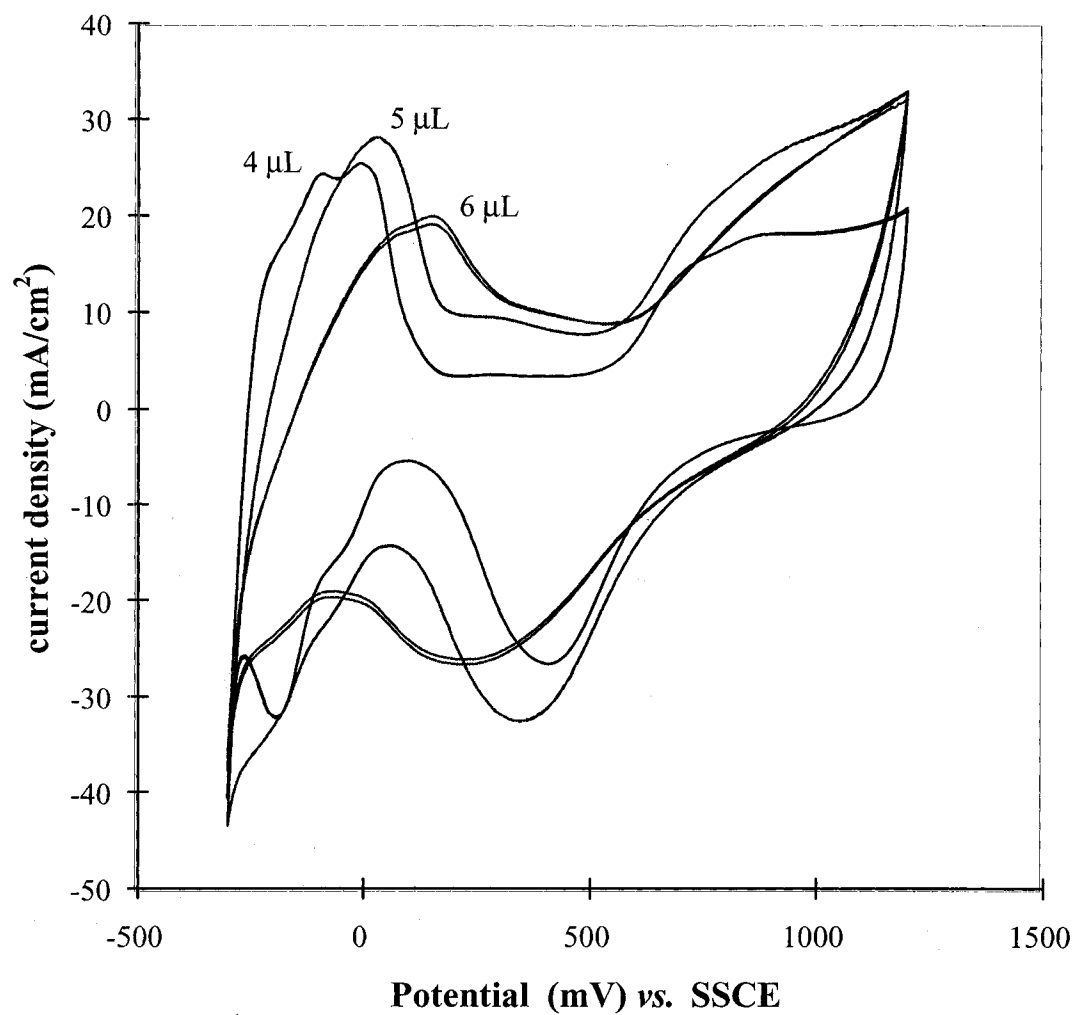


**Figure 7.6:** CVs (100 mV/s) obtained in 0.5 M H<sub>2</sub>SO<sub>4</sub> (aq) with 4 - 6 μ L of catalyst ink applied.

shows the CVs obtained with 4-6  $\mu\text{L}$  of ink. Good definition of the hydrogen adsorption/desorption peaks was obtained when a small amount of ink (1-3  $\mu\text{L}$ ) was used, which allowed for easy integration of the area under those peaks. However, these peaks became less defined as more ink is added, so much so that accurate integration was not possible when 5 and 6  $\mu\text{L}$  of ink was used. The lack of definition of these peaks may be due to increased resistance in the catalyst layer when larger volumes are used (discussed in more detail in the next section). Nonetheless, for 1-4  $\mu\text{L}$  ink, the areas under those peaks do scale linearly with ink volume, as shown in Figure 7.7.

Pt utilization was calculated as the ratio of the area of electroactive Pt, estimated from the charge under the H-adsorption waves ( $0.21 \text{ mC}/\text{cm}^2$ ), to the total area of Pt estimated from the mean particle size (radius  $r$ ) on the assumption that the particles are spheres with surface area  $4\pi r^2$ . Pt utilization was estimated to be ca. 142% for 1-4  $\mu\text{L}$  of ink applied. This method clearly overestimates the active area, which has been previously observed for this catalyst in similar experiments.<sup>10</sup>

### 7.3.2.2 EIS Experiments

Figure 7.8 shows the Nyquist plots obtained with various amounts of catalyst ink applied onto the electrode. From these we can see that the ionic resistance increases with the volume of ink applied (an enlarged view of this region is shown in Figure 7.9). However, there appears to be a larger increase in resistance for electrodes containing 4-6  $\mu\text{L}$  of catalyst ink. This may be in part due to the thickness of the layer. Also, catalyst particles are more likely to “settle out” when applying large volumes. This would lead to

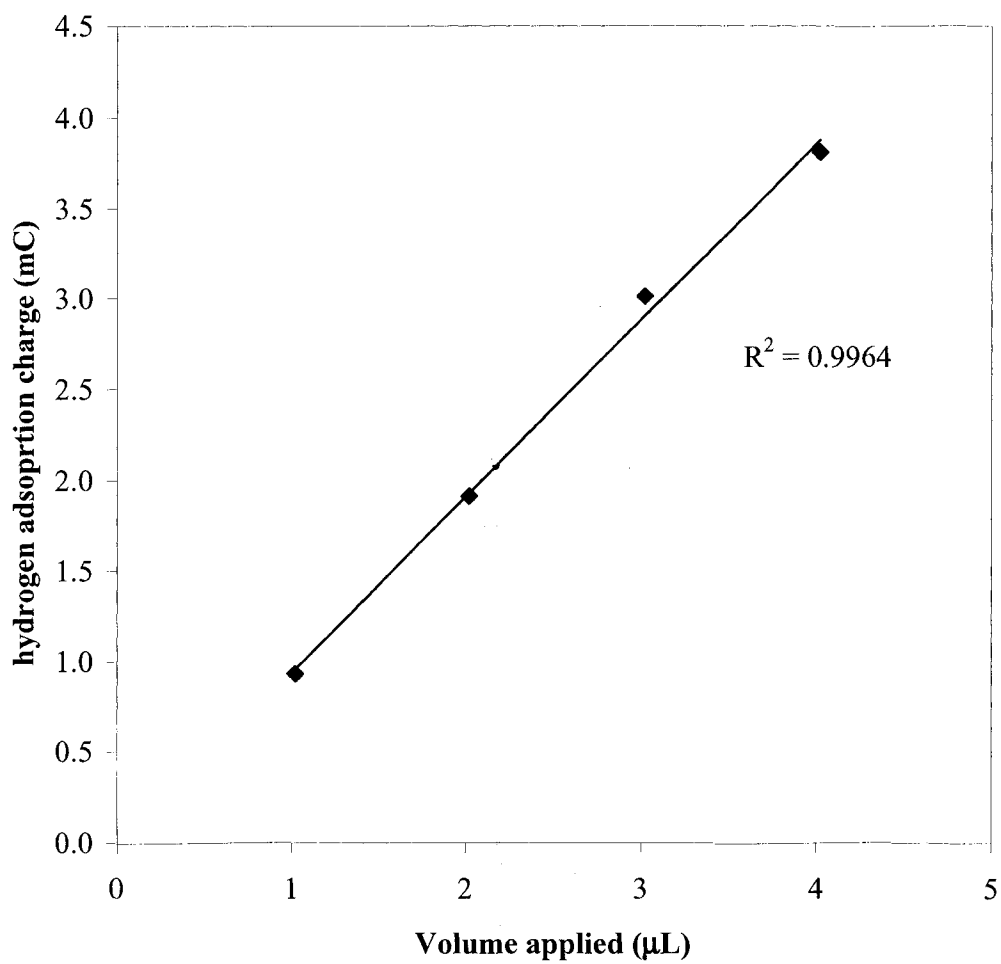


**Figure 7.7:** Hydrogen adsorption charge as a function of the volume of catalyst ink applied.

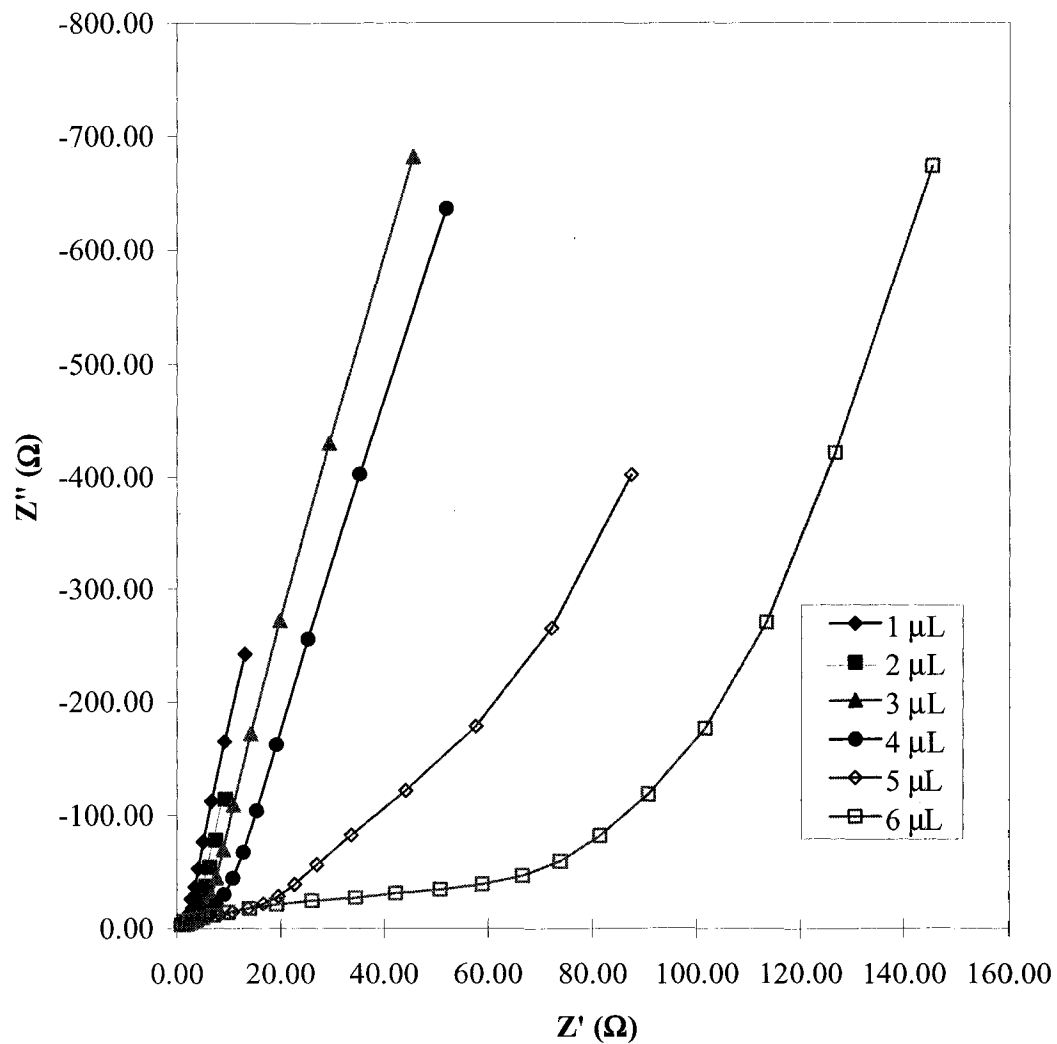


**Figure 7.8:** Nyquist plots obtained for electrodes with various amounts of catalysts ink applied over a frequency range of 100 kHz to 1 Hz.

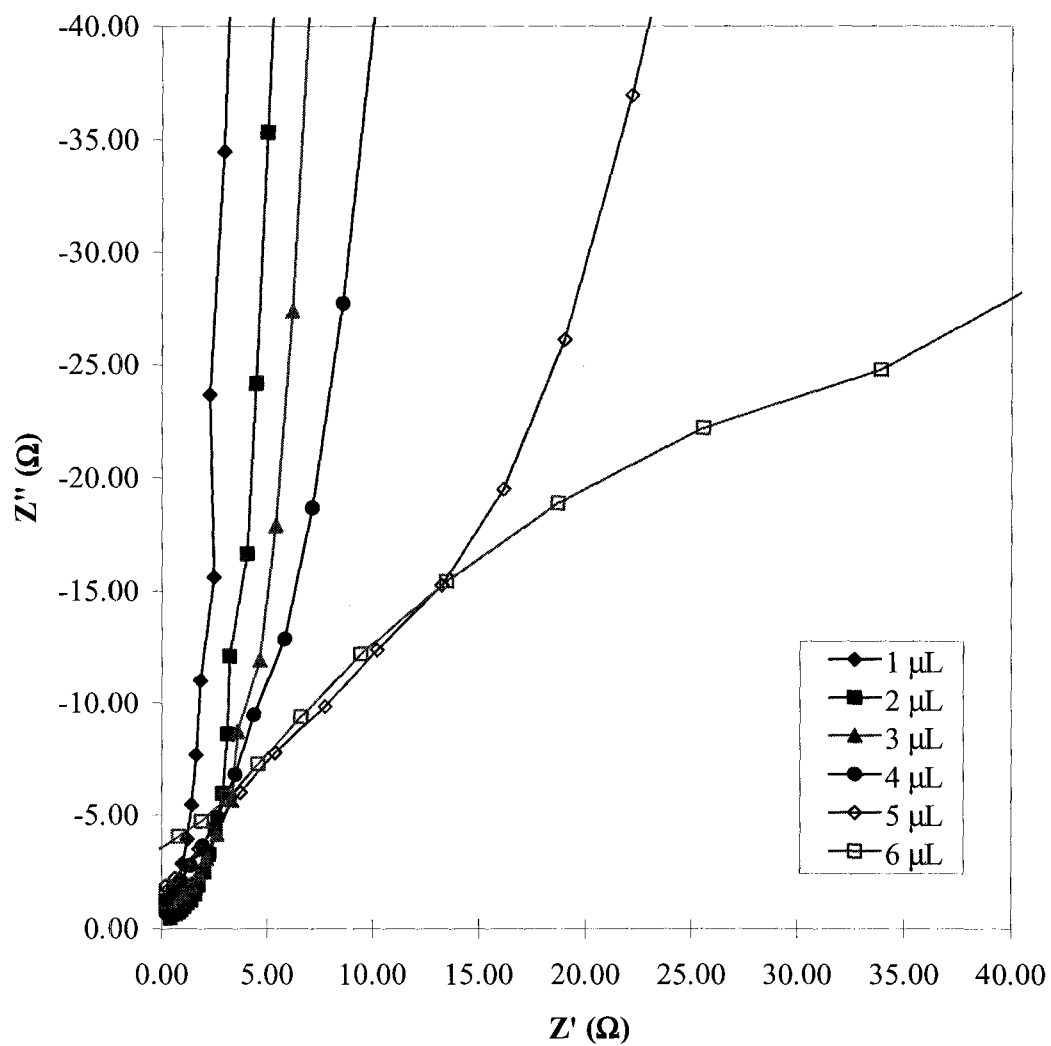


**Figure 7.9:** Enlarged view of Nyquist plots obtained for electrodes with various amounts of catalyst ink applied over a frequency range of 100 kHz to 1 Hz.

a less homogenous and more resistive catalyst layer. This may be a result of the large percentage of Nafion (65%) in the catalyst layer. The increased resistance may also explain the CV results from the previous section.

This increase in ionic resistance can be better visualized through capacitance plots. Figure 7.10 shows capacitance plots obtained for 1-3  $\mu\text{L}$  of catalyst ink applied, Figure 7.11 shows plots obtained for 4-6  $\mu\text{L}$ . We can see that for 1-3  $\mu\text{L}$  of ink, the initial slope (up to half the total capacitance) of each plot is very similar; indicating that the conductivity of each is similar. However, plots obtained for 4-6  $\mu\text{L}$  (Figure 7.11) show much more resistance. This is perhaps better seen in Figure 7.12 where the capacitances have been normalized by dividing them by the volume of ink applied. The increasing resistance is clearly visible.

We can also see from the normalized capacitance plots that the limiting capacitance does scale well with the volume of catalyst ink. Figure 7.13 plots the average limiting capacitance as a function of the volume of catalyst ink. From this, we calculate a capacitance of 0.037 mF/ $\mu\text{g}$  of catalyst. This is a useful parameter that can be applied to fuel cell electrodes to determine utilization (see section 7.4). The linearity of this plot indicates that even though thicker electrodes should have higher resistances, the active area per gram of catalyst of each electrode is approximately the same. This would not necessarily be the case in an operating fuel cell electrode, since a fuel cell electrode would not be as well hydrated as one exposed to sulfuric acid solution, nor would it contain such a large percentage of Nafion.

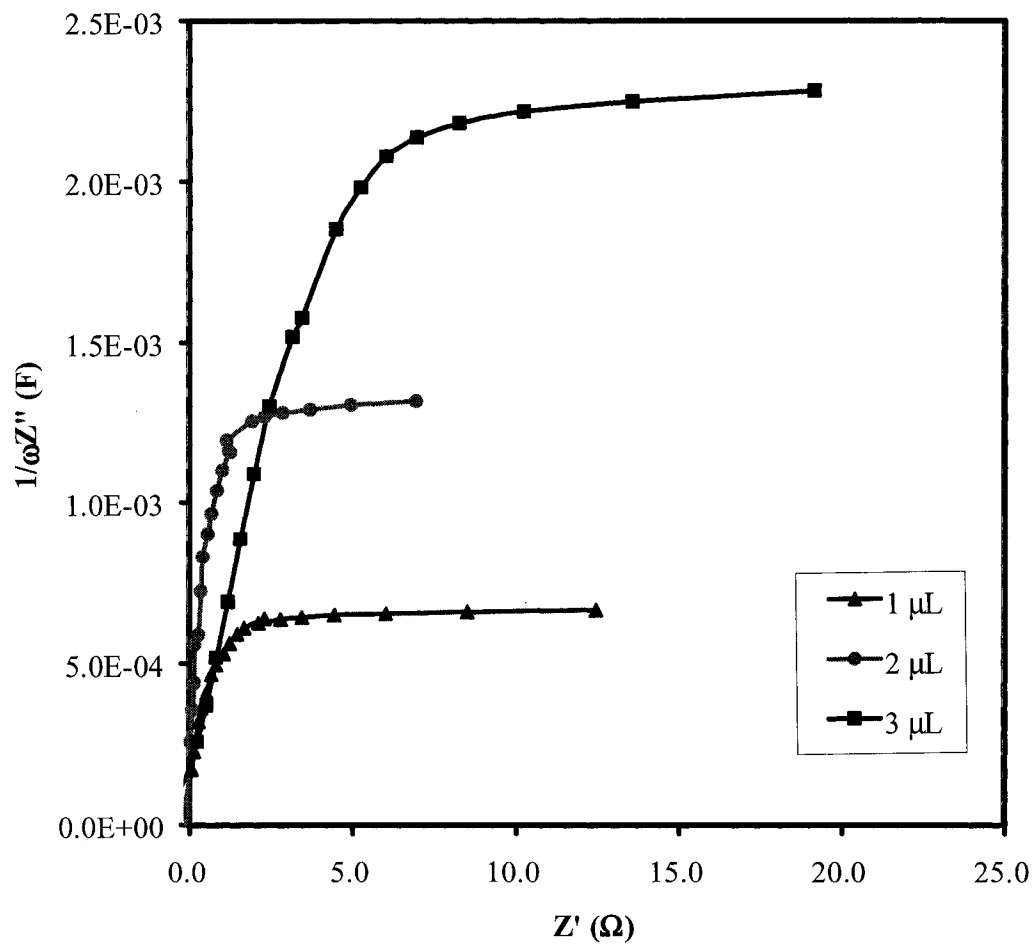


**Figure 7.10:** Capacitance plots obtained for electrodes with 1-3  $\mu$ L of catalyst ink applied.

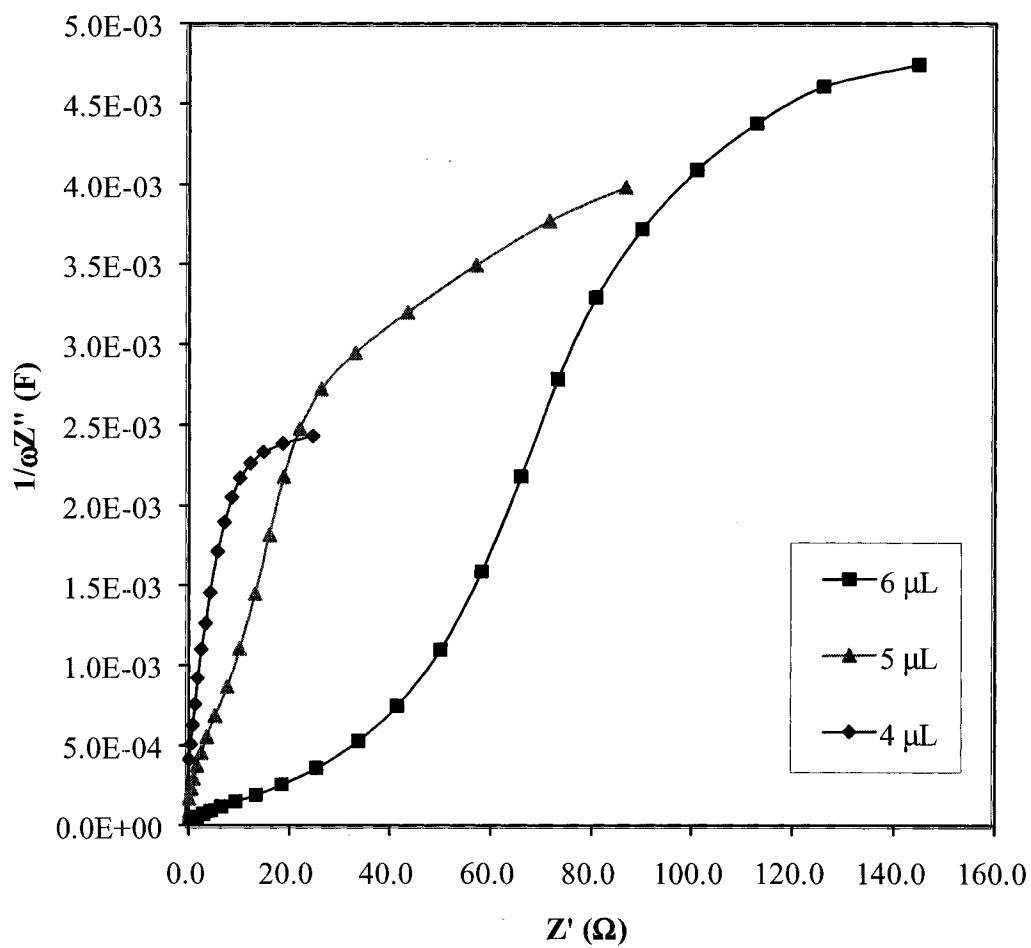


**Figure 7.11:** Capacitance plots obtained for electrodes with 4-6  $\mu\text{L}$  of catalyst ink applied.

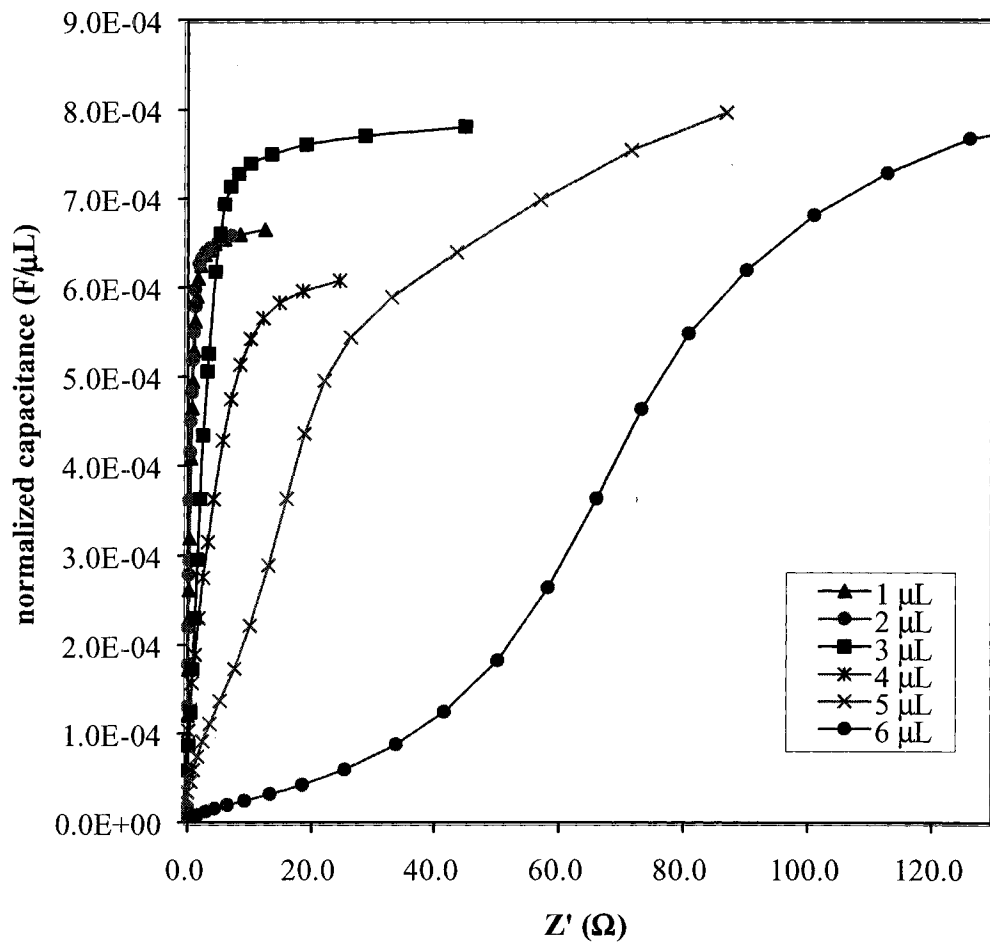


**Figure 7.12:** Volume normalized capacitance plots obtained for electrodes with different volumes of catalyst ink applied over a frequency range of 100 kHz to 1 Hz.

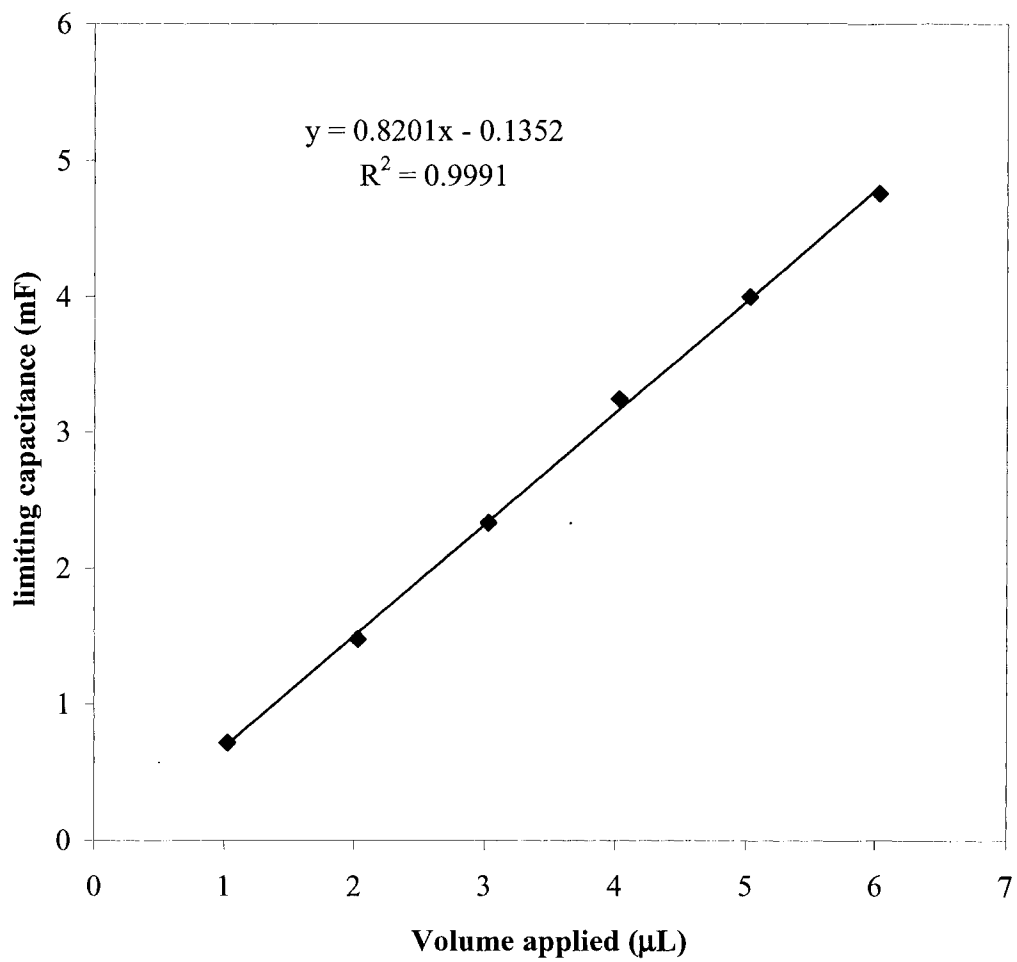


**Figure 7.13:** Limiting capacitance as a function of the volume of catalyst ink applied.

Comparison of these results with those obtained with gas diffusion electrodes is desired to validate the application of EIS to fuel cell electrodes. To do this, a  $1\text{cm}^2$  gas diffusion electrode, containing  $0.85\text{ mg/cm}^2$  of ETEK 20% Pt/C, and  $1.1\text{ mg/cm}^2$  (57%) of Nafion (prepared in a manner similar to that described in Chapters 3 and 4) was tested in the same electrolyte. This loading corresponds to the equivalent of ca.  $2.2\text{ }\mu\text{L}$  of catalyst ink applied onto a  $0.071\text{cm}^2$  electrode. Figure 7.14 compares the capacitance plot obtained with the  $1\text{ cm}^2$  gas diffusion electrode (scaled down to  $0.071\text{cm}^2$ ) to that obtained with  $2\text{ }\mu\text{l}$  of catalyst ink on the  $0.071\text{cm}^2$  electrode. The results are very similar. The slight differences can be attributed to the differences in the Nafion content (65% vs. 57%) and the approximate nature of the calculation. Nevertheless, this shows that impedance measurements taken on gas diffusion electrodes correlate well with data obtained by the more controlled Nafion/catalyst ink on glassy carbon method.

The DC bias potential at which the EIS is acquired can have a significant effect upon the data collected. If the DC bias potential is set at a potential where Faradaic processes occur, then an increase in capacitance will be observed. We have therefore studied the effect of DC bias potential on the EIS response of electrodes prepared from the Pt/C/Nafion ink described above.

Figure 7.15 shows a plot of limiting capacitance vs. DC bias potential. There is a large increase in capacitance between  $-0.2\text{ V}$  and  $0.0\text{ V}$  that can be attributed to the hydrogen adsorption/desorption process on Pt. There are also smaller peaks at higher potentials, which are enlarged in Figure 7.16. The peak at ca.  $0.3\text{V}$  can be attributed to the presence of the electrochemistry of quinone groups present on the carbon surface. The

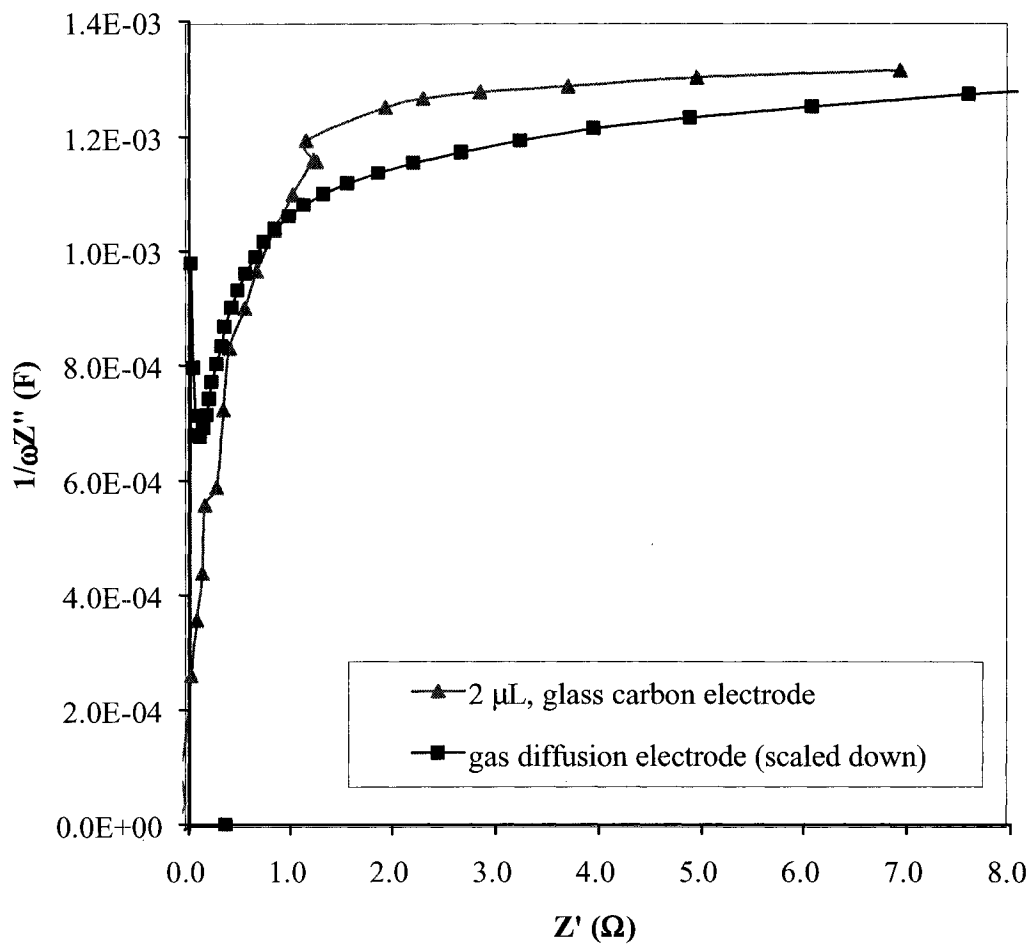


**Figure 7.14:** Comparison of capacitance plots obtained with a 0.071 cm<sup>2</sup> glassy carbon electrode prepared with 2 μL of catalyst ink applied, to that obtained with a 1 cm<sup>2</sup> gas diffusion electrode equivalent to ca. 2.2 μL of catalyst ink.

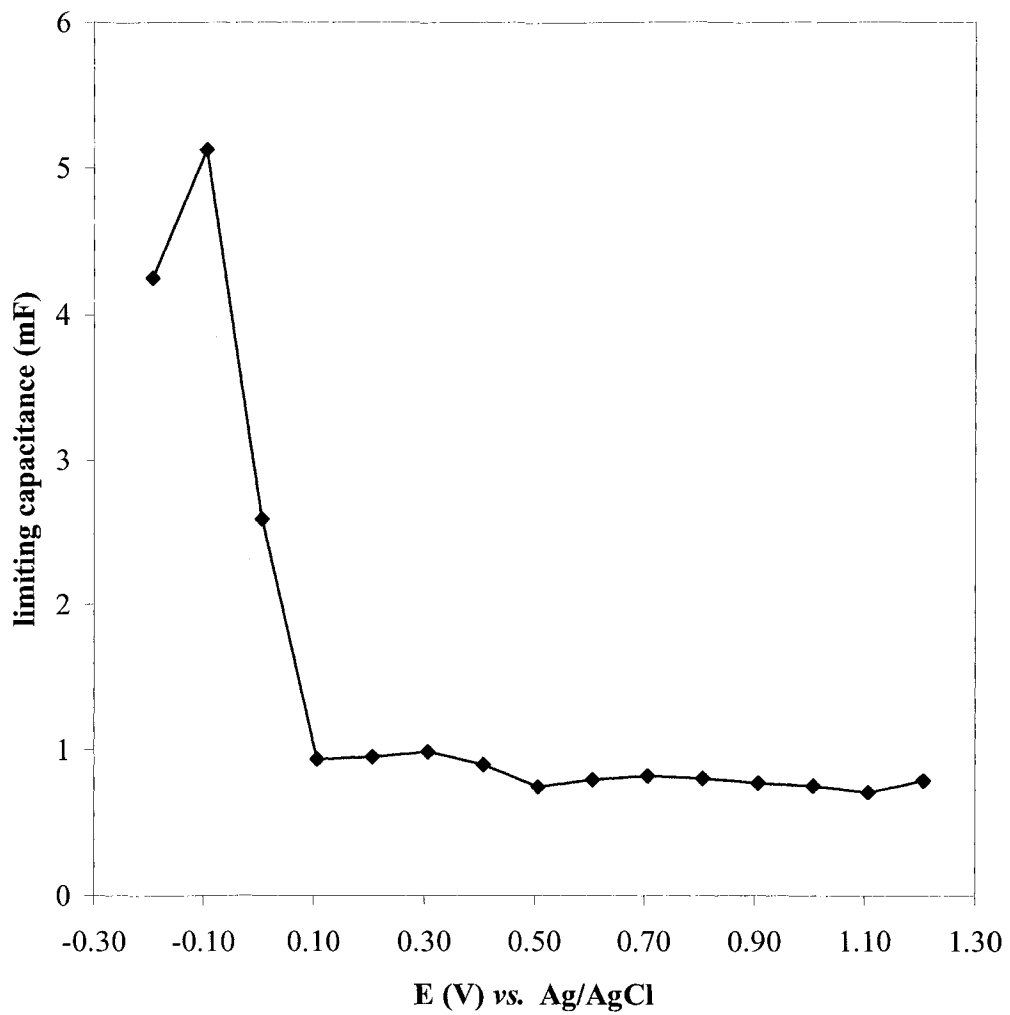


**Figure 7.15:** Limiting capacitance as a function of DC Potential. Data obtained using 1  $\mu\text{L}$  of catalyst ink.

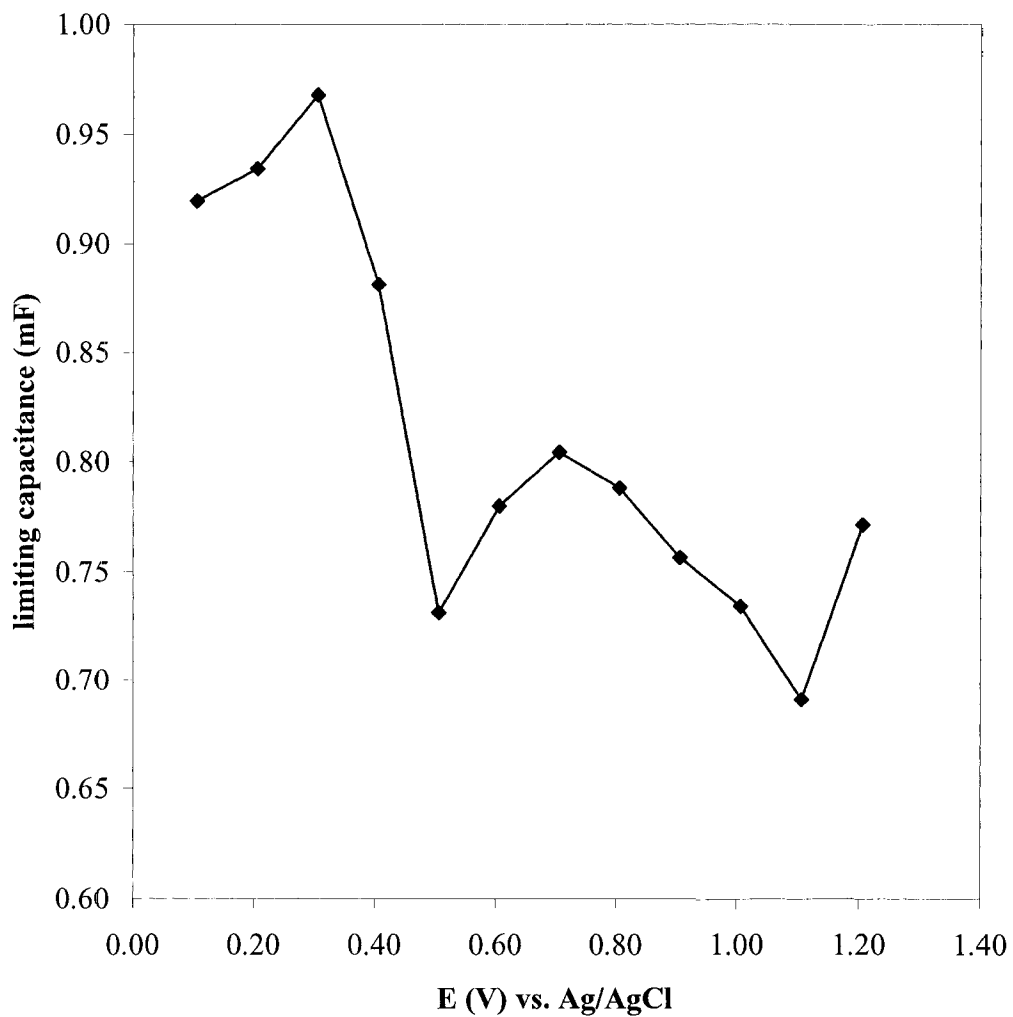


**Figure 7.16:** Limiting capacitance as a function of DC Potential. Expanded view of the area outside the hydrogen adsorption/desorption region. Data obtained using 1  $\mu\text{L}$  of catalyst ink.

peak between 0.6 V and 0.9 V can be attributed to the electrochemistry associated with oxide formation/stripping on the Pt surface.

These plots indicate that EIS data should not be acquired at potentials below 0.1 V (*vs.* SSCE). While there are some Faradaic processes present above 0.1 V, the magnitude is much lower than that for hydrogen adsorption/desorption and should therefore have a smaller effect on the data collected.

#### 7.4 Electrodes Containing Os(bpy)<sub>3</sub><sup>2+</sup> Electroactive Probes

One of the advantages of using an electroactive probe is that it can serve as a reference point for impedance studies (*i.e.* data can be obtained at its redox potential). Hence, we have studied the EIS behavior of electrodes containing Os(bpy)<sub>3</sub><sup>2+</sup> electroactive probes.

Electrodes containing Os(bpy)<sub>3</sub><sup>2+</sup> were prepared and tested (CV, fuel cell polarizations) as described in Chapter 3. Impedance measurements were performed in both the half-cell (0.5M H<sub>2</sub>SO<sub>4</sub> (aq)) and in a fuel cell MEA, both on (0.85V *vs.* NHE, 0.6V *vs.* SSCE) and off (0.65V *vs.* NHE, 0.4V *vs.* SSCE) the Os(II/III) redox wave.

Figure 7.17 shows Nyquist plots obtained on the Os redox wave both in a half-cell and in a full cell. Capacitance plots are shown in Figure 7.18. The most obvious aspect of the capacitance plots is the higher limiting capacitance obtained in the half-cell. This indicates that a significantly smaller quantity of the Os complex is electroactive in the full cell. Based on the values of the limiting capacitance, only ca. 65% of the Os that is electroactive in the half-cell is electroactive in the fuel cell. This value is slightly higher

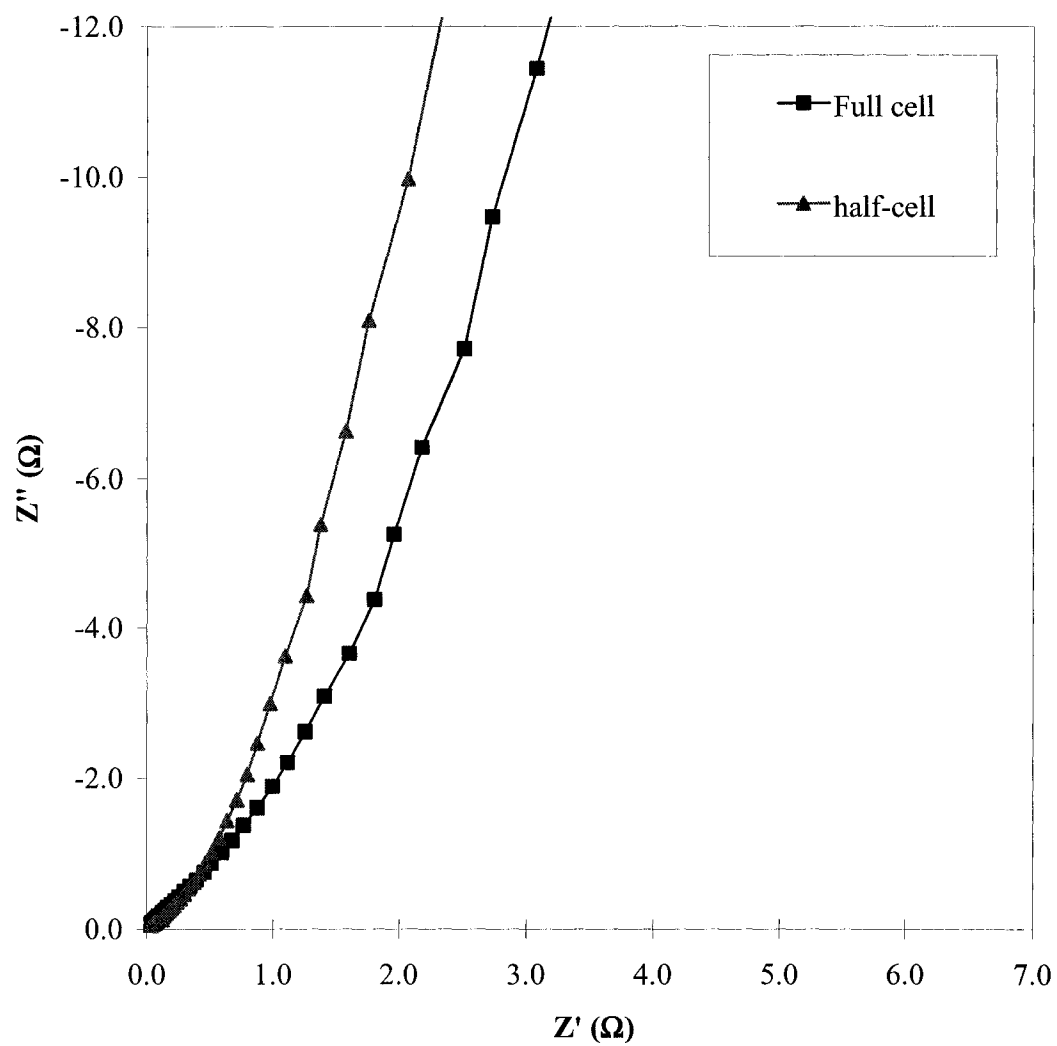


**Figure 7.17:** Comparison of Nyquist plots obtained on the Os redox wave both in a fuel cell and in a half-cell.

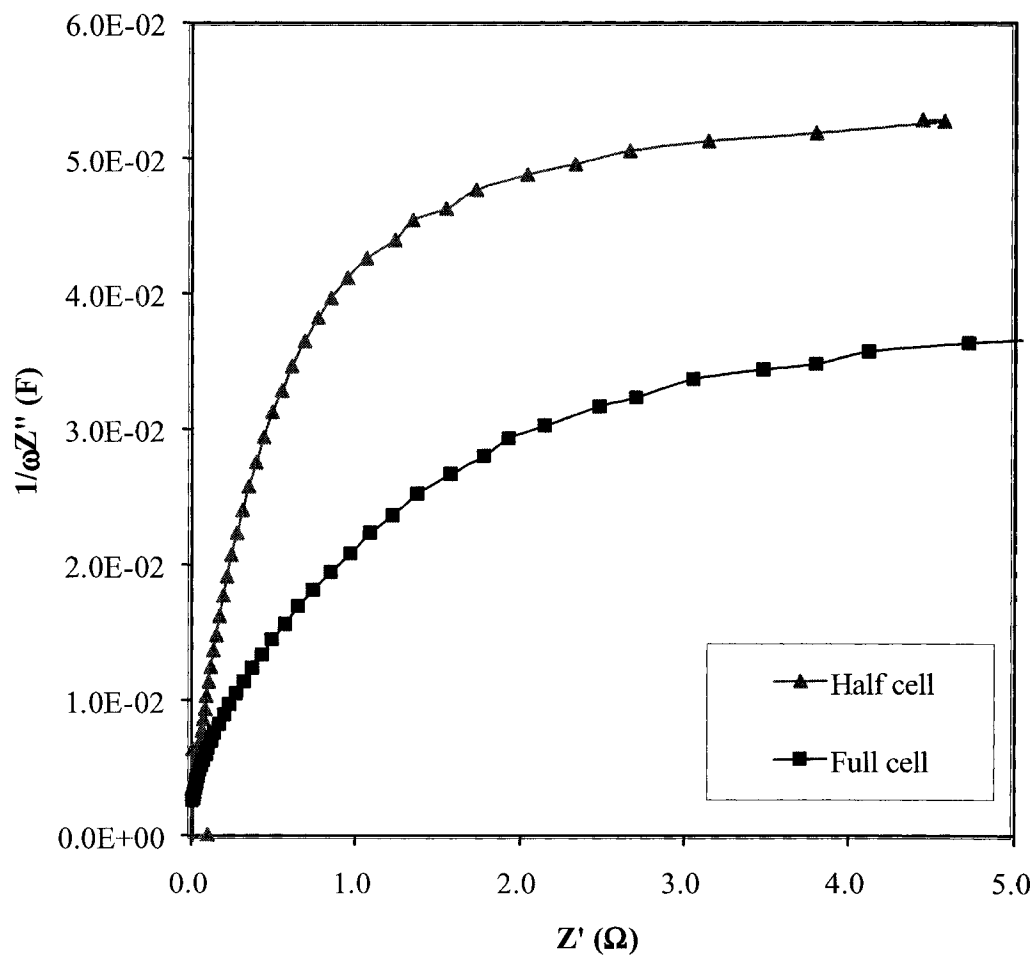


**Figure 7.18:** Comparison of capacitance plots obtained on the Os redox wave, in a fuel cell and in a half-cell.

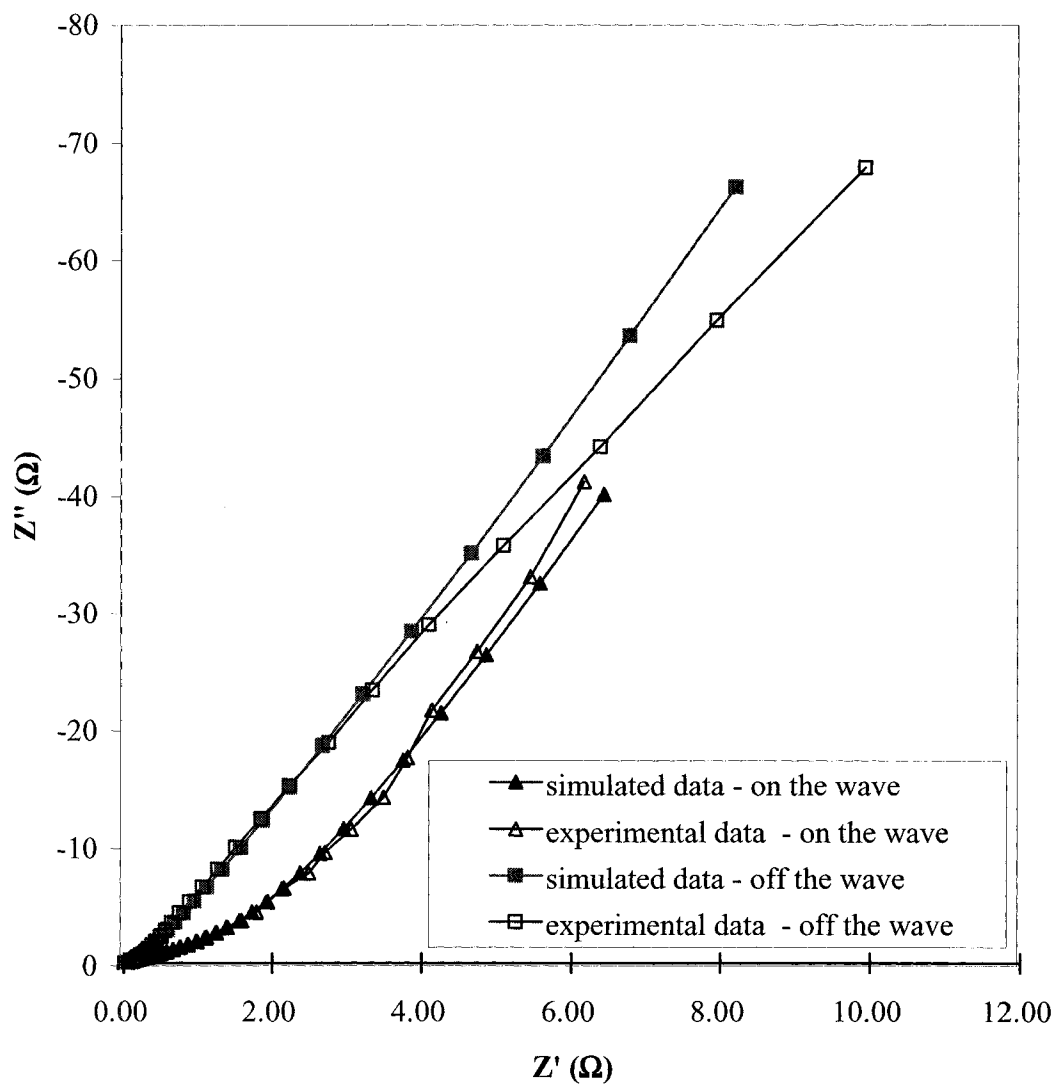
than that obtained by cyclic voltammetry (ca. 55%, section 3.3.1). This discrepancy is most likely due to slight variation in catalyst loading between electrodes and/or variation of the hydration state within the catalyst layers.

A steeper initial slope of the capacitance plot is also observed in the half-cell. This clearly indicates that there is better ionic conductivity in the half-cell compared to the full cell. This confirms our inferences from the CV experiments in chapter 3.

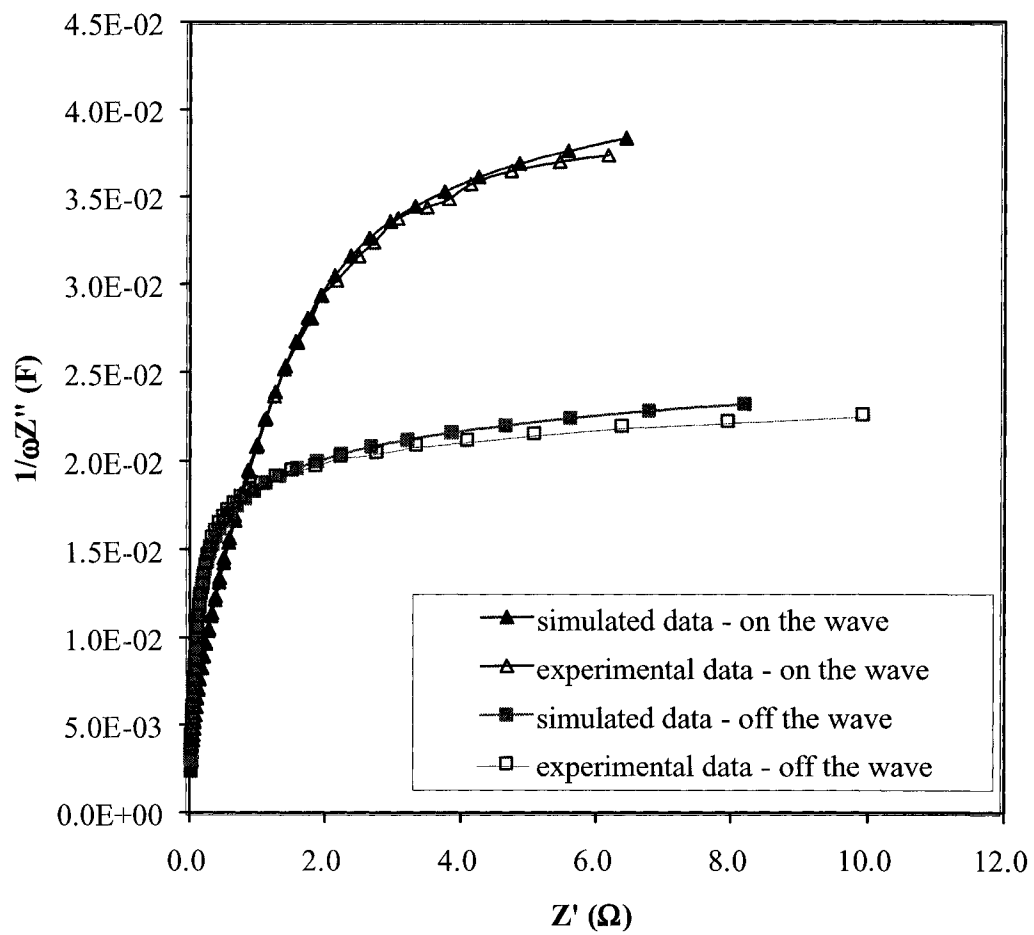
One key issue we wanted to explore was if the acquisition of EIS spectra at the Os redox potential would affect the conductivity profile of the catalyst layer. To study this, full cell impedance spectra were taken both on and off the Os redox wave. Data was then simulated (from a conductivity profile) to fit these experimental results. Simulations were performed in a Microsoft Excel spreadsheet designed by Dr. Pickup.<sup>11</sup>

Figure 7.19 and 7.20 shows the experimental and simulated data, as Nyquist and capacitance plots respectively. Good fits were obtained, especially at high frequencies. There is a much larger limiting capacitance when spectra are obtained on the Os redox wave, which is due to the electrochemistry of the Osmium complex. Based upon the value of 0.037 mF/ $\mu\text{g}$  determined in the previous section, we would expect a limiting capacitance value of ca. 30 mF off the Os wave (if 100% of the layer is electroactive). However, a limiting capacitance of ca. 21 mF is observed off the Os wave, indicating that only ca. 70% of the layer is electroactive.

The conductivity profiles that simulated these fits are shown in Figure 7.21. The distance into the layer is based upon an estimate of 55% of a 30  $\mu\text{m}$  layer being electroactive (from CV experiments in chapter 3). From this we see that the simulated



**Figure 7.19:** Comparison of simulated and experimental Nyquist plots obtained on and off the Os redox wave.



**Figure 7.20:** Comparison of simulated and experimental capacitance plots obtained on and off the Os redox wave.

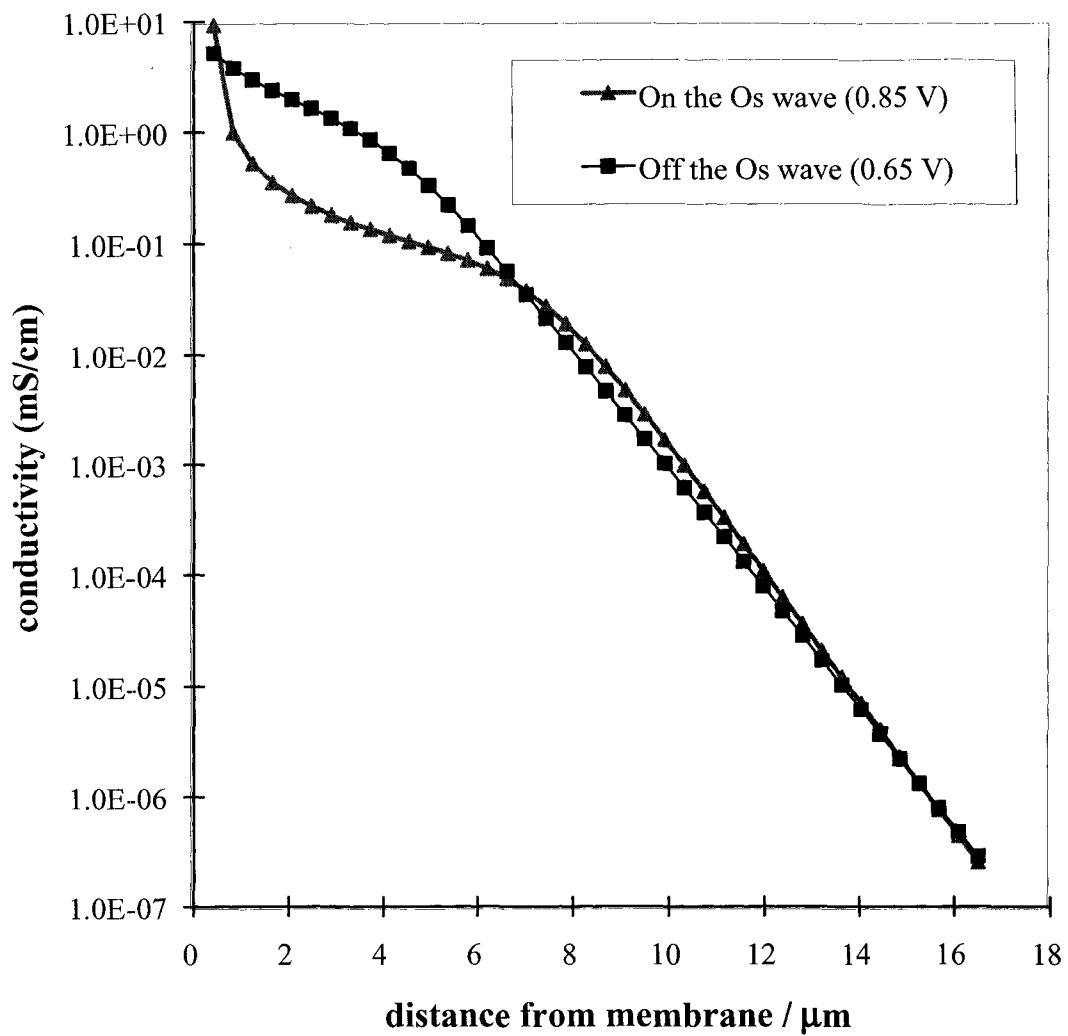


**Figure 7.21:** Conductivity profiles simulated from EIS obtained on and off the Os redox wave.

profiles are almost identical except for the first ca. 6  $\mu\text{m}$  into the layer. The profile simulated on the Os wave deviates from linearity for the first 6  $\mu\text{m}$  into the layer. This deviation is most likely an artifact caused by slow diffusion of the Os complex within the layer. It is well known that the diffusion of  $\text{M}(\text{bpy})_3^{2+}$  (M= Os, Ru, etc.) through Nafion is a relatively slow process compared to other cations.<sup>12</sup> Artifacts from this slow diffusion are most likely to be observed at high frequencies in EIS experiments (but not at low frequencies). This translates into effects seen in the profile at short distances into the catalyst layer, which is what was observed. This highlights the advantage of using an electroactive probe that is tethered directly to the catalyst surface (*i.e.* shorter distances to diffuse). Nonetheless, we can conclude that the conductivity profiles obtained both on and off the Os redox wave are essentially similar, and this supports the hypothesis that the non-ideal behavior of fuel cell electrodes is due to variations of conductivity across the layer, rather than variations in capacitance.

## 7.5 Conclusion

EIS is a powerful tool to study PEMFC catalyst layers. Active area and ionic conductivity within the catalyst layer has been studied as a function of catalyst layer thickness using EIS. We have shown that there is a relationship between the limiting capacitance and the mass of catalyst. Results obtained on more-controlled smaller scale electrodes correlate well with results obtained for larger gas diffusion electrodes. The smaller scale method is therefore suitable for screening different catalyst layer compositions before larger scale tests are performed.

EIS can be used in conjunction with electroactive probes to study ion conductivity and active area in fuel cell electrodes. It can also be used to study slow diffusion processes within the catalyst layer.

Together, these results provide strong evidence that the non-ideal impedance behavior of fuel cell electrodes is due to variation of their ionic conductivity with distance from the membrane.

## References

---

- <sup>1</sup> EG&G Princeton Applied Research Electrochemical Instruments Group. Application Note Ac-1: Basics of AC Impedance Measurements.
- <sup>2</sup> Wagner, N.; Schnurnberger, W.; Muller, B.; Lang, M. *Electrochim. Acta* **1998**, *43*, 3785.
- <sup>3</sup> Daird, J. P.; LeGorrec, B.; Montella, C.; Poinsignon, C.; Vitter, G. *J. Powers Sources* **1999**, *74*, 244.
- <sup>4</sup> Springer, T. E.; Zawodzinski, T. A.; Wilson, M. S.; Gottesfeld, S. *J. Electrochem. Soc.* **1996**, *143*, 87.
- <sup>5</sup> Lefevre, M. C.; Martin, R. B.; Pickup, P. G. *Electrochem. Solid-State Lett.* **1999**, *2*, 259.
- <sup>6</sup> Qi, Z.; Pickup, P. G. *Chem. Comm.* **1998**, 2299.
- <sup>7</sup> Lefevre, M. C.; Qi, Z.; Rana, D.; Pickup, P. G. *Chem. Mater.* **1999**, *11*, 262.
- <sup>8</sup> Jia, N. Y.; Martin, R. B.; Qi, Z. G.; Lefebvre, M. C.; Pickup, P. G. *Electrochim. Acta* **2001**, *46*, 2863-2869.
- <sup>9</sup> Gojkovic, S. L.; Zecevic, S. K.; Savinell, R. F.; *J. Electrochem. Soc.* **1998**, *145*, 3713.
- <sup>10</sup> Shan, J.; Pickup, P. G. *Electrochim. Acta* **2000**, *46*, 119-125.
- <sup>11</sup> Ren, X.; Pickup, P. G. *Electrochim. Acta* **2001**, 4177-4183.
- <sup>12</sup> Martin, C. R.; Dollard, K. A. *J. Electroanal. Chem.* **1983**, *159*, 127-135.

## **Chapter 8**

### **Summary and Future Work**

In this thesis, the chemical modification of fuel cell electrodes and membranes has been a common theme. This has been shown to be an effective method to study processes that occur in a fuel cell (*i.e.* ion transport) and also to improve fuel cell performance. The method of electroactive probes has the potential to improve the diagnostic value of data obtained by techniques such as cyclic voltammetry and Electrochemical Impedance Spectroscopy (EIS). We have shown that the quantity of the probe present can be accurately controlled, and that the percentage that is electrochemically active can be determined. Two examples of chemically modified gas diffusion electrodes were studied to demonstrate the value of electrode functionalization methods in the study of fuel cells. In one example,  $\text{Os}(\text{bpy})_3^{2+}$  was added to the ionomer binder in the active layer of the electrode to measure the fraction of this ionomer that participates in ion transport within the layer. A lower fraction of the Os complex was electrochemically active in the cathode of an operating fuel cell, compared to a similar electrode that was in contact with an aqueous sulfuric acid solution. The difference is attributed to poor hydration of the fuel cell electrode. In a second example, a Ru complex was covalently attached to a carbon black fuel cell catalyst support, allowing for the determination of the fraction of the carbon surface that is in both electronic and ionic contact with the current collector and membrane, respectively.

Future work in the area of electroactive probes should involve the synthesis of acid stable surface bound probes. The use of a silane containing a bi-dentate ligand that directly binds to an electroactive metal center could solve the problem of acid hydrolysis.

Preliminary work has already been started towards the synthesis of a silane containing a 1,10-phenanthroline ligand.

The novel method of treating the catalyst with a sulfonated silane has been shown to be an effective method to increase proton conductivity within the cathode catalyst layers. A 66% reduction of the Nafion content within the catalyst layer was achieved without a significant loss in performance. This was explained by the fact that both of these electrodes contained the optimal total sulfonate loading. This is significant in that it shows that performance is most strongly influenced by the proton conductivity of the electrode, regardless of the origin of the proton conductor. Thus, many other (i.e. less expensive) Nafion alternatives could be used.

Future research in this area should involve the further characterization of these catalysts with EIS, which should clearly illustrate that catalyst layers made with the treated and pretreated catalysts possess increased proton conductivity. Optimization of the silane monomer structure (e.g. tether length) and the treatment of other carbon blacks could also be explored.

Significant improvement in direct methanol fuel cell (DMFC) performance has been achieved from a systematic optimization of the membrane-electrode assembly (MEA). Each component of the anode and cathode has been optimized to yield maximum performance. The effect of Nafion membrane thickness was also explored. Methanol crossover was found to be inversely proportional to membrane thickness, as was anode performance. Nafion 115 and 1135 membranes gave the best DMFC performance. This

was attributed to their balance of good anode performance and intermediate methanol crossover rates.

The reduction of methanol crossover is of paramount importance if DMFCs are to become a viable technology. Polypyrrole/Nafion composite membranes have been shown to decrease the rate of methanol crossover. Composite membranes prepared using  $\text{Fe}^{3+}$  as the oxidizing agent were shown to be significantly less permeable to methanol (ca. 50-80%) than Nafion membranes. However, poor DMFC and anode performance were achieved with these membranes, primary due to poor electrode-interfacial properties. A method to enhance the membrane-electrode interface has been developed, which has resulted in significant performance gains. Composite membranes prepared using  $\text{H}_2\text{O}_2$  as the oxidizing agent exhibit 30-50% less methanol crossover (than Nafion) and have better electrode-interfacial properties than composite membranes prepared using  $\text{Fe}^{3+}$ .

Composite membranes prepared via both methods have been shown to outperform Nafion membranes in a DMFC. This is primarily because of increased cathode activity, resulting from less methanol crossover and a lower water flux across the membrane.

Future studies of these composite systems could involve the use of other conducting polymer. Optimization of the modification technique, specifically to concentrate the polypyrrole in the center of the membrane, could lead to improved results. Also, polypyrrole/Nafion 1135 composite membranes have yet to be studied. Composite membranes based upon other proton exchange membranes (Aciplex, Gore, etc.) could also prove interesting.

EIS is a powerful tool to study fuel cell catalyst layers. We have established a relationship between an electrode's limiting capacitance and its active area. Results obtained with catalyst layers immobilized on glassy carbon electrodes correlated well with results obtained with gas diffusion electrodes. The catalyst layers immobilized on glassy carbon method is therefore suitable for screening different catalyst layer compositions before larger scale tests are performed. EIS studies on electrodes containing the  $\text{Os}(\text{bpy})_3^{2+}$  probes (described above) have also been used to study ion conductivity and active area in fuel cell electrodes. Together, these results provide strong evidence that the non-ideal impedance behavior of fuel cell electrodes is due to variation of their ionic conductivity with distance from the membrane. Future application of the model to different catalyst systems would further enhance its validity.





